ANALYSIS OF TERRESTRIAL RADIONUCLIDES (^{232}TH, ^{238}U, ^{40}K) AND SELECTED HEAVY METALS IN SEDIMENT, WATER, FISH AND FOOD CROPS FROM THE LAKE TURKANA REGION

Vincent Otwori Atambo

A Thesis Submitted in Partial Fulfillment of Requirements for the Degree of Doctor of Philosophy in Physics of Murang'a University of Technology

February, 2025

DECLARATION

Student Declaration

I hereby declare that this thesis is my original work and to the best of my knowledge, it has not been presented for a degree award in this or any other university. I understand what plagiarism is and I am aware of the University's policy in this regard. I understand that any false claim in respect of this work shall result in disciplinary action in accordance with the University Anti-Plagiarism Policy.

_____ _____

Vincent Otwori Atambo Date

Reg no: AS502/5742/2021

Supervisors' Approval

The undersigned certify that they have read and hereby recommended for acceptance of Murang'a University of Technology the thesis entitled "Analysis of Terrestrial Radionuclides (232th, 238u, 40k) and Selected Heavy Metals in Sediment, Water, Fish and Food Crops from the Lake Turkana Region".

_____ _____

Dr. Sharon Kiprotich Date

Department Physical and Biological Sciences

Murang'a University of Technology

_____ _____

Dr. Jeremiah Kebwaro Date

Department of Physical and Biological Sciences

Karatina University

_____ _____

Prof. Sylvia Opiyo Date

Department Physical and Biological Sciences

Murang'a University of Technology

DEDICATION

In dedication of this thesis, I recognize the academia, a realm of relentless inquiry and the pursuit of knowledge. May this work contribute, however modestly, to the human intellect and inspire future generations of researchers to explore, innovate, and challenge the limits of what is known.

ACKNOWLEDGEMENT

My profound gratitude first goes to God, whose grace, strength, and wisdom guided me throughout this academic journey, sustaining me through challenges and providing perseverance. His blessings were the foundation for this achievement.

I extend heartfelt appreciation to my beloved wife and children, whose unconditional love, steadfast encouragement, and immense sacrifices were indispensable. The collective strength and love of my family unit served as an unbreakable support system, cushioning every fall and celebrating every small victory, making this thesis a testament to their unwavering support.

I express immense gratitude to my supervisors, Dr. Sharon Kiprotich, Dr. Jeremiah Kebwaro, and Prof. Sylvia Opiyo. Dr. Kiprotich's meticulous guidance from conception to manuscript, patient clarifications, insightful feedback, and consistent encouragement were transformative, significantly refining my thinking and work quality. Dr. Kebwaro's profound technical expertise and practical advice were crucial for navigating complex methodologies and data analysis. His ability to simplify scientific principles enriched my understanding and ensured the thesis's analytical robustness. Prof. Opiyo's visionary leadership and strategic insights provided a critical framework for this research. Her mentorship inspired critical thinking and fostered an environment of intellectual growth. The collective wisdom and commitment of my supervisory team were the driving force behind the thesis's successful completion.

Finally, I want to express my profound appreciation to all the distinguished members of the Department of Physical and Biological Sciences at Murang'a University of Technology. The department's supportive and collegial atmosphere, along with the moral encouragement, technical assistance, and access to essential resources from faculty and staff, were indispensable. Their readiness to offer advice and engage in discussions significantly contributed to my growth and the research's success.

ABSTRACT

Human activities such as mining and natural processes like earthquakes can release radionuclides and heavy metals into the environment, which are then transported by water into reservoirs, sometimes exceeding safe levels. Elevated concentrations of these elements threaten aquatic ecosystems, reduce water quality, and can bioaccumulate in food chains, posing risks to human health. The Lake Turkana Basin, an important source of water, and livelihoods for surrounding communities, is particularly vulnerable, making baseline data critical for environmental monitoring and public health protection. Previous studies on RiftValley lake systems have indicated that geological formations often contribute to elevated background radiation and mineral leaching into the water column. The objective of this research was to establish a radiological and elemental baseline for the Lake Turkana Basin by quantifying the activity concentrations of ^{232}Th, ^{238}U, and ^{40}K, and assessing heavy metal toxicity in both geological and biological matrices to evaluate the associated public health risks. The objective was realized by studying sediment and water samples collected from the eight centers found along the Weatern shores of Lake Turkana namely Kerio, Eliye, Kalokol, Long'ech, Kataboi, Nachukui, Nareng'ewoi, and Nariokotome. Sediment and water samples were also collected from River Turkwel at Lodwar town and Kang'atosa. Sorghum and cassava were obtained from ten farms at Kang'atosa, and fish were sourced from Kalokol and Long'ech fish markets. The samples for radiometric analysis were dried to remove moisture, homogenized to create a fine, uniform powder, and sealed in standardized counting containers to establish secular equilibrium before measurement. Samples were analyzed for radionuclide concentrations of ^{232}Th, ^{238}U and ^{40}K using a High Purity Germanium (HpGe) detector while Microwave Plasma–Atomic Emission Spectroscopy (MP-EAS) was used to analyze concentrations of the metals lead, copper, arsenic, cadmium, chromium, nickel, zinc and barium in water and fish samples. Before heavy metal analysis, water samples were filtered, immediately acidified with concentrated nitric acid to prevent metal precipitation, fish samples were dried, homogenized, and then underwent wet acid digestion (usually using nitric acid to dissolve the organic matrix and fully release the heavy metals into a liquid solution suitable for MP-AES nebulization. The activity concentrations of ^{232}Th, ^{238}U and ^{40}K were used to determine the radiation hazard indicators in sediment samples such as Absorbed Dose Rate (ADR), Annual Effective Dose (AED), Excess Lifetime Cancer Risk (ELCR), External Hazard Index (H_{ex}), Internal Hazard Index (H_{in}) and the Gamma Index. Also, the activity concentrations of the three radionuclides was used to determine AED in cassava and sorghum samples. Descriptive statistics was used to statistical variables such as the mean, standard error, standard deviation, variance, skewness, kurtosis and range in the data. Analysis of Variance (ANOVA) between groups for different variables in sediment samples was done. Heavy metal concentrations were used to determine water quality indices as well as health risk parameters in fish samples. Pearson correlation was used to determine the correlation between activity concentrations of ^{232}Th, ^{238}U and ^{40}K in fish samples and concentrations of As, Ni, Ba, Cu, Zn, Pb, Cd and Cr in fish samples. Results found sediments from Kalokol to have the highest activity concentration levels of ^{232}Th (75.5 Bq/kg) and ^{238}U (64.5 Bq/kg), while sediments from Nareng'ewoi had the highest activity concentration level of ^{40}K (811.7 Bq/kg). Overall average activity concentrations in sediments from all regions were 38.7 ± 7.53 Bq/kg for ^{232}Th, 30.1 ±

5.80 Bq/kg for ^{238}U, and 664.4 ± 65.43 Bq/kg for ^{40}K. Although average concentration levels of ^{232}Th and ^{238}U were below world averages, ^{40}K exceeded them. All radium equivalent activity values for sediments were safely below the 370 Bq/kg limit. In agricultural products, activity concentration of ^{40}K was notably high in sorghum (699.34 Bq/kg) and cassava (804.42 Bq/kg). Fish species also showed varying radionuclide concentration levels, with Nile Perch having the highest ^{238}U (49.56 ± 2.81 Bq/kg). Radiological hazard indicators in sediments were generally within permissible safety limits. Although the ingestion dose from cassava (0.152 mSv/yr) remained within safe limits, the average dose from sorghum (1.110 mSv/yr) exceeded the ICRP recommended limit. Surface water analysis revealed Arsenic as the most prominent heavy metal (0.756 ± 0.033 mg/L average). The Metal Contamination Index (0.0002–0.0026) was low, but the Heavy Metal Evaluation Index (46.207–122.431) indicated significant pollution, mainly from arsenic (As) and zinc (Zn). Cadmium (Cd) was undetected in fish, while Nile perch showed the highest concentrations of As (0.732 ± 0.045 mg/kg) and Zn (0.769 ± 0.057 mg/kg), as well as the greatest bioaccumulation. Health risk assessment from fish consumption revealed negligible non-carcinogenic risks, with hazard index values below 1. Correlation analysis showed strong positive relationships between ^{238}U and As ($r = 0.900$, $p = 0.001$) and between ^{238}U and Zn ($r = 0.792$, $p = 0.011$). This research establishes a vital geochemical baseline for the Lake Turkana Basin, revealing a complex interplay between natural geological background radiation and anthropogenic heavy metal enrichment. While the radiometric profile characterized by elevated ^{40}K but generally safe levels of ^{232}Th and ^{238}U reflects the unique volcanic lithology of the East African Rift, the significant Arsenic and Zinc signatures in surface waters point toward localized pollution that necessitates active environmental oversight. Crucially, the discovery that sorghum consumption in certain areas may lead to an ingestion dose exceeding ICRP limits (1.110 mSv/yr) underscores a specific public health vulnerability that simple water testing would miss. Ultimately, while the basin remains largely resilient to non-carcinogenic risks at present, these findings serve as a critical early-warning system, advocating for integrated water-soil-food monitoring to ensure that the region's mining and agricultural sectors do not compromise the long-term biological integrity of the ecosystem.

TABLE OF CONTENTS

DECLARATION ..... **ii**
DEDICATION ..... **iii**
ACKNOWLEDGEMENT ..... **iv**
ABSTRACT ..... **v**
LIST OF TABLES ..... **x**
LIST OF FIGURES ..... **xii**
ACRONYMS AND ABBREVIATIONS ..... **xiii**
CHAPTER ONE: INTRODUCTION **1**
1.1 Background of the Study 1
1.2 Statement of the Problem 4
1.3 Justification of the Study 5
1.4 Objectives 6
1.4.1 Main Objective 6
1.4.2 Specific Objectives of the Study 6
1.5 Research Questions 6
1.6 Significance of the Study 7
1.7 Limitations of the Study 7
1.8 Contributions of the Thesis 8
1.9 Organization of the Thesis 10
CHAPTER TWO: LITERATURE REVIEW **11**
2.1 Introduction 11
2.2 Radioactivity in Nature 12
2.2.1 Cosmic Origin 12
2.2.2 Terrestrial Origin 13
2.2.3 Anthropogenic Radiation Sources 14
2.3 The Fundamental Law of Radioactivity 15
2.4 Secular Equilibrium 16
2.5 Types of Decay 18
2.6 Gamma rays' interactions with materials 21
2.6.1 Photoelectric Effect 22
2.6.2 Compton Effect 22
2.6.3 Pair Production 25
2.7 Relative Dominance of Photon Interactions 26
2.8 Effects of Ionizing Radiation on Biological Matter 27
2.8.1 Deterministic Effects 28
2.8.2 Stochastic Effects 28
2.9 Global Averages and Regulatory Limits for Radiological Parameters 29
2.10 Principal Mechanism of a High Purity Germanium (HPGe) Detector 30
2.11 Heavy Metals 34
2.12 Water Quality 47
2.13 Permissible Limits of Heavy Metals in Drinking Water 48
2.14 Principal Mechanism of Microwave Plasma Atomic Emission Spectroscopy (MP-AES) 49
2.15 Related Studies on Radioactivity and Heavy Metal Concentrations 51
2.16 Study Area 54
2.17 Common Fish Species Found in Lake Turkana 57
2.17.1 Nile Perch *(Lates niloticus)* 57

2.17.2 Nile Tilapia (*Oreochromis niloticus*) 58
2.17.3 African Catfish *(Clarias gariepinus)* 60
2.18 Farming along the Turkwel River 61
2.19 Summary 64
CHAPTER THREE: MATERIALS AND METHODS 66
3.1 Introduction 66
3.2 Collection of Samples 66
3.2.1 Sediment Samples 67
3.2.2 Fish Samples 69
3.2.3 Crop Samples 70
3.2.4 Water Samples 71
3.3 Preparation of Samples for Radionuclide Analysis 72
3.3.1 Sediment Samples 72
3.3.2 Fish Samples 73
3.3.3 Cassava and Sorghum Samples 74
3.4 Preparation of Samples for Elemental Analysis 74
3.4.1 Digestion of Water Samples 74
3.4.2 Digestion of Fish Samples 75
3.5 Analysis of NORM in Samples 76
3.5.1 High Purity Germanium (HPGe) γ – Ray Spectrometer 76
3.5.2 Standard Samples 77
3.5.3 Energy and Efficiency Calibration of the HPGe Detector 77
3.5.4 Spectroscopic Analysis of Radionuclides in Sample Matrices 79
3.6 Activity Concentrations 80
3.7 Radiation Hazards Associated with NORM in Sediments, Fish and Crop Samples 81
3.7.1 Equivalent Radium Activity (Ra_{eq}) 81
3.7.2 Absorbed Dose Rate (ADR) 82
3.7.3 Annual Effective Dose (AED) 83
3.7.4 Excess Lifetime Cancer Risk (ELCR) 84
3.7.5 External Hazard Index and Internal Hazard Index 85
3.7.6 Gamma Index (I_γ) 86
3.8 Analysis of Heavy Metals in Samples 87
3.8.1 Heavy Metal Concentration Analysis in Water and Fish 87
3.8.2 Operating Condition for MP-AES 88
3.9 Water Quality Assessment 89
3.10 Health Risk Assessment of Fish Samples 90
3.11 Bioaccumulation Factor (BAF) 92
3.12 Summary 92
CHAPTER FOUR: RESULTS AND DISCUSSION 94
4.1 Introduction 94
4.2 Activity Concentration of ^{238}U, ^{232}Th and ^{40}K in Sediment Samples 94
4.2.1 Descriptive Statistics for Activity Concentrations in Sediment Samples 99
4.2.2 Pearson Correlation Analysis for Sediment Samples 100
4.2.3 Analysis of Variance for sediment samples 101
4.3 Activity Concentration of ^{232}Th, ^{238}U and ^{40}K in Sorghum 102
4.4 Activity Concentration of ^{232}Th, ^{238}U and ^{40}K in Cassava 106
4.5 Activity Concentration of ^{238}U, ^{232}Th and ^{40}K in Fish Samples 108
4.6 Hazard indicators in sediment samples 113

4.6.1 External Hazard Index (H_{ex}) and Internal Hazard Index (H_{in}) in sediment samples 114
4.6.2 Absorbed Dose Rate (ADR) in Sediment Samples 115
4.6.3 Annual Effective Dose Equivalent (AED_{total}) in Sediment Samples 115
4.6.4 Excess Lifetime Cancer Risk (ELCR) in Sediment Samples 116
4.6.5 Gamma Index (Iγ) of Sediment Samples 116
4.6.6 Average Hazard Indicators in Sediment Samples across Sampling Locations 116
4.7 Annual Effective Dose Due to Ingestion of Crop Samples 118
4.8 Heavy Metals Concentration in the Water and Fish Samples 119
4.8.1 Metals Concentration in Surface Water of Lake Turkana 119
4.8.2 Metal Concentration in Surface Water of Turkwel River 125
4.8.3 Comparison of Heavy Metal Concentrations in Water from Lake Turkana and Turkwel River (Present Work) to Other Regions 127
4.9 Water Quality Indices 130
4.9.1 Metal Contamination Index (MCI) 130
4.9.2 Heavy Metal Evaluation Index (HEI) 131
4.10 Heavy Metal Concentrations in Fish Samples 131
4.11 Health Risk Assessment in Fish Samples 139
4.11.1 Estimated Daily Intake (EDI) of Metals from Fish Consumption 139
4.11.2 Target Hazard Quotient (THQ) and Total Hazard Index (HI) 140
4.12 Bioaccumulation Factor in Fish 140
4.13. Correlation between Activity and Heavy Metal Concentrations in Fish Samples 142
4.13.1 Correlation between Heavy Metals Concentration and Activity Concentration of ^{232}Th 144
4.13.2 Correlation between Heavy Metals Concentration and Activity Concentration of ^{238}U 144
4.13.3 Correlation between Heavy Metals Concentration and Activity Concentration of ^{40}K 145
4.14 Summary 145
CHAPTER FIVE: CONCLUSION AND RECOMMENDATIONS 147
5.1 Conclusion 147
5.2 Recommendations 149
5.2.1 Policy Related Recommendations 149
5.2.2 Recommendations for Future Studies 150
REFERENCES 151
APPENDICES 167

LIST OF TABLES

Table 3.1: Sediment sampling plan 68
Table 3.2: Fresh Fish sample collection plan. 69
Table 3.3: Sorghum and cassava sample ID and mass in grams. 70
Table 3.4: Water sample details 71
Table 3.5: Quantification Parameters for Radionuclide Analysis of the HPGe equipment 81
Table 3.6: Operating Condition for MP-AES 89
Table 4.1: Activity concentrations of ^{232}Th, ^{238}U and ^{40}K in sediment samples. 95
Table 4.2: Range and average of ^{232}Th, ^{238}U ^{40}K and Ra_{eq} activity concentrations of sediments. 96
Table 4.3: The activity concentration of ^{238}U, ^{232}Th, ^{40}K and Ra_{eq} in sediment samples in comparison with other regions. 98
Table 4.4: Descriptive statistics of sediment samples of Lake Turkana 100
Table 4.5: Pearson correlation matrix. 101
Table 4.6: ANOVA between groups for different variables in sediment samples 102
Table 4.7: Activity concentrations of the three primordial radionuclides and the resulting effective dose from Sorghum samples 103
Table 4.8: Activity concentrations of the three primordial radionuclides and effective dose in cassava samples. 107
Table 4.9: Activity concentrations of ^{232}Th, ^{238}U, ^{40}K and Ra_{eq} in the fish samples. 108
Table 4.10: Average radionuclide concentration and radiation Ra_{eq} in fish samples of this study and the values of similar studies from other regions. 112
Table 4.11: Hazard indicators for sediment samples. 114
Table 4.12: Hazard indicators of activity of sediment samples across various locations 117
Table 4.13: Calculated annual effective doses via ingestion. 119
Table 4.14: Concentrations of heavy metals in water samples across various sampling locations (mg/l) 121
Table 4.15: Average concentrations of heavy metals in surface water across various sampling locations along shores of L. Turkana 123
Table 4.16: Average concentrations of heavy metals in surface water of Turkwel River 126
Table 4.17: Comparison of heavy metals concentration with reported values and WHO recommended limits for drinking water 129
Table 4.18: MCI and HEI in Lake Turkana and River Turkwel water 130

Table 4.19: Heavy Metals (mg/kg) in Fish Muscle Tissue Samples from Kalokol and Long'ech Markets 132
Table 4.20: Average heavy metal concentrations (mg/kg) in fish samples from the two markets. 135
Table 4.21: Comparison of Heavy Metal Concentrations in Lake Turkana Fish, with values from other studies, and WHO Guidelines.....137
Table 4.22: Non-carcinogenic health risk assessment for metals in fish samples. ..139
Table 4.23: Bioaccumulation factors of selected heavy metals in fish samples 141
Table 4.24: Correlations between heavy metals and activity concentrations of primordial radionuclides in fish samples 143

LIST OF FIGURES

Figure 1.1: Global yearly human encounters with radiation from various origins. 2
Figure 2.1: Diagrammatic representation of secular equilibrium showing activities of long-lived parent and short-lived daughter. 17
Figure 2.2: The interaction pathway of Compton scattering.....24
Figure 2.3: Visual representation of pair production 26
Figure 2.4: Relative dominance of photon interactions 27
Figure 2.5: A visual representation of germanium detector inside a liquid nitrogen dewar. 32
Figure 2.6: FWHM position and resolution types.....33
Figure 2.7: A cartographic representation of the Lake Turkana basin displaying the rivers that drain into the lake, settlements and other geological features in the basin. 56
Figure 3.1: Block diagram of a basic gamma spectrometry system 77
Figure 3.2: Efficiency calibration curve.....79
Figure 4.1: (a): Average activity concentration of ^{232}Th in the sediment samples; (b) Percentage concentration levels of primordial radionuclides in sediments for the study area.....98
Figure 4.2: Average percentage activity concentration of primordial radionuclides in sorghum. 104
Figure 4.3: Correlation of ^{238}U and ^{232}Th Activity Concentrations 105
Figure 4.4: Correlation of ^{238}U and ^{232}K activity concentrations.....106
Figure 4.5: Correlation of ^{40}K and ^{232}Th activity concentrations 106
Figure 4.6: (a) Average percentage activity concentration of primordial radionuclides in fish; (b) Activity concentration levels of radionuclides in the fish. 110
Figure 4.7: (a) Frequency distribution of ^{232}Th; (b) Frequency distribution of ^{238}U; and (c) Frequency distribution of ^{40}K. 113
Figure 4.8: Heavy metal concentrations in; (a) Lake Turkana water and (b) River Turkwel. 127

ACRONYMS AND ABBREVIATIONS

ADR	Absorbed Dose Rate
AED	Annual Effective Dose
ATSDR	Agency for Toxic Substances and Disease Registry
BAF	Bioaccumulation Factor
EDI	Estimated Daily Intake
ELCR	Excess Lifetime Cancer Risk
FAO	Food and Agriculture Organization
HEI	Heavy metal evaluation index
HNO_3	Nitric Acid
HPGe	Hyper pure Germanium
H_{ex}	External hazard index
H_{in}	Internal hazard index
IAEA	International Atomic Energy Agency
ICRP	International Commission on Radiological Protection
MCA	Multi - channel analyzer
MCI	Metal contamination index
MDA	Minimum detectable activity
MP-AES	Microwave plasma atomic emission Spectroscopy
NaI(Tl)	Thallium activated sodium iodide
NORM	Naturally occurring radionuclide material
Ra_{eq}	Radium equivalent
Ppm	Parts per million
THQ	Target Hazard Quotient
USEPA	United States Environmental Protection Agency
UNSCEAR	United Nations Scientific Committee on Effect of Atomic Radiations.
WHO	World Health Organization
^{232}Th	Thorium 232
^{238}U	Uranium 238
^{40}K	Potassium 40

CHAPTER ONE
INTRODUCTION

This chapter provides an essential overview of the research presented in this thesis. It begins by establishing the background of the study, outlining the broader context and existing knowledge relevant to the investigation. Following this, the statement of the problem is articulated, clearly identifying the specific gap in the literature or the unresolved issue that this research aims to address. Subsequently, the justification of the study is presented, providing a precise framework for the inquiry. The objectives of the study are then detailed, outlining the specific goals this research seeks to achieve. Finally, this chapter concludes with a brief overview of the limitations of the research.

1.1 Background of the Study

There is a growing global concern regarding environmental pollution, particularly that caused by radiation. A comprehensive understanding of the extent of human exposure to radiation from both natural and anthropogenic low-level sources is crucial for effective risk assessment and management (UNSCEAR, 2011). Environmental radiation sources are broadly classified into two main categories: natural sources and anthropogenic sources. Natural sources include cosmic radiation from space and terrestrial radiation from naturally occurring radioactive materials in Earth's crust, soil, water, and air. Geological features like granite and phosphate rocks influence natural radiation levels. Anthropogenic sources are human-made. These include medical applications (X-rays, CT scans), nuclear power generation, historical nuclear weapon tests, and industrial uses. Natural sources contribute the vast majority of the global average radiation dose, while medical exposures are the leading anthropogenic contributor (UNSCEAR, 2011).

Radiation exposure can be categorized into two main types: internal and external. Internal exposure happens when a radiation source is inside the body. This typically occurs by inhaling airborne radioactive materials or ingesting them through contaminated food or water. Once inside, these radioactive substances emit rays and particles, irradiating internal body parts. The magnitude of the dose received is

governed by several factors: activity of the radioactive material taken in, its location within the body, how long it remains there, and the specific radiation it releases. For example, a significant portion of the internal dose to the respiratory tract comes from radon and its decay products, which are part of the Uranium-238 decay chain (Friedlander *et al.,* 1981).

Conversely, external exposure occurs when the body, either entirely or partially, is subjected to penetrating radiation from an exogenous origin. Potential external sources of radiation include equipment like X-ray machines, stored radioactive materials, or naturally occurring radionuclides found in the earth's crust. For instance, igneous rocks such as granite are known to be particularly rich in Thorium-232 and Uranium-238. As these naturally present radioactive elements decay, they release gamma rays, contributing to external radiation exposure.

Figure 1.1 illustrates the annual dose to humans received from various sources of radiations averaged over the population of world (UNSCEAR, 2011).

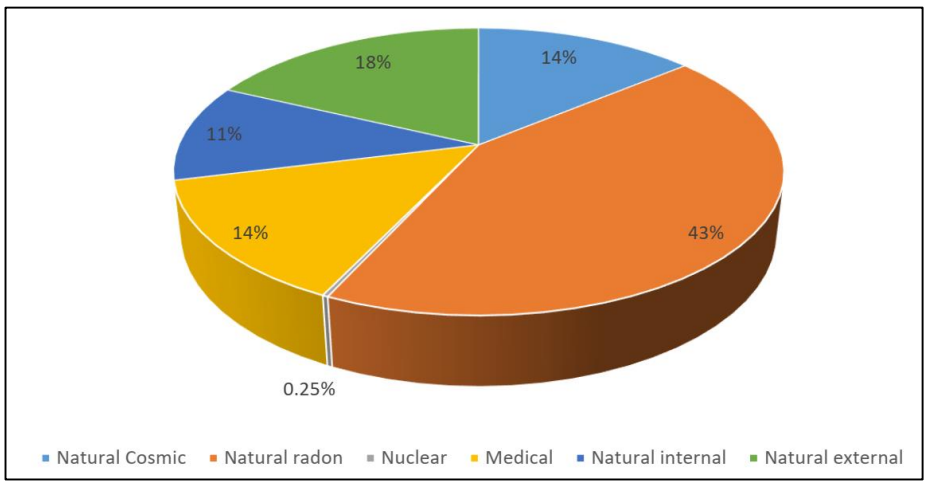


Figure 1.1: Global yearly human encounters with radiation from various origins (Vennart, 1991).

From Figure 1.1, it is noted that more than 85% of the total amount originates from naturally occurring sources, with roughly 50% of it arising from the byproducts of radon decay within residential settings. Medical exposure to patients makes up 14%

of the entire figure, while all remaining artificial sources, including fallout, consumer items, workplace exposure and releases from the nuclear industry contribute about 0.25 % of the total. While natural sources contribute the vast majority of our annual radiation exposure, the health effects are generally minimal at typical background levels. The human body has mechanisms to repair DNA damage caused by low doses of radiation. However, prolonged exposure to elevated natural radiation can still contribute to an increased long-term risk of certain health issues, most notably lung cancer. Children and fetuses are generally more susceptible to the effects of radiation due to their rapidly dividing cells and longer lifespans.

In addition to the radioactive materials found in nature that contribute to environmental radiation, the Earth's crust has also contained heavy metals such as chromium (Cr), manganese (Mn), arsenic (As), selenium (Se), and silver (Ag) since its formation. These elements are primordial, meaning they were incorporated into the planet's structure during its formation and differentiation billions of years ago (Faure, 1986). Unlike radioactive elements that undergo decay, heavy metals are stable elements that persist indefinitely in the environment.

The concern regarding heavy metals stems from their potential toxicity and bioaccumulation in living organisms. While many heavy metals are essential micronutrients at low concentrations, they can become toxic at higher levels, leading to adverse health effects in humans and ecological damage in ecosystems (Violante *et al.,* 2010). Their long residence times in environmental compartments, coupled with their ability to be mobilized by natural processes like weathering and anthropogenic activities such as mining and industrial discharge, make them persistent pollutants (Manahan, 2017).

The continuous interaction between radiation sources and heavy metals in the natural environment presents a complex challenge for environmental management. For instance, the presence of radionuclides can lead to enhanced mobilization of certain heavy metals through radiolysis or by changing reduction-oxidation (redox) conditions in contaminated sites (Q. Li *et al.,* 2022). Conversely, some heavy metals can influence the biogeochemical cycling of radionuclides. This interconnectedness underscores the critical importance of comprehensive monitoring and integrated

management strategies for both radiation exposure and heavy metal contamination to preserve the quality of the environment and the health of the public. The study seeks to quantify the radioactivity levels of uranium-238 (^{238}U), thorium-232 (^{232}Th), and potassium-40 (^{40}K) in selected geological and biological matrices. Furthermore, the study investigated the concentration levels of various heavy metals in water and fish samples (Q. Li *et al.,* 2022).

Various studies have measured NORM concentrations across Kenya, for instance a study at the Kenyan coast particularly at Mombasa showed an average annual effective dose rate that was below 1mSv (Hashim et al., 2004). Studies done to measure radionuclide concentrations in sand samples from Kuja and Migori Rivers showed radiological hazard indices that were near or above permissible levels (Okelo, 2015), A study done at Mrima Hills soil depicted the area to be a High Background Radiation Area (HBRA) (Kebwaro et al., 2011). Others were at Lake Nakuru (Langat et al., 2014), Lake Victoria. (Okelo, 2015), and Kargi (Aguko et al., 2020). NORM studies have also been reported globally including river sediment from Nigeria's Delta State (Iwetan et al., 2015), Port Harcourt in Nigeria (Qureshi et al., 2014), Nile river in Egypt (El-Taher & Abbady, 2012), Bay of Bengal Chattogram, Bangladesh (Biswas et al., 2021) and Jeddah-Saudi Arabia (Safia, 2016). Given the unique volcanic geology of the Turkana Basin and the increasing anthropogenic pressure from oil exploration and localized mining, the absence of baseline radiometric data represents a significant gap in Kenya's environmental health map.

1.2 Statement of the Problem

The Turkana are a pastoral community that live in the Western North Rift region of Kenya. Livestock which is their major source of livelihood has been affected by drought leading to several attacks by neighboring pastoral communities. This has led the Turkana to start crop farming along river basins and fishing as a means of ensuring their food security. Their interaction with water bodies in the region such as the Turkwel and Kerio Rivers as well as Lake Turkana has therefore increased.

The geological setting of Lake Turkana and increased interaction of residents of Turkana County with the Lake pose a radiological risk as well as health problems caused by heavy metals to the residents. River Kerio passes through Kerio Valley is

characterized by the presence of uranium, which is associated with fluorite mineralization (Nderitu *et al.,* 2001) and deposits its water into Lake Turkana. The other two rivers the Omo and Turkwel have several dams constructed along their courses and are utilized for irrigation.

The shift in the Turkana community's livelihood from pure pastoralism to agropastoralism and fishing driven by drought and regional conflict has significantly increased their reliance on Lake Turkana and the Turkwel River for food and water. However, this dietary shift exposes the population to potential geological and environmental hazards. Because Lake Turkana is an endorheic (closed) basin, it acts as a permanent sink for pollutants, including naturally occurring radioactive materials (NORMs) transported by the rivers from uranium-rich zones, and heavy metals concentrated by evaporation and upstream damming. Consequently, this study was necessary to quantify the radiological and heavy metal toxicity risks now present in the community's primary sustenance: water, fish, and irrigated crops (sorghum and cassava) grown in these sedimentary basins.

1.3 Justification of the Study

The utilization of surface water sources potentially containing dissolved radionuclides such as ^{232}Th, ^{238}U and ^{40}K. The radionuclides and heavy metals such lead, arsenic, cadmium, chromium, copper, zinc, barium and nickel constitute a significant health concern, including the potential to cause cancer in humans. Therefore, it is imperative to reduce exposure to natural radionuclides and heavy metals to levels deemed safe for human health. The outcomes of this research can play an essential role in increasing public awareness regarding the radiological safety of naturally occurring radioactive materials and the presence of the heavy metals Zn, Pb, As, Cu, Ni, Cr, Ba and Cd within the specific region under study. Furthermore, the research findings can serve as invaluable foundational data for future studies, facilitating comparisons and enabling a better understanding of evolving radiological and environmental landscape. This knowledge can facilitate the creation of more robust strategies to mitigate the potential hazards that natural radionuclides and heavy metals pose to both human health and environmental quality.

1.4 Objectives

1.4.1 Main Objective

The general objective of this research was to determine concentration levels of terrestrial radionuclides (^{232}Th, ^{238}U, ^{40}K) and selected heavy metals in sediment, water, fish and food crops from the Lake Turkana region

1.4.2 Specific Objectives of the Study

The study aimed to accomplish these specific goals;

i. To determine activity concentration levels of the primordial radionuclides 238U, 232Th and 40K in sediment, crop and fish samples from selected locations in Lake Turkana and its environs.
ii. To determine radiation exposure hazard levels resulting from the presence of naturally occurring radionuclides.
iii. To determine the concentrations levels of selected heavy metals in water from selected sites of Lake Turkana and River Turkwel, and fish samples from Kalokol and Long'ech fish markets.
iv. To establish a correlation between the concentrations of heavy metals and activity levels of primordial radionuclides in fish samples.

1.5 Research Questions

i. What are the activity concentration levels of primordial radionuclides (^{238}U, ^{232}Th, and ^{40}K) in sediment, crop, and fish samples from selected locations in Lake Turkana and its environs?
ii. To what extent do naturally occurring radionuclides contribute to radiation exposure hazard levels in the Lake Turkana ecosystem?
iii. What are the concentration levels of selected heavy metals in water and fish samples from sites within Lake Turkana and its environs?
iv. Is there a significant correlation between the concentrations of heavy metals and the activity levels of primordial radionuclides in the Lake Turkana ecosystem?

1.6 Significance of the Study

Understanding the concentration of radionuclides and heavy metals in water, sediments, crops, and fish is crucial due to the significant risks these contaminants pose to both human health and the environment. Regular monitoring allows early identification of potential threats, enabling the implementation of preventive measures before crises emerge. This proactive approach helps mitigate their impact on human populations and natural habitats. Furthermore, consistent monitoring ensures compliance with stringent national regulations on permissible contaminant levels in water and food, helping industries and local authorities avoid penalties and uphold environmental standards. These contaminants can severely disrupt aquatic ecosystems by degrading habitats and directly harming aquatic organisms. Monitoring tracks these changes, providing vital data to inform conservation strategies and policy decisions aimed at preserving biodiversity. Contaminated fish and crops also pose a direct threat to public health as these harmful substances can enter the human food chain. Regular monitoring acts as a critical checkpoint, ensuring food safety standards are met and protecting consumers from ingestion risks.

Beyond safeguarding health and ecosystems, sharing environmental monitoring results raises public awareness about contamination issues. This empowers communities to understand risks and encourages active participation in pollution prevention. Finally, monitoring provides invaluable data for scientific research, fostering a deeper understanding of how these contaminants behave in different environments, their long-term effects, and the most effective remediation strategies. Ultimately, comprehensive environmental monitoring is essential for predicting, preventing, and managing contamination to ensure a healthier future.

1.7 Limitations of the Study

This research encountered several specific limitations that influenced the scope, precision, and validity of its results, primarily due to the geographical constraints of the expansive study area and the specific chemical parameters analyzed. The study's geographical scope was restricted to the Western shores of Lake Turkana, specifically the centers of Kerio, Eliye, Kalokol, Long'ech, Kataboi, Nachukui, Nareng'ewoi, and Nariokotome alongside the Turkwel River at Lodwar and the agricultural zones of Kang'atosa, meaning the findings may not fully represent the radiological or elemental

profiles of the Eastern or Northern shores. In terms of chemical breadth, the investigation was confined to the terrestrial radionuclides ^{238}U, ^{232}Th, and ^{40}K, and a select suite of heavy metals including As, Ni, Ba, Cu, Zn, Pb, Cd, and Cr. Furthermore, the reliance on a single sampling period failed to capture the spatial and temporal heterogeneity inherent in an endorheic basin, where seasonal fluctuations in water inflow from the Turkwel and Kerio rivers and high evaporation rates significantly impact the concentration and bioaccumulation of these elements in water, sediment, and biological matrices like fish, sorghum, and cassava. Ultimately, these factors, coupled with financial and logistical constraints, define the study as a localized baseline rather than a longitudinal or basin-wide assessment.

1.8 Contributions of the Thesis

The thesis represent a multifaceted advancement in the fields of environmental physics, radioecology, and public health, specifically within the unique context of the Lake Turkana and Turkwel River basins. By integrating the study of Naturally Occurring Radioactive Materials (NORM) with heavy metal toxicity, the research provides a holistic evaluation of environmental stressors that are often studied in isolation. One of the primary scientific contributions is the establishment of a comprehensive radiological baseline for a geographically significant but understudied region. The thesis meticulously quantifies the activity concentrations of $2^{38}U$, ^{232}Th, and ^{40}K across various matrices, including sediments, water, fish (Nile Perch, Nile Tilapia, and African Catfish), and crops like cassava and sorghum. This data is vital for distinguishing between natural background radiation and potential anthropogenic enhancements, providing a benchmark against which all future industrial, agricultural, or mining impacts in Northern Kenya can be measured.

Technologically, the thesis contributes to the application of high-precision analytical methodologies in environmental monitoring. By utilizing High Purity Germanium (HPGe) Gamma-ray Spectrometry and Microwave Plasma Atomic Emission Spectroscopy (MP-AES), the study demonstrates a rigorous approach to detection limits and energy resolution. The detailed exploration of gamma-ray interactions—such as the Photoelectric Effect, Compton Effect, and Pair Production within the context of HPGe detectors offers a localized case study on the efficacy of these instruments in complex environmental matrices. Furthermore, the research advances

the understanding of Secular Equilibrium and radionuclide decay chains in tropical lacustrine environments, contributing theoretical depth to the empirical findings. The systematic preparation and digestion protocols outlined for fish and crop samples also provide a standardized methodological framework that can be replicated by other researchers working in similar arid or semi-arid aquatic ecosystems.

From a socio-economic and public health perspective, the thesis makes a critical contribution by translating raw physical data into human-centric risk assessments. The calculation of the Excess Lifetime Cancer Risk (ELCR) and the Annual Effective Dose (AED) directly informs the community and policymakers about the long-term biological implications of residing near and consuming resources from the Turkwel River and Lake Turkana. By identifying the Bioaccumulation Factor (BAF) for heavy metals in specific fish species, the research highlights which aquatic life poses the highest risk to the local food chain. This is particularly significant for the Turkana people, whose diet and economy are linked to these water bodies. The study's use of the Target Hazard Quotient (THQ) and Total Hazard Index (HI) provides a clear, quantitative signal regarding the safety of fish consumption, effectively bridging the gap between nuclear physics and nutritional safety.

Finally, the thesis offers significant policy-related contributions. By comparing local concentrations of heavy metals and radionuclides against global averages and regulatory limits (such as those set by UNSCEAR and the WHO), the work provides a scientific mandate for environmental protection strategies. It identifies specific hotspots of activity and contamination, allowing for targeted interventions rather than broad, inefficient policies. The correlation analysis between radionuclides and heavy metals further contributes to our understanding of geochemical behavior, suggesting whether these pollutants share common transport mechanisms or origins. Ultimately, this research empowers local authorities with the evidence required to implement water quality standards and agricultural guidelines, ensuring that the development of the Lake Turkana region does not come at the cost of the ecological or physiological health of its inhabitants.

1.9 Organization of the Thesis

This thesis follows a systematic and logical progression, moving from foundational theoretical principles to site-specific empirical analysis and, finally, to actionable public health conclusions. The structure is divided into five cohesive chapters, beginning with Chapter One, which establishes the research framework by outlining the background, problem statement, and the specific objectives concerning the radiological and elemental assessment of the Lake Turkana and Turkwel River ecosystems. This introductory phase justifies the study by highlighting the intersection of environmental safety and human subsistence.

Chapter Two provides an extensive literature review that bridges nuclear physics with environmental chemistry. It explores the origins of radioactivity—cosmic, terrestrial, and anthropogenic—and details the mechanics of gamma-ray interactions, such as the Photoelectric and Compton effects. This chapter also establishes the toxicological context for heavy metals and the operational physics of the High Purity Germanium (HPGe) and Microwave Plasma Atomic Emission Spectroscopy (MP-AES) systems used for detection. Chapter Three details the methodology, documenting the rigorous protocols for collecting and preparing diverse samples, including sediments, water, fish (Nile Perch, Tilapia, and Catfish), and crops like cassava and sorghum. It also defines the mathematical models used to calculate hazard indicators like the Excess Lifetime Cancer Risk (ELCR) and Bioaccumulation Factors (BAF).

The core of the research is contained in Chapter Four, which presents the results and discussions. This section utilizes statistical tools including Pearson correlation and ANOVA to interpret activity concentrations and heavy metal levels, comparing them against global regulatory standards. The thesis concludes with Chapter Five, which synthesizes the findings into a summary of environmental health risks and offers critical policy recommendations for local authorities.

CHAPTER TWO
LITERATURE REVIEW

2.1 Introduction

This chapter provides a comprehensive examination of the theoretical and empirical literature relevant to the assessment of radioactivity and heavy metal concentrations in aquatic environments. The review establishes a foundational understanding of the physical and chemical principles governing the behavior of contaminants in the ecosystem. It begins by exploring the origins and fundamental laws of radioactivity in Section 2.2, Section 2.3, and Section 2.4, followed by a detailed analysis of radioactive decay types and the interaction of gamma rays with matter in Section 2.5, Section 2.6, and Section 2.7. These physical interactions are critical for understanding how radiation affects biological matter, a topic further explored through the deterministic and stochastic effects discussed in Section 2.8.

To provide a framework for safety and environmental health, Section 2.9 evaluates global averages and regulatory limits for radiological parameters, while Section 2.10 details the technical mechanisms of High Purity Germanium (HPGe) detectors used for sample analysis. The review then shifts toward the chemical aspects of the study, examining the nature and toxicity of heavy metals in Section 2.11 and Section 2.12. This is complemented by an overview of water quality standards and permissible limits in drinking water in Section 2.13 and Section 2.14, alongside the operational principles of Microwave Plasma Atomic Emission Spectroscopy (MP-AES) in Section 2.15.

The final portion of the chapter contextualizes these scientific principles within the specific scope of this research. Section 2.16 synthesizes related studies on radioactivity and heavy metal concentrations, highlighting gaps in current knowledge. Finally, Section 2.17, Section 2.18, and Section 2.19 provide vital geographical and ecological context, describing the study area, the common fish species of Lake Turkana—such as Nile Perch, Nile Tilapia, and African Catfish and the impact of agricultural activities along the Turkwel River.

2.2 Radioactivity in Nature

The environment is naturally filled with ionizing radiation, including cosmic rays from space, radioactivity from the earth itself and natural radiation in food, beverages and the air we breathe. Consequently, all individuals are exposed to varying degrees of natural radiation which is the primary source of ionizing radiation exposure making up around 80% of the total exposure to most people. On a global scale, the estimated average effective dose received annually resulting from exposure to natural sources of radiation is 2.4 milliseverts (mSv) (UNSCEAR, 2000). This radiation primarily emanates from two main sources: cosmic rays and naturally occurring radioactive materials (NORM) which are mainly primordial radionuclides within the earth's crust. Notable contributors to NORM are potassium-40 (^{40}K) and the radioactive decay series progenies of uranium-238 (^{238}U) and thorium-232 (^{232}Th) along with radon gas found in air and water sources (Vennart, 1991).

To safeguard against the potential dangers of being exposed to naturally occurring ionizing radiation, the international commission on radiological protection established recommended dose limits. These recommendations are typically enforced by national regulatory authorities, aiming to control and manage human exposure to radiation from natural sources effectively (ICRP, 1991)..

The levels of NORM in terrestrial environments are subject to variations of factors such as the geological composition of rocks and soil, the processes that concentrate these radioactive materials and the mechanisms that immobilize them within geological formations.

2.2.1 Cosmic Origin

Cosmic rays primarily consist of high-energy protons whose origins are uncertain, and reach the atmosphere in consistent amounts. Because these protons are charged particles, they are influenced by the earth's magnetic field, making most of them to enter the atmosphere near the poles rather than the equator. The radiation dose rate is inversely proportional to the distance from the poles, as a result, it increases with higher latitudes. As cosmic rays pass through the atmosphere, they trigger complex reactions and are gradually absorbed, consequently, the radiation dose rate lessens with decreasing altitude. Cosmic radiation is made up of a blend of different radiation

forms, including protons, alpha particles, electrons, and other energetic particles. (Vennart, 1991). At ground level, cosmic radiation mainly consists of muons, neutrons, electrons, positrons and photons, with muons and electrons being major contributors to the radiation dose. According to the United Nations Scientific Committee on the Effects of Atomic Radiation (UNSCEAR), the average yearly effective dose from cosmic rays at ground level is estimated to be around 0.4 mSv. Additionally, typical air travel adds an extra annual dose averaging 0.01mSv for specific populations, especially frequent flyers, but this doesn't affect the global average of 0.4mSv (UNSCEAR, 2010). Radionuclides tritium-3 (^{3}H), carbon-14 (^{14}C), chromium-51 (^{51}Cr), manganese-53, 54 (^{53,54} Mn), beryllium-7 (^{7}Be), sodium-22 (^{22}Na), vanadium-48 (^{48}V), and nickel-59 (^{59}Ni) are of cosmic origin. Cosmic radionuclides move into the terrestrial environment and water bodies via wind and rainfall (UNSCEAR., 2011).

2.2.2 Terrestrial Origin

These radionuclides can be found naturally in every material that makes up the Earth's crust. They contribute significantly to crust formation and temperature maintenance due to natural activity deep within the earth. This energy is predominantly a product of radioactive decay from isotopes including uranium, thorium, and potassium. Uranium-235 (^{235}U) is distributed in rocks, soils and water generating a series of radionuclides, including radon-222 (^{222}Ra). Similarly, ^{232}Th leads to another series of radionuclides, including radon-220 (^{220}Rn) often referred to as thoron. Potassium is more abundant than uranium and thorium, constituting 2.4% of the earth's crust by weight, but ^{40}K, a radionuclide makes up only 120 parts per million of stable potassium. Of these radionuclides, ^{40}K is the most common in water bodies (Harb *et al.,* 2014).

To determine the water cycle radiation dose, radium isotopes and associated progeny are of great significance. ^{226}Ra, is usually in equilibrium with its parent ^{238}U in most rock formations unless the rocks are affected by weathering, hydrological or biological processes. The same applies to ^{228}Ra and ^{224}Ra from the ^{232}Th series. The concentration of radium in water varies between ground and surface water with surface water generally having a lower concentration. This variation is caused by varying geology of the rock formations and disjointed aquifers (Al-Hayani *et al.,* 2021).

According to the UNSCEAR 2000 Report to the United Nations General Assembly, the yearly effective radiation exposure from natural sources varies by type. The typical dose for gamma radiation is between 0.3−0.6 mSv/y, with a global average of 0.5 mSv/y. Cosmic radiation has a typical range of 0.3−1.0 mSv/y, averaging 0.4 mSv/y globally. The dose from internal radiation typically falls between 0.2−0.8 mSv/y, with a global average of 0.3 mSv/y. Lastly, radon inhalation has the widest range, from 0.2−10 mSv/y, and a global average of 1.2 mSv/y. The total natural background radiation is estimated to range from 1.0−10 mSv/y, with a worldwide average of 2.4 mSv/y. Typical annual exposure to natural gamma rays results in an average effective dose of approximately 0.5 mSv. Factors such as local geology and the materials used in residential construction can influence the resulting doses. Consequently, it is advisable to refrain from constructing homes in places or using materials that exhibit exceptionally elevated radiation levels (UNSCEAR, 2000).

Radon gas represents a notable contributor to natural radiation exposure. The decay byproducts of ^{222}Rn and ^{220}Rn consist of radioactive substances with short half-lives. These substances bind to tiny airborne particles, get inhaled and subsequently emit alpha particles that irradiate lung tissues, elevating the likelihood of developing lung cancer. As radon is released into the air from the earth's surface, it becomes dispersed, leading to lower outdoor concentration compared to indoor settings. The average person is exposed to an effective dose of 1.2 mSv annually from radon decay products globally. Additional radioactive elements from the thorium and uranium decay chains, plus the singly existing potassium-40 can be found in the atmosphere, food and water, leading to internal radiation exposure within the body. It is estimated that the average effective radiation dose originating from these internal sources amounts to approximately 0.3 mSv annually, with ^{40}K accounting for roughly half of this exposure (UNSCEAR, 2000).

2.2.3 Anthropogenic Radiation Sources

Human activities, practices and events involving radiation sources that release radioactive materials to the environment constitute anthropogenic sources of radiation. The main human activities that have significantly contributed to ionizing radiation exposure include testing of nuclear weapons and generation of electrical energy by nuclear power reactors. While nuclear power plants are designed with stringent safety

measures and containment systems, routine operations can lead to controlled, low-level emission of radioactive isotopes into the environment. However, the most severe concerns arise from accidents at nuclear power generation plants, such as Chernobyl in 1986 and Fukushima Daiichi in 2011.

These catastrophic events resulted in uncontrolled and extensive releases of radioactive isotopes, causing widespread environmental contamination, requiring massive evacuations, and necessitating long-term remediation efforts. The prolonged persistence of certain radioisotopes released during such accidents pose radiological harm to human health and ecosystems of affected areas (Anzai et al., 2012). In the medical field, diagnostic procedures like X-rays, CT scans, and therapeutic applications such as radiotherapy involve the deliberate use of radioactive materials. While offering immense benefits to healthcare, the production, handling, and eventual disposal of radionuclide wastes from medical facilities pose a continuous radiological contamination risk to the environment. Similarly, various industries employ radioactive sources for diverse applications such as gauging, sterilization of equipment, and non-destructive testing such as industrial radiography using Cobalt-60. These industrial sources require careful management to prevent accidental releases or improper handling that could lead to environmental contamination (UNSCEAR, 2000).

2.3 The Fundamental Law of Radioactivity

The phenomenon of radioactive decay is a fundamental process describing how unstable atomic nuclei spontaneously transform into more stable forms by emitting various types of radiation. While the decay of any single nucleus is a purely random event, the collective behavior of a large number of identical radioactive nuclei follows a precise and predictable statistical pattern. This predictable behavior is captured by the radioactive decay law.

The disintegration rate of a radioactive material is directly dependent on the number of radionuclides N present as demonstrated in Equation 2.1 (Krane, 1987).

$$\frac{dN}{dt} = -\lambda N \quad \text{..... 2.1}$$

with λ being the decay constant.

If $N = N_0$ at $t = t_0$ Equation (2.1) solves exponentially to Equation 2.2.

$N = N_0 e^{-\lambda t}$ 2.2

Let the half-life of the primordial nuclei be represented by $t_{1/2}$ and substitute $N = \frac{N_o}{2}$ in Equation 2.2 to obtain Equation 2.3.

$t_{1/2} = \frac{ln}{\lambda} = \frac{0{\cdot}693}{\lambda}$ ..... 2.3.

Taking the time derivative of Equation 2.2, the element's activity A is obtained as;

$A = \left|\frac{dN}{dt}\right| = \lambda N_0 e^{-\lambda t}$ 2.4

$A(t) = \lambda N(t) = A_0 e^{-\lambda t}$ 2.5

with $A_0 = \lambda N_0$ being activity at $t = 0$. Activity A is measured in becquerel/s (Bqs^{-1}).

2.4 Secular Equilibrium

Secular equilibrium refers to a state in a radioactive disintegration series where the activity (or rate of decay) of the parent radionuclide and its daughter nuclide(s) become approximately equal. It occurs when the system is closed, meaning no material is added or removed, and the duration of decay is considerably greater than the half-life of the daughter nuclide. In such a scenario, the rate of decay of the parent radionuclide is high enough that it continuously produces daughters at a pace that matches the decay rate of the daughter. However, for a state of secular equilibrium to be achieved, the parent radionuclide's half-life must be significantly longer than the half-life of its daughter nuclides. This allows the daughter nuclide to accumulate at a rate that matches the decay of the parent, resulting in a steady state where the parent and its decay product have approximately the same activity. In practical terms, secular equilibrium is often observed in natural radioactive decay chains such as the uranium or thorium decay series where the parent radionuclide has a much longer half-life than its daughters. Figure 2.1 is a graphical demonstration of secular equilibrium between parent and daughter nuclei. The x-axis represents time while the y-axis shows the

activity (decay rate) of both nuclides. Initially, the rate of decay for the parent nuclide is higher as represented by the doted horizontal line on account of its longer half-life, while the daughter nuclide's activity increases over time as represented by the curved dotted line. As time progresses, the rate of decay of the parent slows down and the daughter nuclide's activity approaches that of the parent. This results in a state of equilibrium where the activity of the parent and the activity of the daughter nuclides are approximately equal, illustrating the concept of secular equilibrium. (Chege *et al.,* 2015).

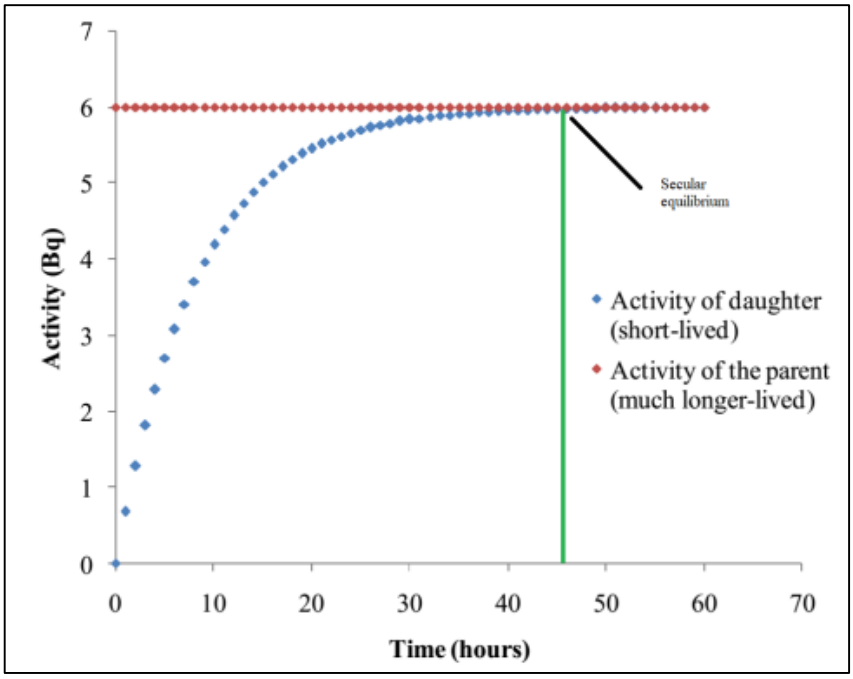


Figure 2.1: Diagrammatic representation of secular equilibrium showing activities of long-lived parent and short-lived daughter.

The principle of secular equilibrium is fundamental to the accurate quantification of ^{238}U and ^{232}Th in the sediment and biological samples, because these parent radionuclides are difficult to measure directly via gamma-ray spectrometry due to their low-intensity gamma emissions, their activity concentrations are instead determined by measuring the high-energy gamma peaks of their short-lived progeny, such as ^{214}Pb and ^{214}Bi for the Uranium series, and ^{208}Tl or ^{228}Ac for the Thorium series. To ensure that the activity of these daughters truly reflected the activity of the parents, samples are dried, homogenized, and hermetically sealed in standardized counting containers for a minimum of 21 to 28 days prior to measurement. This mandatory waiting period

allows the gaseous member of the chain, Radon (^{222}Rn), to reach a state of secular equilibrium with its parent, ^{226}Ra, thereby preventing the underestimation of radioactivity levels that would occur if decay products were allowed to escape. By strictly adhering to this equilibrium protocol, reported values true representative of concentrations of ^{238}U and ^{232}Th in samples.

2.5 Types of Decay

Radioactive decay primarily occurs through three common mechanisms: alpha (α) decay, beta (β) decay, and gamma (γ) decay. Each type involves the emission of distinct particles or energy, leading to different changes in the decaying nucleus and exhibiting unique interaction properties with matter.

Alpha particles are equivalent to helium-4 nuclei (^{4}He). The mass of an alpha particle is 4 atomic mass units (amu). Alpha particles are emitted only from the nuclei of heavy elements like ^{226}Ra, ^{238}U and ^{239}Pu. The speed with which an α particle is emitted depends on the species of the nucleus which has produced it and is about 6% of the velocity of light. This corresponds to an average kinetic energy ranging from 4 – 7 MeV. An α-particle is composed of two protons and two neutrons, giving it a positive charge. α-particles influence photographic plates and are subject to deflection by both electric and magnetic fields. In an electric field, their deflection toward the negative plate is minimal because of their heavy mass. An α – particle is able to ionize 40,000 atoms for every cm of travel through air. Of the radionuclide emissions, alpha rays have the highest ionizing power.

α - particle are the heaviest of the ionizing radiations that result from nuclear decay. Because of their heavy mass α - particles have very short penetration range. In air the penetration range is about 5cm, in soft tissue it is less than 100 μm.

Alpha emission occurs in nuclei having excess protons. Alpha decay is represented by Equation 2.6.

$$^{A}_{Z}X \rightarrow ^{A-4}_{Z-2}Y + ^{4}_{2}\alpha + Q \quad \text{.....2.6}$$

Where Q is decay energy.

When an α-particle is ejected, the nucleus's mass number decreases by 4 and its atomic number decreases by 2. For example Equation 2.7 shows the α-decay sequence of U-238 (Krane, 1987).

$$^{238}_{92}U \rightarrow {}^{234}_{90}Th + {}^{4}_{2}\alpha + Q \quad \text{.....2.7}$$

The range-energy relationship for α-particles is specified using air as the absorbing medium. Equation 2.8 provides the range (Ra in cm) in air for α-particles with an energy (E) between 2 MeV and 8 MeV.

$$Ra = 0.322E^{\frac{3}{2}} \quad \text{.....2.8}$$

Beta (β) particles are emitted by unstable nuclei that have an excess of neutrons. In order to achieve a more stable, lower energy state, one of the neutrons decays into a proton and an electron. The electron is emitted as a β particle, while the proton stays within the nucleus, causing the element to change as it loses a neutron and gains a proton. The total number of nucleons remains unchanged. Beta particles are high-speed electrons, traveling up to 98% of the speed of light, though they possess less energy than alpha particles. As electrons, they have zero atomic mass and their negative charge causes them to be deflected towards the positive plate in an electric field. They are also influenced by magnetic fields and can affect photographic plates. Due to their high speed, beta particles spend little time interacting with the medium they pass through, making them less ionizing than alpha particles but more ionizing than gamma rays. Beta particles can penetrate up to 100 cm in air and 3 cm in soft tissue, which is roughly 100 times more than alpha particles, due to their smaller mass. They can be stopped by a few centimeters of plastic or a few millimeters of metal. However, measuring the absorption of beta particles is complex because they are emitted with a continuous range of energies. Even when monoenergetic beta particles are selected, determining their range is difficult for two main reasons: First, when beta particles are absorbed, they can knock high-speed electrons out of atoms in the absorber, which may be mistaken for real beta particles. Secondly, beta particles are easily deflected, meaning that many of them are scattered away from the detector and are not counted, even if they are absorbed.

When a nucleus undergoes a β- decay, its mass number (A) does not change but its atomic number (Z) increases by 1, as shown in Equation 2.9.

$${}^{A}_{Z}X \rightarrow {}_{Z+1}{}^{A}Y + {}_{-1}{}^{0}e$$ ……2.9

A nucleus may undergo beta decay by either negative β- decay, positive β+ decay or by electron capture. In negative β-decay, a neutron converts to a proton, electron ($e-$) and an anti-neutrino (v). The electron gets expelled from the nucleus as a β- particle while the proton is retained in the nucleus. Equation 2.10 represents a β- decay process.

$${}^{210}_{82}Pb \rightarrow {}^{210}_{83}Bi + e^{-} + v$$ ……2.10

Positive β+ decay occurs in nuclei with more protons than neutrons. The proton will convert to a neutron, positron and neutrino (Krane, 1987). Expression 2.11 depicts a β+ decay process.

$${}^{25}_{13}Al \rightarrow {}^{25}_{12}Bi + e^{+} + v$$ ……...2.11

where $e+$ is a positron and v is a neutrino.

In the process of electron capture, a nucleus assimilates an orbital electron, which subsequently combines with a proton to yield a neutron. This interaction also results in the emission of a neutrino, the energy of which is derived from the mass of the captured electron. Equation 2.12 depicts β-decay process due to electron capture.

$${}^{208}_{83}Bi \rightarrow {}^{208}_{82}Bi + v$$ ……..2.12

Gamma (γ) rays are often emitted alongside alpha or beta particles. After a nucleus undergoes alpha or beta decay, the resulting daughter nucleus can be left with excess energy, putting it in an excited state. To become more stable, this excited nucleus releases that extra energy by emitting a gamma ray. Gamma rays have no mass or charge and possess low ionizing power, about one-hundredth that of beta particles. Since γ-rays are uncharged, they are impervious to electric and magnetic fields, though they can still impact photographic plates or films. Their energy ranges from 100 keV to 3 MeV and they travel at the speed of light. In contrast to alpha (α) and beta (β)

particles, γ-rays cause minimal ionization but have a very high penetrating ability—about 100 times greater than that of alpha β particles. γ-rays also have a very short wavelength, ranging from 10^{-13} m to 10^{-10} m. When γ-rays are emitted, both the atomic and mass numbers of the nucleus remain unchanged, as represented by Equation 2.13

$$^{A}_{Z}X \rightarrow ^{A}_{Z}X + ^{0}_{0}\gamma \quad \text{......} \quad 2.13$$

The resulting daughter nucleus is the same element as the parent but has less energy than the parent nucleus. Many radioactive nuclei emit gamma rays of multiple wavelengths. When γ-rays of a single wavelength are isolated, their absorption follows an exponential function relative to the thickness of the absorbing material (Equation 2.14).

$$I = I_0 e^{-\mu d} \quad \text{......} \quad 2.14$$

Here, *I* represents the intensity of the transmitted gamma rays after passing through a thickness d of the absorber, I_0 is the intensity of the incident gamma rays and μ is the linear absorption coefficient, which depends on the nature of the absorber and the gamma rays' wavelength (Krane, 1987).

2.6 Gamma rays' interactions with materials

Gamma-ray photons undergo multiple types of interactions with atoms in an attenuating medium. The likelihood of these interactions is based on the atomic number of the medium and the photon's energy. The interactions can occur with a free electron, a tightly bound electron, or the nucleus's electromagnetic field. The three key processes through which gamma rays interact with matter are the Compton scattering, photoelectric effect and pair production. High-energy photons such as gamma rays can transfer their energy to electrons in matter, leading to ionization or the emission of secondary particles. The photoelectric effect involves the complete absorption of a gamma ray by an atom, which in turn releases one of its electrons. Compton scattering involves the partial transfer of the gamma ray energy, causing a photon to scatter and ionize an electron. Pair production occurs at very high energies where gamma photons are converted into an electron-positron pair. Understanding these interactions lays a foundation of understanding how γ-rays interact with the detector medium.

2.6.1 Photoelectric Effect

The photoelectric effect refers to the emission of electrons from a material when exposed to light, a phenomenon first discovered by German physicist Heinrich Hertz in 1887. Albert Einstein provided the first comprehensive explanation of the photoelectric effect in 1905. He proposed that electromagnetic radiation is composed of discrete packets of energy, known as photons, each of which has an energy $\hbar\omega$. When a photon strikes the surface of a material, part of its energy is used to free an electron and the remaining energy is converted into the electron's kinetic energy. The electrons most loosely bound to the surface require the least energy to be released. This energy is termed the material's work function (W_0). The maximum kinetic energy (T_{max}) of an emitted electron is given by Equation 2.16, where $\hbar\omega$ is the energy of the photon.

$$T_{max} = \hbar\omega - W_0 = \frac{2\pi\hbar c}{\lambda} - W_0 \quad \text{.....2.16}$$

Electrons that are more tightly bound inside the material are emitted with less kinetic energy. The ejected electron's kinetic energy is influenced by whether it is near the surface or deeper inside the material. The energy that the incident photon loses is utilized within the detector's active area to produce a minor output signal, the size of which corresponds to the energy introduced by the emitted photoelectron (Krane, 1987). When the frequency of the incident radiation (ω_0) is such that the photon energy ($h\omega_0$) is just enough to free the electron, the electron is emitted with zero kinetic energy. This occurs when $h\omega_0 = W_0$ or equivalently, $\frac{2\pi\hbar c}{\lambda} = W_0$.

As noted by Krane (1987), the kinetic energy of this photoelectron is utilized within the detector's active area to produce an electrical output signal. The magnitude of this signal corresponds directly to the energy of the incident gamma photon. This mechanism allows the HpGe detector to register 'Full Energy Peaks' on the spectrum, which serve as unique signatures for identifying specific radionuclides such as ^{40}K, ^{238}U, and ^{232}Th based on their characteristic emission energies.

2.6.2 Compton Effect

The Compton effect or Compton scattering occurs when a gamma ray photon interacts with an electron, typically a free or weakly bound electron in an atom. In this process,

the photon transfers part of its energy to the electron, which results in the electron being ejected or scattered. The energy transferred to the electron depends on the angle at which the photon is scattered. The valence electrons of atoms are the primary participants in this interaction because they are the least tightly bound to the nucleus and are more readily available for scattering.

When the gamma photon collides with the electron, the photon's energy is partially transferred to the electron, causing the electron to gain kinetic energy and be ejected from the atom in a new direction. The remaining energy of the photon is reduced and the photon is deflected at an angle typically denoted as θ, relative to its original trajectory. A key feature of the Compton effect is the altered energy and direction of the scattered photon.

The degree of energy transfer and the scattering angle are governed by the Compton Equation 2.17 which shows the relationship between a scattered photon's change in wavelength and the scattering angle. Compton effect is essential in understanding the behavior of high-energy photons, such as gamma rays in various materials and is instrumental in radiation shielding and detection. It provides insight into the interactions between electromagnetic radiation and matter.

$$hv' = \frac{hv}{1+\frac{hv}{m_0c^2}}(1 - cos\theta) \quad \text{.....2.17}$$

Where θ is the scattering angle, m_o is the rest mass of the ejected electron and c is the speed of light. (Gilmore, 2008). When scattering angle $\theta = 180°$, the scattered electron will receive the highest energy from the incident photon. The scattered electron's direction of motion is aligned with that of the initial photon. When $\theta = 0°$ no energy is transferred from the incident photon to the scattered electron. Equation 2.17 simplifies to a relationship known as the Compton shift.

$$\lambda' - \lambda = \frac{h}{m_o c}(1 - cos\theta) \quad \text{.....2.18}$$

Equation 2.18 highlights that the change in the photon's wavelength, Δλ, is directly related to the scattering angle θ. This change is often expressed as the Compton Equation 2.19:

$$\Delta\lambda = \lambda' - \lambda = \lambda_C(1 - cos\theta) \text{.....2.19}$$

where λ_c represents the Compton wavelength, a fundamental constant defined as:

$$\lambda_C = \frac{h}{m_o c} = 2.4 \times 10^{-12} m \text{ .....2.20}$$

Figure 2.2 illustrates the mechanism of Compton scattering, where an incoming photon interacts with a loosely bound electron.

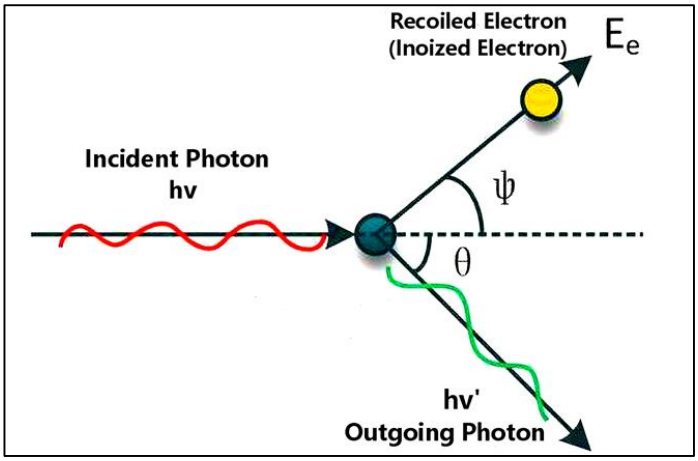


Figure 2.2: The interaction pathway of Compton scattering (Qiao et al., 2021)

According to Podgorsak (2005), the probability of Compton scattering is a function of the atomic number (Z) of the interacting material and the energy (hf) of the gamma ray, as demonstrated in Equation 2.21.

$$Probability\ of\ the\ effect = k.\frac{Z}{hf} \text{.....2.21}$$

Compton scattering significantly impacts gamma-ray spectrometry, especially at lower energies (below 60 keV). In this range, full energy peaks (FEP), which represent the total energy deposited by a gamma-ray in the detector, can overlap with Compton bumps. These bumps are caused by gamma-rays that scatter off electrons within the detector and only deposit a portion of their energy. This overlap creates interference in the spectrum, making it challenging to accurately analyze data and identify specific isotopes. The exact location of these Compton bumps is influenced by both the

incident photon energy and the geometrical setup of the detector and source (Plagnard et al., 2008). Therefore, ensuring the correct detector-source geometry is crucial for minimizing these interferences and enabling accurate spectroscopic analysis.

Unlike the Photoelectric effect which creates the peaks used for identification, Compton Scattering is primarily responsible for the background continuum (noise) in the gamma-ray spectrum. Because the scattering angle varies, this process results in a distribution of partial energy pulses known as the Compton Continuum, rather than a single distinct peak. As noted by Plagnard et al. (2008), these 'Compton bumps' can overlap with Full Energy Peaks (FEP), particularly at energies below 60 keV, creating interference that masks low-energy emissions. Consequently, the analysis of radionuclide concentrations for ^{40}K, ^{238}U, and ^{232}Th. requires careful background subtraction to isolate the true photopeak counts from the noise generated by Compton scattering events.

2.6.3 Pair Production

An electron-positron pair can be created in the nucleus by gamma rays of energy 1.022 MeV when there is a strong electromagnetic field in the neighborhood of a nucleus (Figure 2.3). The positron is a positively charged electron. When the gamma-ray energy surpasses 1.022 MeV, the additional energy is distributed as kinetic energy between the resulting electron and positron. The positron being positively charged cannot survive in the presence of the negatively charged electrons. Therefore, the electron and positron rapidly slowdown in the absorber material and combine in an annihilation process releasing two gamma rays each of energy 0.511 MeV. Annihilation is not limited only to the electron formed during pair production but can occur with any other electron. In a detection event where both of the annihilation gamma rays are successfully absorbed by the detector, a complete energy peak is produced. When one of the annihilation gamma rays leaves the detector, a single peak positioned at 0.511 MeV below the full-energy peak is generated and when both gamma rays escape the detector, a double peak located 1.022 MeV below the full-energy peak will be given. The three peaks' relative heights are dependent upon both the energy of the incoming gamma ray and the physical size of the detector. Escape peaks can occur during measurement of ^{232}Th and ^{238}U samples due to the presence of gamma rays that exceed the pair-production threshold associated with these elements.

The likelihood of occurrence of pair production increases significantly with higher photon energies (above 1.5 MeV) and is also more probable in materials with a higher atomic number (Z), roughly increasing with the square of both the energy above the threshold and the atomic number (i.e., $(E - 1.02)^2 Z^2$). Equation 2.22 can be used to calculate the electron-positron pair's resultant kinetic energy.

$$E_{e-} + E_{e+} = hv - 2m_0c^2 \text{.....2.22}$$

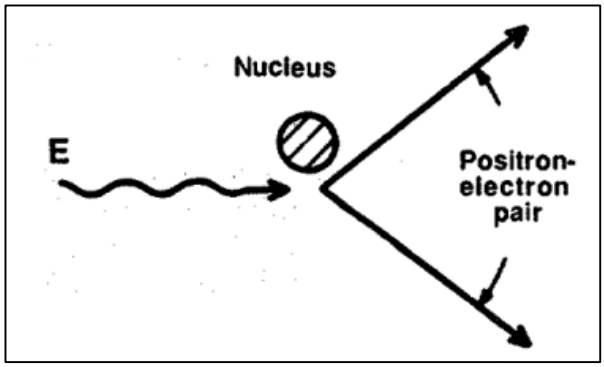


Figure 2.3; Visual representation of pair production (Krane, 1987).

Most environmental gamma rays are low energy. However, the decay chains of terrestrial radionuclides ^{232}Th and ^{238}U contain specific "daughter" isotopes that emit gamma rays well above this threshold. The most prominent high-energy terrestrial gamma ray comes from ^{208}Tl, a daughter of ^{232}Th. It emits a gamma ray at 2.614 MeV. Because 2.614 MeV is much larger than 1.022 MeV, pair production is a highly probable interaction.

2.7 Relative Dominance of Photon Interactions

Figure 2.4 visually delineates the relative predominance of the three primary photon interaction processes: the photoelectric effect, Compton scattering, and pair production. This illustrative diagram highlights how the dominant interaction mechanism changes systematically with varying

photon energy The photoelectric effect dominates at low photon energies, and both phenomena are influenced by the atomic number (Z) of the material. This interaction is the overwhelmingly dominant process, particularly pronounced in materials with a high atomic number. As photon energies increase to intermediate levels, Compton

scattering becomes the predominant interaction. This interaction is less dependent on the atomic number compared to the photoelectric effect, and it is the most significant attenuation mechanism for gamma and X-rays in tissue-equivalent materials (like water and biological soft tissue) and other low-Z materials across a broad energy range (Bajoga et al., 2016). Finally, at high photon energies (exceeding 1.022 MeV), pair production emerges as the dominant interaction. This interaction's probability increases with both photon energy and atomic number, although its Z dependence is less pronounced than that of the photoelectric effect. In essence, Figure 2.4 serves as a critical guide, illustrating these distinct energy and Z-dependent regions of predominance. Understanding these transitions is fundamental for designing effective radiation shielding, developing radiation detectors, optimizing medical imaging techniques, and accurately assessing radiation dosimetry.

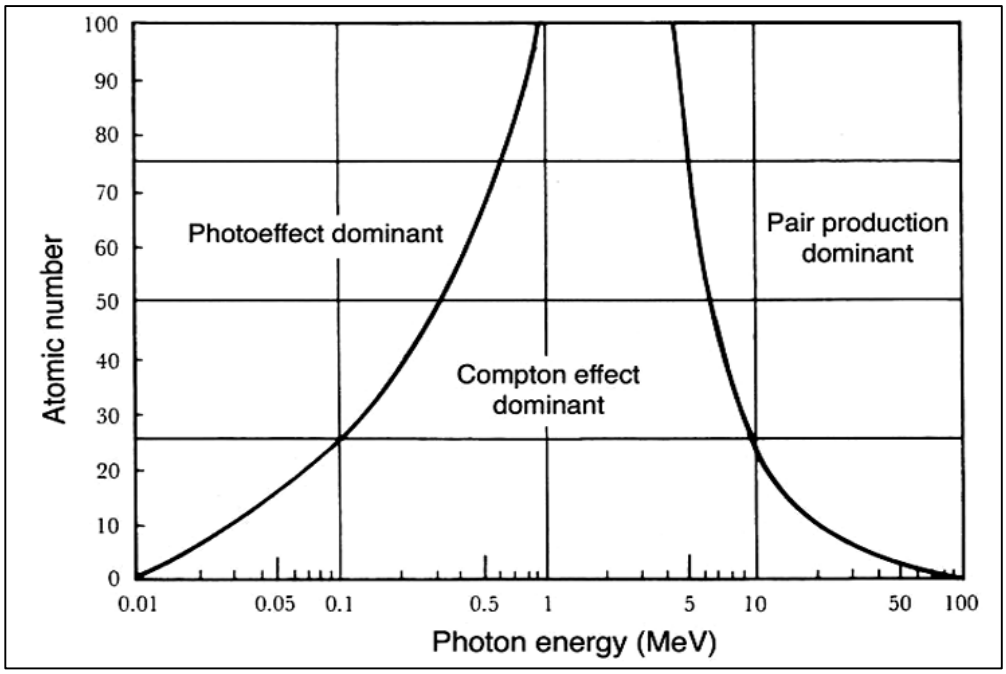


Figure 2.4: Relative dominance of photon interactions (Rosenberg, 2008)

2.8 Effects of Ionizing Radiation on Biological Matter

The human body, composed of specialized cells forming various organs, is susceptible to the effects of ionizing radiation. This radiation possesses sufficient energy to dislodge electrons from the atoms that constitute the molecules within tissues, thereby breaking the molecular bonds, potentially disrupting normal cellular operation.

Exposure to radiation can lead to two main categories of harmful health effects: deterministic and stochastic (ICRP, 1991).

2.8.1 Deterministic Effects

Deterministic effects are direct tissue damage that occur above a threshold radiation dose. These effects are primarily caused by the death or significant damage of a large number of cells within a specific tissue or organ, leading to impaired function. The time it takes for these effects to appear can vary, depending on the dose received and the affected body part. When a sufficient number of cells in a tissue are killed or rendered non-functional by radiation, the tissue's ability to perform its normal functions is compromised, resulting in a deterministic effect. While the body possesses repair mechanisms, it can be overwhelmed if the damage is too extensive or occurs too rapidly (Reisz et al., 2014).

Some examples of deterministic effects and their approximate threshold doses include skin reactions like reddening (erythema) at around 2-5 Gy and hair loss (epilation) at similar doses. More severe and irreversible skin damage can occur at doses of 20-40 Gy or higher. Reproductive health can also be affected, with temporary sterility in males potentially occurring at 0.15 Gy to the testes, and permanent sterility at 4-6 Gy for males and 2.5-7 Gy for females. Furthermore, exposure during critical periods of fetal development, particularly between 8 and 15 weeks of gestation, can lead to developmental abnormalities such as severe mental retardation, with an estimated threshold of 0.1-0.5 Gy (Reisz et al., 2014).

2.8.2 Stochastic Effects

Stochastic effects of ionizing radiation are characterized by their probabilistic nature, meaning they occur by chance rather than with a definite threshold dose. Unlike deterministic effects where the severity increases with dose, the severity of a stochastic effect is independent of the absorbed dose. Instead, it is the probability of the effect occurring that increases proportionally with the radiation dose received. Even at very low doses, there is no absolute certainty that an adverse effect will not occur, which is why there is generally no assumed threshold dose for stochastic effects. The primary stochastic effects of concern are cancer and hereditary (genetic) effects. Cellular DNA can sustain damage from radiation, which can induce mutations. If these mutations

occur in somatic cells (body cells), they can potentially lead to cancer development, often many years after the initial exposure. If the mutations occur in germ cells (reproductive cells), there is a risk of these genetic changes being passed on to future generations (Desouky et al., 2015; Reisz et al., 2014).

A key challenge in attributing a specific cancer or genetic defect to a particular radiation exposure is that these effects can also occur spontaneously in the absence of radiation. Therefore, it is often not possible to conclusively link a specific case of cancer or genetic damage to a prior radiation exposure. Instead, the risk is assessed statistically for a population. The probability of developing a stochastic effect, such as cancer, is generally assumed to increase linearly with dose, particularly at doses above 100 mSv. A fundamental tenet of radiation protection is the linear no-threshold (LNT) model, which argues that the relationship between radiation dose and risk is linear, with no safe threshold. Consequently, radiation protection measures aim to keep exposures as low as reasonably achievable (ALARA) to minimize the probability of these chance occurrences (Desouky et al., 2015).

2.9 Global Averages and Regulatory Limits for Radiological Parameters

Radiological parameters, such as effective dose and equivalent dose, are critical in assessing the potential health risks associated with ionizing radiation exposure. International guidelines, particularly those from the International Commission on Radiological Protection (ICRP), establish maximum permissible limits to safeguard individuals and populations.

The global mean dose equivalent from environmental radiation is approximately 2.4 mSv per year, with variations depending on geographical location and lifestyle factors. For instance, individuals residing at higher altitudes or in areas with elevated radon concentrations may experience higher exposure levels. The ICRP recommends the following annual dose limits:

Occupational Exposure: An effective dose of 20 mSv per year, averaged over five years, with no single year exceeding 50 mSv. Equivalent doses to the lens of the eye, skin, and extremities are also specified to limit potential deterministic effects.

Public Exposure: An effective dose of 1 mSv per year, with higher values permissible in special circumstances, provided the average over five years does not exceed 1 mSv per year.

These limits aim to minimize the risk of stochastic effects, such as cancer, by ensuring that radiation exposure remains within levels deemed acceptable based on current scientific understanding. Adhering to these dose limits is vital for protecting human health and the environment. Regular monitoring and assessment of radiation levels in various settings, including medical facilities, industrial sites, and the natural environment, are essential to ensure compliance with established standards. Implementing these guidelines helps mitigate potential health risks associated with ionizing radiation and promotes public confidence in radiation safety practices.

The worldwide average for Ra_{eq} (radium equivalent activity) is 89 Bq/kg, while the permissible public safety limit is 370 Bq/kg (Joel et al., 2018). The permissible public safety limit for both H_{ex} (external hazard index) and H_{in} (internal hazard index) is 1 (Al-Ghamdi, 2019). The average value for absorbed dose rate is 60 nGy/h, and the permissible public safety limit is 1500 nGy/h (Adewoyin et al., 2018).

2.10 Principal Mechanism of a High Purity Germanium (HPGe) Detector

Germanium stands as the predominant semiconductor material for gamma-ray detection, largely owing to its superior properties compared to silicon. Its significantly higher atomic number ($Z = 32$ for Germanium vs. $Z = 14$ for Silicon) translates to a greater photoelectric absorption cross-section and Compton scattering probability, making it exceptionally effective for the detection of higher-energy gamma radiation. This enhanced interaction probability is crucial for efficient energy deposition and subsequent signal generation from incident photons (Knoll, 2010).

Conceptually, a germanium detector functions akin to a solid-state ionization chamber. It is fundamentally a p-n junction diode configured with a large intrinsic (i) region, forming a p-i-n structure. This intrinsic region, which serves as the active detection volume, is achieved by applying a substantial reverse bias voltage across the diode. This reverse bias creates an extensive depletion region within the intrinsic

semiconductor, where virtually all free charge carriers (electrons and holes) are swept out, rendering it highly resistive (Leo, 1994).

When an incident gamma-ray photon interacts within this depletion region, it transfers its energy to the semiconductor lattice, typically through photoelectric effect, Compton scattering, or pair production. These interactions lead to the liberation of numerous electron-hole pairs. The strong electric field maintained throughout the active volume by the reverse bias voltage then efficiently sweeps these newly generated charge carriers towards their respective collecting electrodes: electrons migrate towards the positive electrode, and holes drift towards the negative electrode (Gilmore, 2008).

The continuous motion of these charge carriers (either electrons or holes) constitutes a transient current pulse that is fed into a charge-sensitive preamplifier that converts it into a voltage pulse whose amplitude is directly proportional to the total charge collected, and therefore, directly proportional to the original energy deposited by the incident gamma-ray photon (Knoll, 2010).

A critical limitation of germanium detectors, however, stems from their small band gap of approximately 0.7 eV. This inherently low band gap means that at room temperature, a significant number of electrons possess sufficient thermal energy to cross the band gap, leading to a large thermally induced leakage current (Bajoga et al., 2016). This leakage current generates substantial electronic noise, which would severely obscure the minute signals produced by gamma-ray interactions, rendering room-temperature operation of germanium detectors impossible for high-resolution spectroscopy (Leo, 1994).

To circumvent this issue and ensure optimal performance by mitigating thermal excitation and minimizing background noise, germanium detectors are invariably operated at very low temperatures, typically 77 K. This is most commonly achieved by cooling the detectors with liquid nitrogen. A standard detector setup designed for cryostatic cooling integrates several essential components: a cooling rod (mostly made of high-thermal-conductivity copper) that physically connects the detector crystal to the cold source, a dewar (a specialized vacuum-insulated container) for storing the

liquid nitrogen (Figure 2.5), and a fill collar to facilitate safe and efficient replenishment of the liquid nitrogen into the dewar. This continuous low-temperature environment is paramount for maintaining the detector's high energy resolution and low noise characteristics (Gilmore, 2008).

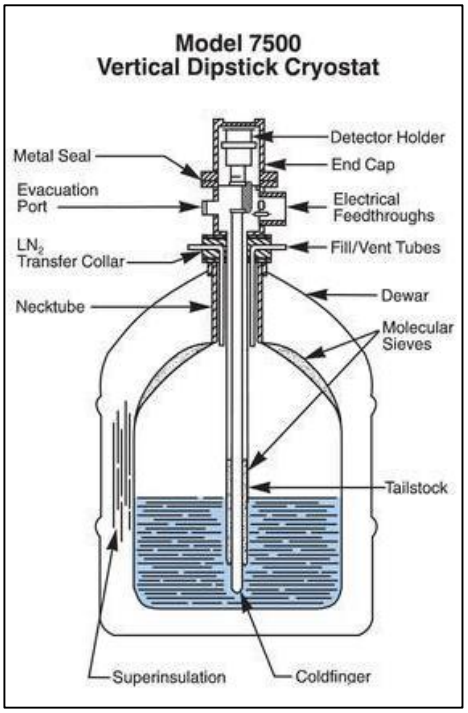


Figure 2.5: A visual representation of germanium detector inside a liquid nitrogen dewar (Khan H. *et al.*, 1993).

Before the detector is put into use, it has to undergo energy resolution. Energy resolution is a measure of the detector's ability to distinguish between two gamma rays with very close energy levels. This is expressed as the Full Width at Half Maximum (FWHM) of a peak on a spectrum, measured at half of its maximum height (Figure 2.6 a). A smaller FWHM value ($\approx$ 1.5 keV for HPGe) means the detector has better resolution and can more accurately separate closely spaced energy peaks. A larger FWHM indicates poorer resolution ($\approx$ 50 keV for NaI(Tl), as the peaks are wider and can overlap, making it difficult to differentiate between two gamma rays of similar energy (Figure 2.6 b) (Knoll, 2010).

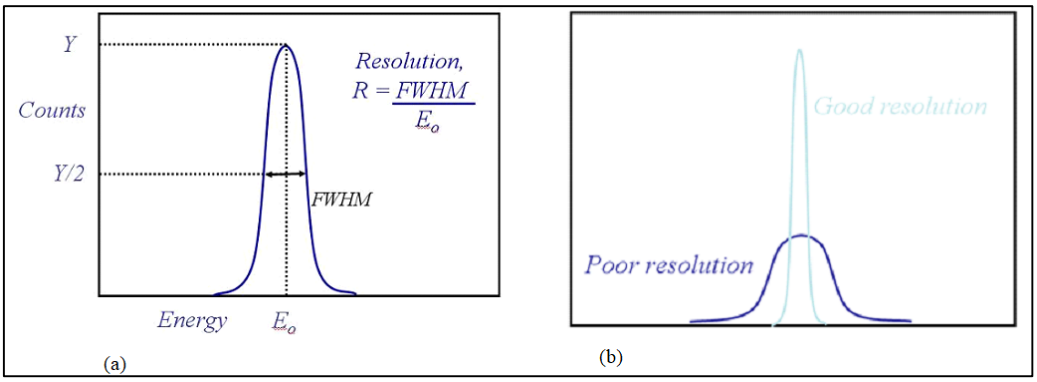


Figure 2.6: FWHM position and resolution types (Knoll, 2010).

The dominant characteristic that underpins the widespread application of germanium detectors in gamma-ray spectroscopy is their excellent energy resolution. This inherent superiority arises from the fundamental difference in the energy required to generate a measurable charge carrier. In germanium, approximately 2.96 eV of energy is needed to produce a single electron-hole pair at cryogenic temperatures (77 K). Conversely, in a NaI(Tl) scintillation detector, higher energies (hundreds of electron volts) are required to generate a single photoelectron (Leo, 1994). This disparity in charge carrier generation efficiency leads to a significantly larger number of charge carriers being produced per unit of absorbed gamma-ray energy in germanium compared to scintillators.

The elevated number of charge carriers per pulse within germanium detectors results in two substantial advantages regarding the achievable energy resolution. Firstly, based on Poisson statistics, the relative statistical fluctuation in the number of collected charge carriers decreases as the total number of carriers increases. Consequently, the inherent statistical uncertainty in the measured charge, which directly dictates the spread of the observed energy, becomes a much smaller fraction of the total signal. Secondly, the intrinsic resolution is further enhanced by the Fano factor (F), which accounts for the fact that the actual variance in charge carrier production is less than what a simple Poisson model predicts, owing to energy conservation constraints during the ionization process (Knoll, 2010). The Fano factor for semiconductors like germanium is much less than 1, further improving their statistical resolution compared to scintillators where analogous statistical processes are less favorable. Consequently, germanium detectors possess the remarkable ability

to clearly separate numerous closely spaced gamma-ray energies that would otherwise appear as a single, unresolved peak in a NaI(Tl) spectrum. This unparalleled capability makes germanium detectors indispensable for virtually all high-resolution gamma-ray spectroscopy applications, particularly when analyzing complex energy spectra originating from multi-nuclide samples or radioactive decay schemes with numerous closely spaced gamma lines. While the intrinsic resolution of germanium detectors is outstanding, at very low gamma-ray energies, the overall resolution may eventually be limited by electronic noise originating from the detector system's preamplifier and associated readout electronics. Therefore, meticulous design and shielding of these electronic components are crucial for achieving optimal low-energy performance (Gilmore, 2008).

2.11 Heavy Metals

Heavy metals are a group of metallic elements characterized by their relatively high density, atomic weight, or atomic number. They are generally considered to have a density greater than 5 g/cm^3. Examples of heavy metals include highly toxic ones like lead (Pb), mercury (Hg), cadmium (Cd), and arsenic (As), as well as those that are also essential nutrients, such as chromium (Cr), copper (Cu), zinc (Zn), and nickel (Ni). It's essential to note that some elements like arsenic are metalloids but are often grouped with heavy metals due to their similar toxicological properties (Duffus, 2002).

These elements occur naturally, anthropogenic activities have impacted the Earth's crust significantly altering their distribution and concentration in the environment. Industrial activities like mining and manufacturing release large amounts of heavy metals into the atmosphere, soil, and water. Heavy metals, once released into the environment, are resistant to degradation. This property leads to their bioaccumulation within ecosystems and biomagnification up the food chain (Tchounwou *et al.,* 2012).

The significance of heavy metals lies in their potential toxicity to living organisms, including humans. While some heavy metals, like zinc and copper, are essential micronutrients in trace amounts, many others are non-essential and exert toxic effects even at low concentrations. Their toxicity arises from their ability to bind to and interfere with the function of biologically active molecules, such as proteins and enzymes, leading to cellular damage, organ dysfunction, and various health problems.

These can range from neurological disorders and kidney damage to developmental issues and cancer (Jarup, 2003). Consequently, monitoring and managing heavy metal contamination are critical environmental and public health concerns.

Heavy metal contamination in aquatic ecosystems represents a significant environmental and public health concern globally. Industrialization, agriculture, and urbanization contribute to the accelerated release of toxic heavy metals such as Cd, As, Pb, Cu, Ni, Ba, Cr and Zn into marine and freshwater environments. Once introduced, these elements are persistent and do not readily degrade, leading to their accumulation in water, sediments, and crucially, in aquatic organisms. This bioaccumulation, and subsequent biomagnification through the food chain, poses substantial risks to aquatic life by disrupting physiological processes, inducing oxidative stress, and causing genetic damage (Ahamad *et al.,* 2024). Ultimately, this contamination threatens biodiversity and presents potential health hazards to humans who consume contaminated seafood (Jarup, 2003).

Lead (Pb)

The extraction of lead, a metal with a density of 11.3 g/cm^3 and an atomic number of 82, is primarily from its ore, galena, as well as cerussite and anglesite. These lead-bearing ores frequently coexist with other valuable metals, including copper, zinc, and cadmium. Lead can also exist in multiple oxidation states, including 0, I, II, and IV with the +2 state being the most bio-accumulated form by aquatic organisms, making it environmentally significant. As a major cause of pediatric heavy metal poisoning, it is the second-most hazardous heavy metal according to the Agency for Toxic Substances and Disease Registry (ATSDR) (Tchounwou *et al.,* 2012). The list ranked based on the heavy metals most commonly associated with severe health risks to humans is as follows: mercury, lead, cadmium, arsenic, chromium, thallium, nickel, antimony, beryllium, tin, bismuth, cobalt, copper, manganese, platinum, silver, zinc, aluminum, vanadium and lithium.

Historically, lead has been a component used in manufacturing pipes, drains, soldering materials, batteries, plumbing components, ammunition, fuel additives, paint pigments and pesticides. Its toxicity, persistence in the environment and ability to bioaccumulate

in aquatic ecosystems are major concerns. Lead accumulates in fish tissues such as bones, gills, liver, kidneys and scales, primarily entering through gaseous exchange across the gills into the bloodstream (Jamil Emon *et al.,* 2023).

Lead poisoning can impair cognitive function by damaging the central nervous system, cause abdominal discomfort, weaken bones by replacing calcium and result in anemia due to enzyme disruption in red blood cell production. It is also associated with reduced fertility, cancer, vomiting, nausea, and headaches (WHO, 2008). High lead exposure can severely damage the brain and kidneys, cause miscarriage, impair sperm production and even lead to death (Wani *et al.,* 2015).

Fish's ability to bioaccumulate lead over time means current metal levels may not accurately reflect real-time concentrations. Studies showed lead levels in fish from the Warri River were below the WHO and FEPA limit of 2.0 mg/kg, indicating their safety for consumption (Ayenimo *et al.,* 2005). However, dry-season concentrations exceeding 2.0 mg/kg were linked to elevated water temperatures, which increased fish activity and pollutant accumulation (Obasohan, 2008).

Lead concentrations in sediments varied widely. For example, Tyume River sediment levels ranged from 0.040 ± 0.005 to 0.067 ± 0.003 mg/kg, while the River Nile exhibited 3.1 to 76.9 mg/kg, surpassing the permissible 35 mg/kg limit and indicating pollution requiring regular monitoring (Awofolu *et al.,* 2005). Elevated sediment lead levels pose direct threats to aquatic ecosystems and indirect risks to humans (Naz *et al.,* 2022). Forcados River sediment samples averaged 9.43 mg/kg, below the WHO limit (Ogbemudia *et al.,* 2023).

Lead concentrations in water from Nairobi River (0.1 mg/L) and Ikpoba River (0.035 mg/L) exceeded the WHO limit of 0.01 mg/L for drinking water, indicating pollution primarily from anthropogenic sources (Oguzie & Okhagbuzo, 2010). While these levels were below the 1 mg/L limit for potable water set by the Federal Ministry of Environment and WHO caution is advised regarding untreated effluent discharge into inland waters. Vegetation along riverbanks has been recommended as a natural purifier for heavy metals.

Nickel (Ni)

With a density of 8.9 g/cm³, nickel readily combines with metals such as iron, aluminum, and copper to form alloys and also dissolves in dilute acids (Briffa *et al.,* 2020). While the most common oxidation state is +2, nickel can also exist in +1, +3, and +4 oxidation states. Nickel (II) compounds are well-known and include sulfides, sulfates, carbonates, hydroxides, carboxylates and halides. Nickel has various industrial applications, such as serving as a catalyst for hydrogenation reactions. Nickel also serves as a cathode in several types of rechargeable batteries. These include nickel-cadmium, nickel-iron, nickel-hydrogen, nickel-metal hydride, and some lithium-ion batteries (Hall *et al.,* 2015). Over 60% of the world's nickel production is allocated to nickel-steels, with a significant portion going into the creation of stainless steel (Obasohan, 2008).

Nickel toxicity is generally low but can cause sub-lethal effects at elevated levels (Gopal *et al.,* 2009). Health effects associated with nickel include skin allergies, lung fibrosis, kidney and cardiovascular poisoning and potential carcinogenicity from nickel sulfide fumes and dust. Nickel carbonyl compounds are especially toxic due to their ability to release carbon monoxide, a highly toxic and explosive gas (Gopal *et al.,* 2009). Fish exposed to high nickel levels can accumulate it in their tissues (Oronsaye *et al.,* 2010).

Studies conducted on the Dhaleswari and Buriganga Rivers in Bangladesh measured nickel concentrations in fish ranging from 9.55–13.35 mg/kg and 0.09–0.48 mg/kg, respectively (Ahmad *et al.,* 2009). In the Ikpoba River, nickel concentrations in the gills of *Chrysichthys nigrodigitatus* averaged 0.02 mg/kg during the rainy season, well below the 0.4 mg/kg safety threshold set by the Food and Agricultural Organization (FAO) and World Health Organization (WHO). Sediments from the Buriganga River showed spatial and temporal nickel variation between 147.06–258.17 mg/kg, indicating partial heavy metal pollution and posing risks to human health and the ecosystem. Increasing industrial activities, pesticide use and untreated sewage discharge may worsen the situation if not addressed (Ahmad *et al.,* 2009).

Unpolluted surface water typically contains nickel concentrations of 5.0 x 10^{-4} mg/L to 0.015–0.020 mg/L (Abd Elnabi *et al.,* 2023). However, studies have recorded varying levels of nickel in rivers compared to the WHO-recommended drinking water limit of 0.07 mg/L (WHO, 2003; Awofolu *et al.,* 2005). For instance, nickel levels in Tyume River water ranged from 0.201–1.777 mg/L, while Nairobi River recorded a mean of 0.03 mg/L (Njuguna *et al.,* 2017). Anthropogenic activities, including fossil fuel combustion, battery waste, stainless steel materials and old coins, are major sources of nickel in surface water. High nickel levels in Tyume River water may contribute to contamination in irrigated vegetables, underscoring the need for regular monitoring (Awofolu *et al.,* 2005). Despite detectable nickel levels, Njuguna *et al.,* (2017)'s the findings showed that the Nairobi River's water was fit for human consumption with regard to nickel.

Manganese (Mn)

Manganese with a density of 7.21g/cm^3 constitutes approximately 1000 ppm (0.1%) in the Earth's crust, where it ranks as the 12th most abundant element (Al-Fartusie & Mohssan, 2017). It primarily occurs in the minerals pyrolusite, psilomelane. Rhodochrosite also serves as a source of manganese, though to a lesser degree. Manganese compounds are known to be strong oxidizing agents and commonly display oxidation states of +4 and +7. Manganese can directly combine with elements such as boron, carbon, sulfur, silicon and phosphorus (Al-Fartusie & Mohssan, 2017). Among its oxidation states, the +2 state is the most stable and essential for biological functions, while other states are toxic to humans. Depending on oxidation state, manganese ions display varying colors and are used industrially as pigments. Manganese dioxide (MnO_2) is a key material for cathodes in disposable dry cells and alkaline batteries. In its metallic form, manganese is vital for industrial alloy production, particularly stainless steel and manganese phosphating, which is applied to prevent rust and corrosion on steel (Zhang & Cheng, 2007).

Although manganese is an essential trace element for all living organisms, excessive exposure, particularly through inhalation, can lead to manganese poisoning in mammals, causing irreversible neurological damage. Other health complications include manganism, characterized by psychiatric and motor disturbances, which has

been reported among workers involved in manganese alloy production (Gopal *et al.,* 2009). Individuals exposed to high environmental manganese levels may experience cerebellar dysfunction and neurological damage as seen in the population of Groote Eylandt, an island just off the northern coast of Australia (Briffa *et al.,* 2020).

Studies have documented manganese levels in fish from various rivers. Fish from the Ogba River showed manganese concentrations ranging between 0.0 and 0.75 mg/kg, while gills of fish from the River Nile contained concentrations as high as 17.37 mg/kg (Obasohan, 2008). The gills' high manganese concentrations were attributed to their biological makeup, which has evolved to maximize the absorption of water. Sediment studies have also highlighted varying manganese concentrations. Nairobi River sediments contained levels ranging between 1598.33 and 4322.83 mg/kg (Kage, 2012), while River Nile sediments ranged between 139.8 and 351.8 mg/kg. River water manganese levels have fluctuated around the WHO-recommended limit of 0.4 mg/L. For example, the River Nile's water recorded levels between 0.033 and 0.14 mg/L, which were within safe limits, but higher levels were observed in Nairobi River (2.5 mg/L) and the River Ganga (0.0226 mg/L) (Boral *et al.,* 2020).

Elevated manganese levels exceeding recommended limits have been linked to rainfall, elevated river discharge, effluents from upstream industrial activities, municipal waste, and the geological characteristics of the riverbeds and catchment basins (Abebe *et al.,* 2023). To prevent further degradation of river water quality, measures such as treating industrial wastewater and upgrading sewage treatment plants are recommended.

Zinc (Zn)

Zinc having a density of 7.14 g/cm^3, is present in the Earth's crust at a concentration of approximately 75 ppm, making it the 24th most abundant element. Zn is commonly found in ores alongside other base metals like copper and lead. It has a greater affinity for sulfur than for oxygen. Typical Zn ores include sphalerite (ZnS), calamite ($ZnCO_3$), and zincite (ZnO). Beyond its role in the creation of alloys such as brass and bronze, zinc is applied in building construction for roofing and cladding. Its applications extend to circuit boards, photocopiers, and dry cell batteries, in addition to serving as

a key component in the chemical and pharmaceutical industries for products like paints, medicines, and nutritional supplements (Al-Fartusie & Mohssan, 2017).

Zinc toxicity is caused by too much zinc being absorbed, which inhibits the absorption of copper and iron. The Zn^{2+} ion is especially toxic to plants, invertebrates, and fish (FAO/WHO, 2016). Zn salts can irritate the intestines, causing nausea and abdominal pain. Long-term high Zn intake can lead to Cu deficiency and anemia. Inhalation of freshly formed Zn oxide during welding of galvanized materials can cause a condition known as "zinc shakes" or "zinc chills." Zn has also been found to damage nasal nerve receptors, potentially causing anosmia, which led to the withdrawal of zinc-based intranasal cold remedies from store shelves.

Analysis of Zn distribution in freshwater cat fish, *Chrysichthys nigrodigitatus* (Siluriformes: Bagridae), of Cross River, Nigeria showed that the highest concentration (0.009 ± 0.001 μg/g) present in the liver tissue collected from Calabar (Station III), a result deemed statistically significant ($p<0.05$). There were also significant disparities in Zn levels between the gills (0.004 ± 0.004 μg/g) and skin (0.003 ± 0.002 μg/g) at Ikom (Station I) and Obubra (Station II), respectively. The lowest observed Zn concentrations (0.002 ± 0.002 μg/g) were consistently found in both the gills and skin at Obubra (Station II) (Olatunji Ayotunde *et al.,* 2012).

Sediments from various rivers have shown Zn levels in excess of the permissible limit of 123 mg/kg. For example, Nile River sediments in the dry period had concentrations of 91.5–307 mg/kg, while Forcados River sediments contained 34.61 mg/kg and Nairobi River sediments fell within the range of 126.33 to 307 mg/kg, with some posing no immediate hazards to aquatic life or humans. The concentration of 0.60 mg/kg detected in Nairobi River sediments did not exceed the recommended limit of 123 mg/kg (Njuguna *et al.,* 2017).

The distribution of heavy metals in river sediments of the main tributaries of Dongting Lake, China was irregular. In the XR river, nearly all metals, particularly arsenic and cadmium, were found in significantly elevated concentrations in the midstream and downstream areas. Specifically, arsenic levels were over 3.5 times greater midstream (113.42 mg/kg) and downstream (111.77 mg/kg) compared to upstream (28.90

mg/kg). Cadmium concentrations showed even more drastic increases, being over 11-fold higher midstream (22.04 mg/kg) and 9-fold higher downstream (18.84 mg/kg) than upstream (2.02 mg/kg). A similar trend of elevated midstream and downstream concentrations was seen in the LR river for most heavy metals, with the notable exception of cadmium, which was markedly elevated upstream (6.00 mg/kg) in this river. For the ZR and YR rivers, zinc, arsenic, and cadmium generally accumulated in the midstream and downstream sections, as did chromium in ZR. However, lead concentrations were significantly higher upstream in YR and midstream in ZR, while copper and chromium in YR peaked in the midstream section (Xu *et al.,* 2018).

High zinc levels, sometimes as high as 20 mg/L, can be found in rivers located near industrial or mining areas. Soils contaminated by mining, refining, or zinc-rich fertilizers can contain several grams of zinc per kilogram of dry soil (Al-Fartusie & Mohssan, 2017). Ganga River showed Zn levels ranging from 7.5 to 15.20 mg/dl, which exceeded the permissible limit of 3 mg/L set by the WHO in 1993 (Dubey, 2021). A study on the Nairobi River in Kenya indicated that industrial discharge and electronic waste are likely sources of heavy metals like Cr, Pb, Zn, Cu, and Ni found in the water. High concentrations of these metals were particularly noted downstream of the Ngong River in the industrial zone. For example, during the rainy season, the Kayole area (situated along the Ngong River) showed the highest levels of Zn (154.23 µg/L), Pb (4.5 µg/L), and arsenic (3.98 µg/L). The average Zn concentration for the entire river was 104.86 µg/L. Elevated Zn levels were attributed to agricultural runoff, residential and industrial effluents, and land use activities. A downstream decrease in pollutants due to dilution and self-purification was observed. Recommendations include continuous monitoring of heavy metal contamination and using riverine vegetation to absorb heavy metals as a purification method (Njuguna *et al.,* 2017).

Cadmium (Cd)

Cadmium with a density of 8.65 g/cm^3 typically exhibits an oxidation state of +2, forming various inorganic compounds such as sulphates, chlorides and acetates, many of which are water-soluble. Cd is primarily a by-product of Pb and Zn mining and smelting and is widely used in nickel-cadmium batteries and as a pigment in paints. Additionally, Cd contamination in soils often originates from agricultural activities

involving pesticides and fertilizers. Ingestion of Cd can quickly lead to symptoms such as nausea, vomiting, abdominal cramps, headaches, diarrhea and shock. The Itai-itai disease in Japan was linked to Cd exposure in areas where rice fields were irrigated with Cd-contaminated water. Cd targets multiple organs.

In fish, lower mean Cd levels ranging from 0.79 to 0.98 mg/kg were recorded in specimens from Ikpoba River, while higher levels of 2.16 mg/kg were observed in Forcados River. Although these levels were below the recommended safety limits, caution is warranted due to the potential cumulative effects that could harm aquatic life and humans who consume contaminated fish (Oronsaye *et al.,* 2010). Cd levels in *Oreochromis niloticus* (Nile tilapia) from the Challawa River varied from 0.066 ± 0.021 to 0.189 ± 0.038 mg/kg. These concentrations suggest potential toxicity risks for both aquatic life and human consumers, highlighting the importance of consistent monitoring to evaluate the impact of heavy metals on the river's ecosystem (Sani *et al.,* 2022).

Sediment samples also revealed concerning Cd concentrations. In the River Nile, levels ranged narrowly between 0.81 and 2.3 µg/kg (Al-Afify & Abdel-Satar, 2022). Conversely, sediments from Tyume River showed Cd levels between trace amounts and 0.005 ± 0.003 mg/kg, within the South African Target Water Quality Range (TWQR) for domestic and irrigation purposes (Awofolu *et al.,* 2005). In Wadi Hanifah River sediments, a mean Cd concentration of 71.7 ppb was recorded (Abdel-Baki *et al.,* 2011). Heavy metal contamination in sediments can degrade water quality, promote bioaccumulation in aquatic organisms, and have long-term adverse effects on human health and ecosystems (Fernandes *et al.,* 2007).

Cd levels in river water frequently exceed the WHO recommended limit of 0.003 mg/L. For example, River Nile water exhibited Cd concentrations between 0.002 and 0.02 mg/L, and Nairobi River showed mean levels of 0.02 mg/L, both surpassing the safe limit and rendering the water unsuitable for consumption (Osman & Kloas, 2010). Similarly, Cd concentrations in Tyume River water ranged from 0.030 ± 0.002 to 0.044 ± 0.003 mg/L, surpassing the TWQR guideline of 0 to 0.005 mg/L for domestic use (Awofolu *et al.,* 2005). Sources of these elevated Cd levels include agricultural runoff, sediment-bound metal release, industrial waste, and atmospheric dust deposition

(Osman & Kloas, 2010). Consequently, Tyume River water was deemed unsuitable for domestic use, with potential chronic health implications for users. Regular monitoring and assessment of contamination levels are thus strongly recommended (Awofolu *et al.,* 2005).

Chromium (Cr)

Cr has a density of 7.2 g/cm³ and ranks as the 21st most abundant element in the Earth's crust, with an average concentration of 100 ppm (Al-Fartusie & Mohssan, 2017). Cr compounds naturally occur in the environment due to the erosion of Cr-containing rocks and their presence in animals, plants, and soil. These compounds can exist as solids, liquids, or gases. Cr primarily exists in oxidation states of +3 and +6, with Cr (III) being the more stable form, producing compounds such as oxides, chlorides and sulphates (Gonzalez *et al.,* 2005). Cr is widely used in metal alloys like stainless steel, protective metal coatings through electroplating, magnetic tapes and pigments for paints, cement, paper and rubber. Additionally, its soluble forms are utilized in wood preservatives and as corrosion inhibitors in water systems for industrial and cooling purposes (Barnhart, 1997).

Hexavalent chromium (Cr VI) is highly toxic and mutagenic when inhaled and is classified as a human carcinogen (Wise et al., 2022). Exposure to elevated levels of Cr VI can cause irritation to the nasal lining, respiratory problems such as asthma, cough and wheezing, and, over long periods, damage to the liver, kidneys, circulatory and nervous systems as well as skin irritation (Shin *et al.,* 2023).

Cr levels in fish have often exceeded the recommended limit of 0.15 mg/kg (Adebiyi et al., 2024). For instance, fish from Wadi Hanifah River showed an average Cr concentration of 386 mg/kg, while samples from Ogba River in Benin City, Nigeria, reported Cr levels ranging from 0.01 mg/kg to 1.16 mg/kg, both above the recommended threshold (Obasohan, 2008). Sediments are significant reservoirs of metals and other pollutants in aquatic environments, which can adversely affect water quality and lead to metal bioaccumulation in aquatic organisms, with long-term implications for human health and ecosystems (Fernandes *et al.,* 2007). Elevated Cr levels in agricultural soils, potentially affecting crops, can result from sewage sludge

application and atmospheric deposition of industrial fumes. Sediments from Wadi Hanifah River recorded an average Cr concentration of 9500 µg/kg (Abdel-Baki *et al.,* 2011). Cr concentrations in water often deviate from the recommended domestic water limit of 0.05 mg/L. For example, Wadi Hanifah River water samples showed Cr concentrations of 6.4 ppb, while Msimbazi River water ranged from 1.414 mg/L to 0.01 mg/L, influenced by industrial effluents such as those from the textile sector (Abdel-Baki *et al.,* 2011; Mwegoha & Kihampa, 2010). By contrast, Cr levels in Nairobi River water averaged 0.02 mg/L, staying within the recommended limit of 0.05 mg/L for drinking water, making it suitable for domestic use regarding Cr content (Njuguna *et al.,* 2017).

Iron (Fe)

Iron having a density of 7.9g/cm^3, is one of the most abundant elements on Earth that is majorly produced through fusion in high mass stars and forms most of the earth's outer and inner core, making up about 5% of the Earth's crust (Frey & Reed, 2012). It ranks as the fourth most abundant element and the second most abundant metal, after aluminum. Iron occurs naturally in various forms, including in ores such as hematite (Fe_2O_3), magnetite (Fe_3O_4), limonite ($FeO(OH)\cdot nH_2O$), and siderite ($FeCO_3$). These ores are typically mined for use in the production of iron and steel. Iron is also a key component of Earth's core and is present in trace amounts in soil, water and biological systems. In aquatic environments, iron exists primarily in two oxidation states: ferrous iron (Fe^{2+}), which is soluble in water, and ferric iron (Fe^{3+}), which tends to form insoluble hydroxides and oxides. The concentration of iron in natural waters is influenced by factors such as pH, redox (reduction oxidation) conditions, and the presence of organic matter (Lasheen *et al.,* 2008).

Iron is essential in various industries including construction and manufacturing where it is used in steel production for building structures, vehicles and machinery. It also has a biological significance where it plays a vital role in living organisms, being a key component of hemoglobin in red blood cells and myoglobin in muscles, both crucial for oxygen transport and storage. In addition, iron is used in water treatment and as a coagulant to remove impurities. Iron is an essential trace element for human health, but both its deficiency and excess can cause significant health problems. Iron

deficiency can lead to anemia, condition characterized by reduced hemoglobin levels, leading to symptoms such as fatigue, weakness, shortness of breath and pale skin. In children, iron deficiency can cause delayed cognitive and physical development. Iron deficiency also causes impaired immune function where the body's ability to fight infections is reduced. Common causes of iron deficiency include poor dietary intake, chronic blood loss (e.g., gastrointestinal bleeding or heavy menstruation) and increased requirements during pregnancy or growth spurts (Abbaspour *et al.,* 2014).

Excessive iron in the body, a condition known as iron overload or hemochromatosis, can lead to damage of organs such as the liver, heart and pancreas. This can cause conditions like cirrhosis, diabetes and heart failure. Excess iron can catalyze the formation of free radicals, leading to cell and tissue damage. Excess iron can also cause joint problems resulting to result in arthritis. Though iron is not considered highly toxic, high concentrations of iron in water can lead to taste and staining issues and harm aquatic ecosystems by promoting eutrophication. Excessive iron in soils can inhibit plant growth and nutrient uptake (Dev & Babitt, 2017).

Arsenic (As)

Arsenic is a naturally occurring element found in the Earth's crust. It is typically present in trace amounts in soil, water and air, and often occurs in combination with other elements, particularly sulfur forming arsenic minerals such as arsenopyrite (FeAsS)**,** realgar (As_4S_4) and orpiment (As_2S_3)**.** Arsenic is also found in small amounts in coal, oil and other fossil fuels. It can leach into groundwater, leading to elevated levels in drinking water, particularly in geographic regions with arsenic-rich minerals. Arsenic has a density of 5.727 g/cm^3**,** making it relatively heavy compared to many other elements, although lighter than metals like lead and copper (Reis & Duarte, 2019).

Some notable uses of arsenic include wood preservation to protect against rot, pests and fungi. However, due to its toxicity, this use has been reduced, especially in residential areas. Arsenic is used in the production of semiconductors, particularly in gallium arsenide (GaAs), which is a critical material for high-speed electronic devices such as microchips and solar cells. Arsenic is used in small amounts in certain alloys,

such as lead alloys to improve their durability and resistance to corrosion. Arsenic is used in the production of glass to improve the glass's clarity and to remove bubbles during the manufacturing process.

Arsenic is highly toxic to humans and poses serious health risks even at low exposure levels. Its health effects depend on the form and level of exposure (organic vs. inorganic arsenic), the duration of exposure and the route of entry (inhalation, ingestion, or dermal contact). Ingestion or inhalation of high levels of arsenic can result in acute arsenic poisoning, which may cause nausea, vomiting, abdominal pain, diarrhea, shock and death in extreme cases, usually from multi-organ failure. Long-term exposure to lower levels of arsenic can cause severe health issues, including cancers of the skin, lungs, liver, kidneys and bladder. Prolonged exposure to arsenic has also been associated with an increased risk of cardiovascular diseases, including hypertension and arterial damage. Arsenic toxicity may cause neurological problems such as nerve damage leading to headaches, confusion and memory loss. Arsenic exposure during pregnancy can affect fetal development, leading to birth defects, low birth weight and developmental delays (Hong *et al.,* 2014).

The most significant health risk arises from arsenic-contaminated drinking water, particularly in regions with natural arsenic-rich groundwater. Prolonged consumption of contaminated water can lead to various chronic diseases, including cancer. The World Health Organization has set a guideline limit of 0.01 mg/L (10 ppb) for arsenic in drinking water due to its carcinogenic and toxic effects at higher levels. Arsenic levels in food and soil are regulated to minimize exposure through dietary intake. Foods such as rice, which tends to accumulate arsenic more than other grains, have been a focus of concern (Navas-Acien & Nachman, 2013).

Copper (Cu)

Cu is a reddish-brown metal with a high thermal and electrical conductivity, making it one of the earliest metals used by humans. It is the 26th most abundant element in Earth's crust, occurring at about 50 ppm. Copper is found both in its native state (as pure metal) and in minerals such as: chalcopyrite ($CuFeS_2$)**,** malachite ($Cu_2CO_3(OH)_2$)**,** azurite ($Cu_3(CO_3)_2(OH)_2$) and Bornite (Cu_5FeS_4). Cu is extracted from its ores. It is

commonly found in association with other metals such as Zn, Pb and Ni. Cu has a density of 8.96 g/cm³, making it relatively heavy compared to many other metals (Henckens & Worrell, 2020). This property contributes to its durability and utility in industrial applications. Cu is an excellent conductor of electricity, making it essential for wiring, cables and electrical components. Cu is used in plumbing, roofing and architectural structures due to its durability and corrosion resistance. Cu forms important alloys like brass (copper and zinc) and bronze (copper and tin), used in various industries. Cu is used in automotive radiators, brake systems and electric vehicle components. Copper sulfate is widely used as a fungicide and pesticide in agriculture. Cu compounds are used in pigments and catalysts. Cu has antimicrobial properties, making it useful in medical equipment, surfaces and water treatment. Cu is an essential trace element for humans, playing a crucial role in various physiological processes such as formation of red blood cells, maintenance of healthy bones, blood vessels and nerves. Cu leaching from corroded pipes into drinking water can lead to elevated Cu intake (Bost *et al.,* 2016).

Cu deficiency is rare but can result in anemia (due to impaired iron metabolism), weakness and fatigue, osteoporosis and bone abnormalities. Excessive Cu exposure can lead to toxicity, with symptoms varying based on the duration and level of exposure. Acute toxicity symptoms include nausea, vomiting, abdominal pain, and diarrhea. Long-term exposure, often from contaminated water, may cause liver and kidney damage. Neurological effects include headaches, dizziness, and cognitive dysfunction (Kumar, 2006). The World Health Organization recommends a maximum Cu concentration of 2 mg/L in drinking water.

2.12 Water Quality

Water quality is heavily influenced by the presence and concentration of various metals. While some metals are essential micronutrients for biological life, others, particularly heavy metals, can become potent pollutants at elevated concentrations, posing significant risks to ecosystems and human health. Metals enter water bodies through a diverse range of natural and anthropogenic pathways. Natural sources include weathering of rocks and soils, volcanic activity, and geothermal processes, which release metals like Fe, Mn, and even trace amounts of arsenic into water systems (Briffa *et al.,* 2020). However, human activities often exacerbate metal loading in

aquatic environments. Industrial discharges from mining operations, metallurgy, electroplating, and chemical manufacturing are major contributors of heavy metals such as Pb, Cd, Cu, Zn, Ni, and Cr (Vardhan *et al.,* 2019). Agricultural runoff, carrying pesticides and fertilizers, can introduce metals like Cu and Zn, while urban runoff from roads and impervious surfaces can transport metals from vehicle wear, brake pads, and atmospheric deposition (Saravanan *et al.,* 2024). Additionally, inadequate wastewater treatment and the leaching from waste disposal sites can further contribute to metal contamination in surface and groundwater.

Once introduced into water, the behavior of metals is complex and influenced by various physicochemical parameters, including pH, presence of organic matter, and the concentration of other ions. Metals can exist in different chemical forms, or "species," such as free ions, complexes with organic or inorganic ligands, or adsorbed onto suspended particles. Speciation dictates a metal's solubility, mobility, and bioavailability, directly impacting its toxicity. For instance, Cr(III) is less mobile and generally less toxic than Cr(VI), which is highly soluble and readily taken up by organism (Prasad *et al.,* 2021). Similarly, the mobility of As is highly sensitive to redox conditions. The impact of elevated metal concentrations on water quality is multifaceted. Environmentally, metals can be acutely toxic to aquatic organisms, disrupting their physiological processes, growth, and reproduction. Chronic exposure can lead to bioaccumulation, where metals concentrate in organisms over time, and biomagnification, where concentrations increase up the food chain, eventually affecting top predators, including humans who consume contaminated fish or other aquatic products (Dey *et al.,* 2024).

2.13 Permissible Limits of Heavy Metals in Drinking Water

Aquatic environments are polluted with significant amounts of heavy metals from both natural deposits and human activities (Hama Aziz *et al.,* 2023). Human activities such as industrial and municipal wastewater, along with non-point source runoff, are the primary contributors of metals to rivers. The introduction of heavy metals into aquatic systems can lead to shifts in both species diversity and ecosystem structure, primarily because of their toxic nature and capacity for bioaccumulation (Al-Weher, 2008). The presence of dissolved heavy metals in water presents a danger to the public, particularly those who use it for drinking or irrigation. The use of such water for

agricultural purposes facilitates the entry of heavy metals into the food chain, leading to their subsequent ingestion by humans (Hama Aziz *et al.,* 2023).

Different regulatory bodies and countries have established varying permissive limits for heavy metals in drinking water, measured in mg/L. The U.S. Environmental Protection Agency (USEPA) sets limits for Cadmium (Cd) at 0.005, Chromium (Cr) at 0.1, Manganese (Mn) at 0.05, Lead (Pb) at 0.01, and Zinc (Zn) at 5 (Ab Razak et al., 2015). The European Union (EU) also allows 0.005 for Cd, along with 0.05 for both Cr and Mn, and 0.01 for Pb, but has no specified limit for Zn (World Health Organization, 2011). The World Health Organization (WHO) has established limits of 0.003 for Cd, 0.05 for Cr, 0.4 for Mn, 0.01 for Pb, and 3 for Zn (World Health Organization, 2011). In contrast, the Iranian limits are 0.01 for Cd, 0.05 for Cr, 0.5 for Mn, and 0.05 for Pb, with no set value for Zn (Alidadi et al., 2019).

2.14 Principal Mechanism of Microwave Plasma Atomic Emission Spectroscopy (MP-AES)

There are various methods of analyzing heavy metal concentrations, including Inductively Coupled Plasma Mass Spectroscopy (ICP-MS), Flame Atomic Absorption Spectroscopy (AAS), Inductively Coupled Plasma Atomic Emission Spectroscopy (ICP-AES) and Microwave Plasma Atomic Emission Spectroscopy (MP-AES). For this study, MP-AES was used due to its extra sensitivity and low cost of operation. MP-AES uses cheap consumables such as hollow cathode lamps since it is an atomic emission technique (Balaram, 2020). The MP-AES equipment consists of several key components that work together to generate a microwave plasma, analyze emitted light and quantify elemental concentrations.

The process begins with the microwave source, typically a magnetron, which generates high-energy microwave radiation, often at 2.45 GHz. This radiation is crucial for creating the plasma. The plasma torch is where the sample is introduced and atomized. It usually consists of a quartz tube surrounded by a coil, through which argon gas flows. When the microwave energy is focused into this chamber containing low-pressure argon gas, it causes the gas molecules to ionize, forming a high-temperature (exceeding 6000K) optically transparent plasma. The sample introduction system then precisely delivers the sample into this plasma torch. Depending on

whether the sample is solid or liquid, different methods are employed. Solid samples are atomized and converted into an aerosol or vapor via a nebulizer before entering the plasma, while liquid samples are typically aspirated using a peristaltic pump or an auto-sampler. Once the sample is in the plasma, it emits light. The optical emission spectrometer acts as the detection system, analyzing this emitted light. It uses a diffraction grating or prism to disperse the light into its individual wavelengths. A photodetector, such as a photomultiplier tube, then measures the intensity of the light at specific wavelengths, which correspond to the unique elemental transitions of interest (W. Li *et al.,* 2013).

The data acquisition and processing system transforms the raw light signals into meaningful analytical results. This sophisticated system acts as the central hub, meticulously collecting and analyzing the spectral data streamed from the optical emission spectrometer. The system typically features advanced software designed to manage every aspect of the analysis, including precise instrument control for optimal data collection. Once the light emitted by the plasma is captured, the software takes over for spectral data acquisition, converting the light intensity at various wavelengths into digital information. Significantly, the system performs quantitative analysis, translating these spectral signatures into actual elemental concentrations. This is often achieved by comparing the acquired data against calibration curves or reference standards. Beyond just numbers, the system is also equipped with powerful tools for data visualization, allowing scientists to easily interpret complex spectral patterns. Furthermore, it facilitates comprehensive interpretation of results and generates detailed reports, providing a clear summary of the elemental composition of the analyzed sample. This system converts light into actionable insights, making it indispensable for precise and reliable MP-AES analysis (Jung *et al.,* 2019).

MP-AES offers significant advantages over other spectroscopic techniques. These include high sensitivity, low detection limits, and the capability to simultaneously analyze a wide range of elements. Additionally, it requires minimal sample preparation compared to methods like Inductively Coupled Plasma Optical Emission Spectroscopy (ICP-OES) or Inductively Coupled Plasma Mass Spectrometry (ICP-MS), making it a more efficient and user-friendly option for various analytical applications.

2.15 Related Studies on Radioactivity and Heavy Metal Concentrations

To avert health problems that may arise from radionuclides in water bodies such as lakes and oceans, there is need to study concentration levels of radionuclides in the water bodies. This can be done analyzing activity concentrations in sediment and water samples.

Average radionuclides activity concentration values in water of Tigris river in Iraq were found to be (315.6, 30.8, 12.04, and 509.2) Bq/L for ^{226}Ra, ^{212}Pb, ^{137}Cs and ^{40}K respectively. The study also found an average outdoor effective dose of 0.911mSv/y (Al-Hayani *et al.,* 2021). A study done at an ex-mining site at Kolej University Islam Antarabangsa Selangor lake in Malaysia found average activity concentrations in water of (0.44 ± 0.31) Bq/L, (0.04 ± 0.02) Bq/L, (0.19 ± 0.11) Bq/L, (0.62 ± 0.37) Bq/L for ^{238}U, ^{232}Th, ^{226}Ra and ^{40}K respectively. The water was declared safe for drinking since the radionuclide activity concentration values obtained were low hence could pose no significant hazards to users. Of the heavy metals that were studied, zinc had the highest concentration of (17.34 ± 15.79) mg/kg in the sediments and arsenic had the highest concentration of (0.58 ± 0.26) µg/L in water (Radzali *et al.,* 2018). Samples of beach sediments collected from beach sediments of north east coast of Tamilnadu, India had their activity concentrations determined by gamma ray spectrometry with multivariate statistical approach. The range and average activity concentration resulting from the singly occurring ^{40}K in the samples was found to be 250.9–560.4 Bq/kg and 349.60 Bq/kg respectively. The average calculated annual effective dose was 0.621 mSv (SureshGandhi *et al.,* 2014).

Radionuclide concentration levels of NORM were measured in Mombasa, Malindi and Gazi along the Kenyan coast. Mombasa was found to have the highest concentration levels of (22.8 ± 1.8) Bq/kg for ^{238}U, (26.2 ± 1.7) Bq/kg for ^{232}Th and (479.8 ± 24.2) Bq/kg for ^{40}K. The average annual effective dose rate in Mombasa was (0.12 ± 0.01) mSv (Hashim *et al.,* 2004). The average natural radioactivity concentrations and absorbed dose-rates of radionuclides ^{40}K, ^{238}U and ^{232}Th in air were determined from soil samples collected from Mrima hills. The activity concentration values gave an annual absorbed dose rate of (441 ±17) nGy/h (Kebwaro *et al.,* 2011). A study done at Kargi area of Marsabit county in Kenya found mean values of

activities for ^{40}K of 52.68±25.07 Bq/l, for ^{232}Th the mean activity value was 2.20±2.74 Bq/l and ^{226}Ra had a mean value of 3.55±3.04 Bq/l (Aguko *et al.,* 2020).

Sand samples were collected from sand mines at the estuaries of the Kuja and Migori Rivers, as well as several smaller streams in Migori County. Analysis of these samples revealed average activity concentrations of 64.5 ± 3.3 $Bqkg^{-1}$ for ^{238}U, 146.0 ± 4.4 $Bqkg^{-1}$ for ^{232}Th, and 1222.8 ± 43.3 $Bqkg^{-1}$ for ^{40}K. The average absorbed dose rate from these sites was 171.2±3.4 nGy/h, with a range of 123 ± 2.4 to 236 ± 4.8 nGy/h. The annual effective dose rates for gamma radiation ranged from 0.302 ± 0.006 mSv/y to 0.579 ± 0.012 mSv/y. The study also calculated average internal and external hazard indices, which were 0.99 ± 0.02 and 1.17 ± 0.02 respectively (Okelo, 2015).

Water and sediment samples from dams in Tunisia and Algeria were analyzed. The mean radioactivity rates in the Tunisian dam water were 1.72 $Bq \cdot L^{-1}$ for ^{238}U, 0.068 $Bq \cdot L^{-1}$ for ^{232}Th, and 94.6 $Bq \cdot L^{-1}$ for ^{40}K, while Algerian dam water samples showed slightly higher rates of 1.9 $Bq \cdot L^{-1}$ for ^{238}U, 0.09 $Bq \cdot L^{-1}$ for ^{232}Th, and 131.43 $Bq \cdot L^{-1}$ for ^{40}K. In sediment samples, the Tunisian dam had mean activity concentrations of 2.67 $Bq \cdot kg^{-1}$ for ^{238}U, 0.18 $Bq \cdot kg^{-1}$ for ^{232}Th, and 197.87 $Bq \cdot kg^{-1}$ for ^{40}K, whereas the Algerian dam sediment had higher concentrations of 4.34 $Bq \cdot kg^{-1}$ for ^{238}U, 0.27 $Bq \cdot kg^{-1}$ for ^{232}Th, and 287.61 $Bq \cdot kg^{-1}$ for ^{40}K. Across both locations and sample types, ^{40}K consistently showed the highest activity concentration, followed by ^{238}U and then ^{232}Th (Hamed et al., 2024).

The concentrations and spatial distribution of naturally occurring radionuclides, specifically ^{238}U, ^{232}Th, and ^{40}K, were determined at Luilu and Dilala rivers, both located in the mining district of Kolwezi in the Lualaba Province of the Democratic Republic of Congo. The average concentrations of ^{238}U, ^{232}Th, and ^{40}K in the analyzed samples from the Luilu river were 154 ± 6 $Bq \cdot kg^{-1}$, 28 ± 2 $Bq \cdot kg^{-1}$and 211 ± 76 $Bq \cdot kg^{-1}$ respectively, while for the Dilala river, they were 378 ± 13 $Bq \cdot kg^{-1}$, 30 ± 6 $Bq \cdot kg^{-1}$, and 95 ± 13 $Bq \cdot kg^{-1}$ respectively (Atibu et al., 2021).

The concentrations of ^{238}U and ^{232}Th were determined in water and sediment samples from an environment affected by amang processing. The maximum activity concentration of uranium was 78.53 $Bq \cdot L^{-1}$ in water and 860.57 $Bq \cdot kg^{-1}$ in sediment,

while the maximum activity concentration of thorium was 6.90 $Bq \cdot L^{-1}$ in water and 637.61 $Bq \cdot kg^{-1}$ in sediment. The study found that concentrations of both radionuclides were consistently higher in sediment than in water. Furthermore, radionuclide concentrations were elevated in sediments from ponds that used a closed water recycling system compared to those from open water systems (Nasirian et al., 2008).

A study investigated the activity concentrations of ^{40}K, ^{232}Th, and ^{238}U in 26 river sediment samples collected from eleven oil-producing and two non-oil producing communities in Nigeria's Delta State. Using a High Purity Germanium (HPGe) detector for radionuclide analysis, the study found that radioactivity concentrations in sediments from oil-producing areas averaged 302.15 $Bq \cdot kg^{-1}$ for ^{40}K, 11.66 $Bq \cdot kg^{-1}$ for ^{232}Th, and 8.66 $Bq \cdot kg^{-1}$ for ^{238}U. The radiological assessment indices were within permissible limits, indicating a negligible radiation hazard (Iwetan et al., 2015).

Using gamma-ray spectrometry with a high-purity germanium (HPGe) detector, the activity concentrations of ^{226}Ra, ^{232}Th, and ^{40}K were determined in six fish samples collected from the Shatt Al-Arab River in southern Iraq. The concentrations of ^{226}Ra ranged from 0.86 ± 0.21 $Bq \cdot kg^{-1}$ to 6.41 ± 0.81 $Bq \cdot kg^{-1}$ with an average of 2.79 ± 0.61 $Bq \cdot kg^{-1}$. For ^{232}Th, concentrations varied from 1.18 ± 0.17 $Bq \cdot kg^{-1}$ to 5.69 ± 0.13 $Bq \cdot kg^{-1}$, averaging 3.23 ± 0.44 $Bq \cdot kg^{-1}$. The highest concentrations were observed for ^{40}K, ranging from 86.34 ± 18.21 $Bq \cdot kg^{-1}$ to 120.21 ± 28.74 $Bq \cdot kg^{-1}$ with an average of 101.52 ± 19.06 $Bq \cdot kg^{-1}$. The study's findings indicate that the measured radionuclide concentrations in these fish samples were higher than globally reported values (Aswood et al., 2018).

Concentrations of six metals in water and the edible tissue of Tilapia (Oreochromis niloticus) and Barbus (Labeobarbus intermedius) fish species from Lakes Chamo and Abaya were determined using Flame Atomic Absorption Spectroscopy. The results revealed that the average heavy metal concentrations in water samples were; 0.017 mg/L, 0.077 mg/L, 7.50 mg/L, 0.033 mg/L, 0.264 mg/L and 1.731 mg/L for Zn, Cu, Fe, Cr, Cd and Pb respectively. The average concentration of heavy metals in fish samples were; 0.062 mg/kg, 0.047 mg/kg, 2.270 mg/kg, 0.041 mg/kg, 0.045 mg/kg and 1.78 mg/kg for Zn, Cu, Fe, Cr, Cd and Pb respectively in both fish species (Dugasa & Endale, 2019).

A study on wastewater in Central Ethiopia's Eastern industrial zone measured the levels of heavy metals and their potential toxicity. The results showed that the concentrations of all measured metals (Cr, Cd, Zn, Fe, Pb, and Cu) were above the recommended limits from both the WHO and FAO. The specific concentration ranges (in mg/L) found were: Cr (0.20-1.04), Cd (0.04-0.08), Zn (0.07-0.21), Fe (2.89-5.15), Pb (3.11-45), and Cu (0.30-0.99) (Dagne *et al.,* 2019).

2.16 Study Area

The Lake Turkana Basin is situated within the geographical coordinates of approximately 35° 45 minutes to the east and 36° 48 minutes to the east longitude and latitudes 2° 25 minutes to the north and 4° 38 minutes to the north latitude as illustrated in figure 3.1. The lake lies within the northern Kenya Rift Valley, extending into Ethiopia at its furthest northern point. To the west of Lake Turkana is Turkana County and to the East is Marsabit county. Its area size is 6405 km^2 with a shore line of about 240 km and a maximum depth of about 120 m. The rock formations in the Turkana basin are mainly composed of granite, tuffs, gneisses and limestone. The island at the center of the Lake is a live volcano that releases vapor. South of the lake is the volcanic Mt. Nyiru constituting of an area that is composed of numerous lava flows that form a series of terraces that lead into the lake. To the south eastern part of the lake there are two volcanic complexes namely mount Kulal and Longipi hills from which eroded soils form the Lake Turkana marginal sediments at Loiyangalani, El Molo and Pori towns. To the western part of River Kerio are deeply eroded volcanic rocks that form the Chibelet, Emuruabwin and Kaling basalts. They all deposit their sediments into river Kerio which eventually deposits them at the low lying Kerio plains and into the lake. The lower region of river Turkwel is also a plain full of deposits of sediments from higher lying mountains to the west of the lake. The Auwerwer basalts have a thickness of approximately 300 meters and are accompanied by thinly interbedded sediments. Overlying the lavas are recent layers of sand and gravel. The Pliocene-recent sediments in the area comprise various rock deposits such as alluvium, recent basalts and ashes. The Turkana rift's subsidence has triggered the deposition of these sediments along the pre-existing drainage networks in the region. Newer sedimentary layers are found on top of volcanic rocks. These layers are composed of unorganized, large-grained (reaching boulder size) matrix-supported

sandstones and mixes with extensive erosional surfaces that span hundreds of meters. The deposits are believed to represent alluvial fan sediments that were formed in close proximity to their source (Feibel, 2011).

In the northern region of the Lokichar basin, there is a collection of rock formations consisting of various types, such as volcanic sandstones, arkosic sandstones, altered mafic tuffs and trachytic tuffs. These rocks overlay Oligocene-Miocene basalts which in turn are covered by Miocene-Pleistocene volcanic materials and sediment layers. The entire formation has a substantial thickness, measuring 580 meters. These rocks were formerly known as Turkana grits (Feibel, 2011)

The water volume of Lake Turkana is largely contributed by the Omo River from Ethiopia which contributes over 90% while the Kerio and Turkwel rivers collectively contribute less than 10%. The Omo catchment is made up of approximately 68% volcanic deposits, along with 25% alluvial deposits and a portion of granite deposits. A cartographic representation of the study area is shown in Figure 2.7.

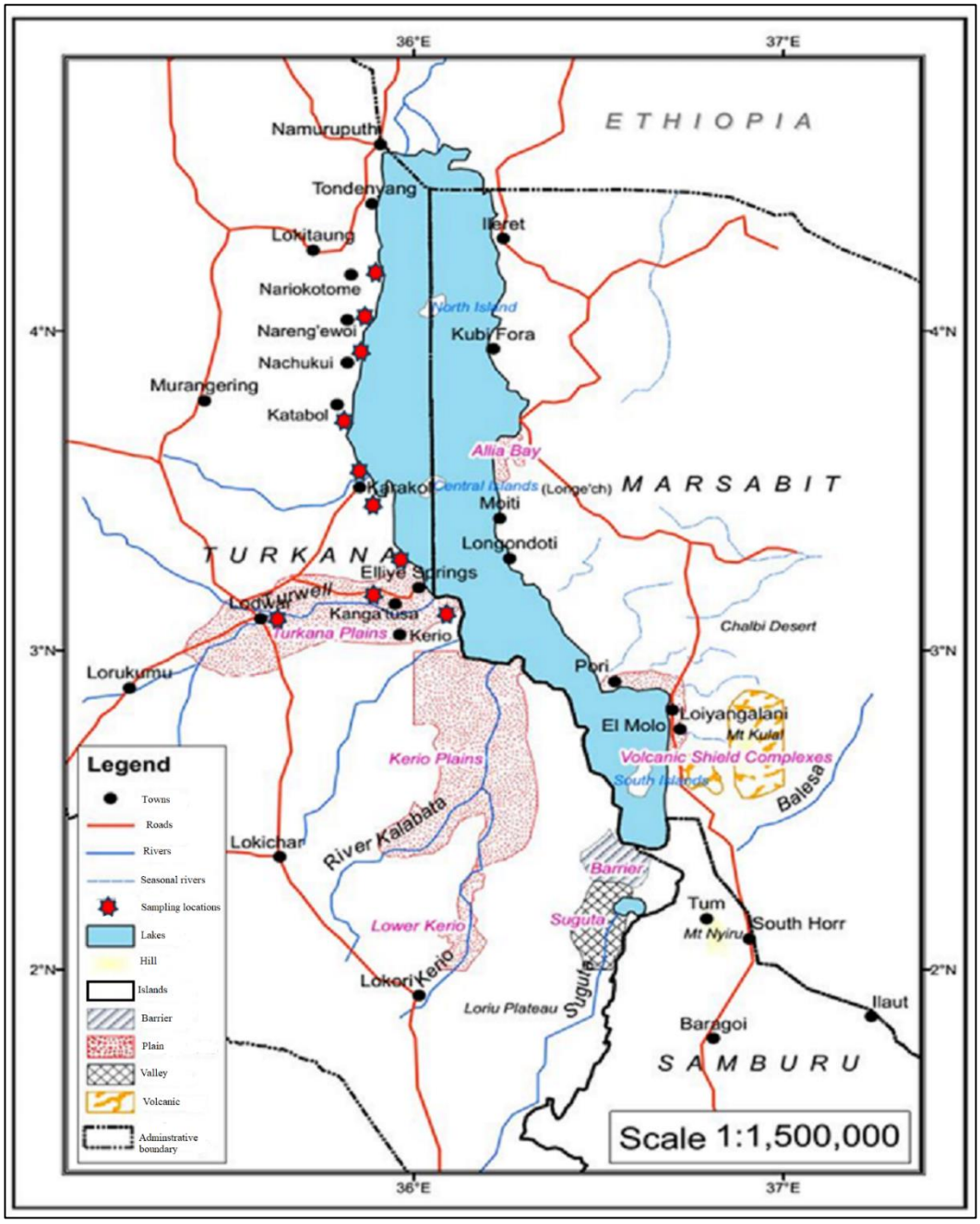


Figure 2.7: A cartographic representation of the Lake Turkana basin displaying the rivers that drain into the lake, settlements and other geological features in the basin.

2.17 Common Fish Species Found in Lake Turkana

Lake Turkana, despite its arid surroundings, is a significant aquatic ecosystem in Kenya, hosting a diverse fish fauna. It is estimated to harbor around 79 fish species, with a notable number, approximately 10 to 12, being endemic to the lake, meaning they are found nowhere else in the world. Among the commercially important species, the Nile perch (*Lates niloticus*), various tilapia species, particularly the Nile tilapia (*Oreochromis niloticus*), and African Catfish *(Clarias gariepinus)* are prominent (Obiero *et al.,* 2023).

2.17.1 Nile Perch *(Lates niloticus)*

The Nile perch (*Lates niloticus*) is a freshwater fish indigenous to several African regions. It holds substantial ecological and economic significance, particularly in East Africa, though its introduction into non-native habitats has triggered considerable ecological disruption. The Nile perch belongs to the family Latidae, formerly categorized under Centropomidae, and falls under the order Perciformes. This striking fish is typically silvery with a blue tint, featuring distinct dark-black eyes encircled by a bright yellow ring. Its body is elongated, boasting a large, protrusible mouth and a prominent lower jaw lined with numerous villiform teeth. It possesses two dorsal fins and a rounded caudal, or tail, fin. As one of the largest freshwater fish species, it can reach nearly 2 meters (6 ft 7 in) in length and weigh up to 200 kg. While many are caught before reaching this maximum size, mature individuals commonly measure between 1.21 and 1.37 meters (Barlow & Lisle, 1987)

Naturally, the Nile perch is widely distributed across much of the Afrotropical realm, found in the Congo, Nile (below Murchison Falls), Senegal, Niger, Volta, and Lake Chad basins, as well as Lake Turkana. Adults generally prefer deeper waters with adequate oxygen levels, whereas juveniles typically reside in shallow or nearshore environments. The Nile perch is a formidable and adaptable predator, with a flexible diet that quickly adjusts to available prey (Olagbemide & Owolabi, 2023). Younger and juvenile Nile perch primarily feed on invertebrates such as zooplankton, crustaceans like *Caridina nilotica* prawns, and insects such as mayfly nymphs and odonate nymphs. As they mature, Nile perch become increasingly piscivorous, preying mainly on other fish species, including their own kind (cannibalism) (Aloo *et al.,* 2017). Their diet can also include molluscs and larger crustaceans. In introduced

environments such as Lake Victoria, they extensively prey on smaller native fish (Wanink & Goudswaard, 1994)

Nile perch exhibit high reproductive rates, particularly in warm, oxygen-rich waters. They can reproduce year-round in warm tropical areas, with spawning peaks often occurring during the rainy season. They typically favor shallow, sheltered nearshore waters for breeding (Dadebo *et al.,* 2006).

The Nile perch holds significant economic and food-security importance, especially in East Africa. Its introduction into Lake Victoria, despite its controversial nature, spurred a boom in the local fishing industry. It is highly valued for its white, flaky, and boneless meat, which is widely accepted in international markets across Europe, the Middle East, and Asia, making it a major export commodity for countries like Uganda, Tanzania, and Kenya (Asnake, 2018). Nile perch fishing industry supports livelihoods of thousands in the East African region, contributing substantially to local economies through fishing, processing (filleting factories), and trade. Furthermore, Nile perch meat is rich in protein and omega-3 fatty acids, offering considerable nutritional value, while its skin provides zinc, iron, calcium, lipids, and protein (Asnake, 2018).

2.17.2 Nile Tilapia (*Oreochromis niloticus*)

The Nile tilapia is one of the most widely recognized and extensively cultured freshwater fish species globally. Originating from Africa and the Middle East, its remarkable adaptability, rapid growth, and palatable flesh have led to its widespread introduction and significant role in aquaculture worldwide. The Nile tilapia, *Oreochromis niloticus*, belongs to the family Cichlidae. Natural Nile tilapia from the wild are usually brown or gray, and they often have faint, unclear bands on their sides and distinct, regular dark stripes on their caudal (tail) fin (Kpelly *et al.,* 2022). During the breeding season, males can become reddish, particularly on their fins. This species can grow to a maximum length of about 63 cm (25 in) and weigh up to 4.3 kg, with an average size of around 20 cm (8 in). It is closely related to, and sometimes confused with, the blue tilapia (*Oreochromis aureus*), but can generally be distinguished by the number of dorsal spines (16-18 for Nile tilapia vs. 15-16 for blue tilapia) and the distinct banding on its caudal fin (Kpelly *et al.,* 2022)

The Nile tilapia is native to tropical and subtropical Africa and the Middle East. Its natural range includes the Nile River basin including Lake Albert, Edward, and Tana, the Niger and Benue river basins, the Volta and Senegal rivers, and lakes Chad, Kivu, and Tanganyika. It is also found in various smaller drainages and lakes in western and eastern Africa, and in the Middle East, such as the Yarkon River in Israel. This species successfully inhabits a broad spectrum of freshwater environments, from flowing rivers and streams to stagnant ponds and reservoirs, and it can be found at altitudes reaching 1,830 m (6,000 ft) above sea level. While primarily a freshwater species, it can tolerate brackish water but cannot survive long-term in full saltwater. It has been recorded in water temperatures between 8 and 42 °C, although it typically prefers temperatures above 13.5 °C and has an upper lethal limit of around 39–40 °C (Munguti *et al.,* 2022). Recent studies have also explored its adaptability to varying environmental conditions within its native range, highlighting its broad ecological niche. Nile tilapia is highly valued in aquaculture because it can thrive in diverse environmental conditions, grow quickly, reproduce successfully, and adapt their feeding to various food sources. These very characteristics, however, also enable them to become exceptionally successful invasive species when introduced to new subtropical and temperate environments (Grammer *et al., 2012*)

Though primarily herbivorous, the Nile tilapia displays omnivorous behavior, especially in its early life. Its diet is centered on phytoplankton and algae, with macrophytes being a notable food source for some populations. Detritus, aquatic insects, and crustaceans have also been documented as part of its diet (Assefa & Getahun, 2015). Feeding typically occurs during the daytime, though nocturnal feeding can also be observed in crowded habitats, where it is often driven by the need to compete for limited food resources (Alzeny *et al., 2024*).

Nile tilapia are prolific breeders, a trait that contributes significantly to their success in aquaculture. They are maternal mouth brooders, meaning the female incubates the fertilized eggs and cares for the fry in her mouth (buccal cavity) until they hatch and are large enough to be released. Reproduction typically begins when water temperatures exceed 24°C. The breeding process starts with the male establishing and fiercely guarding a circular, crater-like spawning nest, often created by mouth-digging. After a short courtship, the female spawns her eggs in the nest, which are then

immediately fertilized by the male (Nyakuni, 2009). Nile tilapia can reach sexual maturity in as little as 5 to 6 months under good growth conditions in ponds, even at weights of 150-200 grams. A female can lay eggs every three to four months, with the number of eggs proportional to her body weight; a 100g female might produce around 100 eggs, while a 1kg female can produce 1,000 to 1,500 eggs (Munguti *et al.,* 2022). Males can fertilize eggs from a succession of females. This rapid and continuous reproduction is a key factor in their success in aquaculture but can also lead to overpopulation and stunting in ponds if not managed (Nyakuni, 2009).

2.17.3 African Catfish *(Clarias gariepinus)*

Clarias gariepinus belongs to the family Clariidae, known as air-breathing catfishes. It is considered one of the most widely distributed fish in Africa. Due to its suitability for aquaculture, it has been widely introduced to many countries outside its native range, including Brazil, Vietnam, Indonesia, and India (DiEnye *et al.,* 2021). This species is incredibly adaptable and can be found in a wide variety of freshwater environments, including lakes, rivers, streams, swamps, and temporary floodplains. They are particularly tolerant of turbid waters and low dissolved oxygen levels, often being one of the last or only fish species to survive in remnant pools of drying rivers. They prefer calm, shallow, swampy areas with soft, muddy substrates, but can also be found in fast-flowing rivers and rapids.

Clarias gariepinus is a large, elongated fish with an eel-like body. Adults typically reach 1 to 1.5 meters in length, with a maximum recorded length of 1.7 meters and a weight of up to 60 kg. Their coloring is typically dark grey or black dorsally (on the back), fading to a cream or white belly. Adults may have a dark longitudinal line on either side of the head. A defining characteristic is their well-developed accessory breathing organ, often referred to as "pseudo-lungs," which are modified gill arches. This organ allows them to breathe atmospheric air directly, enabling survival in oxygen-depleted waters or even out of water for extended periods (Dessie *et al.,* 2024).

Clarias gariepinus has a wide diet, and is generally considered an opportunistic, omnivorous predator. Their diet varies with size and availability of prey. Juveniles primarily consume zooplankton and chironomids (FAO: North African catfish - Natural food and feeding habits). Adults feed on a diverse range of items including

insects, phytoplankton and zooplankton, various invertebrates (snails, crabs, shrimp), other fish, birds, reptiles, amphibians, small mammals, carrion, and plant matter like fruits and seeds. They are capable of swallowing relatively large prey whole due to their wide mouths and can even hunt in packs to herd and trap smaller fish. While typically bottom feeders, they can adapt to filter feeding at the water surface when food sources permit. They are primarily nocturnal feeders (Bruton, 1979).

Clarias gariepinus is a vital source of protein, especially in developing countries where animal protein can be scarce and expensive. Its cultivation contributes significantly to food security and helps address protein deficiencies (DiEnye *et al.,* 2021). Its popularity stems from several key attributes. They exhibit rapid growth rates and can attain a large size, leading to efficient biomass production (Aladetohun *et al.,* 2021). Their ability to tolerate low dissolved oxygen levels and varying water quality allows for high stocking densities in culture systems (El-Shebly, 2006).

2.18 Farming along the Turkwel River

Following Kenya's independence, a concise policy emerged to foster investment and development of the Turkana region, with both the new government and international organizations initiating ambitious programs to provide alternative ways of life for the Turkana community. This push was underpinned by a prevailing belief that severe events like droughts, raids, insecurity, and diseases were consequences of overstocking and desertification, a perspective that promoted destocking and the relocation of impoverished herders (Catley *et al.,* 2013).

The profound effects of drought served as a catalyst for planners to champion a transition from a pastoralist way of life to one based on irrigated agriculture and fishing. It was believed that irrigated farming would offer a stable livelihood and encourage settlement which would facilitate the delivery of essential government services like clean water, healthcare, and education. Intriguingly, planners considered irrigation a "privileged" technological solution, often overlooking existing local knowledge and practices. Despite this, East Africa was not wholly unfamiliar with the practice of irrigation; for instance, the Turkana themselves had a simple indigenous irrigation practice of cultivating sorghum in the Kerio and Turkwel River floodplains (Akall, 2021).

From 1966 to 1978, Turkana launched small-scale irrigation projects with the goal of reducing food aid dependency and boosting fishing, restocking, and land restoration efforts. The widespread belief was that irrigation held immense potential for helping locals adapt to drought and strengthen food security and resilience, with pastoralists envisioned primarily as operators of these schemes (Catley, *et al.,* 2013). A significant development occurred in 2013 when United Nations Educational, Scientific, and Cultural Organization (UNESCO) identified two vast underground water aquifers in the Lotikipi plains and near Lodwar, whose reserves were estimated to be sufficient to supply the entire country of Kenya for 70 years (Akall, 2021).

Farming along the Turkwel River, represents a crucial attempt to diversify livelihoods and enhance food security in a predominantly arid and semi-arid region historically reliant on pastoralism (Francis Ekiru, 2023). Despite the challenging climatic conditions characterized by low and erratic rainfall, the Turkwel River offers a vital water source for irrigation, supporting several schemes along its banks. Numerous small-scale irrigation projects in the region rely on the Turkwel River water or connected shallow boreholes. As of 2013, the total irrigated area was estimated at 18 square kilometers (Hirpa *et al.,* 2018) and it has continued to grow since then. Irrigation schemes such as Katilu, Namakat, Nawepeto, Natuntun, Napak, Napool, and Nadapal utilize water from the Turkwel River to cultivate a range of crops, including maize, sorghum, green grams, groundnuts, cowpeas, and various vegetables and fruits like pawpaw, apple mangoes, and watermelons. The introduction of crops like groundnuts has been particularly transformative, contributing to improved soil fertility, diversified incomes, and enhanced household nutrition (FAO in Kenya, 2025).

However, farming along the Turkwel River faces numerous challenges. Climate change impacts, such as increased temperatures and altered precipitation patterns lead to unpredictable water availability, with the river experiencing both shrinking dry periods and sudden flash floods (Akuja & Kandagor, 2019). The Turkwel Gorge Dam, while providing hydroelectric power, also presents complexities in water management, impacting downstream flows crucial for irrigation. Despite these hurdles, ongoing efforts by government bodies and non-governmental organizations aim to enhance irrigation infrastructure, provide farmer training, and promote climate-smart

agricultural practices to build resilience and improve livelihoods in the Turkwel River Basin (FAO in Kenya, 2025).

Two crops of particular importance in the current study are Cassava *(Manihot esculenta)* and Sorghum (*Sorghum bicolor* (L.). Cassava is a versatile perennial woody shrub recognized globally as a vital staple food, particularly in tropical and subtropical regions (Irunkwor *et al.,* 2023). Originating from tropical America, it was introduced to Africa by the Portuguese around 1558 and has since become a cornerstone of food security and economic sustenance for millions, especially in sub-Saharan Africa. The plant is primarily cultivated for its starchy, tuberous roots, which grow in clusters at the base of the stem, typically ranging from 1 to 4 inches in diameter and 8 to 15 inches in length, though some can grow significantly larger.

Nutritionally, cassava roots are primarily a rich source of carbohydrates, with starch content ranging from 25% to 30% of their fresh weight. They are, however, notably low in protein (typically 0.7% to 1.3% fresh weight) and lipids. The protein content of cassava flour, peels, and leaves is also relatively low, necessitating supplementation, particularly with amino acids like methionine and lysine, when cassava forms a major part of the diet (Ola & Adedayo, 2020). Despite their caloric density, cassava tubers and leaves also contain anti-nutritional substances, prominently cyanogenic glycosides, which can release toxic hydrogen cyanide upon consumption. Other anti-nutrients include oxalate and phytate. This necessitates proper processing methods to reduce or eliminate these toxic compounds before consumption (Ola & Adedayo, 2020).

Sorghum is a vital annual grass and one of the world's top five cereal crops, originating in Africa and crucial for food security in arid and semi-arid regions. This resilient plant, growing 1 to 4 meters tall with a dense grain-bearing panicle, is exceptionally tolerant to drought and heat, due to its deep root system and water-conserving waxy leaves. It also thrives in diverse, often marginal, soil conditions including those with low fertility, salinity, and acidity (Hossain *et al.,* 2022).

Nutritionally, sorghum grains are a valuable energy source, rich in starch, and provide a good amount of protein (8-12%), along with beneficial dietary fiber. It is naturally

gluten-free, making it suitable for those with sensitivities, and contains essential micronutrients like iron, zinc, magnesium, and vitamins B (Thilakarathna *et al.,* 2022). Sorghum's versatility extends to various uses beyond direct human consumption, where it's processed into flours for traditional foods, porridges, and fermented products, and used in brewing. It serves as a significant and cost-effective feed grain for livestock, and its starch finds applications in industries like textiles and paper. Furthermore, specific varieties are cultivated for biofuel production, particularly ethanol, due to their high biomass and sugar content. This multifaceted nature positions sorghum as a key crop for global food security, nutrition, and sustainable energy (Khoddami *et al.,* 2023).

2.19 Summary

The chapter presents a comprehensive examination of the theoretical and empirical literature relevant to the assessment of radioactivity and heavy metals in aquatic environments. The review establishes that ionizing radiation is an omnipresent natural phenomenon, contributing approximately 80% of the total radiation exposure to the global population. This natural background radiation, which carries a global average annual effective dose of 2.4 mSv, originates from both cosmic and terrestrial sources. Cosmic radiation consists of high-energy particles from space that interact with the Earth's atmosphere, while terrestrial radiation arises from primordial radionuclides embedded in the Earth's crust, such as ^{40}K, ^{238}U, and ^{232}Th. A critical focus is placed on Radon gas, which poses a significant health risk through inhalation, and the review distinguishes these natural sources from anthropogenic contributors such as nuclear power accidents (Chernobyl and Fukushima) and medical diagnostic procedures.

The mathematical foundation of the study is rooted in the fundamental law of radioactivity and the concept of secular equilibrium. The latter is a physical state where the activity of a long-lived parent radionuclide equals that of its short-lived daughters, a principle essential for gamma-ray spectrometry. This allows researchers to accurately quantify difficult-to-measure parent isotopes by analyzing the high-energy peaks of their progeny after a mandatory sealing period. The review further details the three primary decay mechanisms, namely; alpha, beta, and gamma, noting that while alpha particles have the highest ionizing power, gamma rays possess the greatest penetrating ability, necessitating specialized shielding and detection methods.

Understanding the interaction of gamma rays with matter is crucial for interpreting the data collected during this research. The literature identifies three primary interaction mechanisms: the photoelectric effect, Compton scattering, and pair production. The photoelectric effect is the ideal interaction for detection as it produces the "Full Energy Peaks" used to identify specific radionuclides. In contrast, Compton scattering creates a background continuum or noise in the spectrum that can mask low-energy emissions. Pair production, which occurs at energies above 1.022 MeV, is particularly relevant for measuring high-energy terrestrial isotopes like Thallium-208 (^{208}Tl). These physical principles are applied through the use of High Purity Germanium (HPGe) detectors, which are favored for their superior energy resolution and ability to separate closely spaced gamma-ray peaks.

The review then transitions to the chemical aspects of the study, focusing on the toxicity of heavy metals such as Lead, Cadmium, and Mercury within aquatic ecosystems. Unlike organic pollutants, heavy metals are non-biodegradable and undergo bioaccumulation and biomagnification through the food chain, posing severe risks to human health including neurological damage and organ failure. The operational principles of Microwave Plasma Atomic Emission Spectroscopy (MP-AES) are detailed as the primary method for detecting these metal concentrations. By synthesizing global regulatory standards and water quality limits, the chapter provides a benchmark for evaluating the safety of the study area.

Finally, the chapter contextualizes these scientific principles within the specific geographical and ecological scope of Lake Turkana and the Turkwel River. It identifies key fish species—Nile Perch, Nile Tilapia, and African Catfish as vital nutritional sources and primary indicators of environmental health for the local population. The inclusion of agricultural activities along the Turkwel River highlights the potential for anthropogenic runoff to introduce contaminants into the lake. By bridging the gap between nuclear physics and environmental toxicology, this literature review establishes the necessary framework for the radiological and chemical assessment of the Lake Turkana basin.

CHAPTER THREE
MATERIALS AND METHODS

3.1 Introduction

This chapter provides a comprehensive overview of the materials and methods employed in the study. For the geological and aquatic matrices, sediment samples were collected using mason's trowel, while surface water was gathered from Lake Turkana and the Turkwel River using 500 ml polyethylene bottles. These water samples were filtered through 0.45 μm filters for particulate removal and concentrated nitric acid for stabilization. Fish samples were sourced from local markets and transported in paper envelops, while agricultural products, specifically sorghum and cassava, were harvested using a stainless-steel knife.

The preparation of these materials involved laboratory-grade equipment including drying oven, and muffle furnace, analytical balances for precise mass determination, and electric pulverizes for homogenization. To facilitate radiometric analysis, the processed samples were hermetically sealed in standardized counting containers using aluminum foils and cello tape. The primary detection of radionuclides was conducted using a High Purity Germanium (HpGe) detector. For heavy metal analysis, biological and water samples underwent wet acid digestion to dissolve organic matrices before being analyzed for Arsenic, Lead, Cadmium, and other trace metals using Microwave Plasma–Atomic Emission Spectroscopy (MP-AES). Finally, the resulting data were processed using specialized statistical software to perform ANOVA and Pearson correlation tests.

3.2 Collection of Samples

Getting accurate measurements of radionuclide and elemental concentrations is dependent on how carefully samples were collected and prepared. Sample collection, was vital because it directly impacted how reliable the subsequent analysis was done. Once collected, samples needed various preparation steps to make them suitable for analysis. This include physical treatments like drying to remove moisture or grinding to make the sample uniform. For samples rich in organic material, ashing (either dry or wet) was done to eliminate organic matter that could interfere with the analysis. This section discusses collection of sediment, fish, crop, and water samples.

3.2.1 Sediment Samples

The study was divided into 10 sampling locations (Areas) found along the shores of Lake Turkana, particularly Kerio, Nariokotome, Nareng'ewoi, Nachukui, Kataboi, Kalokol, Long'ech and Eliye as well as from sites along the Turkwel River in Lodwar Town and Kang'atosa. At each sampling location, three sampling sites were selected. 30 sediment samples each weighing approximately 400g were collected from different sites in the Lake Turkana Basin using purposive/judgmental sampling method. Table 3.1 summarizes the sediment sampling plan. The sampling sites in each location were between 30m and 50m apart.

Table 3.1: Sediment sampling plan

Region	Sample ID	Mass (grams)
Nareng'ewoi	NARE 1	375
	NARE 2	356
	NARE 3	372
Kalokol	KAL 1	378
	KAL 2	387
	KAL 3	381
Nachukui	NACH 1	388
	NACH 2	365
	NACH 3	389
Kang'atosa	KANG 1	393
	KANG 3	384
	KANG 3	399
Kerio	KERIO 1	410
	KERIO 2	402
	KERIO 3	404
Eliye	ELI 1	387
	ELI 2	396
	ELI 3	386
Lodwar	LOD 1	375
	LOD 2	379
	LOD 3	367
Long'ech	LONG 1	388
	LONG 2	390
	LONG 3	393
Nariokotome	NARI 1	389
	NARI 2	403
	NARI 3	383
Kataboi	KATA 1	382
	KATA 2	387
	KATA 3	378

The samples were collected from a depth of up to 20 cm using a mason's trowel and placed in polythene bags. A label detailing the sample collection location was affixed to the bag. To minimize the risk of contamination, all sampling equipment were thoroughly cleaned before handling subsequent samples. Each sediment sample was

sun-dried on clean fabric to remove moisture, followed by manual removal of debris. The samples were then weighed, placed in non-polythene bags and labeled for identification.

3.2.2 Fish Samples

Three different species of fish samples were bought from Kalokol and Long'ech markets. These two fish sampling sites provide a good representation of the entire lake basin considering that fishing boasts dock on these places. The sampled fish comprised of Synodonis catfish (*Synodontis schall*), Nile tilapia (Oreochromis *niloticus*) and Nile perch (*Lates niloticus*).

For radionuclide analysis, three samples of fresh/wet fish of each fish species were collected. At the time of collection, each sample was cut into tiny pieces using a knife that was cleaned before being used to cut the next sample, weighed and placed in a clean non-polythene paper bag that was properly labeled. Table 3.2 gives details of the different fresh fish species that were sampled.

Table 3.2: Fresh Fish sample collection plan.

Region	Sample ID	Sample type	Mass (grams)
Kalokol	CF 1	Catfish	254
	CF 2	Catfish	189
	CF 3	Catfish	256
Kalokol	NT 1	Tilapia	170
	NT 2	Tilapia	180
	NT 3	Tilapia	176
Long'ech	NP1	Nile perch	250
	NP2	Nile perch	250
	NP3	Nile perch	250

For heavy metal analysis, eighteen (18) sun-dried fish samples were collected from the Kalokol and Long'ech fish markets. From each market, three samples of Synodontis catfish, Nile tilapia and Nile perch were purchased, totaling nine samples

per market. Upon collection, the three individual samples of each fish species from each market were cut into smaller pieces and then thoroughly mixed together to create a single, composite sample for that species and market. Each composite sample was then placed in a clean, non-polythene paper bag, and appropriately labeled for identification.

3.2.3 Crop Samples

Mature sorghum flower heads were collected from ten distinct farms in Kang'atosa ward, where irrigation relied on the Turkwel River, while cassava tubers were randomly obtained from four of the farms. To ensure representative sampling for sorghum, three heads were gathered from different locations within each farm, and the seeds were subsequently removed from these heads and combined to form a single composite sample for that specific farm. Similarly, three cassava tubers collected from three different locations within each farm were cut into small pieces and thoroughly mixed, creating a composite sample for each the farm. The crop sample summary is highlighted in Table 3.3.

Table 3.3: Sorghum and cassava sample ID and mass in grams.

SAMPLE ID	MASS (grams)
SOR 1	300
SOR 2	320
SOR 3	305
SOR 4	290
SOR 5	310
SOR 6	299
SOR 7	285
SOR 8	301
SOR 9	313
SOR 10	303
CAS 1	304
CAS 2	320
CAS 3	318
CAS 4	327

3.2.4 Water Samples

Thirty surface water samples were collected using grab sampling method from various locations along the shores of Lake Turkana and the Turkwel River. Along Lake Turkana's shores, eight distinct sampling locations were chosen: Kerio, Nariokotome, Nareng'ewoi, Nachukui, Kataboi, Kalokol, Long'ech, and Eliye. For the Turkwel River, two sampling locations, Lodwar and Kang'atosa, were selected. These riverine sites were approximately 50 km apart, representing upstream and downstream points. At each of these ten primary sampling locations, three individual sampling sites were established, spaced between 30 and 50 meters apart.

The water samples were collected in 500ml plastic bottles. Prior to collection, all bottles underwent a rigorous cleaning procedure involving washing with dilute hydrochloric acid to prevent the adsorption of radionuclides onto the container walls. Each bottle was carefully filled to the brim, ensuring complete air removal from the water, before being tightly capped. Three samples were collected from each specific sampling point. Immediately after collection, each sampling bottle was clearly labeled with its unique sample identity (ID) and collection location using durable waterproof tape for identification.

Table 3.4 provides a detailed overview of the water samples collected, outlining the region of collection, sample identification labels, and the number of samples obtained from each specific site.

Table 3.4: Water sample details

Region	Sample ID
Nareng'ewoi	NARE 1
	NARE 2
	NARE 3
Kalokol	KALO 1
	KALO 2
	KALO 3
Nachukui	NACH 1
	NACH 2
	NACH 3
Kang'atosa	KANG 1

	KANG 2
	KANG 3
Kerio	KERIO 1
	KERIO 2
	KERIO 3
Eliye	ELIYE 1
	ELIYE 2
	ELIYE 3
Lodwar	LOD 1
	LOD 2
	LOD 3
Long'ech	LONG 1
	LONG 2
	LONG 3
Nariokotome	NARI 1
	NARI 2
	NARI 3
Kataboi	KATA 1
	KATA 2
	KATA 3
Total	30

3.3 Preparation of Samples for Radionuclide Analysis

This section details the critical steps undertaken to prepare the collected sediment, fish and crop samples for radionuclide analysis. Accurate and consistent sample preparation is paramount in radionuclide investigations, as it directly impacts the reliability and precision of the subsequent measurements. The procedures outlined herein ensured the samples were in an optimal state for the detection and quantification of radionuclides, minimizing potential interferences and ensuring the integrity of the analytical results.

3.3.1 Sediment Samples

Each sediment sample underwent a thorough preparation process to ensure accurate radionuclide analysis. Initially, each sample was thoroughly sun-dried on a clean fabric, ensuring no cross-contamination between samples. Once sun-dried, the samples were individually pulverized into a fine powder using a clean mortar and pestle, with the equipment thoroughly cleaned after each sample to maintain sample

integrity. The powdered samples were then transferred to a non-polyethylene bag, which was appropriately labeled for identification.

To eliminate any residual moisture, the samples underwent a secondary drying phase in an oven maintained at a temperature of 105°C for 24 hours. After oven drying, each sample was carefully transferred into a pre-weighed plastic container that was similar to those holding the reference gamma (RG) standard samples from International Atomic Energy Agency (IAEA) used to calibrate the gamma spectrometry equipment used for radionuclide analysis. Each sample container was covered with aluminium foil, and then tightly corked to prevent the escape of radon gas. The sealed container, along with its contents, was re-weighed to accurately determine the net sample mass. A sticker bearing the sample ID, determined sample mass, and the date of sealing was affixed to each container for comprehensive tracking. To ensure secular equilibrium between parent and daughter radionuclides, the sealed samples were stored for one month prior to analysis (Kessaratikoon *et al.,* 2007).

3.3.2 Fish Samples

The fish samples were thoroughly sun-dried to remove initial moisture. The samples were then individually pulverized into a fine powder using a thoroughly cleaned mortar and pestle. The powdered samples were carefully transferred into pre-weighed plastic containers, consistent in design and material with those recommended by the IAEA for radionuclide analysis. To eliminate any remaining significant moisture and achieve a constant dry weight, each sample underwent a secondary drying process in a convection oven, maintained at a temperature of 105°C for a duration of 24 hours. These containers were then covered with aluminum foil and tightly corked to create an airtight seal. The sealed container, including its contents, was re-weighed to precisely determine the net sample mass. A durable sticker containing the sample ID, the determined sample mass, and the date of sealing was then affixed to each container for sample tracking.

To ensure that secular equilibrium was established between parent radionuclides and their respective daughter products, the airtight containers were stored for a minimum of thirty days prior to analysis (Kessaratikoon *et al.,* 2007).

3.3.3 Cassava and Sorghum Samples

Both crop samples were initially sun-dried to a constant weight to eliminate bulk moisture and stabilize their masses. The dried samples were individually pulverized into a fine, homogenous powder using a grinder. To ensure uniform particle size, the powdered material was then sieved through a 2-mm mesh and transferred to appropriately labeled, containers similar to those of IAEA. These containers were specifically chosen to match the dimensions and geometry of International Atomic Energy Agency standard reference materials, ensuring consistent counting geometry during gamma spectroscopy. To further reduce moisture content and achieve complete dryness, all samples underwent a secondary drying phase in the laboratory oven, maintained at a constant temperature of 105°C for 24 hours. To effectively impede the escape of gaseous radon isotopes ^{222}Ra and ^{220}Rn and their short-lived decay products, the containers were carefully sealed with aluminum foil and then tightly corked. The sealed samples were subsequently stored for a minimum of 30 days prior to laboratory analysis to allow for the establishment of secular equilibrium between parent radionuclides and their respective daughter radionuclides (Kessaratikoon *et al.,* 2007).

3.4 Preparation of Samples for Elemental Analysis

The subsections below describe in detail the digestion methods applied to both water (Section 3.7.1) and fish samples (Section 3.7.2), outlining the reagents, conditions, and preparatory steps undertaken to produce clear, homogeneous solutions for elemental analysis using atomic emission spectrometry.

3.4.1 Digestion of Water Samples

The precise and accurate determination of elemental concentrations in water samples necessitates a robust sample preparation procedure to ensure complete dissolution of analytes and matrix compatibility with the analytical instrument. The method involved a two-stage digestion process followed by careful dilution and filtration, culminating in samples ready for atomic emission spectrometry.

Approximately 0.5 liters of each water sample was accurately measured and transferred into a clean digestion flask. To this, a measured acid mixture consisting of 9 mL of concentrated nitric acid (HNO_3) and 3 mL of concentrated hydrochloric acid (HCl) was added. This specific acid combination, often referred to as aqua regia

provided a powerful oxidizing and complexing medium, ensuring the complete dissolution of various inorganic species and the destruction of organic matter in the samples. The acid-sample mixture was then heated in a fume chamber. This facilitated the digestion process, indicated by the evolution of brownish fumes, primarily composed of nitrogenous compounds such as nitrogen dioxide, (NO_2). Heating continued until these fumes were completely expelled, signifying complete oxidation of organic constituents and the dissolution of target analytes. Following digestion, the samples were cooled to room temperature to prevent loss of volatile analytes and ensure safe handling.

To prepare the digested samples for analysis, they were first diluted with distilled water to a volume of approximately 100 ml. This initial dilution helps to reduce the acid concentration and bring the analyte concentrations into a suitable range for the subsequent analytical technique. The diluted digestates were then subjected to a two-step filtration process. First, they were filtered through Whatman No. 42 filter papers into 100 ml volumetric flasks to remove larger particulate matter. Subsequently, a finer filtration step was performed, using 0.22 µm pore size filters directly into plastic reagent bottles. This final filtration step was critical to prevent nebulizer clogging and minimize scattering effects during atomic emission spectrometry, ensuring a clean and homogeneous solution for instrumental analysis. These prepared solutions were then used for atomic emission spectrometry.

3.4.2 Digestion of Fish Samples

For the quantitative determination of heavy metals in fish samples, a two-stage dry ashing digestion method was employed to ensure complete decomposition of the organic matrix. A 2.0 g portion of each homogenized, powdered fish sample was transferred into a clean crucible. To facilitate initial decomposition and prevent spattering during subsequent heating, 6.0 mL of deionized water and 4.0 mL of 35% nitric acid (HNO_3) were carefully added to the crucible. The crucibles were then slowly heated on a hotplate, with the temperature gradually increased to evaporate the liquid phase and achieve complete dryness. This preliminary heating step helps to char the organic material and prepare the sample for the high-temperature ashing process.

Following the initial drying, the crucibles containing the charred samples were transferred to a muffle furnace where they were subjected to an elevated temperature of 550°C for a duration of 1 hour for complete organic removal.

Upon completion of the ashing process, the crucibles were removed from the furnace and allowed to cool to room temperature. The inorganic ash was then re-dissolved by adding a suitable volume of deionized water, followed by careful mixing to ensure the analytes were fully solubilized. The resulting solution was then filtered through Whatman No. 42 filter papers into 100 mL volumetric flasks to remove any undissolved particulate matter (Bilalo *et al.,* 2024).

To ensure the stability of the analytes and establish a consistent matrix for instrumental analysis, the volumetric flasks were subsequently diluted to the 100 mL mark with a 2% nitric acid solution. This acidic medium helps to prevent precipitation of metal ions and maintain them in a stable, soluble form. The mixture within the volumetric flasks was then thoroughly shaken to achieve complete homogenization. Prior to instrumental analysis, the prepared solutions underwent a final filtration step, passing through 0.22 μm pore size filters directly into plastic reagent bottles suitable for the MP-AES. These solutions were then introduced into the MP-AES for the quantitative determination of elemental concentrations.

3.5 Analysis of NORM in Samples

This section introduces the analytical methodologies employed to determine the concentration levels of terrestrial radionuclides in sediments, fish, and crop samples. High Purity Germanium gamma-ray spectrometry was utilized for the quantitative analysis of radionuclides, capitalizing on its superior energy resolution and detection efficiency. The data generated from these analyses was a critical input for evaluating the health risks associated with the observed radionuclide levels, thereby providing essential information for environmental management and public health protection.

3.5.1 High Purity Germanium (HPGe) γ – Ray Spectrometer

A gamma spectroscopy system is made up of several key components namely, a gamma ray detector, high voltage power supply, preamplifier, amplifier, Analogue to Digital Converter (ADC), and Multi-Channel Analyzer (MCA) (Figure 3.1).

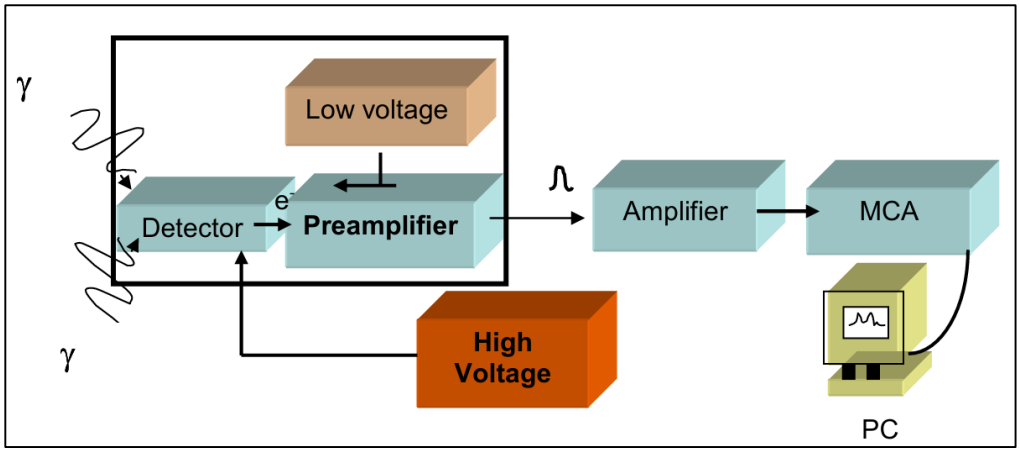


Figure 3.1: Block diagram of a basic gamma spectrometry system

A gamma spectroscopy system works by converting the energy from gamma rays into a digital signal that can be analyzed. This process begins when a gamma ray hits the detector crystal, creating a burst of electrons. This burst forms a tiny electrical pulse, which is then strengthened by a preamplifier and an amplifier. The now-stronger pulse is converted into a numerical value by an ADC. This digital information is then sent to the MCA, which acts as the system's core processor. The MCA sorts these numerical values by their energy, collecting the data in real time and displaying it as a spectrum on a computer. Specialized spectrum analysis software can then be used to examine this data and identify the specific isotopes present.

3.5.2 Standard Samples

Three primary standards from the International Atomic Energy Agency (IAEA) were used to calibrate a gamma spectroscopy system and analyze data: RGK-1 for ^{40}K, RGU-1 for ^{238}U, and RGTH-1 for ^{232}Th. Each standard had a known activity for its primary element and was used to calibrate the system for accurate measurements. An additional combined standard, RGMIX, was also used to help analyze the full gamma spectrum.

3.5.3 Energy and Efficiency Calibration of the HPGe Detector

Accurate and reliable radionuclide analysis hinges on a well calibrated gamma spectrometry system. To yield meaningful results, including precise isotope identification and both qualitative and quantitative analyses, energy and efficiency calibration are indispensable.

The process of energy calibration creates a link between a spectrometer's channel numbers and the energy of the gamma rays it detects. This crucial step was performed by identifying prominent gamma ray peaks within the spectrum of the standard reference materials and correlating their known energies with the corresponding channel numbers at which they were detected. This correlation allows the system to accurately convert raw channel data into energy spectra. This is a fundamental step in radionuclide identification, as it allows for the precise determination of the radionuclides present based on their unique gamma energy signatures.

Efficiency calibration of the detector is the process of quantifying its sensitivity to gamma rays across various energies. It is the fraction of emitted gamma rays that the detector successfully counts. This was achieved by measuring known radioactive sources and comparing the observed counts to their known emission rates, allowing for the creation of an efficiency curve that plots detector efficiency against gamma-ray energy (Alnour *et al.,* 2014). This calibration ensured accurate quantitative determination of radionuclide activities in samples, which was crucial for environmental monitoring and health risk assessment, ultimately transforming raw count data into meaningful activity concentrations.

The calibration of the HPGe detector's energy and efficiency was performed with gamma lines 352 keV for ^{214}Pb, 609 keV for ^{214}Bi, 238 keV for ^{212}Pb, 911 keV for ^{228}Ac and 1460 keV for ^{40}K. Figure 3.2 shows the efficiency calibration curve in the 77-1460.29 KeV range. At low energies, efficiency quickly increases. This happens because the attenuation within the radioactive source, detector cap, or inner dead layer sharply decreases. Beyond a few hundred keV, the efficiency steadily declines.

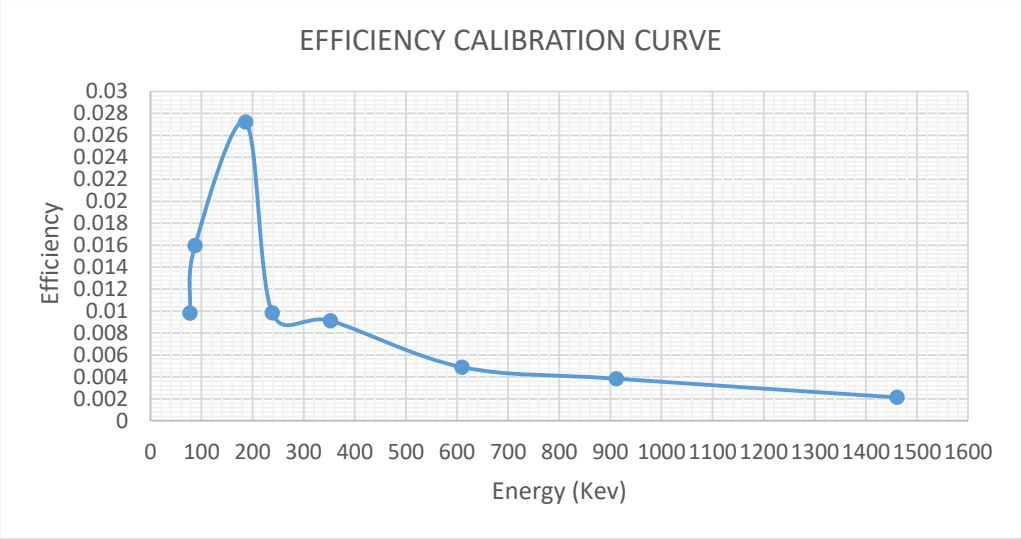


Figure 3.2: Efficiency calibration curve

3.5.4 Spectroscopic Analysis of Radionuclides in Sample Matrices

The radionuclide spectra of the samples were determined using a high-resolution, p-type coaxial HPGe γ-ray spectrometer. The detector, which had an active volume of 144 mm^3, a dead layer thickness of 600 microns, and a detector-to-window distance of less than 5 mm, was enclosed within a 10 cm thick lead shield with a 2 mm copper lining. This shielding effectively reduced background gamma radiation in the lab. The detector's performance was confirmed by its 1.8 keV energy resolution for ^{60}Co and an efficiency of 31.6%. During data collection, the detector crystal was maintained at 77 K with liquid nitrogen to preserve the high resolution of energy peaks (Matsitsi et al., 2020). Each sample was placed on the thin front window and analyzed for at least 28,800 seconds, with the spectral data saved using Maestro-32 software.

The resulting gamma-ray spectra were thoroughly examined to identify prominent photopeaks exhibiting statistically significant counts above the continuum. A comprehensive Region of Interest (ROI) report was subsequently generated for each identified peak. This report expressed critical parameters essential for further data processing, including: Gross Peak Area, representing the total number of counts within the defined ROI; Net Peak Area, the number of counts specifically attributed to the photopeak, obtained after subtracting the background continuum, which represents the true signal from the radionuclide; Peak Centroid Energy, the precise energy corresponding to the maximum count within the photopeak, characteristic of a specific

gamma-ray emission; and Radionuclide Library Information, which linked each identified photopeak to its corresponding radionuclide species by cross-referencing the peak centroid energy with a pre-established library of known gamma-ray emissions.

To ensure accurate quantification of radionuclide activity in the field samples, the net characteristic count for each photopeak was determined by subtracting the measured background count from the gross measured count. This background subtraction was crucial for isolating the signal originating solely from the radionuclides within the sample, thereby mitigating interference from environmental background radiation.

3.6 Activity Concentrations

Based on the gamma ray emission profiles of the samples, nuclide identification reports were compiled for all samples. The activity concentrations for ^{238}U, ^{232}Th, and ^{40}K were then calculated from the measured counts using Equation 3.1 and the spectroscopic parameters provided in Table 3.5 (Radzali *et al.,* 2018).

$$A = \frac{N}{\varepsilon_f P_\gamma t_S M}$$

…….3.1

where $N = N_S - N_B$ is the γ-ray's net counts, N_S - sample spectrum's counts, N_B - counts of the background spectrum, ε_f - the γ-ray's detection efficiency, t_s – the sample spectrum's collection time in seconds, M - the mass of the sample (kg), P_γ - emission probability of the γ-ray.

The quantitative analysis of ^{238}U and ^{232}Th was based on the principle of secular equilibrium. As described by Chege et al. (2015), when a radioactive system is closed and the parent half-life significantly exceeds that of the daughters, the activities of the parent and daughter nuclides become approximately equal. Since ^{238}U and ^{232}Th are poor gamma emitters, their activity concentrations were determined indirectly by measuring the gamma emissions of their progeny (such as ^{214}Pb and ^{214}Bi for the Uranium series, and ^{228}Ac and ^{212}Pb for the Thorium series under the assumption that secular equilibrium had been established within the sealed samples.

For instance, the activity of ^{40}K was calculated from its 1460.81 keV γ-line, while activity of ^{232}Th was calculated using its 238.36 keV and 911.19 keV γ-lines as detailed in Table 3.5

Table 3.5: Quantification Parameters for Radionuclide Analysis of the HPGe equipment

Primordial radionuclide	Emitter nuclide	Energy (keV)	Emission probability of the γ-ray (P_γ)	γ-ray's detection efficiency (ε_f)
^{238}U	Pb-214	351.92	0.356	0.009123567
	Bi-214	609.31	0.4549	0.004896875
^{232}Th	Pb-212	238.36	0.436	0.009837521
	Ac-228	911.19	0.258	0.00383998
^{40}K		1460.81	0.107	0.00213234

3.7 Radiation Hazards Associated with NORM in Sediments, Fish and Crop Samples

In this section, key radiological hazard indicators used in evaluating the risks associated with NORM are discussed. These include equivalent radium activity, absorbed dose rate, and annual effective dose. Other radiological hazard indicators discussed in the section are; excess lifetime cancer risk, external and internal hazard indices and lastly gamma index. Together, these indices offer a comprehensive framework for determining whether radionuclide levels in environmental samples exceed internationally recommended safety limits. Their application in sediments, crops, and fish from Lake Turkana and its environs ensures a clear understanding of radiation exposure pathways and informs risk management strategies aimed at safeguarding both ecosystems and human health.

3.7.1 Equivalent Radium Activity (Ra_{eq})

Radium equivalent activity is a crucial radiological indicator used to assess and quantify the total radiation hazard posed by materials containing various naturally occurring radioactive elements. This standardized measure expresses the cumulative effect of radiation from multiple radionuclides present in a given material, particularly the key radionuclides ^{226}Ra, ^{232}Th and ^{40}K. These radionuclides are commonly found

in natural environments with ^{226}Ra originating from the decay of uranium, ^{232}Th from thorium and ^{40}K from the natural potassium found in soil and rocks.

The concept of Ra_{eq} allows for the aggregation of radiation doses from these different isotopes into a single value, providing a simplified method to assess the overall radiological risk posed by a material. Since these radionuclides emit gamma radiation, Ra_{eq} is primarily used to assess the possible amount of gamma radiation exposure. Ra_{eq} is especially important in evaluating the safety of building materials such as concrete, bricks, and tiles as well as soils and industrial waste that may contain elevated levels of naturally occurring radioactive materials (NORM). It helps to determine whether the levels of radiation from these materials exceed safety thresholds established by regulatory agencies which are designed to protect public health. For instance, exposure to high levels of gamma radiation over time can raise the risk of developing health issues such as cancer, particularly lung cancer and bone cancer, due to the ionizing nature of gamma radiation. The Ra_{eq} in (Bq/kg) was computed using Equation 3.2.

$$Ra_{eq} = (C_K \times 0.077) + (C_U) + (C_{Th} \times 1.43) \quad \text{.....3.2}$$

where C_K, C_U and C_{Th} are concentration rates of ^{40}K, ^{238}U and ^{232}Th respectively. Permissible values of Ra_{eq} should not exceed 370 Bq/kg (Alaamer, 2012).

3.7.2 Absorbed Dose Rate (ADR)

The Absorbed Dose Rate is a critical concept in radiation dosimetry, quantifying the rate at which energy from ionizing radiation is deposited in a unit mass of matter. It is expressed in units such as gray per second (Gy/s), milligray per second (mGy/s), or rad per hour (rad/h), depending on the context and measurement system used. ADR represents the intensity or strength of a radiation field, indicating how much energy is imparted to a material over time.

ADR is vital in various fields, including medical radiology, nuclear safety, and environmental monitoring. In medical settings, understanding ADR helps in assessing the appropriate radiation dose during diagnostic imaging or therapeutic procedures, ensuring efficacy while minimizing potential harm to patients. In environmental

contexts, measuring ADR assists in evaluating radiation levels in soil or air, which is crucial for public health and safety.

Using Equation 3.3, the rate of absorbed dose from terrestrial sources was determined based on the activity concentrations of the corresponding radionuclides.

$$D\left(\frac{nGy}{h}\right) = 0.462\ A_U + 0.604\ A_{Th} + 0.0417\ A_K \ldots\ldots\ldots\ldots\ldots\ldots\ldots 3.3$$

The terms A_K, A_U, and A_{Th} represent the average activity concentrations of three specific naturally occurring radionuclides: ^{40}K, ^{238}U, and ^{232}Th respectively. (Ali *et al.,* 2015). United Nations Scientific committee on effects of atomic radiation came up with the values 0.462, 0.604 and 0.0417 as dose conversion factors for ^{238}U, ^{232}Th and ^{40}K respectively (Atambo, 2011).

3.7.3 Annual Effective Dose (AED)

Annual Effective Dose (ADR) is a quantity that relates the annual ionizing radiation dose received by the human body to health effects it will cause on the human body. The estimation of annual effective dose received from natural radionuclides depend on the radionuclide concentration at a place. Exposure to natural ionizing radiation considers the duration of time humans spend indoors and outdoors. This time duration is categorized as outdoor and indoor and is known as occupancy factor.

The indoor, outdoor and total annual effective dose were calculated using Equations 3.4 a, b and c respectively (Soh et al., 2018).

$$AED_{out}(mSv/y) = D(nGy/h) \times 8760(h/y) \times 0.2 \times 0.7(Sv/Gy) \times 10^{-6} \ldots\ldots\ldots\ldots\ldots 3.4\ a$$

$$AED_{int}(mSv/y) = D(nGy/h) \times 8760(h/y) \times 0.8 \times 0.7(Sv/Gy) \times 10^{-6} \ldots\ldots\ldots\ldots\ldots 3.4\ b$$

$$AED_{total}(mSv/y) = AED_{out} + AED_{int} \ldots\ldots\ldots\ldots\ldots\ldots\ldots\ldots 3.4\ c$$

where 0.8 and 0.2 are the average indoor and outdoor occupancy factors (Hashim *et al.,* 2004). The absorbed dose in the air was converted into an adult's effective dose using a conversion coefficient of 0.7 Sv/Gy.

The activity concentration levels of ^{238}U, ^{232}Th and ^{232}K in crop samples were used to calculate the effective dose E (mSv/y) in crop using Equation 3.5 (Chege *et al.,* 2015).

$$E = y\sum(A_i X_i) \quad \text{.....3.5}$$

where A_i is the activity of radionuclide *i* and X_i is the corresponding dose coefficient equivalent to $0.00023\, msVBq^{-1}$ for ^{232}Th, $0.00028\, msVBq^{-1}$ for ^{238}U and $0.0000062\, msVBq^{-1}$ for ^{40}K for adult public members; y is the annual ingested quantity of food/water. The annual effective dose was calculated based on the assumption that an average adult person in Kang'atosa consumes 90 kg of sorghum and 10 kg of cassava tubers annually.

3.7.4 Excess Lifetime Cancer Risk (ELCR)

Excess Lifetime Cancer Risk (ELCR) is a probabilistic measure used to estimate the likelihood that an individual will develop cancer due to exposure to carcinogenic agents over a lifetime. This metric is commonly employed in environmental health, radiological protection and occupational safety to quantify the cancer risk posed by exposure to harmful substances such as ionizing radiation, toxic chemicals or heavy metals. ELCR accounts for cumulative exposure to a carcinogen over an individual's expected lifespan, typically considered to be about 70 years. It integrates the effects of dose, duration and frequency of exposure (Najam *et al.,* 2019).

Carcinogens are substances or forms of energy that can lead to cancer. They include chemical agents such as benzene, asbestos and formaldehyde; physical agents like ultraviolet radiation and ionizing radiation; biological agents such as certain viruses like human papilloma virus (HPV). These substances lead to contamination of the environment for example particulate matter like benzene and polycyclic aromatic hydrocarbons contaminate air while pesticides, radionuclides, heavy metals and industrial chemicals contaminate soil and water. Regulatory agencies such as the U.S. Environmental Protection Agency (EPA), UNSCEAR and the International

Commission on Radiological Protection (ICRP) establish guidelines for acceptable ELCR levels typically ≤ 0.5%. ELCR was calculated using Equation 3.6 (Taskin *et al.,* 2009).

$$ELCR = AED_{total} \times LE \times PC \quad \text{.....3.6}$$

where the total annual effective dose is calculated using two key variables: an assumed life expectancy (LE) of 70 years and the probability coefficient (PC), which is the risk of cancer per unit of radiation dose. For the general population ICRP use $PC = 0.055Sv^{-1}$ (Taskin *et al.,* 2009).

3.7.5 External Hazard Index and Internal Hazard Index

The external hazard index (H_{ex}) and internal hazard index (H_{in}) are important tools for assessing radiological risks from naturally occurring radionuclides in the environment. These indices are particularly relevant for construction materials, soil, and rocks used in building infrastructure, as they provide a quantitative estimate of potential radiation exposure (Estokova et al., 2022).

The external hazard index measures exposure to gamma radiation from materials like rocks, soil, or construction products. Gamma radiation is a major issue, largely because of its elevated penetration power, which allows it to travel through materials and reach the human body. If the H_{ex} value exceeds a specific threshold, it indicates a potential health risk, especially for individuals spending significant time near materials with high levels of naturally occurring radioactive materials (NORM).

The internal hazard index, assesses the risk from inhaling radon gas or its decay products, which can emanate from building materials. Radon is a radioactive gas that occurs naturally and is created when uranium and thorium decay. As it is odorless, colorless, and tasteless, it can build-up in poorly ventilated buildings. High concentrations of radon in building materials can lead to elevated indoor radon levels, especially in poorly ventilated buildings. Prolonged radon inhalation is linked to a higher risk of developing lung cancer, making the monitoring of H_{in} levels essential for public health and safety.

Both indices focus on risks from gamma radiation and radon. Gamma rays are highly energetic and can travel long distances, making them the primary concern for external exposure assessments. Alpha and beta particles, in contrast, have limited penetration power. H_{ex} was computed using Equation 3.7 (Ali *et al.,* 2015).

$$H_{ex} = \frac{A_U}{370} + \frac{A_{Th}}{259} + \frac{A_K}{4180} \quad \text{.....3.7}$$

where A_U, A_{Th} and A_K are the activities of ^{238}U, ^{232}Th and ^{40}K in Bq/kg, respectively. The constants 370, 259, and 4810 are normalization factors based on permissible activity concentrations that limit radiation exposure to safe levels corresponding to a dose limit of 1(UNSCEAR, 2010). H_{in} was computed using Equation 3.8 (Ali *et al.,* 2015).

$$H_{in} = \frac{A_U}{185} + \frac{A_{Th}}{259} + \frac{A_K}{4180} \text{.....3.8}$$

where A_U, A_{Th} and A_K are the activities of ^{238}U, ^{232}Th and ^{40}K in Bq/kg, respectively. The denominator for radium changed to 185, which is more conservative to account for the higher risk associated with radon inhalation. The internal hazard index should also ideally not exceed 1, ensuring that internal exposure risks remain within recommended safety thresholds.

3.7.6 Gamma Index (I_γ)

The gamma index (Iγ) is used to estimate the potential radiation hazard from naturally occurring radionuclides in a given material. It helps determine the risk of gamma radiation exposure to people. A gamma index value of 1 or less ($I\gamma \leq 1$) indicates that the annual effective dose from the material is likely to be less than or equal to 1 mSv. This is a common regulatory limit for public radiation exposure. A value of 0.5 or less ($I\gamma \leq 0.5$) suggests that the annual effective dose is likely 0.3 mSv or less. This lower threshold is often used to assess the safety of materials used for building construction. Gamma index in sediment samples was calculated using Equation 3.9 (Turhan et al., 2008).

$$I_\gamma = \frac{A_K}{3000} + \frac{A_{Th}}{200} + \frac{A_U}{300} \text{.....3.9}$$

where A_K, A_{Th}, and A_U are the ^{40}K, ^{232}Th and ^{238}U activity concentrations (Bq/kg) in the sediment samples respectively.

3.8 Analysis of Heavy Metals in Samples

This section introduces the analytical methodologies used to measure the concentration levels of heavy metals in water and fish. Microwave Plasma Atomic Emission Spectrometer was utilized for the quantitative analysis of heavy metal concentrations. The data generated from these analyses was a critical input for evaluating the health risks associated with the observed heavy metal concentration levels, thereby providing essential information for environmental management and public health protection.

3.8.1 Heavy Metal Concentration Analysis in Water and Fish

An Agilent 4210 Microwave Plasma Atomic Emission Spectrometer (MP-AES) was used to precisely quantify the concentrations of the specific heavy metals Zn, Ba, Cd, Pb, Cu, As, Ni, and Cr in the prepared samples. This instrument operates on the principle of atomic emission, where the sample is introduced into a high-temperature microwave-induced plasma. The intense energy of the plasma excites the atoms of the target elements, making them release light at certain characteristic wavelengths. The emitted light is then detected and its intensity measured, with the intensity directly proportional to the concentration of the element in the sample.

To establish the quantitative relationship between emission intensity and elemental concentration, an eight-point calibration curve was meticulously constructed. This involved preparing a series of multi-element standard solutions across a relevant concentration range (Umar *et al.,* 2023). Each point on the calibration curve represented a known concentration of all eight target elements, allowing for the accurate determination of unknown concentrations in the samples in emission mode. This calibration approach ensured the linearity and reliability of the analytical measurements across the expected concentration spectrum of the analytes.

To assess the performance and validity of both the MP-AES technique and the overall experimental procedures, comprehensive quality control (QC) tests were implemented. A key component of this quality assurance protocol involved matrix

spiking. Specifically, a representative pre-digested sample (meaning a sample that had already undergone the complete digestion process but without prior elemental determination) was spiked with a known concentration of the target analytes. This spike was prepared by adding a portion of a 5 mg/kg standard solution, which itself was derived through serial dilution from a high-concentration 1000 mg/kg stock standard solution.

The purpose of this spiking procedure was to evaluate the analytical method's accuracy and recovery efficiency in the presence of the complex sample matrix (Yue *et al.,* 2022). By comparing the measured concentration in the spiked sample to the original concentration plus the known amount added, the percentage recovery was calculated. The final concentrations of the heavy metals in each fish sample were then determined based on these validated MP-AES measurements.

3.8.2 Operating Condition for MP-AES

The operating conditions for MP-AES are summarized in Table 3.6. A critical aspect of data acquisition involved implementing automatic background correction for most analytes, ensuring the accurate subtraction of spectral interferences. Sample introduction was facilitated by a OneNeb series 2 nebulizer, which consistently delivered the sample into the plasma at a controlled flow rate of 0.5 liters per minute (L/min). This precise flow rate was crucial for maintaining plasma stability and efficient atomization of the analytes. The analytical cycle incorporated specific timing protocols to ensure reliable and reproducible measurements: defined read time for data acquisition, rinse time to minimize carryover between samples, stabilization time to allow the plasma and system to equilibrate before each measurement, and uptake time for the sample to reach the nebulizer and plasma.

Table 3.6: Operating Condition for MP-AES

Parameters	Settings
Background correction	Auto
Replicates	3
Nebulizer	One neb series 2, with nitrogen humidifier
Nebulizer flow (L/min)	0.5
Viewing position	0
Read time (s)	3
Rinse time (s)	30
Stabilization time (s)	15
Uptake time (s)	120
Sample tubing	Orange/green
Pumps speed (rpm)	15
Calibration fit	Linear/Rational
Spray chamber	Double-pass
Drain tubing	Blues
Total run time (min)	5

The sample delivery system utilized orange/green sample tubing for identification. The peristaltic pump, responsible for drawing the sample, operated at a consistent pump speed of 15 revolutions per minute (rpm), further contributing to the stable sample flow. A double-pass spray chamber was employed, a design feature that enhances the efficiency of aerosol generation and helps remove larger droplets, leading to a more stable and less noisy signal. The entire analytical sequence for each sample or set of samples was completed within a total run time of 5 minutes, reflecting an optimized balance between analytical thoroughness and sample throughput.

3.9 Water Quality Assessment

Water quality was determined by evaluating the Heavy Metal Contamination Index (MCI) and HEI used to assess the overall level of heavy metal contamination in water (Munene *et al.,* 2023 b). It combines the concentration of various metals in water with their toxicity to create an overall pollution index.

The MCI was determined using Equation 3.10 (Munene *et al.,* 2023 b).

$$MCI = (C_{Zn} \times C_{Pb} \times C_{Cu} \times C_{Cd} \times C_{Cr} \times C_{Ba} \times C_{As} \times C_{Ni})^{1/3} \quad \ldots\ldots 3.10$$

where C_{Zn}, C_{Pb}, C_{Cu}, C_{Cd}, C_{Cr}, C_{Ba}, C_{As} and C_{Ni} are the concentrations of metals of interest in mg/l.

Based on the mean MCI values obtained, the water was categorized as good quality water having low metal pollution if the MCI value fell within the range of 0 to 1. If $1 < MCI \leq 5$, the metal pollution of the water was moderate and had some negative impact on the ecosystem and when $MCI > 5$, the metal pollution in the water was high, hence could harm both aquatic life and humans (Munene *et al.,* 2023 b). The Heavy metal Evaluation Index (HEI) was calculated using Equation 3.11 (Munene *et al.,* 2023 b).

$$HEI = \sum \frac{C_i}{MAC} \quad \ldots\ldots 3.11$$

where C_i is the concentration of heavy metals and MAC is the maximum allowable concentration of the heavy metal in drinking water. The water is classified as highly polluted when the average HEI value exceeds 10 (Ojekunle *et al.,* 2016).

3.10 Health Risk Assessment of Fish Samples

The assessment of non-carcinogenic health risks was carried out by calculating the Estimated Daily Intake (EDI), Target Hazard Quotient (THQ), and Hazard Index (HI). The EDI quantifies the average daily exposure of an individual to a specific substance, such as a metal, based on dietary intake. The EDI is commonly expressed in units of milligrams per kilogram of body weight per day (mg/kg bw/day). It was calculated using Equation 3.12 (Esilaba *et al.,* 2020).

$$EDI = \frac{CF \times IR \times MC}{BW} \quad \ldots\ldots 3.12$$

MC represents the concentration of metal in the fish muscle is measured in milligrams per kilogram of dry weight. IR is the assumed ingestion rate of 0.0123 kg/person/day, while BW is the average body weight of an African adult, set at 60.7 kg (Esilaba *et al.,* 2020). A conversion factor (CF) of 0.21 was used to convert the dry weight metal

results to wet weight, based on the assumption of 79% moisture content in the fish (Samantara *et al.,* 2023).

The non-carcinogenic risk to human health was assessed by calculating the THQ using the formula provided in Equation 3.13 (Samantara *et al.,* 2023). This metric helps quantify the potential health effects that may arise from consumption of fish that is contaminated with heavy metals.

$$THQ = \frac{EDI}{RfD} \text{ .....3.13}$$

Where each metal has an oral reference dose (RfD**)**, expressed in milligrams per kilogram per day (mg/kg/day). These values represent the estimated daily exposure to a substance that is unlikely to cause adverse health effects over a lifetime. The specific RfD values mentioned are; As: 0.00006 mg/kg/day, Cd: 0.001 mg/kg/day, Ba: 0.2 mg/kg/day, Cr: 0.003 mg/kg/day, Cu: 0.04 mg/kg/day, Ni: 0.02 mg/kg/day, Pb: 0.0035 mg/kg/day and Zn: 0.3 mg/kg/day (Samantara *et al.,* 2023).

A THQ value less than 1 indicates that the daily exposure level is safely below the reference dose (RfD) (Esilaba *et al.,* 2020). This indicates that adverse health effects are unlikely to occur over an individual's lifetime. Conversely, when the THQ value is greater than 1, it suggests that consuming the fish contaminated with heavy metals could pose a non-carcinogenic health risk to the exposed population. A higher THQ value indicates an increased probability of adverse health effects (Esilaba *et al.,* 2020).

The total health risk attributed to the presence of multiple metals in fish was determined by calculating a Hazard Index (HI). Consequently, the HI provides a comprehensive representation of the combined risk posed by all the metals identified. This index is derived by summing the individual Target Hazard Quotient (THQ) values for each metal as indicated in Equation 3.14 (Esilaba *et al.,* 2020).

$$HI = \sum_{i=1}^{n} THQ_i \text{ .....3.14}$$

where THQ_i measures the risk from a single heavy metal. The HI represents the combined risk from all eight heavy metals (n=8) included in this study. When the HI is less than one, there's no significant risk of non-carcinogenic effects and when the

HI is greater than one, there is a probability of non-carcinogenic risk effects occurring(Alabi *et al.,* 2024).

3.11 Bioaccumulation Factor (BAF)

The bioaccumulation factor is a ratio that compares the concentration of the substance in the organism to the concentration in the surrounding environment. A BAF value greater than 1 indicated that the concentration of the metal in the fish is higher than in the surrounding water, signifying occurrence of bioaccumulation of the metal in fish. Conversely, a BAF value less than 1 suggest failure in accumulation of the metal, or that the rate of excretion being higher than the rate of uptake. BAF was calculated using Equation 3.15 (Rajeshkumar & Li, 2018).

$$\text{BAF} = \frac{\text{Average concentration of metal X in fish}}{\text{Average concentration of metal X in water}} \ldots\ldots\ldots\ldots\ldots\ldots\ldots\ldots\ldots\ldots 3.15$$

This value helps researchers understand the potential for a substance to build up in the food chain and pose a risk to higher-level predators, including humans, who may consume the fish.

3.12 Summary

Chapter three presents a comprehensive technical roadmap of the methodology used to assess radiological and elemental risks in the Lake Turkana Basin and Turkwel River. The study adopts a multidisciplinary approach, analyzing four distinct matrices—sediment, water, fish, and agricultural crops—to evaluate NORM and heavy metals. By integrating systematic field sampling with laboratory techniques like HPGe gamma-ray spectrometry and MP-AES, the research establishes a rigorous framework for quantifying environmental safety.

The geographical scope included ten primary locations, such as Kalokol and Lodwar, where sampling was conducted using purposive methods. Sediment was collected at 20 cm depths, while surface water was gathered in acid-washed bottles to prevent mineral adsorption. Biological monitoring involved three fish species (Catfish, Tilapia, and Nile perch) and irrigated crops (sorghum and cassava). A significant portion of the methodology involves transforming these raw samples into analytical specimens through a multi-stage drying process. Solid samples were sun-dried, oven-

dried at 105°C, pulverized, and sieved. Crucially, these were hermetically sealed for 30 days to achieve secular equilibrium, ensuring that parent radionuclides and their daughter products reached a stable ratio for accurate measurement.

For elemental analysis of heavy metals like Lead and Cadmium, the study employed specific acid digestion protocols. Water samples were treated with aqua regia and heated, while fish samples underwent "dry ashing" in a muffle furnace at 550°C to remove the organic matrix. The resulting inorganic residues were filtered through 0.22 µm pores to create homogeneous solutions for MP-AES analysis. Radioactivity quantification relied on a shielded HPGe detector maintained at 77 K with liquid nitrogen. The system was calibrated using IAEA standard reference materials to link energy peaks to specific isotopes, such as the 1460.81 keV line of ^{40}K.

Finally, the chapter establishes a mathematical framework to translate activity concentrations into human health risk factors. This includes calculating Radium Equivalent Activity (Ra_{eq}), which aggregates the effects of various radionuclides, and the ADR to measure radiation field intensity. To ensure scientific robustness, the data were processed using ANOVA and Pearson correlation tests to identify significant relationships between locations and pollutant levels. This methodology ensures that the study's findings are based on standardized, reproducible, and internationally recognized scientific protocols.

CHAPTER FOUR
RESULTS AND DISCUSSION

4.1 Introduction

In this section, the data obtained from the analytical instruments is analyzed and interpreted in line with the four objectives of the study. These interpretations and discussions of the results formed the basis for the conclusions. Results and discussions concerning objective one, which was to determine activity concentration levels of the primordial radionuclides ^{238}U, ^{232}Th and ^{40}K in sediment, crop and fish samples from selected locations in Lake Turkana and its environs, are captured in Sections 4.2 to 4.5. Objective two, was to determine radiation exposure hazard levels resulting from the presence of naturally occurring radionuclides. Its results and discussions are captured in sections 4.6 and 4.7. Sections 4.8 to 4.12 discuss the third objective which was to find the concentration of selected heavy metals in water and fish samples from selected sites of Lake Turkana and its environs. Finally, the fourth Objective which was to establish a correlation between the concentrations of heavy metals and activity levels of primordial radionuclides in the Lake Turkana ecosystem, is discussed in Sections 4.13.

4.2 Activity Concentration of ^{238}U, ^{232}Th and ^{40}K in Sediment Samples

Table 4.1 displays the activity concentrations of the three primordial radionuclides found in sediment samples from all sampling locations. The highest ^{232}Th activity was in KAL 3 (89.52 ± 15.01 Bq/kg) and the lowest was in LONG 2 (11.36 ± 1.76 Bq/kg). The highest ^{238}U activity was also in KAL 3 (80.97 ± 14.68 Bq/kg) with the lowest in LONG 2 (9.62 ± 1.18 Bq/kg). The highest ^{40}K activity was in ELI 3 (1054.38 ± 145.21 Bq/kg) and the lowest was in KAL 3 (236.7 ± 28.47 Bq/kg). These variations in activity could be attributed to differences in geological characteristics at each sampling site.

Table 4.1: Activity concentrations of ^{232}Th, ^{238}U and ^{40}K in sediment samples.

Sampling location	Sample ID	Activity Concentration in Bq/kg		
		^{232}Th	^{238}U	^{40}K
Eliye	ELI 1	57.06 ± 12.13	27.56 ± 5.22	706.78 ± 78.12
	ELI 2	69.62 ± 13.12	22.35 ± 6.9	554.89 ± 63.06
	ELI 3	52.04 ± 11.12	37.56 ± 10.03	1054.38 ± 145.21
Kerio	KERIO 1	42.54 ± 9.31	30.23 ± 11.61	864.56 ± 82.12
	KERIO 2	14.6 ± 1.03	11.03 ± 2.01	745.02 ± 74.22
	KERIO 3	32.8 ± 9.24	22.68 ± 4.23	672.82 ± 85.37
Lodwar	LOD 1	47.47 ± 10.01	42.94 ± 12.15	559.85 ± 59.09
	LOD 2	28.48 ± 5.91	21.27 ± 3.84	497.32 ± 55.67
	LOD 3	17.45 ± 1.25	13.48 ± 1.08	774.91 ± 78.37
Kalokol	KAL 1	50.19 ± 12.12	32.63 ± 8.62	966.24 ± 97.32
	KAL 2	86.8 ± 14.08	79.88 ± 14.51	274.90 ± 32.36
	KAL 3	89.52 ± 15.01	80.97 ± 14.68	236.7 ± 28.47
Kataboi	KATA 1	29.93 ± 4.03	23.4 ± 3.01	706.78 ± 64.65
	KATA 2	20.95 ± 3.27	21.16 ± 2.27	784.27 ± 71.41
	KATA 3	33.57 ± 0.04	28.16 ± 4.42	731.71 ± 65.32
Nachukui	NACH 1	42.68 ± 9.95	38.4 ± 4.29	571.77 ± 45.93
	NACH 2	19.77 ± 1.03	15.25 ± 1.08	514.2 ± 54.15
	NACH 3	43.29 ± 9.03	35.18 ± 9.12	656.75 ± 55.51
Kang'atosa	KANG 1	26.59 ± 4.32	25.24 ± 3.11	718.3 ± 65.46
	KANG 2	41.93 ± 7.54	39.00 ± 7.69	591.72 ± 53.87
	KANG 3	33.63 ± 8.37	28.31 ± 4.21	570.68 ± 49.05
Long'ech	LONG 1	44.33 ± 10.74	37.43 ± 8.22	709.58 ± 75.09
	LONG 2	11.36 ± 1.76	9.62 ± 1.18	550.5 ± 53.19
	LONG 3	36.39 ± 8.61	30.68 ± 6.32	630.85 ± 60.02
Nariokotome	NARI 1	15.32 ± 1.09	15.83 ± 2.25	818.27 ± 72.33
	NARI 2	37.19 ± 9.15	31.48 ± 7.93	486.63 ± 34.51
	NARI 3	29.3 ± 7.22	18.77 ± 2.04	546.18 ± 55.07
Nareng'ewoi	NARE 1	14.02 ± 1.36	11.02 ± 0.98	764.64 ± 59.93
	NARE 2	47.85 ± 12.94	36.44 ± 4.77	868.48 ± 80.06
	NARE 3	42.79 ± 11.08	34.66 ± 6.12	801.83 ± 67.99
Overall average		38.67 ± 7.53	30.09 ± 5.80	664.38 ± 65.43

Table 4.2 presents the calculated range and average of Ra_{eq} as well as the average level of radioactivity for ^{232}Th, ^{238}U and ^{40}K in the analyzed sediments from the ten sampling locations.

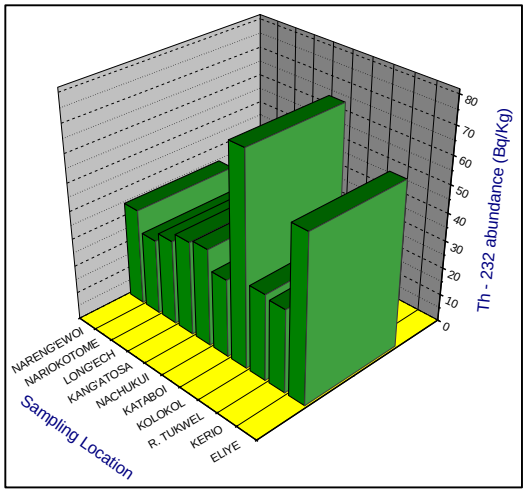
The highest average concentration of ^{232}Th was in Kalokol (75.5 Bq/kg) and the lowest in Nariokotome (27.3 Bq/kg), showing significant variation across sampling locations (Figure 4.1a). Kalokol also had the highest ^{238}U concentration (64.5 Bq/kg), while Kerio had the lowest (21.3 Bq/kg). Nareng'ewoi showed the highest ^{40}K concentration (811.7 Bq/kg), with Kalokol having the lowest (492.6 Bq/kg). The study area's average concentrations were 38.7 Bq/kg for ^{232}Th, 30.1 Bq/kg for ^{238}U, and 664.4 Bq/kg for ^{40}K. These were more than the world averages of 30 and 400 Bq/kg for ^{232}Th and ^{40}K respectively but less than the world average of 35 Bq/kg for ^{238}U.(Tzortzis & Tsertos, 2004).

Table 4.2: Range and average of ^{232}Th, ^{238}U ^{40}K and Ra_{eq} activity concentrations of sediments.

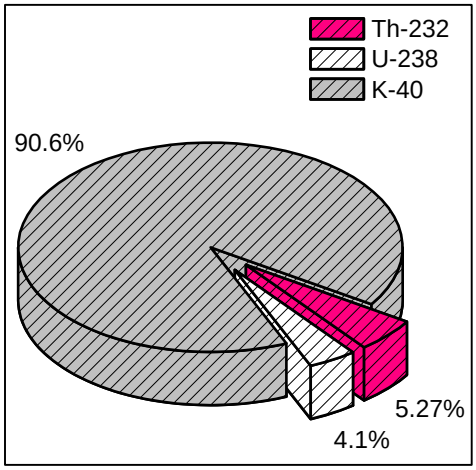
Sampling location	**Activity concentration (Bq/kg)**						**Ra_{eq} (Bq/kg)**	
	^{232}Th		^{238}U		^{40}K			
	Range	Average	Range	Average	Range	Average	Range	Average
Eliye	52 - 69.6	59.6	22.4 - 37.6	29.2	554.9-1054.4	772.0	163.6 - 193.2	173.8
Kerio	14.6 - 42.5	30.0	11.0 - 30.2	21.3	672.8 - 864.6	760.8	89.3 - 157.6	122.8
Lodwar	17.5 - 47.5	31.1	13.5 - 42.9	25.9	497.3 - 774.9	610.7	98.1 - 153.9	117.4
Kalokol	50.2-89.5	75.5	32.6 - 81	64.5	236.7 - 966.2	492.6	178.8-227.2	210.4
Kataboi	20 - 33.6	28.2	21.2 - 28.2	24.2	706.8 - 784.3	740.9	111.5-132.5	121.6
Nachukui	19.8 - 43.3	35.3	15.3 - 38.4	29.6	514.2 - 656.8	580.9	83.1 - 147.7	124.7

Kang'atosa	26.6 - 41.9	34.1	25.2 - 39	30.9	570.7 - 718.3	626.9	118.6 - 144.5	127.8
Long'ech	11.6 - 44.3	30.7	9.6 - 37.4	25.9	550.5 - 709.6	630.3	68.3 - 155.5	118.3
Nariokotome	15.3 - 37.2	27.3	15.8 - 31.5	22.0	486.6 - 818.3	617.0	100.8 - 122.1	108.5
Naraeng'ewoi	14.0 - 47.9	34.9	11 - 36.4	27.4	746.6 - 868.5	811.7	89.9 - 171.7	139.8
Overall Average		38.7		30.1		664.4		124.1

The crustal abundance of ^{40}K in the studied sediments was notably higher than that of ^{232}Th and ^{238}U (Figure 4.1 b), a typical geological characteristic observed in most marine sediments (Arriola-Velásquez *et al.*, 2021). Ra_{eq} varied between 108.5 to 210.4 Bq/kg, with a mean of 124.1 Bq/kg. In the current study, all sediments were found to have Ra_{eq} values below the recommended maximum of 370 Bq/kg (Alaamer, 2012). The low Ra_{eq} values in sediments suggest that the geological composition of the area is not rich in uranium or thorium, the sediments were therefore considered to pose a negligible radiological threat to humans. This means that using these sediments for purposes like agriculture, construction, or as a component in building materials would not expose people to dangerous levels of external gamma radiation.



a



b

Figure 4.1: (a): Average activity concentration of ^{232}Th in the sediment samples; (b) Percentage concentration levels of primordial radionuclides in sediments for the study area

Table 4.3 presents a comparison between the average activity concentrations found in this study's sediment samples and those from other parts of Kenya and different global regions.

Table 4.3: The activity concentration of ^{238}U, ^{232}Th, ^{40}K and Ra_{eq} in sediment samples in comparison with other regions.

Country	**Activity concentration (Bq/kg)**			
	^{238}U	^{232}Th	^{40}K	Ra_{eq}
Kenya, Lake Turkana (Current study)	30.09	38.65	664.38	124.10
Kenya, Kargi.(Aguko *et al.,* 2020)	7	8	355	46
Kenya, Lake Nakuru.(Langat *et al.,* 2014)	37	44	708	152
Kenya, Lake Victoria. (Okelo, 2015)	65	146	1223	…
Iraq, Fuel facility (Rasheed *et al.,* 2016)	16	14	306	60
India, Tamilnadun(Raghu *et al.,* 2017)	116	44	300	201
Nigeria, Port Harcourt (Qureshi *et al.,* 2014)	5	4	16	11
Egypt, Nile river (El-Taher & Abbady, 2012)	29	45	123	100

The results from Lake Turkana showed moderate radionuclide concentrations compared to other regions. It had average ^{238}U, ^{232}Th and ^{40}K concentrations of 30.09, 38.65 and 664.38 Bq/kg respectively. Lake Nakuru showed higher ^{238}U (37 Bq/kg) and ^{232}Th (44 Bq/kg) concentrations possibly due to it being surrounded rocks like rhyolites, pumice, and volcanic sediments, all of which are volcanic in origin. It also had a concentration of in ^{40}K (708 Bq/kg) that could result from the small scale farms along rivers Njoro and Ngosur that are the main sources of its water.(Langat *et al., 2014)* The Nile River had lower levels of ^{238}U (29 Bq/kg), ^{232}Th (45 Bq/kg) and ^{40}K

(123 Bq/kg). This was attributed to the sediments studied, which were primarily derived from basic volcanic rocks, as well as acidic and metamorphic rocks. (El-Taher & Abbady, 2012).

It can be concluded that Lake Turkana's sediments primarily originate from volcanic rocks, which generally have lower radionuclide concentrations than those found in Lakes Nakuru and Victoria. Furthermore, Lake Turkana's catchment is less impacted by industrial and agricultural activities compared to the catchments of Lakes Victoria and Nakuru.

4.2.1 Descriptive Statistics for Activity Concentrations in Sediment Samples

The data presented in Table 4.4 provide an overview of the radionuclide activity levels of ^{232}Th, ^{238}U and ^{40}K in the sediment samples. The mean activity was highest for ^{40}K (664.38 Bq/kg), followed by ^{232}Th (38.65Bq/kg) and ^{238}U (30.09Bq/kg).

The arithmetic mean and standard deviation of the activity levels were calculated across all samples and locations to describe the data's central tendency and variability. Skewness measures the asymmetry of the probability distribution of a real-valued random variable. Many models assume that data follow a normal distribution, meaning they are symmetrically distributed around the mean. A normal distribution has a skewness of zero. However, in practice, the data may not always exhibit perfect symmetry (Ravisankar *et al.,* 2014). Positive skewness refers to a distribution with an asymmetrical tail extending toward higher values, while negative skewness indicates a tail extending toward lower values. Lower skewness values typically suggest a more normal distribution. In the current study, the activity concentrations of ^{232}Th and ^{238}U radionuclides exhibited positive skewness, indicating that their distributions were asymmetrical while ^{40}K had negative skewness. Kurtosis measures the "peakedness" of the probability distribution of a real-valued random variable. Kurtosis measures how the peak and tails of a distribution compare to a normal distribution. A distribution with positive kurtosis has a sharper peak and fatter tails, while one with negative kurtosis has a flatter peak and thinner tails. In the current study, the distributions for ^{232}Th and ^{238}U showed positive kurtosis, indicating they were more peaked, whereas the distribution for ^{40}K exhibited a negative kurtosis, indicating a flatter shape (Raghu

et al., 2017). The standard deviation, variance and range were largest for ^{40}K, indicating higher variability in its activity levels.

Table 4.4: Descriptive statistics of sediment samples of Lake Turkana

Variables	**^{232}Th**	**^{238}U**	**^{40}K**
Mean	38.65	30.09	664.38
Standard Error	5.03	3.95	32.07
Median	32.59	26.64	628.61
Std Deviation	15.91	12.49	101.43
Variance	253.01	155.97	10287.98
Kurtosis	2.75	8.34	-0.91
Skewness	1.89	2.79	-0.03
Range	48.23	43.18	319.04
Minimum	27.27	21.31	492.61
Maximum	75.50	64.49	811.65

4.2.2 Pearson Correlation Analysis for Sediment Samples

Table 4.5 displays the Pearson correlation coefficients, which were calculated to determine the relationships between the naturally occurring radioactive materials and the potential health risks in the sediment. Strong positive correlations were observed between ^{232}Th and other parameters such as Ra_{eq} (0.986 Bq/kg) and H_{ex} (0.981), indicating that higher levels of ^{232}Th are closely associated with increased radiological hazard values. ^{238}U and ^{232}Th are often found in the same natural environments. The strong correlation between them (0.867) suggests that they come from the same sources, which are generally linked to a mineralogical component (Raghu et al., 2017). ^{238}U also showed strong correlations with Ra_{eq} (0.870 Bq/kg) and H_{ex} (0.854). However, ^{40}K had a negative correlation with ^{232}Th (-0.317) and ^{238}U (-0.609), suggesting an inverse relationship between these radionuclides.

Radiological parameters such as Ra_{eq}, H_{ex}, H_{in}, ADR, AED_{total} and % ELCR showed extremely high positive correlations with each other, ranging from 0.985 to 1.000. This indicates that these parameters are highly interdependent and reflect similar trends in radiological hazard assessment. The high correlations suggest that variations in the radionuclide activities are strongly linked to radiation risk metrics.

Table 4.5: Pearson correlation matrix.

Variables	^{232}Th	^{238}U	^{40}K	Ra_{eq}	H_{ex}	H_{in}	ADR	AED_{total}	% ELCR
^{232}Th	1.000								
^{238}U	0.867	1.000							
^{40}K	-0.317	-0.609	1.000						
Ra_{eq}	0.986	0.870	-0.222	1.000					
H_{ex}	0.981	0.854	-0.186	0.999	1.000				
H_{in}	0.978	0.924	-0.316	0.992	0.988	1.000			
ADR	0.978	0.849	-0.172	0.999	1.000	0.987	1.00		
AED_{total}	0.975	0.846	-0.163	0.997	0.999	0.985	0.99	1.000	
% ELCR	0.975	0.846	-0.163	0.997	0.999	0.985	0.99	1.000	1.000

4.2.3 Analysis of Variance for sediment samples

ANOVA, or Analysis of Variance, is a statistical test used to determine if the average values of two or more groups are significantly different from each other. A smaller p-value (typically less than 0.05) indicates that there are significant differences between the group means.

Table 4.6 shows the results of a test of ANOVA for different variables (^{232}Th, ^{40}K, Ra_{eq}, H_{ex}, H_{in}, ADR, AED_{total} and ELCR). Significant differences were found in the groups for the following variables (since their p-values were < 0.05): ^{232}Th, Ra_{eq}, H_{ex}, H_{in}, ADR, AED_{total}, and ELCR. ^{40}K did not show significant differences across groups (p-value = 0.492).

Table 4.6: ANOVA between groups for different variables in sediment samples

Variable		Sum of Squares	Df	Mean Square	F-Statistic	P-Value
^{232}Th	Between Groups	6832.775	9	759.197	3.742	0.007
^{40}K	Between Groups	277755.749	9	30861.75	0.97	0.492
Ra_{Eq}	Between Groups	26887.775	9	2987.531	3.356	0.012
H_{ex}	Between Groups	0.193	9	0.021	3.299	0.013
H_{in}	Between Groups	0.356	9	0.04	3.04	0.018
ADR	Between Groups	4972.999	9	552.555	3.206	0.014
AED_{total}	Between Groups	0.19	9	0.021	3.4	0.011
ELCR	Between Groups	0	9	0	3.4	0.011

4.3 Activity Concentration of ^{232}Th, ^{238}U and ^{40}K in Sorghum

The results for activity concentrations of ^{232}Th, ^{238}U and ^{40}K in sorghum samples are detailed in the table 4.7.

Table 4.7: Activity concentrations of the three primordial radionuclides and the resulting effective dose from Sorghum samples

Sample ID	Activity concentration (Bq/kg)			Effective dose (mSv/y)
	^{232}Th	^{238}U	^{40}K	
SOR 1	14.62	13.95	710.50	1.051
SOR 2	19.89	15.18	612.99	1.136
SOR 3	19.98	15.56	771.98	1.237
SOR 4	16.31	14.51	710.05	1.100
SOR 5	16.97	15.77	672.94	1.124
SOR 6	18.47	15.74	813.78	1.233
SOR 7	16.06	11.31	707.22	1.012
SOR 8	13.12	10.81	631.79	0.896
SOR 9	17.35	14.31	752.61	1.140
SOR 10	19.94	16.59	609.56	1.171
AVERAGE	17.27	14.37	699.34	1.110

The average activity concentration of ^{232}Th was 17.27 Bq/kg, with individual values ranging from 13.12 to 19.98 Bq/kg. This was consistent with findings from other regions, such as southwestern Nigeria, where the average for ^{232}Th in agricultural soils was 17.02 Bq/kg (Oladele *et al.,* 2023). The average concentration of ^{238}U is 14.37 Bq/kg, with a range from 10.81 to 16.59 Bq/kg. This aligns with global averages for uranium in soils, which are typically around 33 Bq/kg (Oladele *et al., 2023)*. The average concentration of ^{40}K is 699.34 Bq/kg with values ranging between 609.56 and 813.78 Bq/kg, these concentrations are higher than the global average for potassium in soils, which is approximately 420 Bq/kg. A study in the Bale Zone of Ethiopia reported average concentrations of 4.39 Bq/kg for ^{238}U, 11.30 Bq/kg for ^{232}Th, and 112.64 Bq/kg for ^{40}K in sorghum samples (Abdissa, 2021) . These values are notably lower than those in the current study. However, the activity concentrations observed in these sorghum samples are within the typical ranges found in agricultural products globally (Darko *et al.,* 2015). The average abundance of ^{40}K (699.34 Bq/kg) in sorghum was notably higher than that of ^{232}Th (17.27 Bq/kg) and 14.37 Bq/kg for ^{238}U (Figure 4.2).

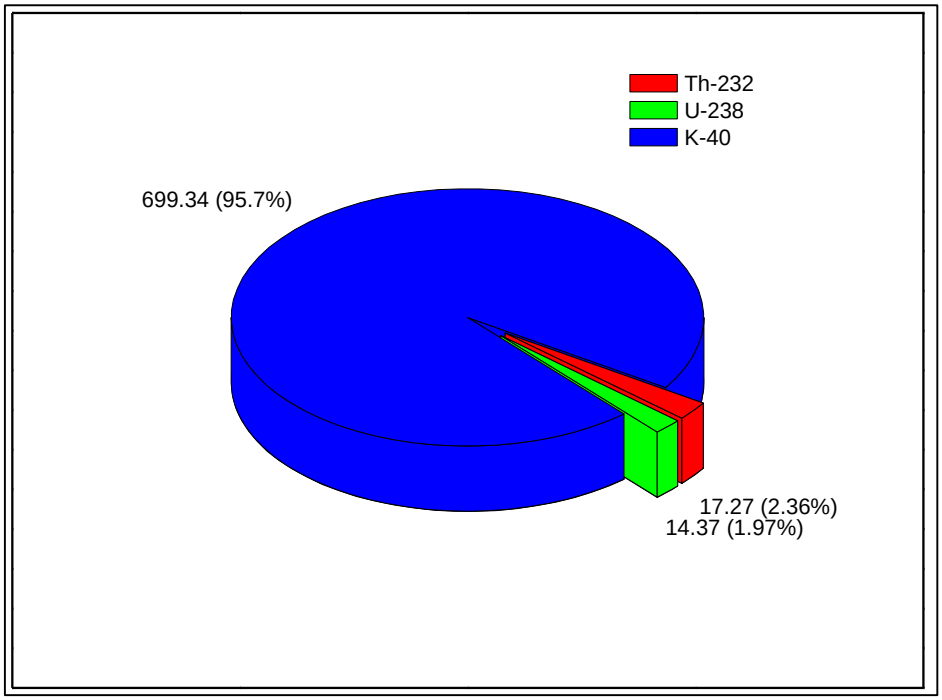


Figure 4.2: Average percentage activity concentration of primordial radionuclides in sorghum.

Regression analysis of radionuclide concentrations in sorghum samples revealed varying degrees of correlation among the three radionuclides studied. A strong, positive correlation was observed between ^{232}Th and ^{238}U, with an R^2 value of 0.6222 (Figure 4.3). This finding suggests a significant relationship between the concentrations of these two radionuclides. The relatively high R^2 value indicates that over 62% of the variability in one radionuclide's concentration can be explained by the other's concentration. This strong correlation is likely due to the similar geochemical behavior of thorium and uranium. Both are heavy elements that tend to be found in similar geological formations, such as certain types of igneous rocks and mineral deposits. As such, they are often leached from the same source rocks in the soil and absorbed by the sorghum plant through similar pathways. The presence of one radionuclide, therefore, serves as a reasonably good predictor of the other's presence.

In contrast, the correlations involving ^{40}K were very weak, indicating little to no relationship with either of the other two radionuclides. The R^2 value for ^{238}U and ^{40}K was 0.0156 (Figure 4.4), and for ^{232}Th and ^{40}K it was 0.0059 (Figure 4.5). These

extremely low values suggest that less than 2% of the variability in these pairs can be explained by the linear models. This is an expected result, as potassium is a vital macronutrient for plants and is absorbed based on the plant's metabolic needs, which are independent of the concentrations of thorium and uranium. Potassium is highly mobile in the soil and is readily available for plant uptake. Conversely, thorium and uranium are generally less mobile and are taken up through different mechanisms, often as trace elements or contaminants.

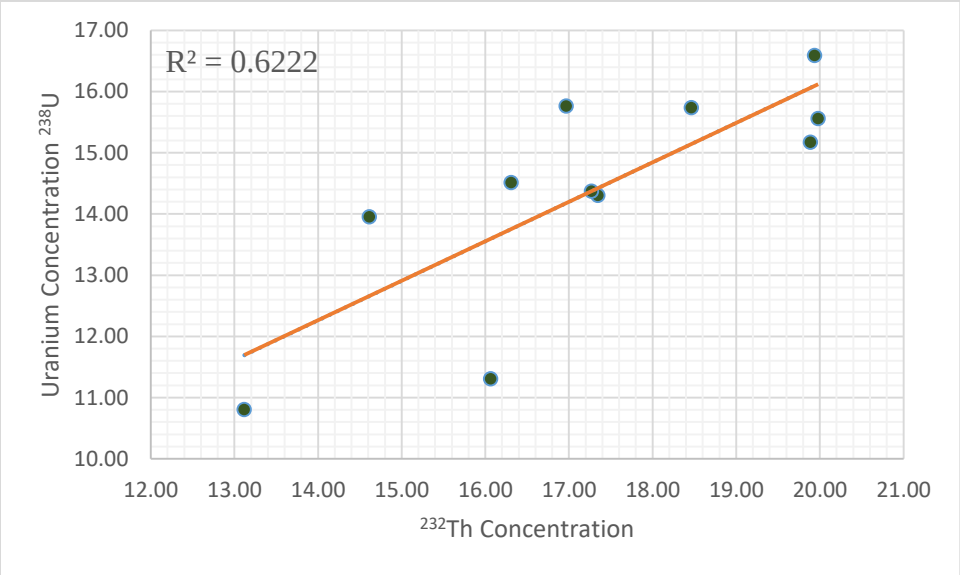


Figure 4.3: Correlation of ^{238}U and ^{232}Th Activity Concentrations

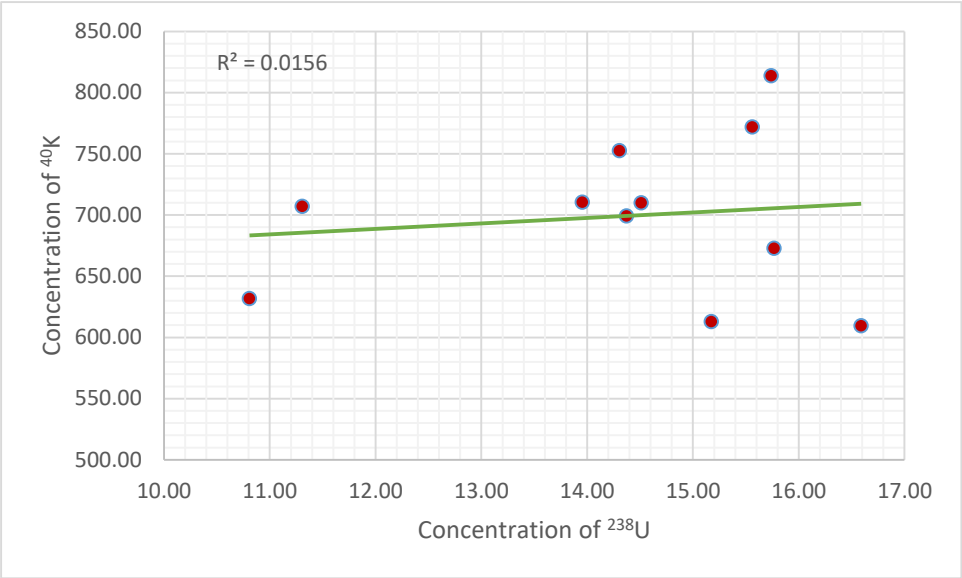


Figure 4.4: Correlation of ^{238}U and ^{232}K activity concentrations

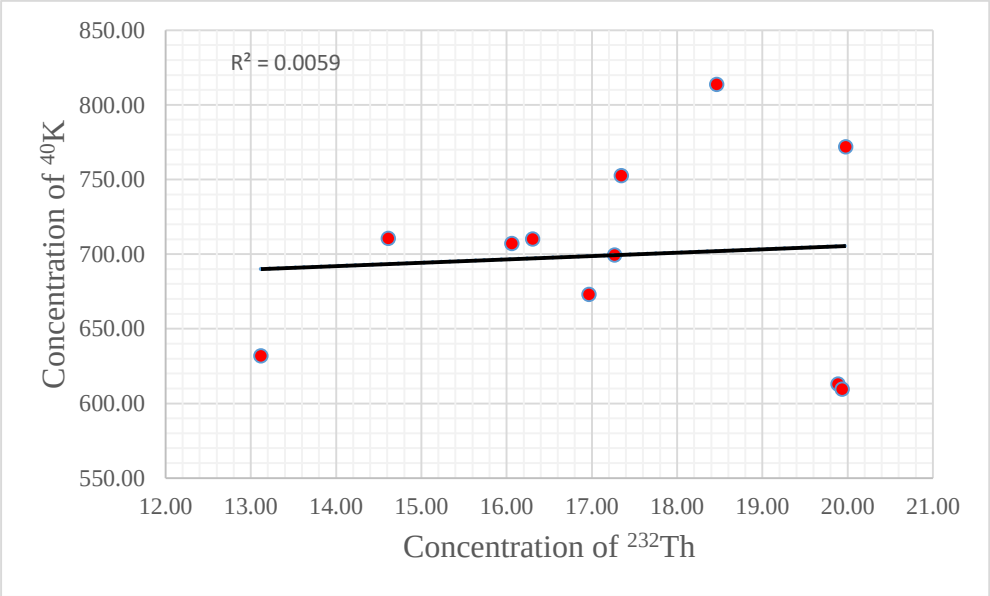


Figure 4.5: Correlation of ^{40}K and ^{232}Th activity concentrations

4.4 Activity Concentration of ^{232}Th, ^{238}U and ^{40}K in Cassava

Table 4.8 presents the activity concentrations of naturally occurring radionuclides ^{232}Th, ^{238}U and ^{40}K in cassava samples (CAS 1 to CAS 4). These radionuclides exist naturally in the soil and can be taken up by plants, including food crops like cassava. The table also includes the calculated "Effective dose (mSv/y).

Table 4.8: Activity concentrations of the three primordial radionuclides and effective dose in cassava samples.

Sample ID	Activity concentration (Bq/kg)			Effective dose (mSv/y)
	^{232}Th	^{238}U	^{40}K	
CAS 1	23.75	18.05	903.69	0.161
CAS 2	21.33	16.59	714.32	0.140
CAS 3	18.20	22.09	827.57	0.155
CAS 4	20.57	20.57	772.10	0.153
AVERAGE	20.96	19.33	804.42	0.152

The activity concentrations of ^{232}Th in the cassava samples range from 18.20 Bq/kg to 23.75 Bq/kg. The average concentration for ^{232}Th is 20.96 Bq/kg. Generally, the uptake of thorium by plants is relatively low, because thorium is not highly soluble and tends to bind strongly to soil particles, limiting its uptake by plants. The activity concentrations of ^{238}U in the samples vary from 16.59 Bq/kg to 22.09 Bq/kg. The average concentration for ^{238}U is 19.33 Bq/kg Similar to thorium, uranium up take by plants is generally low. The activity concentration values of ^{40}K are substantially higher than those of ^{232}Th and ^{238}U, as expected, given potassium′s essential role as a nutrient for plants. Cassava, being a root crop, readily takes up potassium from the soil. The values range from 714.32 Bq/kg to 903.69 Bq/kg with an average concentration of 804.42 Bq/kg.

Comparatively, a study in Ghana reported cassava ^{232}Th concentrations ranging from 1.82 to 10.32 Bq/kg and ^{238}U concentrations ranged from 0.38 to 6.73 Bq/kg (Darko *et al.,* 2015). Thus, the levels in Kang'atosa Ward are higher than those observed in Ghana. The average activity concentrations of ^{226}Ra ^{232}Th and ^{40}K, in cassava tubers from Kilimambogo region in Kenya were 46 ± 5, 105 ± 13 and 555 ± 13 Bq kg^{-1} respectively (Njoroge & Nyambura, 2024). The levels in Kang'atosa ward were lower than those in Kilimambogo for ^{238}U/^{226}Ra and ^{232}Th but higher for ^{40}K. In a Nigerian study, the concentration of ^{226}Ra, ^{232}Th and ^{40}K in cassava tubers was 21.89, 817.17 and 565.31 respectively (Ononugbo *et al.,* 2019). Like in Kilimambogo, the levels in Kang'atosa ward were lower for ^{238}U/^{226}Ra and ^{232}Th but higher for ^{40}K.

4.5 Activity Concentration of ^{238}U, ^{232}Th and ^{40}K in Fish Samples

Table 4.9 presents the calculated activity concentrations of ^{232}Th, ^{238}U, ^{40}K and Ra_{eq} in the analyzed fish samples as well as the average concentration in each fish species. Additionally, the overall mean activity concentrations, minimum, maximum and standard deviation for the radionuclides across all fish samples are also included.

Table 4.9: Activity concentrations of ^{232}Th, ^{238}U, ^{40}K and Ra_{eq} in the fish samples.

Sample type	Sample ID	Radionuclide Activity (Bq/kg)			Ra_{eq} (Bq/kg)
		^{232}Th	^{238}U	^{40}K	
African cat fish	CF 1	1.45 ± 1.48	25.34 ± 4.22	557.65 ± 130.22	70.42
	CF 2	5.95 ± 0.28	26.70 ± 5.45	433.04 ± 169.08	68.55
	CF 3	2.67 ± 0.28	18.55 ± 3.02	510.24 ± 93.22	61.65
MEAN		3.36 ± 1.52	23.55 ± 4.23	500.31 ± 130.84	66.87
Nile perch	NP 1	7.99 ± 5.80	42.98 ± 2.58	444.78 ± 76.28	88.66
	NP 2	27.59 ± 6.90	56.72 ± 3.06	377.86 ± 95.48	125.27
	NP 3	15.13 ± 6.20	48.98 ± 2.77	470.81 ± 81.22	106.87
MEAN		16.90 ± 6.3	49.56 ± 2.81	431.15 ± 84.32	106.93
Nile Tilapia	NT 1	27.94 ± 9.05	19.16 ± 4.03	452.08 ± 125.66	93.93
	NT 2	24.41 ± 9.90	21.86 ± 3.39	526.36 ± 141 15	97.29
	NT 3	21.89 ± 9.27	22.26 ± 4.11	519.60 ± 133.86	93.57
MEAN		24.75 ± 9.41	21.09 ± 4.18	499.38 ± 133.56	94.93
OVERAL MEAN		15.00 ± 5.74	31.40 ± 3.74	476.95 ± 116.24	89.58
Minimum		1.45 ± 1.48	18.55 ± 3.02	377.86 ± 95.48	61.65
Maximum		27.94 ± 9.05	56.72 ± 3.06	557.65 ± 130.22	125.27
Standard deviation		9.20 ± 054	7.88 ± 1.25	68.81 ± 41.45	16.25

^{40}K consistently exhibited the highest activity concentrations across all fish species. The overall mean for ^{40}K was 476.95 ± 116.24 Bq/kg. This was an expected finding, as potassium is an essential element for all living organisms and its radioactive isotope, ^{40}K, is naturally abundant. In contrast, ^{238}U showed moderate activity concentrations, with an overall mean of 31.40 ± 3.74 Bq/kg, while ^{238}Th generally presented the lowest concentrations, having an overall mean of 15.00 ± 5.74 Bq/kg. The Ra_{eq}, which provided a single index for the radiological hazard from these radionuclides, had an

overall mean of 89.58 Bq/kg, ranging from a minimum of 61.65 Bq/kg to a maximum of 125.27 Bq/kg. The standard deviation for Ra_{eq} across all samples was 16.25 Bq/kg.

African Catfish samples showed mean activity concentrations of 3.36 ± 1.52 Bq/kg for ^{232}Th, 23.55 ± 4.23 Bq/kg for ^{238}U, and 500.31 ± 130.84 Bq/kg for ^{40}K, resulting in a mean Ra_{eq} of 66.87 Bq/kg. These values were relatively consistent among the catfish samples, indicating a stable uptake pattern for these radionuclides in this species. Nile Perch samples, however, displayed notably higher mean concentrations for both ^{232}Th (16.90 ± 6.30 Bq/kg) and ^{238}U (49.56 ± 2.81 Bq/kg) compared to the African Catfish. The mean ^{40}K concentration in Nile Perch (431.15 ± 84.32 Bq/kg) was slightly lower than in African Catfish. The elevated concentrations of ^{238}U and ^{232}Th in Nile Perch contributed to a significantly higher mean Ra_{eq} of 106.93 Bq/kg for this species, indicating a greater radiological burden compared to the African Catfish. The variability, as indicated by the standard deviations, was also higher for ^{232}Th (6.30 Bq/kg) and ^{238}U (2.81 Bq/kg) in Nile Perch, suggesting more diverse individual uptake or environmental exposure. Nile Tilapia samples exhibited the highest mean ^{232}Th activity concentration at 24.75 ± 9.41 Bq/kg, while their mean ^{238}U concentration (21.09 ± 4.18 Bq/kg) was comparable to that of African Catfish but considerably lower than Nile Perch. The mean ^{40}K concentration for Nile Tilapia (499.38 ± 133.56 Bq/kg) was very similar to that of African Catfish. The Ra_{eq} for Nile Tilapia averaged 94.93 Bq/kg, placing it between African Catfish and Nile Perch in terms of overall radiological hazard. The standard deviations for ^{232}Th in Nile Tilapia (9.41 Bq/kg) were quite large, suggesting considerable variation in thorium uptake among individual tilapia samples.

Overall, the results highlighted that while ^{40}K was the most abundant radionuclide across all sampled fish, the concentrations of ^{238}U and ^{232}Th, and consequently the radiological hazard (Ra_{eq}), varied significantly among different fish species. Nile Perch showed the highest accumulation of ^{238}U and the highest Ra_{eq}, while Nile Tilapia demonstrated the highest ^{232}Th levels. These variations likely reflected differences in the feeding habits, habitat preferences, and metabolic processes of each fish species within the Lake Turkana ecosystem. The reported standard deviations indicated a degree of natural variability in radionuclide uptake even within the same species. The

overall standard deviations across all samples were 9.20 ± 0.54 Bq/kg for ^{232}Th, 7.88 ± 1.25 Bq/kg for ^{238}U, and 68.81 ± 41.45 Bq/kg for ^{40}K.

The average abundance of ^{40}K in the studied fish was notably higher than that of ^{232}Th and ^{238}U (Figure 4.6a).

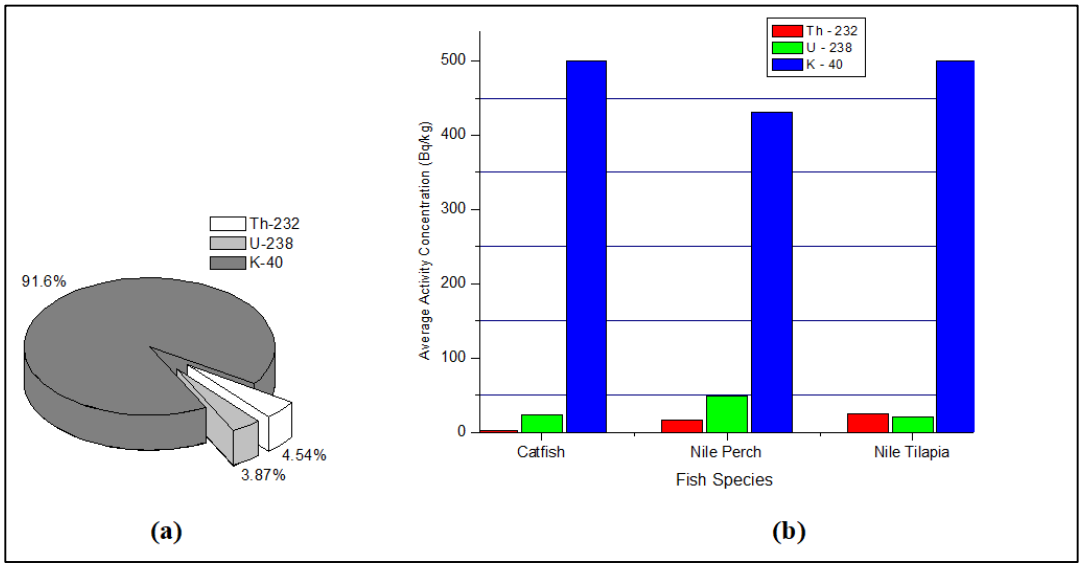


Figure 4.6: (a) Average percentage activity concentration of primordial radionuclides in fish; (b) Activity concentration levels of radionuclides in the fish.

The activity concentrations of the three radionuclides varied significantly across the fish species. The variation was attributed to differences in habitats where the fish live, feeding habits and individual fish metabolism which influence the bioaccumulation of radionuclides. The activity concentration of ^{40}K was relatively high across all species (Figure 4.6b). This was expected since potassium is a naturally occurring element in biological systems.

Table 4.10 presents average radionuclide activity concentrations (in Bq/kg) in fish samples from various global locations, offering a comparative overview that includes data from the current work on Lake Turkana. ^{40}K consistently showed the highest activity concentrations across almost all locations, a common finding in biological samples due to its essential role in biological processes and relatively high natural abundance. Lake Turkana's fish exhibited the highest ^{40}K concentration among those listed in the studies (476.95 ± 116.24 Bq/kg), surpassing values from River Kubanni

of 270.14 Bq/kg (Adigun & Sodipo, 2024), Bay of Bengal of 250 ± 50 Bq/kg (Biswas *et al.,* 2021), and Epe Waterside Region of 282.7 ± 17.9 Bq/kg (Olurin, 2024). The lowest ^{40}K values (86.65 Bq/kg) were reported in Hong Kong (Yu *et al.,* 1997).

^{232}Th activity concentrations varied significantly among fish from different global locations. Fish from the Epe Waterside Region of Lagos, Nigeria (245.80 ± 7.7 Bq/kg) reported by Olurin (2024) showed an exceptionally high ^{232}Th level, considerably higher than those from most of the other locations. In contrast, fish from Jeddah-Saudi Arabia that gave 1.66 Bq/kg (Safia, 2016) and Hong Kong (0.47 Bq/kg) (Yu *et al.,* 1997) had very low ^{232}Th levels. For fish from Lake Turkana, ^{232}Th concentration (15.00 ± 5.74 Bq/kg) is relatively low compared to fish from sites like River Kubanni (77.24 Bq/kg) (Adigun &Sodipo, 2024) and Kainji Lake (94.82 Bq/kg) (Adamu *et al.,* 2013), but higher than those from Jeddah and Hong Kong. ^{238}U data was reported only in fish from Jeddah-Saudi Arabia (1.63 Bq/kg), Hong Kong (0.018 Bq/kg), and Lake Turkana (31.40 ± 3.74 Bq/kg). Among these, Lake Turkana's fish had a substantially higher ^{238}U concentration compared to those from Jeddah and Hong Kong. This highlights a potential regional difference in uranium uptake or availability in the aquatic environment. Ra_{eq} was presented in a few locations such as the Eastern Libyan Coast which had a Ra_{eq} of 103.40 ± 3.64 Bq/kg, that was relatively close to Lake Turkana's value of 89.58 Bq/kg. ^{40}K concentration in Lake Turkana's fish was notably the highest, suggesting a significant natural presence of potassium in the lake's ecosystem.

Table 4.10: Average radionuclide concentration and radiation Ra_{eq} in fish samples of this study and the values of similar studies from other regions.

Location	Average Radionuclide Activity in fish samples (Bq/kg)				
	^{232}Th	^{226}Ra	^{238}U	^{40}K	Ra_{eq} (Bq/kg)
Eastern Libyan Coast (R. Hamad *et al.*, 2023)	16.84±0.92	86.40±0.98	….	146.63±0.05	103.40 ±3.64
River Kubanni in Nigeria (Adigun & Sodipo, 2024)	77.24	46.86	….	270.14	….
Bay of Bengal Chattogram, Bangladesh (Biswas *et al.,* 2021)	67 ± 9	5 ± 2	….	250 ± 50	….
Epe Waterside Region of Lagos, Nigeria (Olurin, 2024)	245.80 ± 7.7	80.15 ± 65.40	….	282.7 ± 17.9	….
Jeddah-Saudi Arabia (Safia, 2016)	1.66	1.6	1.63	208.13	…..
Hong Kong (Yu *et al.,* 1997)	0.47	0.005	0.018	86.65	….
Kainji lake (Adamu *et al.,* 2013)	94.82	37.22	….	384.98	….
Lake Turkana (Current study)	15.00 ± 5.74	….....	31.40 ± 3.74	476.95 ± 116.24	89.58

In summary, the data in Table 4.10 revealed significant variability in radionuclide concentrations in fish across different geographical locations, which likely stemmed from diverse geological backgrounds, environmental conditions, and specific aquatic ecosystem characteristics. The fish samples from Lake Turkana generally exhibited moderate to high concentrations of the measured primordial radionuclides, particularly for ^{40}K and ^{238}U, when compared to the available global data.

Figure 4.7 a-c displays histograms showing the frequency distribution for all the radioactive variables measured in the analyzed fish. These histograms approximate the

probability distribution of these continuous variables. Notably, the graphs for ^{232}Th and ^{40}K suggest that these radionuclides follow a normal, or bell-shaped, distribution (Raghu et al., 2017) while that of ^{238}U has minimal skewness to the right.

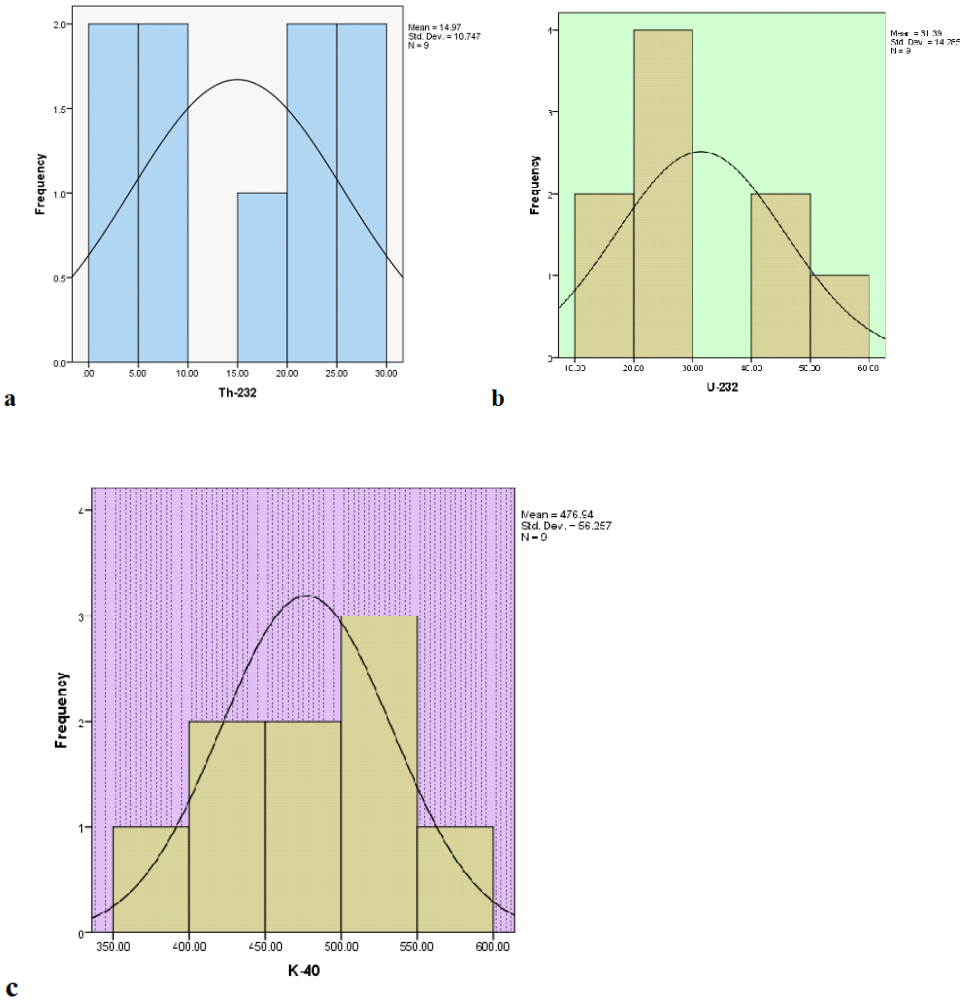


Figure 4.7: (a) Frequency distribution of ^{232}Th; (b) Frequency distribution of ^{238}U; and (c) Frequency distribution of ^{40}K.

4.6 Hazard indicators in sediment samples

Table 4.11 presents radiation hazard indicators in sediment samples collected from various sample sites. The parameters presented include Absorbed Dose Rate (ADR), Total Annual Effective Dose (AED_{tot}), Excess Lifetime Cancer Risk (ELCR), Hazard Indices (H_{ex} and H_{in}), and Gamma Index(I_γ). These indicators provide crucial insights into the potential radiological risks associated with the sediments, helping to assess environmental safety and potential health impacts on residents and ecosystems. The data is for regions including Kerio, Eliye, Kalokol, Nachukui and Nareng'ewoi.

Table 4.11: Hazard indicators for sediment samples.

Sample ID	Hazard indicator					Gamma Index (I_γ)
	H_{ex}	H_{in}	ADR (nGy/h)	AED_{total} (mSv/y)	% ELCR	
ELI 1	0.464	0.538	76.667	0.470	0.018	0.613
ELI 2	0.462	0.522	75.513	0.463	0.018	0.608
ELI 3	0.555	0.656	92.749	0.569	0.022	0.737
KERIO 1	0.453	0.534	75.712	0.464	0.018	0.602
KERIO 2	0.265	0.294	45.007	0.276	0.011	0.358
KERIO 3	0.349	0.410	58.344	0.358	0.014	0.464
LOD 1	0.433	0.549	71.852	0.411	0.016	0.567
LOD 2	0.286	0.344	47.767	0.293	0.011	0.379
LOD 3	0.289	0.326	49.078	0.301	0.012	0.39
KAL 1	0.513	0.601	85.684	0.525	0.020	0.682
KAL 2	0.617	0.833	100.795	0.618	0.024	0.792
KAL 3	0.621	0.840	101.348	0.621	0.024	0.796
KATA 1	0.348	0.411	58.364	0.358	0.014	0.463
KATA 2	0.326	0.383	55.132	0.338	0.013	0.437
KATA 3	0.381	0.457	63.798	0.391	0.015	0.506
NACH 1	0.405	0.509	67.363	0.413	0.016	0.532
NACH 2	0.241	0.282	40.430	0.248	0.010	0.321
NACH 3	0.419	0.514	69.785	0.428	0.016	0.553
KANG 1	0.343	0.411	57.671	0.354	0.014	0.457
KANG 2	0.409	0.514	68.017	0.417	0.016	0.537
KANG 3	0.343	0.419	57.187	0.351	0.014	0.453
LONG 1	0.442	0.543	73.657	0.452	0.017	0.583
LONG 2	0.202	0.228	34.259	0.210	0.008	0.272
LONG 3	0.374	0.457	62.456	0.383	0.015	0.495
NARI 1	0.298	0.340	50.690	0.311	0.012	0.402
NARI 2	0.345	0.430	57.297	0.351	0.014	0.453
NARI 3	0.295	0.345	49.146	0.301	0.012	0.391
NARE 1	0.267	0.297	45.443	0.279	0.011	0.362
NARE 2	0.491	0.589	81.952	0.503	0.019	0.65

4.6.1 External Hazard Index (H_{ex}) and Internal Hazard Index (H_{in}) in sediment samples

For all samples, both the H_{ex} and H_{in} values were less than 1. This suggested that the radiation hazard from both external and internal exposure pathways due to these sediment samples was below the internationally recognized safe limits. This indicates

that, based on these indices, the sediments posed a negligible radiological health risk in terms of direct exposure and potential intake of radionuclides. The values generally ranged from around 0.202 to 0.621 for H_{ex} and 0.228 to 0.840 for H_{in}. The highest values for both H_{ex} and H_{in} were observed in the KAL series (KAL 1, KAL 2, KAL 3), particularly KAL 2 (H_{ex} = 0.617, H_{in} = 0.833) and KAL 3 (H_{ex} = 0.621, H_{in} = 0.840). While these were the highest in the dataset, they still remained well below the unity threshold, indicating safety.

4.6.2 Absorbed Dose Rate (ADR) in Sediment Samples

ADR measurements showed a wide range of values, with the lowest recorded being 34.259 nGy/h (from the LONG 2 sample) and the highest at 101.348 nGy/h (from the KAL 3 sample). Higher ADR values were notably concentrated in the ELI and KAL series. ELI 3 had an ADR of 92.749 nGy/h, while KAL 1, KAL 2, and KAL 3 showed consistently high values of 85.684, 100.795, and 101.348 nGy/h respectively. These values were considerably higher than the typical global average outdoor absorbed dose rate from terrestrial gamma rays, which is often cited around 59 nGy/h. This suggests that while still within acceptable hazard index limits, the instantaneous exposure in these areas might be higher than average. Lower ADR values were seen in samples like NACH 2 (40.430 nGy/h), KERIO 2 (45.007 nGy/h), LODW 2 (47.767 nGy/h), and LONG 2 (34.259 nGy/h). These sites represent areas with lower ambient gamma radiation levels from the sediment.

4.6.3 Annual Effective Dose Equivalent (AED_{total}) in Sediment Samples

The AED_{total} values ranged from 0.008 mSv/y (LONG 2) to 0.024 mSv/y (KAL 2 and KAL 3). All the AED_{total} values were below the global average outdoor effective dose equivalent from terrestrial gamma radiation (0.07 mSv/y). This was a very reassuring finding, as it implied that the annual radiation dose received by individuals from these sediments is less than the natural background radiation from terrestrial sources in many parts of the world. Similar to ADR, the KAL samples (KAL 1, KAL 2, KAL 3) exhibit the highest AED_{total} values (0.020, 0.024, and 0.024 mSv/y respectively), indicating a slightly higher, though still safe, annual dose.

4.6.4 Excess Lifetime Cancer Risk (ELCR) in Sediment Samples

The ELCR values were relatively low across all samples, ranging from 0.008% (LONG 2) to 0.024% (KAL 2 and KAL 3). These values represented the additional probability of developing cancer over a lifetime due to exposure to radiation from these sediment samples. Given the magnitude of these percentages (all below 0.03%), the excess lifetime cancer risk was very low for all samples. This meant that the contribution of these sediments to an individual's overall cancer risk was minimal. The KAL samples (KAL 1, KAL 2, KAL 3) again gave the highest ELCR values (0.020%, 0.024%, and 0.024% respectively), consistent with their higher ADR and AED_{total} values. However, even these highest values were considered to be very small in the context of overall cancer risk. In conclusion, these hazard indicators for the sediment samples painted a reassuring picture regarding radiological safety. While there were variations in radioactivity levels across different samples, all measured parameters fell within internationally accepted safety limits, suggesting a low risk of exposure of the population to radiation from these sediments.

4.6.5 Gamma Index (Iγ) of Sediment Samples

All sediment samples from the Eliye, Kerio, Lodwar, Kalokol, Kataboi, Nachukui, Kang'atosa, Long'ech, Nariokotome, and Nareng'ewoi locations had a gamma index value below 1. The highest values were found in samples KAL 2 ($I\gamma = 0.792$) and KAL 3 ($I\gamma = 0.796$), followed by ELI 3 ($I\gamma = 0.737$). Despite these being the highest values, they still fall well below the critical threshold of 1. The lowest gamma index value was for sample LONG 2 ($I\gamma = 0.272$), which indicates a very low radiological risk from the radionuclides in that sample. The results consistently show that none of the samples pose a significant radiological hazard based on the gamma index criterion. Therefore, all sampled sediment were considered safe from a radiological perspective.

4.6.6 Average Hazard Indicators in Sediment Samples across Sampling Locations

Table 4.12 presents the average hazard indicators derived from sediment samples collected at different locations.

Table 4.12: Hazard indicators of activity of sediment samples across various locations

Sampling location	H_{ex}	H_{in}	ADR (nGy/h)	AED_{total} (mSv/y)	% ELCR	Gamma Index (I_γ)
Eliye	0.493	0.572	81.643	0.501	0.019	0.653
Kerio	0.355	0.413	59.688	0.366	0.014	0.475
Lodwar	0.336	0.406	56.232	0.335	0.013	0.445
Kalokol	0.584	0.758	95.942	0.588	0.023	0.757
Kataboi	0.351	0.417	59.098	0.362	0.014	0.469
Nachukui	0.355	0.435	59.193	0.363	0.014	0.469
Kang'atosa	0.365	0.448	60.958	0.374	0.014	0.482
Long'ech	0.339	0.409	56.791	0.348	0.013	0.45
Nariokotome	0.312	0.372	52.378	0.321	0.012	0.415
Nareng'ewoi	0.403	0.477	67.563	0.414	0.016	0.536
AVERAGE	0.389	0.471	64.949	0.397	0.015	0.515

For all sampled locations, both the H_{ex} and H_{in} were below 1. The H_{ex} values ranged from 0.312 (Nariokotome) to 0.584 (Kalokol). Similarly, H_{in} values ranged from 0.372 (Nariokotome) to 0.758 (Kalokol). While all values were safe, Kalokol consistently showed the highest values for both H_{ex} and H_{in} among the individual locations, suggesting a slightly higher, though still safe, concentration of radionuclides compared to the other areas. The Study Area Average for H_{ex} was 0.389 and for H_{in} was 0.471, reinforcing the overall low hazard.

The Absorbed Dose Rate (ADR) ranged from 52.378 nGy/h (Nariokotome) to 95.942 nGy/h (Kalokol). Kalokol stood out with the highest ADR at 95.942 nGy/h. Eliye also showed a relatively high ADR of 81.643 nGy/h. Conversely, locations like Nariokotome, Lodwar, and Long'ech exhibited lower ADR values, indicating less ambient gamma radiation from their sediments. The study area average ADR was 64.949 nGy/h, which was slightly above the global average, indicating that, on average, the region had slightly elevated natural background radiation from its sediments. The AED_{total} ranged from 0.321 mSv/y (Nariokotome) to 0.588 mSv/y (Kalokol). The study area average AED_{total} was 0.397 mSv/y, which was also well above the global average. This indicates that residents in these areas are exposed to a

higher annual radiation dose from the sediment compared to the global average for natural terrestrial sources.

The ELCR ranged from 0.012% to 0.023%. Kalokol again showed the highest ELCR at 0.023%. The study area average ELCR was 0.015%, which was also very low. This suggested that despite the higher AED_{total} values compared to the global average, the additional lifetime cancer risk attributable specifically to these sediments was still quite low. In summary, the sediments in these sampling locations contributed to a higher natural background radiation compared to many other parts of the world, but the levels were generally not considered to pose an alarming health risk based on these standard hazard indicators.

All ten sampling locations, including the overall study area average, had a gamma index value below the critical threshold of 1. The highest gamma index was recorded at Kalokol ($I\gamma = 0.757$), followed by Eliye ($I\gamma = 0.653$). While these were the highest values, they are still well below the safety limit. The lowest gamma index value was at Nariokotome ($I\gamma = 0.415$), indicating the lowest radiological risk among the samples. The average gamma index for the entire study area was 0.515. This value is also significantly less than 1, reinforcing the conclusion that, on average, the sediment samples from this area do not pose a significant radiological hazard. The results are consistent across all samples, showing that the naturally occurring radiation levels in the sediments from these locations are not a cause for concern.

4.7 Annual Effective Dose Due to Ingestion of Crop Samples

Table 4.13 presents results for the AED from ingestion of cassava tubers and sorghum. The AED from cassava tubers ranged from 0.14 to 0.161 mSv/y. The average AED of 0.152 mSv/y from cassava ingestion was well below the international safety limit of 1 mSv/yr recommended by the International Commission on Radiological Protection (ICRP).

The AED from sorghum ranged from 0.896 to 1.237 mSv/y. The average AED of 1.110 mSv/yr from sorghum ingestion exceeded the 1 mSv/yr safety limit and $0.38 \pm 0.07 \mu Sv/y$ in sorghum from Villy at the West Central Region of Burkina Faso (Bangou *et al.,* 2024). While 1.110 mSv/yr was higher than the recommended limit, it

was still within the typical range of natural background radiation doses to which individuals are exposed globally.

Table 4.13: Calculated annual effective doses via ingestion.

Exposure pathway	Effective dose (mSv/y)		
	Minimum	Maximum	Average
Cassava tubers	0.140	0.161	0.152
Sorghum	0.896	1.237	1.110

4.8 Heavy Metals Concentration in the Water and Fish Samples

This section examines heavy metal concentrations in surface waters and fish samples, providing an integrated assessment of contamination patterns and associated risks. Subsection 4.8.1 focuses on metal concentrations in surface water from Lake Turkana, while 4.8.2 presents corresponding findings from the Turkwel River. Subsection 4.8.3 compares the observed concentrations with values reported in other regional studies and World Health Organization (WHO) drinking water standards. To provide a more holistic evaluation, 4.8.4 introduces water quality indices. Finally, 4.8.5 investigates metal concentrations in fish muscle tissue, highlighting patterns of bioaccumulation across species and their implications for food safety.Together, these subsections offer a comprehensive overview of heavy metal contamination in the Lake Turkana Basin, establishing baseline data essential for environmental monitoring, public health protection, and resource management.

4.8.1 Metals Concentration in Surface Water of Lake Turkana

Table 4.14 presents the concentrations of heavy metals (Zn, Cd, Ba, Cu, Ni, As, Pb, Cr) in water samples from different locations. The data highlights the variability in concentrations across the sampling sites, providing insights into regional water quality and potential environmental concerns. Some values were recorded as < 0.01, indicating that the specific elements in certain samples were below the detection limit of the MP-AES equipment.

Arsenic (As) appeared to be the most prevalent heavy metal across almost all sampling locations, with concentrations often exceeding 0.3 mg/L. The highest arsenic

concentrations were observed in Eliye, particularly Eliye 3 (1.20 mg/L), Eliye 1 (1.13 mg/L), and Eliye 2 (1.11 mg/L). Kerio also had elevated As levels, with Kerio 3 reaching 1.09 mg/L and Kerio 2 at 0.90 mg/L. Kang'atosa similarly showed high values, with Kang 1 at 0.93 mg/L and Kang 2 at 0.92 mg/L. Kataboi samples generally had lower As levels compared to other locations, with KATA 1 showing 0.28 mg/L and Nachukui samples also exhibiting relatively low concentrations. Zinc concentrations varied significantly across locations. Eliye stood out with exceptionally high Zn concentrations, especially Eliye 1 (4.58 mg/L) and Eliye 2 (3.81 mg/L). This was a significant finding and warranted further investigation. Other locations had much lower Zn levels, generally below 1 mg/L. For instance, Nariokotome and Kataboi had very low Zn concentrations, typically below 0.1 mg/L. Lodwar had a high value of Zn in LODW 2 (1.88 mg/L). Cadmium concentrations were remarkably low across all samples, mostly at 0.01 mg/L or 0.02 mg/L. Some samples such as Eliye 3 had a concentration that was too low to be measured, falling below 0.01 mg/L. KANG 1 and Kang 3 had slightly elevated Cd levels at 0.03 mg/L, though still very low overall. Barium concentrations showed moderate variability. LOD 1 had the highest Ba concentration at 0.63 mg/L. Most other locations showed Ba concentrations ranging from 0.01 mg/L to 0.18 mg/L. Eliye 2 had a very low concentration of <0.01 mg/L. Copper concentrations were generally low, mostly ranging from 0.01 mg/L to 0.08 mg/L. Eliye 1 showed a Cu concentration of 0.13 mg/L, and Eliye 3 had 0.10 mg/L. Kalokol also had slightly higher values in KALO 1 (0.06 mg/L) and KALO 3 (0.04 mg/L). Nickel concentrations were consistently low across all samples, often at or below 0.01 mg/L. Many samples had concentrations that were too low to be measured, falling below 0.01 mg/L. KATA 2 showed a notable elevation in Ni concentration at 0.59 mg/L, which was significantly higher than any other sample. Lead concentrations were generally low, with many samples showing levels at 0.01 mg/L or 0.02 mg/L. Several samples were below the detection limit (<0.01 mg/L). LOD 1 had a significantly higher Pb concentration at 0.32 mg/L. Chromium concentrations were consistently very low across all samples. Most samples showed concentrations of 0.01 mg/L or below the detection limit (<0.01 mg/L). Eliye 1 showed the highest Cr concentration at 0.12 mg/L, followed by Eliye 2 at 0.08 mg/L and Eliye 3 at 0.09 mg/L.

Table 4.14: Concentrations of heavy metals in water samples across various sampling locations (mg/l)

Sampling location	Sample ID	Metal concentration (mg/L)							
		Zn	Cd	Ba	Cu	Ni	As	Pb	Cr
Nariokotome	NARI 1	0.04	0.01	0.08	0.02	0.03	0.48	0.03	0.01
	NARI 2	0.08	0.01	0.18	0.01	0.03	0.62	0.05	0.01
	NARI 3	0.12	0.02	0.01	0.01	0.02	0.59	0.02	0.02
Kerio	KERIO 1	0.33	0.01	0.17	0.03	0.05	0.86	<0.01	<0.01
	KERIO 2	0.23	0.01	0.09	0.02	<0.01	0.9	0.02	<0.01
	KERIO 3	0.11	0.02	0.16	0.02	0.04	1.09	0.01	<0.01
Eliye	ELIYE 1	4.58	0.01	0.08	0.13	0.01	1.13	0.02	0.12
	ELIYE 2	3.81	0.011	<0.01	0.04	0.01	1.11	0.01	0.08
	ELIYE 3	1.94	<0.01	0.09	0.1	0.01	1.2	0.01	0.09
Kang'atosa	KANG 1	0.6	0.03	0.16	0.04	0.01	0.93	0.02	0.01
	KANG 2	1.24	0.01	0.06	0.02	0.02	0.92	0.03	0.02
	KANG 3	0.8	0.03	0.08	0.02	0.02	0.78	0.04	0.01
Kalokol	KALO 1	0.12	0.02	0.09	0.06	0.01	0.84	0.03	0.01
	KALO 2	0.11	0.01	0.1	0.02	0.012	0.51	<0.01	<0.01
	KALO 3	0.03	0.01	0.07	0.04	0.01	0.38	0.03	<0.01
Kataboi	KATA 1	0.05	0.01	0.12	0.02	0.01	0.28	<0.01	<0.01
	KATA 2	0.06	0.01	0.18	0.01	0.59	0.46	0.01	<0.01
	KATA 3	0.02	0.01	0.13	0.02	0.02	0.42	0.01	<0.01
Lodwar	LOD 1	0.35	0.03	0.63	0.01	0.03	0.39	0.32	0.01
	LOD 2	1.88	0.01	0.15	0.02	<0.01	0.54	<0.01	<0.01
	LOD 3	0.21	0.02	0.03	0.03	<0.01	0.53	0.02	0.01
Nareng'ewoi	NARE 1	0.87	0.01	0.04	0.02	<0.01	0.57	<0.01	<0.01
	NARE 2	0.41	0.01	0.12	0.04	0.01	0.47	<0.01	<0.01
	NARE 3	0.04	0.01	0.08	0.04	0.01	0.65	0.02	<0.01
Long'ech	LONG 1	0.12	0.01	0.15	0.05	<0.01	0.6	<0.01	0.01
	LONG 2	0.12	0.01	0.18	0.08	0.02	0.67	0.01	0.01
	LONG 3	0.06	0.01	0.08	0.03	0.01	0.51	0.02	<0.01
Nachukui	NACH 1	0.21	0.02	0.04	0.02	<0.01	0.41	<0.01	<0.01
	NACH 2	0.06	0.01	0.02	0.02	<0.01	0.34	<0.01	<0.01
	NACH 3	0.16	0.03	0.04	0.01	<0.01	0.36	0.03	<0.01
Drinking water limit (WHO, 2011)		5	0.003	0.7	2	0.07	0.01	0.01	0.05

Based on the heavy metal concentration data in Table 4.14, the water quality across the study area, the heavy metal concentrations frequently exceeding the World Health

Organization (WHO) 2011 drinking water guidelines. Both Arsenic and Lead exceed the WHO limit of 0.01 mg/L for drinking water. Every single sampling location, from the upstream river Turkwel site at Lodwar to the various lake shores like Eliye and Kerio, recorded levels significantly higher than this limit. For instance, Arsenic reached a dangerous peak of 1.31 mg/L at Eliye, while Lead concentrations were recorded as high as 1.2 mg/L at the same location. This universal exceedance suggests a widespread contamination issue that affects the entire hydrological system of the basin, rendering the water unsafe for direct consumption without treatment.

Beyond Arsenic and Lead, other metals show significant localized spikes that further degrade water quality. Nickel often exceeded its 0.07 mg/L limit, particularly at Lodwar (0.63 mg/L) and Nariokotome (0.59 mg/L). While Zinc levels generally remain within the safe limit of 3.0 mg/L for most sites, the Eliye shoreline was a notable exception, recording a concentration of 4.58 mg/L, which was well above the safety threshold. Similarly, Cd presents a specific risk in the riverine area; while most lake sites are near the limit, Lodwar recorded 0.03 mg/L, which is ten times the stringent WHO limit of 0.003 mg/L, indicating a significant source of Cadmium pollution upstream.

Geographically, the data indicates that the Turkwel River acts as a major transport pathway for these contaminants. The high concentrations of Ni, As, and Cd found upstream at Lodwar persist downstream at Kang'atosa, eventually feeding into the lake. Among the lake shore locations, Eliye appears to be the most heavily contaminated "hotspot," consistently registering the highest maximum values for Zn, As, and Pb. Consequently, the distinct pattern of heavy metal accumulation particularly at Eliye and Lodwar indicates that the water poses severe health risks, ranging from potential neurotoxicity to carcinogenic effects, if used as a primary source of drinking water.

Table 4.15 provides a comprehensive analysis of the average concentrations of eight heavy metals—Zn, Cd, Ba, Cu, Ni, As, Pb, and Cr—across eight distinct water sampling locations along the shores of Lake Turkana. All concentrations are expressed in milligrams per liter (mg/L), and each is accompanied by its standard deviation, which indicates the variability of measurements at that specific site. The overall

average concentration for each element across all locations is also presented, rounded to three decimal places.

Table 4.15: Average concentrations of heavy metals in surface water across various sampling locations along shores of L. Turkana

Sampling Location	Average concentration (mg/L)							
	Zn	Cd	Ba	Cu	Ni	As	Pb	Cr
Nariokotome	0.080 ±0.023	0.013 ± 0.003	0.130 ± 0.041	0.013 ± 0.003	0.027 ± 0.003	0.563 ± 0.043	0.033 ± 0.009	0.013 ± 0.001
Kerio	0.223 ± 0.063	0.013 ± 0.003	0.140 ± 0.025	0.023 ± 0.003	0.045 ± 0.004	0.950 ± 0.0	0.010 ± 0.004	ND
Eliye	0.443 ± 0.784	0.011 ± 0.001	0.085 ± 0.004	0.09 ± 0.004	0.010 ± 0.0	1.147 ± 0.027	0.013 ± 0.003	0.047 ± 0.012
Kalokol	0.087 ± 0.029	0.013 ± 0.003	0.087 ± 0.009	0.04 ± 0.012	0.011 ± 0.001	0.577 ± 0.137	0.030 ± 0.0	0.010 ± 0.0
Kataboi	0.043 ± 0.012	0.010 ± 0.0	0.143 ± 0.019	0.017 ± 0.003	0.008 ± 0.002	0.478 ± 0.002	0.010 ± 0.0	ND
Nareng'ewoi	0.440 ± 0.240	0.010 ± 0.0	0.080 ± 0.023	0.033 ± 0.007	0.010 ± 0.0	0.768 ± 0.002	0.020 ± 0.0	ND
Long'ech	0.100 ± 0.020	0.010 ± 0.0	0.137 ± 0.030	0.053 ± 0.015	0.015 ± 0.004	0.984 ± 0.028	0.015 ± 0.004	0.010 ± 0.0
Nachukui	0.143 ± 0.044	0.020 ± 0.006	0.033 ± 0.007	0.019 ± 0.033	ND	0.579 ± 0.023	0.030 ± 0.0	ND
Overall average	0.195 ± 0.152	0.013 ± 0.002	0.104 ± 0.020	0.036 ± 0.01	0.016 ± 0.002	0.756 ± 0.033	0.020 ± 0.003	0.010 ± 0.002
Drinking water limit (WHO, 2011)	5	0.003	0.7	2	0.07	0.01	0.01	0.05

Arsenic showed the highest overall average concentration, which was 0.756±0.033 mg/L. This element exhibited consistently elevated levels across most locations. Its concentrations ranged from a low of 0.478±0.002 mg/L at Kataboi to a significant peak of 1.147±0.027 mg/L at Eliye. Other sites like Kerio (0.950±0.0 mg/L) and Longéch (0.984±0.028 mg/L) also displayed concentrations approaching 1.0 mg/L. Despite these high average concentrations, the standard deviations for As were generally low, indicating a consistent and prevalent presence of this element across the sampled areas. Cadmium had a remarkably low and consistent overall average concentration of 0.013±0.002 mg/L. Individual site concentrations generally varied between 0.010±0.0 mg/L and 0.020±0.006 mg/L (Nachukui). Lead also registered low overall average concentrations, measuring 0.020±0.003 mg/L. Its distribution across sites was fairly consistent, with concentrations ranging from 0.010±0.0 mg/L at Kerio, Kataboi, and Narengéwoi to 0.033±0.009 mg/L at Nariokotome. Chromium presented the lowest overall average concentration among all elements, at 0.010±0.002 mg/L. It was detected at specific locations such as Nariokotome (0.013±0.001 mg/L), Eliye (0.047±0.012 mg/L), Kalokol (0.010±0.0 mg/L), and Longéch (0.010±0.0 mg/L). However, Cr was reported as "ND" at Kerio, Kataboi, Narengéwoi, and Nachukui, suggesting its absence or presence below detectable limits in nearly half of the sampled areas. Eliye showed the highest detected concentration and also exhibited the highest variability for Cr.

Zinc had an overall average concentration of 0.195±0.152 mg/L. Individual concentrations of Zn varied widely, from a low of 0.043±0.012 mg/L at Kataboi to higher levels such as 0.443±0.784 mg/L at Eliye and 0.440±0.240 mg/L at Narengéwoi. Barium had an overall average concentration of 0.104±0.020 mg/L. Its concentrations ranged from 0.033±0.007 mg/L at Nachukui to 0.143±0.019 mg/L at Kataboi. Other locations like Nariokotome (0.130±0.041 mg/L) and Kerio (0.140±0.025 mg/L) also showed relatively higher levels. Copper registered an overall average concentration of 0.036±0.010 mg/L. Concentrations ranged from 0.013±0.003 mg/L at Nariokotome to a peak of 0.090±0.004 mg/L at Eliye. Nickel had an overall average concentration of 0.016±0.002 mg/L. Its levels were generally low, ranging from 0.008±0.002 mg/L at Kataboi to 0.045±0.004 mg/L at Kerio. Ni was not detected at Nachukui.

In conclusion, arsenic was the most prominent heavy metal in terms of concentration across these sampling locations, with its high and consistent levels presenting significant potential public health risks. While Cd, Pb, and Cr were found at much lower concentrations, their inherent toxicity necessitates continued vigilance. The varying concentrations and standard deviations across locations underscore the importance of site-specific assessments and further investigation into the sources and pathways of these heavy metals to mitigate potential health impacts.

4.8.2 Metal Concentration in Surface Water of Turkwel River

Table 4.16 displays the average concentrations of selected heavy metals in the Turkwel River at the two sampling locations. The heavy metal concentrations in the river vary between Kang'atosa and Lodwar, with some notable differences.

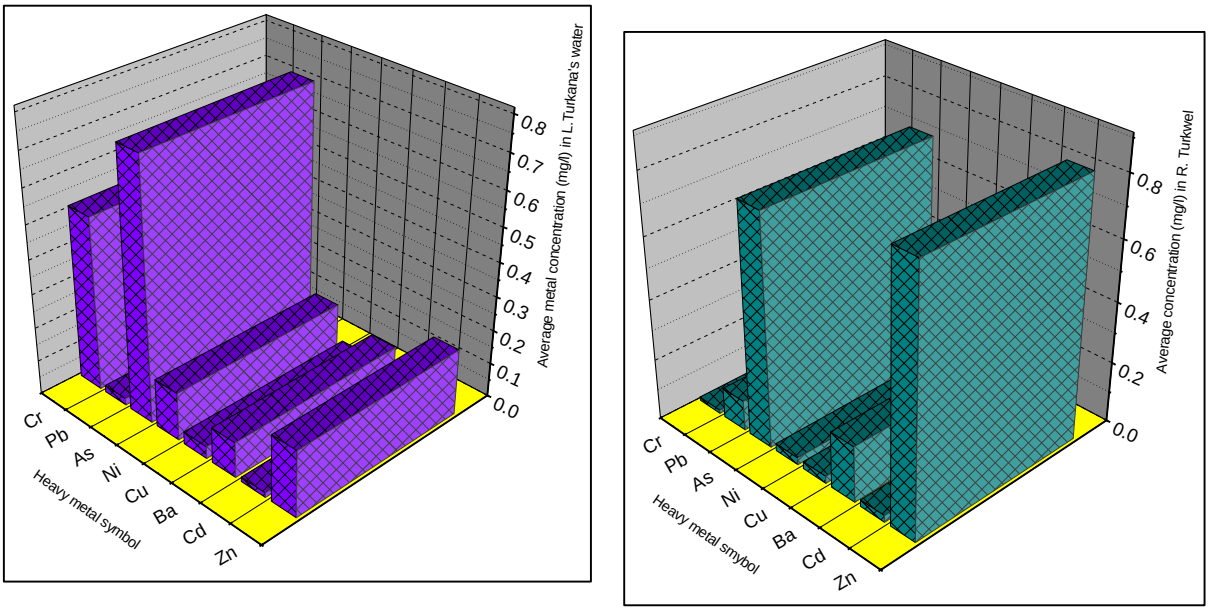
Both Kang'atosa (0.88 ± 0.189 mg/L) and Lodwar (0.813 ± 0.539 mg/L) showed relatively high average concentrations of zinc. Kang'atosa had a marginally higher average zinc concentration than Lodwar, with a difference of 0.067 mg/L. The higher presence of zinc at Kang’atosa could be attributed to zinc related fertilizers used in farms found in the Turkana plains and anthropogenic activities upstream. The overall average zinc concentration in the Turkwel River was 0.846 ± 0.364 mg/L. Cadmium levels were consistently very low at both locations, with averages of 0.023 ± 0.007 mg/L at Kang'atosa and 0.02 ± 0.006 mg/L at Lodwar. The difference between the two locations was negligible (0.003 mg/L), and the overall average was 0.022 ± 0.007 mg/L. This was a positive finding as cadmium is highly toxic. Lodwar (0.27 ± 0.183 mg/L) showed significantly higher average barium concentrations compared to Kang'atosa (0.100 ± 0.031 mg/L). The difference was substantial (0.170 mg/L), indicating a localized influence on barium levels. The overall average was 0.185 ± 0.107 mg/L. Copper concentrations were low and very similar at both locations, with 0.027 mg/L at Kang'atosa and 0.020 mg/L at Lodwar. The overall average for copper was 0.024 ± 0.007 mg/L. Nickel levels were low at both sites, with 0.017 ± 0.003 mg/L at Kang'atosa and 0.030 mg/L at Lodwar. Lodwar had a slightly higher average nickel concentration than Kang'atosa. The overall average was 0.024 ± 0.002 mg/L. Arsenic was the most prominent heavy metal in terms of concentration. Kang'atosa recorded a significantly higher average arsenic concentration (0.877 ± 0.048 mg/L) compared to Lodwar (0.487 mg/L). The difference of 0.390 mg/L highlighted a notable variation in

arsenic levels between the two sampling points. The overall average was 0.755 ± 0.042 mg/L. The presence of arsenic at these levels is a significant concern due to its toxicity. Lodwar showed a considerably higher average lead concentration (0.170 mg/L) compared to Kang'atosa (0.030 mg/L). This represented a substantial difference (0.140 mg/L), indicating a potential localized source at Lodwar. The overall average was 0.100 mg/L. Chromium levels were consistently very low at both locations, with 0.013 mg/L at Kang'atosa and 0.010 mg/L at Lodwar. The difference was negligible (0.003 mg/L), and the overall average was 0.012 mg/L.

Table 4.16: Average concentrations of heavy metals in surface water of Turkwel River

Sampling Location	Average concentration (mg/L)							
	Zn	Cd	Ba	Cu	Ni	As	Pb	Cr
Kang'atosa	0.88 ± 0.189	0.023 ± 0.007	0.1 ± 0.031	0.027 ± 0.007	0.017 ± 0.003	0.877 ± 0.048	0.03 ± 0.006	0.013 ± 0.002
Lodwar	0.813 ± 0.539	0.02 ± 0.006	0.27 ± 0.183	0.02 ± 0.006	0.03 ± 0.0	0.487 ± 0.034	0.17 ± 0.123	0.01 ± 0.0
Overall average	0.846 ± 0.364	0.022 ± 0.007	0.185 ± 0.107	0.024 ± 0.007	0.024 ± 0.002	0.755 ± 0.042	0.100 ± 0.065	0.012 ± 0.001

Figure 4.8 (a) and (b) show bar graphs of the average concentrations of heavy metals in water for both Lake Turkana and the Turkwel River respectively. Figure 4.8(a) illustrates that arsenic (As) had the highest concentration in the Lake's water while in the Turkwel River, Zn had the highest concentration followed by arsenic (As) as illustrated in Figure (b).



(a) (b)

Figure 4.8: Heavy metal concentrations in; (a) Lake Turkana water and (b) River Turkwel.

4.8.3 Comparison of Heavy Metal Concentrations in Water from Lake Turkana and Turkwel River (Present Work) to Other Regions

The concentration of heavy metals in the current study was compared to concentrations of selected elements in studies reported by other researchers in water from other lakes and one of the rivers found in the Kenyan Rift valley and results are presented in Table 4.17 which also presents WHO recommended limits for drinking water.

The average Zn concentration in Lake Turkana was 0.195 mg/L. This was well below the WHO recommended limit of 5 mg/L, indicating that zinc levels were generally safe for drinking water. With an average concentration of 0.036 mg/L, Cu in Lake Turkana was also significantly below the WHO limit of 2 mg/L, suggesting no immediate concern. The average Pb concentration in Lake Turkana was 0.02 mg/L. This exceeded the WHO recommended limit of 0.01 mg/L. This was a significant concern as lead is highly toxic even at low concentrations, particularly for children. The average Cd concentration was 0.013 mg/L. This exceeded the WHO recommended limit of 0.003 mg/L by a substantial margin. Cadmium is highly toxic

and its elevated presence was a major concern. The average Cr concentration in Lake Turkana was 0.51 mg/L. This was ten times higher than the WHO recommended limit of 0.05 mg/L. At 0.104 mg/L, the average Ba concentration was well below the WHO limit of 0.7 mg/L. The average arsenic concentration was 0.756 mg/L. This was massively higher than the WHO recommended limit of 0.01 mg/L. The average Ni concentration was 0.016 mg/L. This was lower than the WHO recommended limit of 0.07 mg/L. The findings of concentrations of cadmium and lead in water from selected sites at Lake Turkana by Munene et al, 2023 were consistent with those observed in the current study. The concentrations of Pb, Cr, and As were higher in Lake Turkana when compared to concentrations of corresponding elements in both Lake Elmentaita and Lake Nakuru. This was primarily due to its unique geological characteristics, combined with the effects of evaporation in a closed basin.

The average Zn concentration in Turkwel River was 0.846 mg/L which was well below the WHO limit of 5 mg/L. At 0.024 mg/L, Cu was well below the WHO limit of 2 mg/L. The average Pb concentration was 0.1 mg/L. This was ten times higher than the WHO recommended limit of 0.01 mg/L. The concentration of Cu and Pb was found to be higher in River Sosian compared to River Turkwel in the current study. However, the concentration of Zn in River Turkwel's water was higher than that of River Sosian. The higher Zn in the Turkwel River could be from fertilizers used in farming activities found along its course that is largely through a semi-arid region. On the other hand, River Sosian flows through regions with high rainfall and therefore its water was not utilized in farming activities as much. Concentrations of Cd, Ni, As, Pb, and Cr were higher in the current study compared to corresponding WHO recommended levels for drinking water.

Table 4.17: Comparison of heavy metals concentration with reported values and WHO recommended limits for drinking water

Source	**Study area**	**Metal concentration (mg/l)**								**Reference**
		Zn	Cu	Pb	Cd	Cr	Ba	As	Ni	
Lake water	L. Turkana, Kenya	0.195	0.036	0.02	0.013	0.51	0.104	0.756	0.016	Current study
Lake water	L.Turkana			>0.11	>0.03	>0.03				(P. M. Munene *et al.,* 2023)
River water	R. Turkwel, Kenya	0.846	0.024	0.1						Present work
River water	R. Sosian, Kenya	0.291	0.407	0.106						(E. N. Munene *et al.,* 2023)
Lake water	L. Elmentaita, Kenya			0.014	0.003			0.010		(Verwoerd, 2017)
Lake water	L. Nakuru, Kenya			0.012		0.005		0.002		(Verwoerd, 2017)
Drinking water Standard limit		5	2	0.01	0.003	0.05	0.7	0.01	0.07	(World Health Organization, 2011)

4.9 Water Quality Indices

Table 4.18 presents water quality data focusing on two distinct water quality indices: the Metal Contamination Index (MCI) and the Heavy Metal Evaluation Index (HEI). These indices were calculated for specific sampling locations across Lake Turkana and the Turkwel River, offering a quantifiable assessment of metal contamination and heavy metal pollution in these vital water bodies.

Table 4.18: MCI and HEI in Lake Turkana and River Turkwel water

Water body	Sampling Location	Water quality indices	
		MCI	HEI
Lake Turkana	Nariokotome	0.0002	64.910
	Kerio	0.0018	101.844
	Eliye	0.0016	122.431
	Kalokol	0.0002	65.625
	Kataboi	0.0009	46.207
	Nareng'ewoi	0.0011	62.028
	Long'ech	0.0002	64.823
	Nachukui	0.0026	46.751
Turkwel River	Lodwar	0.0013	73.554
	Kang'atosa	0.0007	99.281

4.9.1 Metal Contamination Index (MCI)

The MCI values for all sampled locations, from both Lake Turkana and the Turkwel River, were consistently low, ranging from 0.0002 to 0.0026. Within Lake Turkana, the sampling locations of Nariokotome, Kalokol, and Long'ech displayed the lowest MCI values at 0.0002, which indicated minimal overall metal contamination. Even Nachukui, which registered the highest MCI value in Lake Turkana of 0.0026, was also low. Similarly, the Turkwel River sites, Lodwar (0.0013) and Kang'atosa (0.0007), also exhibited MCI values that remained consistently low, reinforcing a broad finding of a low level of general metal presence across all sampled areas as indicated by the MCI.

4.9.2 Heavy Metal Evaluation Index (HEI)

In contrast to the MCI, the HEI values presented a different and often more elevated perspective on water quality. These values were significantly higher in magnitude, ranging from 46.207 to 122.431. Within Lake Turkana, HEI values showed considerable variation. Kataboi recorded the lowest HEI at 46.207. However, higher values were observed at Kerio (101.844) and Eliye (122.431). These elevated HEI values for Eliye and Kerio indicated a greater degree of heavy metal pollution at these specific Lake Turkana locations. For the Turkwel River, Kang'atosa recorded a higher HEI of 99.281 when compared to Lodwar's 73.554, suggesting more significant heavy metal pollution at Kang'atosa. The HEI values obtained for the Turkwel River generally fell within the range observed at Lake Turkana locations. These high HEI values suggest that the water was polluted with heavy metals to a considerable extent, primarily due to arsenic and zinc.

4.10 Heavy Metal Concentrations in Fish Samples

Table 4.19 summarizes the average concentrations of various heavy metals in muscle tissue of fish specimens from Kalokol and Long'ech markets. The samples were categorized into three groups: Catfish, Nile Perch, and Nile Tilapia. The metals analyzed were: Cu, Zn, Pb, Ni, Cr, Ba, As, and Cd. The concentrations are reported in milligrams per kilogram (mg/kg) on a dry weight basis.

Table 4.19: Heavy Metals (mg/kg) in Fish Muscle Tissue Samples from Kalokol and Long'ech Markets

Metal	Kalokol market			Long'ech market		
	Catfish	Nile Perch	Nile Tilapia	Catfish	Nile Perch	Nile Tilapia
As	0.510 ± 0.015	0.723 ± 0.082	0.363 ± 0.027	0.480 ± 0.010	0.740 ± 0.070	0.357 ± 0.028
Ba	0.060 ± 0.012	0.053 ± 0.006	0.027 ± 0.006	0.063 ± 0.006	0.047 ± 0.011	0.020 ± 0.006
Cd	ND	ND	ND	ND	ND	ND
Cr	0.013 ± 0.003	0.027 ± 0.015	0.017 ± 0.006	0.017 ± 0.006	0.028 ± 0.011	0.016 ± 0.006
Cu	0.373 ± 0.027	0.400 ± 0.015	0.213 ± 0.006	0.357 ± 0.037	0.400 ± 0.015	0.193 ± 0.048
Ni	0.026 ± 0.003	0.047 ± 0.006	0.010 ± 0.001	0.023 ± 0.006	0.043 ± 0.006	0.017 ± 0.006
Pb	0.020 ± 0.006	0.023 ± 0.006	0.013 ± 0.006	0.020 ± 0.006	0.023 ± 0.006	0.010 ± 0.006
Zn	0.560 ± 0.081	0.767 ± 0.042	0.323 ± 0.048	0.557 ± 0.086	0.770 ± 0.072	± 0.033

ND*: Not Detected

The heavy metal concentrations on dry weight basis, in Catfish, Nile Perch, and Nile Tilapia sourced from Kalokol and Long'ech markets revealed distinct patterns. Notably, Cd was consistently ND across all sampled fish species in both markets. This is a significant positive finding, suggesting either extremely low environmental levels of Cd in the fish's habitat or concentrations below the detection limits of the MP-AES. Given that Cadmium is a highly toxic metal known for its bioaccumulative properties, its absence is a favorable indicator for food safety. The lack of detection points to minimal industrial or agricultural Cd pollution, or perhaps its limited bioavailability within the aquatic ecosystem.

Among the detected metals, Zn, As, and Cu consistently exhibited the highest concentrations. Zinc, an essential trace element, was found in the highest amounts, with average concentrations ranging from 0.323±0.048 mg/kg in Nile Tilapia from Kalokol market to 0.770±0.072 mg/kg in Nile Perch from Long'ech market. Its

elevated presence could stem from its widespread use in industries like galvanizing and batteries, and from domestic waste entering aquatic systems. Arsenic also appeared in relatively high concentrations, particularly in Nile Perch, with values spanning from 0.357±0.028 mg/kg in Nile Tilapia (Long'ech) to 0.740±0.070 mg/kg in Nile Perch (Long'ech). Naturally occurring and anthropogenic activities such as mining, agricultural practices, and industrial discharges can significantly elevate arsenic levels in water bodies due to its high mobility and the varying toxicity of its chemical forms (Irunde et al., 2022). Copper concentrations were likewise notable, ranging from 0.193±0.048 mg/kg in Nile Tilapia (Long'ech) to 0.400±0.015 mg/kg in Nile Perch (both markets). Although Copper is an essential micronutrient, it can become toxic at high levels, with potential sources being agricultural runoff from fungicides and industrial effluents.

Conversely, Pb, Cr, Ni, and Ba generally presented the lowest detected concentrations. Lead levels were remarkably low across the board, ranging from 0.010±0.006 mg/kg in Nile Tilapia (Long'ech) to 0.023±0.006 mg/kg in Nile Perch (both markets). This low level is highly positive given lead's non-essential and highly toxic nature, potentially reflecting reduced environmental lead pollution from sources like phased-out leaded gasoline or limited industrial discharges in the fish's habitat. Chromium concentrations ranged from 0.013±0.003 mg/kg (Catfish, Kalokol) to 0.028±0.011 mg/kg (Nile Perch, Long'ech), and Nickel from 0.010±0.001 mg/kg (Nile Tilapia, Kalokol) to 0.047±0.006 mg/kg (Nile Perch, Kalokol). These metals are often associated with industrial processes, but their relatively low levels suggest limited specific industrial contamination. Barium concentrations were also low, spanning from 0.020±0.006 mg/kg (Nile Tilapia, Long'ech) to 0.063±0.006 mg/kg (Catfish, Long'ech), reflecting its natural occurrence and potentially limited bioavailability.

Significant species-specific differences in metal accumulation were evident, largely correlating with their trophic levels (i.e., the position an organism occupies in a food chain) and feeding habits (Balzani et al., 2022). Nile Perch consistently exhibited the highest concentrations for most detected heavy metals, including Arsenic (e.g., 0.723±0.082 mg/kg in Kalokol and 0.740±0.070 mg/kg in Long'ech) and Zinc (e.g., 0.767±0.042 mg/kg in Kalokol and 0.770±0.072 mg/kg in Long'ech). As a large, top

predatory fish, Nile Perch occupies a higher trophic level, making it highly susceptible to biomagnification, where contaminants increase in concentration up the food chain. Its longer lifespan and larger body size also provide more time for the bioaccumulation of metals from its diet, primarily consisting of smaller fish. Catfish generally displayed intermediate heavy metal concentrations, such as Arsenic at 0.510±0.015 mg/kg (Kalokol) and 0.480±0.010 mg/kg (Long'ech). Being benthic omnivores (organisms that live on or near the seafloor), Catfish feed on a diverse array of organic matter and invertebrates found near the lakebed, exposing them to metals accumulated in sediments and lower trophic organisms. In contrast, Nile Tilapia consistently showed the lowest concentrations for almost all detected metals, with Arsenic at 0.363±0.027 mg/kg (Kalokol) and 0.357±0.028 mg/kg (Long'ech), and Zinc at 0.323±0.048 mg/kg (Kalokol) and 0.330±0.033 mg/kg (Long'ech). This is likely due to their lower trophic level, as they primarily feed on phytoplankton, zooplankton, and aquatic plants, thus encountering fewer biomagnified contaminants. Their generally faster growth rates and shorter lifespans may also limit the total metal accumulation in their tissues.

A striking observation was the remarkable consistency in heavy metal concentrations for each fish species between Kalokol market and Long'ech market. The differences in mean values and their standard deviations were minimal across the two locations. This strong similarity strongly suggests that the fish sold in both markets originate from the same or very similar aquatic environments, most likely Lake Turkana itself. This indicates a relatively uniform distribution of heavy metal contaminants across the fishing grounds supplying these markets, implying the absence of significant localized pollution sources that would differentially impact the fish sold in one market over the other. This consistency further supports the reliability of the observed species-specific accumulation trends.

Table 4.20 presents the average heavy metal concentrations in mg/kg, along with their standard errors (SE), for Catfish, Nile Perch, and Nile Tilapia, averaged across the two markets. This consolidated view allows for a clearer understanding of metal accumulation patterns across different fish species.

Table 4.20: Average heavy metal concentrations (mg/kg) in fish samples from the two markets.

Metal	Average heavy metal concentration ± SE (mg/kg) for the two markets		
	Catfish	Nile Perch	Nile Tilapia
As	0.495 ± 0.013	0.732 ± 0.045	0.360 ± 0.055
Ba	0.062 ± 0.009	0.050 ± 0.009	0.024 ± 0.006
Cd	ND	ND	ND
Cr	0.015 ± 0.005	0.028 ± 0.013	0.017 ± 0.006
Cu	0.365 ± 0.032	0.400 ± 0.021	0.203 ± 0.027
Ni	0.025 ± 0.005	0.045 ± 0.006	0.014 ± 0.004
Pb	0.020 ± 0.006	0.023 ± 0.006	0.012 ± 0.006
Zn	0.559 ± 0.084	0.769 ± 0.057	0.327 ± 0.041

ND*: Not Detected

Notably, Cd was consistently not detected in all fish species, mirroring the findings from the individual market data. Among the detected metals, Zn and As consistently showed the highest average concentrations across all fish species. Zinc concentrations ranged from 0.327 ± 0.041 mg/kg in Nile Tilapia to 0.769 ± 0.057 mg/kg in Nile Perch. Arsenic levels were similarly high, varying from 0.360±0.055 mg/kg in Nile Tilapia to 0.732 ± 0.045 mg/kg in Nile Perch. These elevated levels of both essential and toxic elements such as such Zn and As respectively, warrant further consideration regarding their environmental sources and potential long-term impacts. Copper also registered notable concentrations, ranging from 0.203 ± 0.027 mg/kg in Nile Tilapia to 0.400 ± 0.021 mg/kg in Nile Perch, indicating its consistent presence in the aquatic environment.

Conversely, Pb, Cr, Ni, and Ba were found at significantly lower concentrations. Lead levels were particularly low, ranging from 0.012 ± 0.006 mg/kg in Nile Tilapia to 0.023 ± 0.006 mg/kg in Nile Perch. Similarly, Chromium concentrations varied from 0.015 ± 0.005 mg/kg in Catfish to 0.028±0.013 mg/kg in Nile Perch, while Nickel ranged from 0.014 ± 0.004 mg/kg in Nile Tilapia to 0.045±0.006 mg/kg in Nile Perch. Barium levels were also relatively low, from 0.024 ± 0.006 mg/kg in Nile Tilapia to 0.062±0.009 mg/kg in Catfish. The relatively low concentrations of these metals, especially lead, are generally favorable from a public health perspective.

A clear trend in heavy metal accumulation emerged across the different fish species, largely explained by their ecological roles and feeding habits. Nile Perch consistently exhibited the highest average concentrations for most heavy metals, including Zinc (0.769 ± 0.057 mg/kg) and Arsenic (0.732 ± 0.045 mg/kg). Catfish showed intermediate concentrations, such as Zinc at 0.559 ± 0.084 mg/kg and arsenic at 0.495 ± 0.013 mg/kg. Nile Tilapia consistently exhibited the lowest average concentrations for nearly all metals, including Zinc (0.327 ± 0.041 mg/kg) and Arsenic (0.360 ± 0.055 mg/kg). This consolidated data reinforces the significant influence of an organism's position in the food web on its heavy metal burden.

Table 4.21 offers a comparative analysis of heavy metal concentrations in fish muscle tissue (in mg/kg) from Lake Turkana, Kenya (current study), compared with studies conducted at Omo Delta, Ethiopia, Gilgel Gibe (I), and the Maximum Permissible Limits (MPLs) established by the Food and Agriculture Organization (FAO) and World Health Organization (WHO). The concentrations are reported in milligrams per kilogram (mg/kg) on a wet weight basis.

Table 4.21: Comparison of Heavy Metal Concentrations in Lake Turkana Fish, with values from other studies, and WHO Guidelines

Trace element concentration levels in muscle tissue of fish (mg/kg)								
Metal	**Current study**			**Lake.Turkana**	**Omo delta**		**Gilgel Gibe (I)**	**MPL**
	Catfish	Nile Perch	Nile Tilapia	Red belly Tilapia	Catfish	Nile Perch	Nile Tilapia	
As	0.495 ± 0.013	0.732 ± 0.045	0.360 ± 0.055					
Ba	0.062 ± 0.009	0.050 ± 0.009	0.024 ± 0.006					
Cd	ND	ND	ND	<0.005	ND	ND	ND	0.200
Cr	0.015 ± 0.005	0.028 ± 0.013	0.017 ± 0.006	0.232	ND	0.039 ± 0.085	10.31	0.150
Cu	0.365 ± 0.032	0.400 ± 0.021	0.203 ± 0.027	0.808	0.071 ± 0.198	0.129 ± 0.283	4.64	3.000
Ni	0.025 ± 0.005	0.045 ± 0.006	0.014 ± 0.004		0.013 ± 0.006	0.019 ± 0.003		0.500
Pb	0.020 ± 0.006	0.023 ± 0.006	0.012 ± 0.006	<0.007	0.597 ± 0.153	0.89 ± 0.099	8.39	0.500
Zn	0.559 ± 0.084	0.769 ± 0.057	0.327 ± 0.041	26.900	0.394 ± 0.26	0.428 ± 0.393		40
Reference				(Plessl *et al.,* 2017)	(Andemo *et al.,* 2024)	(Andemo *et al.,* 2024)	(Gure *et al.,* 2019)	(World Health Organization *et al.,* 2016)

ND*: Not Detected

A critical finding across the current study for Catfish, Nile Perch, and Nile Tilapia was the consistent non-detection of Cadmium. This aligned with Catfish and Nile Perch from the Omo Delta. However, Plessl et al (2017) reported a detectable Cd level of <0.005 mg/kg for Redbelly Tilapia. The WHO Maximum Permissible Limit (MPL) for Cd is 0.200 mg/kg. Chromium concentrations in Lake Turkana fish from the current study were relatively low: 0.015 ± 0.005 mg/kg for Catfish, 0.028 ± 0.013 mg/kg for Nile Perch, and 0.017 ± 0.006 mg/kg for Nile Tilapia. These values were considerably lower than the 0.232 mg/kg reported for Redbelly Tilapia in Lake Turkana and the 10.31 mg/kg reported for Nile Tilapia in Gilgel Gibe I. Cr concentrations in the current study were below the FAO/WHO MPL of 0.150 mg/kg. Copper concentrations in this work range from 0.203 ± 0.027 mg/kg in Nile Tilapia to 0.400 ± 0.021 mg/kg in Nile Perch. These levels were lower than the 0.808 mg/kg reported for Redbelly Tilapia in Lake Turkana and the 4.64 mg/kg found in Nile Tilapia from Gilgel Gibe (I). Compared to the FAO/WHO MPL of 3.000 mg/kg, Cu levels in Lake Turkana fish this study were well within safe limits. The Omo Delta study reported lower Copper concentrations for Catfish (0.071 ± 0.198 mg/kg) and Nile Perch (0.129 ± 0.283 mg/kg). Nickel concentrations in Lake Turkana fish were low, ranging from 0.014 ± 0.004 mg/kg in Nile Tilapia to 0.045±0.006 mg/kg in Nile Perch. These are comparable to the values from Omo Delta (Catfish: 0.013±0.006 mg/kg, Nile Perch: 0.019 ± 0.003 mg/kg) and are well below the FAO/WHO MPL of 0.500 mg/kg. Pb concentrations in this study were also very low, ranging from 0.012 ± 0.006 mg/kg in Nile Tilapia to 0.023 ± 0.006 mg/kg in Nile Perch. These values were lower than the <0.007 mg/kg for Redbelly Tilapia from Lake Turkana. Crucially, the Pb levels in the current study were significantly lower than the 0.597 ± 0.153 mg/kg for Catfish and 0.89 ± 0.099 mg/kg for Nile Perch in the Omo Delta study, and also much lower than the 8.39 mg/kg for Nile Tilapia in Gilgel Gibe I. All Pb concentrations in the current study were well below the FAO/WHO MPL of 0.500 mg/kg, indicating a very low lead burden in these fish.

Zinc (Zn) concentrations in this study were the highest among the detected metals, varying from 0.327 ± 0.041 mg/kg in Nile Tilapia to 0.769 ± 0.057 mg/kg in Nile Perch. These levels were substantially lower than the 26.900 mg/kg reported for

Redbelly Tilapia in Lake Turkana and are also lower than the FAO/WHO MPL of 40 mg/kg. The Omo Delta study reported slightly lower zinc concentrations for Catfish (0.394±0.26 mg/kg) and Nile Perch (0.428±0.393 mg/kg) compared to the values from the current study.

4.11 Health Risk Assessment in Fish Samples

Table 4.22 presents the average EDI, THQ and HI due to heavy metals resulting from the commonly consumed fish species in Kalokol and Long'ech markets.

Table 4.22: Non-carcinogenic health risk assessment for metals in fish samples.

Metal	EDI (mg/kg)			THQ		
	Catfish	Nile Perch	Nile Tilapia	Catfish	Nile Perch	Nile Tilapia
As	0.0000221	0.0000245	0.0000206	0.3680881	0.4088686	0.3439745
Ba	0.0000022	0.0000020	0.0000017	0.0000109	0.0000101	0.0000084
Cd	ND	ND	ND	ND	ND	ND
Cr	0.0000008	0.0000009	0.0000008	0.0002695	0.0003156	0.0002766
Cu	0.0000143	0.0000146	0.0000124	0.0003574	0.0003644	0.0003093
Ni	0.0000011	0.0000013	0.0000010	0.0000574	0.0000654	0.0000495
Pb	0.0000008	0.0000008	0.0000007	0.0002310	0.0002401	0.0002006
Zn	0.0000235	0.0000257	0.0000211	0.0000783	0.0000857	0.0000702
HI	------	------	------	0.3690927	0.4099500	0.3448890

ND*: Not Detected

4.11.1 Estimated Daily Intake (EDI) of Metals from Fish Consumption

The data presented in Table 4.22 provide insights into the potential health risks associated with the consumption of Catfish, Nile Perch, and Nile Tilapia, based on the estimated daily intake (EDI) and target hazard quotient (THQ) for various metals. The EDI values for all analyzed metals across the three fish species were exceedingly low, ranging from 0.0000008 mg/kg for chromium and lead in Nile Tilapia to 0.0000257 mg/kg for zinc in Nile Perch. Arsenic generally had the highest EDI among the metals, with Nile Perch having the highest EDI for Arsenic (0.0000245 mg/kg) compared to Catfish (0.0000221 mg/kg) and Nile Tilapia (0.0000206 mg/kg). Cd was consistently not detected in all fish samples, indicating its absence or presence below the detection limits, which was a positive finding from a health risk perspective. The

other metals, Ba, Cr, Cu, Ni, Pb, and Zn, all exhibited very low EDIs across all fish types, suggesting minimal daily exposure through consumption.

4.11.2 Target Hazard Quotient (THQ) and Total Hazard Index (HI)

The Target Hazard Quotient (THQ) was used to assess the non-carcinogenic health risk from individual metals. Arsenic presented the highest THQ values across all fish species. Nile Perch again showed the highest THQ for arsenic (0.4088686), followed closely by Catfish (0.3680881) and Nile Tilapia (0.3439745). While these values were notably higher than those for other metals, all individual THQ values remained significantly below 1. A THQ value less than 1 generally indicated that the exposure level was unlikely to cause adverse non-carcinogenic health effects over a lifetime (Emurotu et al., 2024). For other metals like Ba, Cr, Cu, Ni, Pb, and Zn, their respective THQ values were considerably lower, well within the safe limits, further reinforcing the minimal individual risk. Similar to EDI, Cadmium's THQ was also not detected due to its non-detection.

Finally, the HI, which represented the cumulative non-carcinogenic risk from multiple metals, aggregated the individual THQ values. The calculated HI values for Catfish (0.3690927), Nile Perch (0.4099500), and Nile Tilapia (0.3448890) were all less than 1. This was a critical finding, as an HI value below 1 suggested that there was no significant cumulative non-carcinogenic health risk associated with the combined consumption of these metals from the respective fish species (Nyarko et al., 2023). While Nile Perch exhibited a slightly higher overall HI compared to Catfish and Nile Tilapia, all three species fell within the acceptable risk range. Therefore, based on the provided data for these specific metals, the consumption of Catfish, Nile Perch, and Nile Tilapia pose negligible non-carcinogenic health risk to consumers.

4.12 Bioaccumulation Factor in Fish

Table 4.23 presents the Bioaccumulation Factor (BAF) for six different heavy metals As, Ba, Cr, Cu, Ni, Pb, and Zn across measured across three common fish species (Catfish, Nile Perch, and Nile Tilapia).

Table 4.23: Bioaccumulation factors of selected heavy metals in fish samples

Fish Species	Bioaccumulation Factor (BAF)						
	As	Ba	Cr	Cu	Ni	Pb	Zn
Catfish	0.687	0.490	1.900	9.333	1.688	0.950	2.829
Nile Perch	0.763	0.457	2.225	9.514	1.922	0.988	3.099
Nile Tilapia	0.642	0.377	1.950	8.076	1.453	0.825	2.538

The results revealed distinct patterns of bioaccumulation across the various metals. Cu, Zn, Cr, and Ni consistently showed BAF values greater than 1 for all three fish species. This indicates a clear tendency for these metals to accumulate in the tissues of Catfish, Nile Perch, and Nile Tilapia from the lake environment. In contrast, As, Ba, and Pb consistently showed BAF values less than 1 across all species. This suggests that these metals were not accumulating in the fish tissues to concentrations higher than those found in the water.

Copper and Zinc exhibited the highest BAF values, with Cu being the most bioaccumulative metal overall. The BAF for Cu ranged from 8.076 in Nile Tilapia to 9.514 in Nile Perch. Similarly, the BAF for Zn ranged from 2.538 in Nile Tilapia to 3.099 in Nile Perch. The high BAF values for these two essential metals suggest that they were not only accumulating but also potentially being actively absorbed by the fish for metabolic functions, as both are crucial micronutrients. Chromium and Nickel also showed moderate bioaccumulation, with BAF values ranging from 1.900 to 2.225 for Cr and 1.453 to 1.922 for Ni. This indicates that these non-essential metals were accumulating in the fish, albeit at a lower rate than Cu and Zn. As, Ba, and Pb had minimal accumulation, with all BAF values below 1. These results suggest that these metals were either not readily absorbed by the fish or were efficiently excreted from their bodies, indicating a lower risk of bioaccumulation compared to the other metals studied.

Comparing the three fish species revealed slight differences in their bioaccumulation potential. Nile Perch generally showed the highest BAF values for most of the metals studied (As, Cr, Cu, Ni, Pb, and Zn). This suggests that Nile Perch may have had a higher capacity or rate of bioaccumulation for these metals compared to Catfish and Nile Tilapia. Catfish showed intermediate BAF values for most metals, while Nile

Tilapia consistently exhibited the lowest BAF values for all the metals. This could have been due to differences in Nile Tilapia's diet, metabolism, or physiology.

4.13. Correlation between Activity and Heavy Metal Concentrations in Fish Samples

Table 4.24 contains Pearson correlation coefficients (r - values), two-tailed significance values (p-values), and the sample size (N=9). A Pearson correlation coefficient (r) indicates the strength and direction of a linear relationship between two variables, with values close to +1 indicating a strong positive relationship, values close to -1 indicating a strong negative relationship, and values near zero (0) indicating a weak or no linear relationship (Di Leo & Sardanelli, 2020). The p-value helps determine whether a correlation is statistically significant; typically, a p-value less than 0.05 is considered significant, and less than 0.01 is considered highly significant (Andrade, 2019).

Table 4.24: Correlations between heavy metals and activity concentrations of primordial radionuclides in fish samples

Metal	Correlation type	As	Ba	Cr	Cu	Ni	Pb	Zn	^{232}Th	^{238}U	^{40}K
As	Pearson Correlation	1	0.367	0.334	0.764*	-0.294	0.688*	0.866**	-0.145	0.900**	-0.463
	Sig. (2-tailed)		0.331	0.380	0.017	0.443	0.040	0.003	0.709	0.001	0.210
Ba	Pearson Correlation	0.367	1	0.211	0.832**	-0.411	0.362	0.378	-0.638	0.271	-0.156
	Sig. (2-tailed)	0.331		0.586	0.005	0.272	0.338	0.316	0.065	0.481	0.689
Cr	Pearson Correlation	0.334	0.211	1	0.270	0.158	-0.017	0.179	0.291	0.618	-0.398
	Sig. (2-tailed)	0.380	0.586		0.481	0.684	0.966	0.645	0.447	0.076	0.289
Cu	Pearson Correlation	0.764*	0.832**	0.270	1	-0.318	0.627	0.765*	-0.634	0.617	-0.308
	Sig. (2-tailed)	0.017	0.005	0.481		0.404	0.071	0.016	0.066	0.077	0.420
Ni	Pearson Correlation	-0.294	-0.411	0.158	-0.318	1	-0.341	-0.194	0.221	-0.088	0.199
	Sig. (2-tailed)	0.443	0.272	0.684	0.404		0.369	0.617	0.568	0.822	0.608
Pb	Pearson Correlation	0.688*	0.362	-0.017	0.627	-0.341	1	0.582	-0.244	0.527	-0.287
	Sig. (2-tailed)	0.040	0.338	0.966	0.071	0.369		0.100	0.528	0.145	0.453
Zn	Pearson Correlation	0.866**	0.378	0.179	0.765*	-0.194	0.582	1	-0.237	0.792*	-0.666
	Sig. (2-tailed)	0.003	0.316	0.645	0.016	0.617	0.100		0.538	0.011	0.050
Th	Pearson Correlation	-0.145	-0.638	0.291	-0.634	0.221	-.244	-0.237	1	0.172	-0.349
	Sig. (2-tailed)	0.709	0.065	0.447	0.066	0.568	0.528	0.538		0.658	0.357
U	Pearson Correlation	0.900**	0.271	0.618	0.617	-0.088	0.527	0.792*	0.172	1	-0.662
	Sig. (2-tailed)	0.001	.481	0.076	0.077	0.822	0.145	0.011	0.658		0.052
K	Pearson Correlation	-0.463	-.156	-0.398	-0.308	0.199	-0.287	-0.666	-0.349	-0.662	1
	Sig. (2-tailed)	0.210	.689	0.289	0.420	0.608	0.453	0.050	0.357	0.052	

*. Correlation is significant at the 0.05 level (2-tailed), **. Correlation is significant at the 0.01 level (2-tailed).

4.13.1 Correlation between Heavy Metals Concentration and Activity Concentration of ^{232}Th

Thorium-232 (^{232}Th) generally exhibited weak to moderate, and predominantly non-significant, inverse relationships with most of the heavy metals. For instance, there was a very weak negative correlation between ^{232}Th and As ($r = -0.145$, $p = 0.709$), which was not statistically significant. A moderate negative correlation existed between ^{232}Th and Ba ($r = -0.638$, $p = 0.065$), nearing statistical significance at the 0.05 level. This suggested a potential trend where higher Ba concentrations might be associated with lower ^{232}Th. Similarly, ^{232}Th showed a moderate negative correlation with Cu ($r = -0.634$, $p = 0.066$), also close to significance, hinting at a possible inverse relationship. Conversely, ^{232}Th's correlations with Cr, Ni, Pb, and Zn were weak and not statistically significant. In summary, ^{232}Th did not show strong or consistently significant correlations with the analyzed heavy metals however, its moderate negative correlations with Ba and Cu are worthy noting for being near the significance threshold, implying a need for further investigation.

4.13.2 Correlation between Heavy Metals Concentration and Activity Concentration of ^{238}U

Uranium-238 (^{238}U) presented a distinct pattern, displaying strong and statistically significant positive correlations with several heavy metals, particularly As and Zn, which suggests shared geochemical behaviors or origins. There was a very strong positive correlation between ^{238}U and As ($r = 0.900$, $p = 0.001$), indicating a highly significant tendency for their concentrations to increase or decrease together. Likewise, ^{238}U exhibited a strong positive correlation with Zn ($r = 0.792$, $p = 0.011$), which was also statistically significant. Moderate positive correlations were observed between ^{238}U and Cr ($r = 0.618$, $p = 0.076$) and ^{238}U and Cu ($r = 0.617$, $p = 0.077$). While these correlations were not statistically significant at the 0.05 level, they were close, suggesting a tendency for these elements to increase together. ^{238}U's correlations with Ba, Ni, and Pb were weak and not significant. Thus, Uranium showed a strong and highly significant positive relationship with Arsenic and a strong and significant positive relationship with Zinc, implying that ^{238}U, As, and Zn might have shared common sources, transport mechanisms, or geochemical processes.

4.13.3 Correlation between Heavy Metals Concentration and Activity Concentration of ^{40}K

Potassium-40 (^{40}K) generally showed weak to moderate negative correlations with most heavy metals, with one relationship bordering on statistical significance. Its correlation with As was weak and negative ($r = -0.463$, $p = 0.210$) and not significant. Similar weak negative correlations were found with Ba, Cr, Cu, and Pb, none of which were statistically significant. A very weak positive correlation was observed with Ni ($r = 0.199$, $p = 0.608$), also not significant. However, a moderate negative correlation existed between ^{40}K and Zn ($r = -0.666$, $p = 0.050$), which was precisely at the conventional threshold for statistical significance. This suggested that as ^{40}K concentrations increased, Zn concentrations tended to decrease, and this relationship was on the borderline of being considered statistically significant. Overall, ^{40}K generally displayed weak to moderate negative relationships with the heavy metals, with the moderate negative correlation with Zinc being the most notable for its near-significance, potentially indicating differing geological sources or geochemical controls.

4.14 Summary

The chapter provides a detailed analysis of the radiological and elemental data gathered from the Lake Turkana ecosystem, focusing on the activity concentrations of primordial radionuclides and heavy metal levels. The study successfully met its primary objective by quantifying the presence of ^{238}U, ^{232}Th, and ^{40}K across various environmental matrices. In sediment samples, Potassium-40 emerged as the most abundant radionuclide, a finding consistent with the crustal characteristics of marine sediments. The highest activity levels for Thorium and Uranium were recorded in Kalokol, while Nareng'ewoi exhibited the peak concentration for ^{40}K. Despite these variations, the calculated radium activity for all sediment samples remained well below the internationally recommended safety threshold of 370 Bq/kg, suggesting that the geological composition of the area poses a negligible radiological threat for construction or agricultural use.

In agricultural products, specifically sorghum and cassava, the study found that ^{40}K levels were notably higher than global soil averages, reflecting the plant's metabolic requirement for this essential macronutrient. Sorghum samples showed a strong

positive correlation between Uranium and Thorium, likely due to their similar geochemical behaviors and absorption pathways from the soil. Conversely, Potassium showed no significant correlation with the other two radionuclides, confirming its independent uptake based on plant biology. Cassava samples from the Kang'atosa Ward displayed higher radionuclide concentrations compared to similar studies in Ghana but were generally lower than those found in other regions of Kenya, such as Kilimambogo.

The analysis of fish species revealed distinct patterns of radionuclide accumulation. ^{40}K consistently exhibited the highest activity concentrations in all species. However, Nile Perch showed the greatest accumulation of ^{238}U and the highest overall radiological burden, while Nile Tilapia demonstrated the highest levels of ^{232}Th. These discrepancies are attributed to the diverse feeding habits, metabolic processes, and habitat preferences of the fish within the Lake Turkana basin.

Statistical tools, including Pearson correlation and ANOVA, were employed to validate the relationships between the data points. The Pearson matrix indicated extremely high positive correlations between the various radiological hazard indices, such as the ADR and the ELCR, confirming that these metrics are highly interdependent. ANOVA testing further revealed significant geographical differences in the distribution of Thorium and Uranium, although ^{40}K distribution was relatively uniform across the sampling sites. Collectively, the chapter interprets these findings to conclude that while the Lake Turkana ecosystem contains moderate levels of natural radioactivity, the current concentrations in sediments, crops, and fish do not exceed safety limits that would pose an immediate health risk to the local population.

CHAPTER FIVE
CONCLUSION AND RECOMMENDATIONS

5.1 Conclusion

The general objective of this research was to assess the levels of naturally occurring radionuclides ^{232}Th, ^{238}U and ^{40}K in sediment, crop, and fish samples and heavy metal contamination in water and fish samples from the Lake Turkana ecosystem. The associated exposure risks resulting from naturally occurring radionuclides, and potential correlations between radionuclide activity and heavy metal concentrations were also investigated.

The results revealed varying radionuclide concentrations in sediments. Kalokol had the highest activity concentrations of ^{232}Th (75.5 Bq/kg) and ^{238}U (64.5 Bq/kg), while Nareng'ewoi had the highest concentration of ^{40}K (811.7 Bq/kg). Overall averages of activity concentrations of radionuclides in sediments were 38.7 ± 7.53 Bq/kg for ^{232}Th, 30.1 ± 5.80 Bq/kg for ^{238}U, and 664.4 ± 65.43 Bq/kg for ^{40}K. While ^{232}Th and ^{238}U averages were below world averages, ^{40}K was above the world averages. All sediment Ra_{eq} values averaged at 124.1 Bq/kg and were safely below the 370 Bq/kg limit. In sorghum, the average ^{232}Th concentration was 17.27 Bq/kg, ^{238}U concentration averaged at 14.37 Bq/kg, and the average concentration of ^{40}K was 699.34 Bq/kg, which was notably higher than the global average, though within typical agricultural product ranges. Radionuclide concentrations in cassava averaged at 20.96 Bq/kg for ^{232}Th, ^{238}U averaged at 19.33 Bq/kg and, as expected due to its nutrient role, ^{40}K levels in cassava were significantly higher, averaging 804.42 Bq/kg, reflecting cassava's efficient potassium absorption. The average activities of ^{232}Th in Nile tilapia, Nile perch, and African catfish were 24.75 ± 9.41 Bq/kg, 16.90 ± 6.3 Bq/kg, and 3.36 ± 1.52 Bq/kg, respectively. For ^{238}U, the corresponding average activities were 21.09 ± 4.18 Bq/kg, 49.56 ± 2.81 Bq/kg, and 23.55 ± 4.23 Bq/kg, respectively, and for ^{40}K, the corresponding activities were 499.38 ± 133.56 Bq/kg, 431.15 ± 84.32 Bq/kg, and 500.31 ± 130.84 Bq/kg, respectively.

The study's hazard indicators in sediment samples revealed that while all locations were safe, Kalokol consistently exhibited the highest values. H_{ex} ranged from 0.312 to 0.584, and H_{in} from 0.372 to 0.758, and both were below 1. The average ADR was

64.949 nGy/h with Kalokol at 95.942 nGy/h having the highest. The average AED_{total} was 0.397 mSv/y, and the average ELCR was 0.015%, with Kalokol having 0.023% again being the highest. Despite higher background radiation, the overall health risk remained low. The average annual effective dose due to ingestion of cassava was 0.152 mSv/yr, which is below the safety limit of 1 mSv/yr recommended by the ICRP. However, sorghum's average AED of 1.110 mSv/yr exceeded the ICRP limit. The gamma index value for all sediment samples was less than 1.

Heavy metal concentration in Lake Turkana's surface water identified Arsenic as the most prominent heavy metal, with an overall average concentration of 0.756 ± 0.033 mg/L. Concentrations peaked at Eliye (1.147 ± 0.027 mg/L). In contrast, Cd, Pb, and Cr exhibited much lower overall averages of 0.013 ± 0.002 mg/L, 0.020 ± 0.003 mg/L, and 0.010 ± 0.002 mg/L, respectively. Despite lower concentrations for some metals, their inherent toxicity warrants continued monitoring and site-specific assessments. The Turkwel River's surface water showed varied heavy metal concentrations between sampling locations. Arsenic with an average concentration of 0.755 mg/L and Zn with an average concentration of 0.846 mg/L were prominent. Lodwar showed higher Ba (0.27 ± 0.183 mg/L) and Pb (0.170 ± 0.123 mg/L) concentrations, while Kang'atosa had elevated As (0.877 ± 0.048 mg/L) concentration. Conversely, Cd (0.022 ± 0.007 mg/L), Cu (0.024 ± 0.007 mg/L), and Cr (0.012 ± 0.001 mg/L) concentration levels remained consistently low.

MCI values in water were consistently low, ranging from 0.0002 to 0.0026, indicating minimal overall metal contamination. However, HEI values were significantly higher, ranging from 46.207 to 122.431. Eliye with 122.431 and Kerio with 101.844 in Lake Turkana, and Kang'atosa with 99.281 in Turkwel River showed elevated HEI. This suggested considerable heavy metal pollution, primarily from arsenic and zinc, despite low MCI readings. Heavy metal analysis in fish samples revealed that Cd was consistently undetected. Among the detected metals, Zn and As exhibited the highest average concentrations across all fish species. Nile Perch recorded 0.769 ± 0.057 mg/kg for Zn and 0.732 ± 0.045 mg/kg for As, while Nile Tilapia had 0.327 ± 0.041 mg/kg for Zn and 0.360 ± 0.055 mg/kg for As. In contrast, Pb, Cr, Ni, and Ba were found at significantly lower concentrations. A clear trend of bioaccumulation was observed, with Nile Perch exhibiting the highest metal concentrations and Nile Tilapia

the lowest, indicating the strong influence of feeding habits and trophic level on heavy metal burden in fish.

The health risk assessment for fish consumption revealed consistently low Estimated Daily Intake (EDI) values for all analyzed metals, ranging from 0.0000008 mg/kg (Cr, Pb in Nile Tilapia) to 0.0000257 mg/kg (Zn in Nile Perch). Arsenic generally had the highest EDI, with Nile Perch recording 0.0000245 mg/kg. Cd was consistently undetected. Individual Target Hazard Quotient (THQ) values were all significantly below 1, with arsenic showing the highest at 0.4088686 (Nile Perch). The cumulative Hazard Index also remained below 1 for Catfish (0.3690927), Nile Perch (0.4099500), and Nile Tilapia (0.3448890). These results suggest negligible non-carcinogenic health risks from consuming these fish species.

Correlation analysis between heavy metal concentrations and primordial radionuclide activity levels in fish samples revealed distinct patterns. ^{232}Th generally showed weak, non-significant inverse relationships. In contrast, ^{238}U exhibited strong, statistically significant positive correlations with As ($r = 0.900$, $p = 0.001$) and Zn ($r = 0.792$, $p = 0.011$), strongly suggesting shared geochemical behaviors or common origins. ^{40}K typically displayed weak to moderate negative correlations; however, its moderate negative correlation with Zn ($r = -0.666$, $p = 0.050$) was exactly at the significance threshold, potentially indicating differing geological sources or geochemical controls.

5.2 Recommendations

5.2.1 Policy Related Recommendations

i. Given the dynamic nature of environmental systems and potential influences like seasonal changes, water level fluctuations, and geological processes in the Turkana Basin, it is recommended that long-term monitoring programs be established to assess temporal variations in the activity concentrations of terrestrial radionuclides in various environmental matrices from the Lake Turkana ecosystem.
ii. Despite the generally low health risks from radionuclides, the elevated 40K in sediments and crops, along with higher absorbed dose rates in some areas, necessitates continuous radiological monitoring.

iii. The annual effective dose from sorghum ingestion exceeding the ICRP limit suggests a need for public awareness regarding potential long-term exposure.

iv. Given the consistently high concentrations of Arsenic in surface water and fish, particularly in locations such as Eliye and Kang'atosa, it is recommended that measures be implemented to mitigate significant potential public health risks.

5.2.2 Recommendations for Future Studies

i. Further studies on dietary intake and local consumption patterns for sorghum are advisable.

ii. Further investigation into the sources and pathways of arsenic, and strategies for mitigation, are strongly recommended.

iii. The clear trend of heavy metal bioaccumulation in fish, particularly in Nile Perch, warrants further research into the trophic transfer of these elements and their potential impact on the aquatic ecosystem and human consumers.

iv. The significant correlations, particularly between 238U, arsenic, and zinc, suggest shared geochemical origins or processes. Further detailed geochemical studies would be beneficial to understand the underlying mechanisms controlling their distribution and bioavailability.

REFERENCES

Abbaspour, N., Hurrell, R., & Kelishadi, R. (2014). Review on iron and its importance for human health. *Journal of Research in Medical Sciences: The Official Journal of Isfahan University of Medical Sciences*, *19*(2), 164–174.

Abd Elnabi, M. K., Elkaliny, N. E., Elyazied, M. M., Azab, S. H., Elkhalifa, S. A., Elmasry, S., Mouhamed, M. S., Shalamesh, E. M., Alhorieny, N. A., Abd Elaty, A. E., Elgendy, I. M., Etman, A. E., Saad, K. E., Tsigkou, K., Ali, S. S., Kornaros, M., & Mahmoud, Y. A.-G. (2023). Toxicity of Heavy Metals and Recent Advances in Their Removal: A Review. *Toxics*, *11*(7), 345-356. https://doi.org/10.3390/toxics11070580

Abdel-Baki, A. S., Dkhil, M. A., & Al-Quraishy, S. (2011). Bioaccumulation of some heavy metals in tilapia fish relevant to their concentration in water and sediment of Wadi Hanifah, Saudi Arabia. *African Journal of Biotechnology*, *10*(13), 167-178.

Abdissa, S. (2021). Measurement of Radioactivity Levels and Health Risk in Maize and Sorghum Grown in the Bale zone Oromia Region, Ethiopia, by Using Gamma Ray Spectrometer (HPGe). *MSc Thesis, Addis Ababa University*.

Abebe, Y., Alamirew, T., Whitehead, P., Charles, K., & Alemayehu, E. (2023). Spatio-temporal variability and potential health risks assessment of heavy metals in the surface water of Awash basin, Ethiopia. *Heliyon*, *9*(5), e15832. https://doi.org/10.1016/j.heliyon.2023.e15832

Adamu, R., Zakari, Y., Ahmed, A., Abubakar, S., & Vatsa, A. M. (2013). Analysis of activity concentrations due to natural radionuclides in the fish ofKainji lake. *Advances in Applied Science Research*, 283–287.

Adebiyi, F. M., Ore, O. T., & Owolafe, O. S. (2024). Human health risk assessment of potentially toxic metals in fish (Cynoglossus sp.) commonly consumed in Nigeria. *Discover Toxicology*, *1*(1), 7. https://doi.org/10.1007/s44339-024-00009-3

Adewoyin, O. O., Omeje, M., Joel, E. S., Akinwumi, S. A., Ehi-Eromoseled, C. O., & Embong, Z. (2018). Radionuclides proportion and radiological risk assessment of soil samples collected in Covenant University, Ota, Ogun State Nigeria. *MethodsX*, *5*, 1419–1426. https://doi.org/10.1016/j.mex.2018.10.023

Adigun, M., & Sodipo, B. (2024). Determination of 40K, 238U and 232Th Activity Levels in Fishes from River Kubanni in Nigeria. *Science Letters*, *12*(2), 65–69. https://doi.org/10.47262/SL/12.2.132024270

Aguko, W. O., Kinyua, R., & Githiri, J. G. (2020). Natural Radioactivity and Excess Lifetime Cancer Risk Associated with Soil in Kargi Area, Marsabit-Kenya. *Journal of Geoscience and Environment Protection*, *8*(12), 127-143. https://doi.org/10.4236/gep.2020.812008

Ahamad, M. I., Yao, Z., Ren, L., Zhang, C., Li, T., Lu, H., Mehmood, M. S., Rehman, A., Adil, M., Lu, S., & Feng, W. (2024). Impact of heavy metals on aquatic life and human health: A case study of River Ravi Pakistan. *Frontiers in Marine Science*, *11,* 121-128. https://doi.org/10.3389/fmars.2024.1374835

Akall, G. (2021). Effects of development interventions on pastoral livelihoods in Turkana County, Kenya. *Pastoralism*, *11*(1), 23. https://doi.org/10.1186/s13570-021-00197-2

Akuja, T. E., & Kandagor, J. (2019). A review of policies and agricultural productivity in the arid and semi-arid lands (ASALS), Kenya: The case of Turkana County. *Journal of Applied Biosciences*, *140*(1), 14304. https://doi.org/10.4314/jab.v140i1.9

Alaamer, A. S. (2012). Measurement of Natural Radioactivity in Sand Samples Collected from Ad-Dahna Desert in Saudi Arabia. *World Journal of Nuclear Science and Technology*, *02*(04), 187–191. https://doi.org/10.4236/wjnst.2012.24029

Alabi, O. D., Gounden, A., Naidoo, K. K., Mellem, J. J., & Paul, V. (2024). The Detrimental Influence of Heavy Metals and Contaminants on Food Production and Consumption. *Journal of Environmental Protection*, *15*(12), 1035–1055. https://doi.org/10.4236/jep.2024.1512062

Al-Afify, A. D. G., & Abdel-Satar, A. M. (2022). Heavy Metal Contamination of the River Nile Environment, Rosetta Branch, Egypt. *Water, Air, & Soil Pollution*, *233*(8), 302–318. https://doi.org/10.1007/s11270-022-05759-7

Al-Fartusie, F. S., & Mohssan, S. N. (2017). Essential Trace Elements and Their Vital Roles in Human Body. *Indian Journal of Advances in Chemical Science*, *5*(3), 127–136.

Al-Ghamdi, A. H. (2019). Health risk assessment of natural background radiation in the soil of Eastern province, Saudi Arabia. *Journal of Radiation Research and Applied Sciences*, *12*(1), 219–225. https://doi.org/10.1080/16878507.2019.1637045

Al-Hayani, A. H., Al-Mashhadani, A. H., & Tawfiq, N. F. (2021). *Radioactivity Investigation In Water of Tigris River in Salah Al-Din Governorate, Iraq*. *1999*(1), 12–25. https://doi.org/10.1088/1742-6596/1999/1/012057

Alnour, I. A., Wagiran, H., Ibrahim, N., Hamzah, S., Siong, W. B., & Elias, M. S. (2014). New approach for calibration the efficiency of HpGe detectors. 38–44. https://doi.org/10.1063/1.4866101

Aloo, P. A., Njiru, J., Balirwa, J. S., & Nyamweya, C. S. (2017). Impacts of Nile Perch, Lates niloticus, introduction on the ecology, economy and conservation of Lake Victoria, East Africa. *Lakes & Reservoirs: Science, Policy and Management for Sustainable Use*, *22*(4), 320–333. https://doi.org/10.1111/lre.12192

Al-Weher, S. M. (2008). *Levels of Heavy Metal Cd, Cu and Zn in Three Fish Species Collected from the Northern Jordan Valley, Jordan*. *1*(1), 41–46.

Alzeny, A., Abdel-Aziz, N. E., El-Ghobashy, A. E., & El-Tohamy, W. S. (2024). Diet Composition and Feeding Habits of Fish Larvae of Five Species in the Burullus Lake, Egypt. *Thalassas: An International Journal of Marine Sciences*, *40*(2), 1145–1157. https://doi.org/10.1007/s41208-024-00677-3

Andemo, A., Yimer, G. T., Sota, S. S., & Berego, Y. S. (2024). Level of Heavy Metals in Fish and Associated Human Health Risk From the Omo Delta in Southern

Ethiopia: A First-Hand Report. *Environmental Health Insights*, *18*, 11786302241238180. https://doi.org/10.1177/11786302241238180

Andrade, C. (2019). The P Value and Statistical Significance: Misunderstandings, Explanations, Challenges, and Alternatives. *Indian Journal of Psychological Medicine*, *41*(3), 210–215. https://doi.org/10.4103/IJPSYM.IJPSYM_193_19

Anzai, K., Ban, N., Ozawa, T., & Tokonami, S. (2012). Fukushima Daiichi Nuclear Power Plant accident: Facts, environmental contamination, possible biological effects, and countermeasures. *Journal of Clinical Biochemistry and Nutrition*, *50*(1), 2–8. https://doi.org/10.3164/jcbn.D-11-00021

Arriola-Velásquez, A. C., Tejera, A., Guerra, J. G., Geibert, W., Stimac, I., Cámara, F., Alonso, H., Rubiano, J. G., & Martel, P. (2021). ^{226}Ra, ^{228}Ra and ^{40}K as tracers of erosion and accumulation processes: A 3-year study on a beach with different sediment dynamics. *CATENA*, *207*, 105705. https://doi.org/10.1016/j.catena.2021.105705

Asnake, W. (2018). Nile Perch (Lates niloticus): The Promising White Meat of the World. *Journal of Nutrition & Food Sciences*, *08*(02), 680.

Assefa, W. W., & Getahun, A. (2015). *The Food and Feeding Ecology of Nile Tilapia, Oreochromis niloticus, in Lake Hayq, Ethiopia*. *41*, 55–66.

Aswood, M. Sh., Al-Hamzawi, A. A., & Khadayeir, A. A. (2018). Natural radionuclides in six selected fish consumed in south Iraq and their committed effective doses. *SN Applied Sciences*, *1*(1), 21–26. https://doi.org/10.1007/s42452-018-0019-6

Atambo, O. V. (2011). Determination of Naturally Occurring Radioactive Elements and Radiation Exposure Levels in the Soapstone Quarries of Tabaka Region of Kisii District, Kenya (No. INIS-KE--060). Jomo Kenyatta University of Agriculture and Technology, Nairobi (Kenya). https://inis.iaea.org/records/rrt82-9j395

Atibu, E. K., Oliveira, J. M., Malta, M., Santos, M., Mulaji, C. K., Mpiana, P. T., & Carvalho, F. P. (2021). Assessment of Natural Radioactivity in Rivers Sediment and Soil from the Copper Belt Artisanal Mining Region, Democratic Republic of the Congo. *Journal of Geoscience and Environment Protection*, *9*(7), 1-20. https://doi.org/10.4236/gep.2021.97001

Awofolu, O. R., Mbolekwa, Z., Mtshemla, V., & Fatoki, O. S. (2005). Levels of trace metals in water and sediment from Tyume River and its effects on an irrigated farmland. *Water SA*, *31*(1), 87–94. https://doi.org/10.10520/EJC116227

Ayenimo, J. G., Adeeyinwo, C. E., & Amoo, I. A. (2005). *Heavy Metal Pollutants In Warri River, Nigeria*. 43–50.

Bajoga, A. D., Alazemi, N., Shams, H., Regan, P., & Bradley, D. (2016). Evaluation of naturally occurring radioactivity across the State of Kuwait using high-resolution gamma-ray spectrometry. *Radiation Physics and Chemistry*, *137*, 203–209. https://doi.org/10.1016/j.radphyschem.2016.02.013

Balaram, V. (2020). Microwave plasma atomic emission spectrometry (MP-AES) and its applications – A critical review. *Microchemical Journal*, *159*, 105483. https://doi.org/10.1016/j.microc.2020.105483

Balzani, P., Kouba, A., Tricarico, E., Kourantidou, M., & Haubrock, P. J. (2022). Metal accumulation in relation to size and body condition in an all-alien species community. *Environmental Science and Pollution Research International*, *29*(17), 25848–25857. https://doi.org/10.1007/s11356-021-17621-0

Bangou, C., Yameogo, Z., Hie, K., Nitiema, E., Zerbo, I., & Zoungrana, M. (2024). Assessment of Natural Radioactivity and Radiological Hazards in Soil, Sorghum, and Water in Villy at the West Central Region of Burkina Faso. *Applied and Environmental Soil Science*, *2024*(1), 2002878. https://doi.org/10.1155/2024/2002878

Barlow, C. G., & Lisle, A. (1987). Biology of The Nile Perch *Lates niloticus* (Pisces: Centropomidae) with reference to its proposed role as a sport fish in Australia. *Biological Conservation*, *39*(4), 269–289. https://doi.org/10.1016/0006-3207(87)90129-7

Barnhart, J. (1997). Occurrences, Uses, and Properties of Chromium. *Regulatory Toxicology and Pharmacology*, *26*(1), S3–S7. https://doi.org/10.1006/rtph.1997.1132

Bilalo, S. Q., Andayi, A. A., Njagi, E. C., & Ptoton, B. M. (2024). *Concentrations of Selected Heavy Metals in Soil and Tomatoes (Lycopersicon Esculenta Mill.) Grown in Kirinyaga County, Kenya*. *11*(2), 932–942.

Biswas, K. P., Hossain, S., Deb, N., Bhuian, A. K. M. S. I., Gonçalves, S. C., Hossain, S., & Hossen, M. B. (2021). Assessment of the Levels of Pollution and of Their Risks by Radioactivity and Trace Metals on Marine Edible Fish and Crustaceans at the Bay of Bengal (Chattogram, Bangladesh). *Environments*, *8*(2), 232-243. https://doi.org/10.3390/environments8020013

Boral, S., Sen, I. S., Tripathi, A., Sharma, B., & Dhar, S. (2020). Tracking Dissolved Trace and Heavy Metals in the Ganga River From Source to Sink: A Baseline to Judge Future Changes. *Geochemistry, Geophysics, Geosystems*, *21*(10), e2020GC009203. https://doi.org/10.1029/2020GC009203

Bost, M., Houdart, S., Oberli, M., Kalonji, E., Huneau, J.-F., & Margaritis, I. (2016). Dietary copper and human health: Current evidence and unresolved issues. *Journal of Trace Elements in Medicine and Biology*, *35*, 107–115. https://doi.org/10.1016/j.jtemb.2016.02.006

Briffa, J., Sinagra, E., & Blundell, R. (2020). Heavy metal pollution in the environment and their toxicological effects on humans. *Heliyon*, *6*(9), e04691. https://doi.org/10.1016/j.heliyon.2020.e04691

Bruton, M. N. (1979). The food and feeding behaviour of Clarias gariepinus (Pisces: Clariidae) in Lake Sibaya, South Africa, with emphasis on its role as a predator of cichlids. *The Transactions of the Zoological Society of London*, *35*(1), 47–114. https://doi.org/10.1111/j.1096-3642.1979.tb00057.x

Catley, Andy, Lind, Jeremy, & Scoones, Ian. (2013). *Pastoralism and Development in Africa*. https://library.oapen.org/handle/20.500.12657/102413

Chege, M. W., Hashim, N. O., Merenga, A. S., & Tschiersch, J. (2015). Analysis of internal exposure associated with consumption of crops and groundwater from

the high background radiation area of Mrima Hill, Kenya. *Radiation Protection Dosimetry*, *167*(1–3), 276–278.

Dadebo, E., Ahlgren, I., & Ahlgren, G. (2006). Maturation, sex ratio and fecundity of the Nile perch <I>Lates niloticus</I> (L.) (Pisces: Centropomidae) in Lake Chamo, Ethiopia. *SINET: Ethiopian Journal of Science*, *28*(2), 151–160.

Dagne, B. B., Endale, T., Tesfahun, K., & Negash, D. (2019). Levels of some toxic heavy metals (Cr, Cd and Pb) in selected vegetables and soil around eastern industry zone, central Ethiopia. *African Journal of Agricultural Research*, *14*(2), 92–101. https://doi.org/10.5897/ajar2018.13324

Darko, G., Faanu, A., Akoto, O., Acheampong, A., Goode, E. J., & Gyamfi, O. (2015). Distribution of natural and artificial radioactivity in soils, water and tuber crops. *Environmental Monitoring and Assessment*, *187*(6), 339. https://doi.org/10.1007/s10661-015-4580-9

Desouky, O., Ding, N., & Zhou, G. (2015). Targeted and non-targeted effects of ionizing radiation. *Journal of Radiation Research and Applied Sciences*, *8*(2), 247–254. https://doi.org/10.1016/j.jrras.2015.03.003

Dessie, A., Mingist, M., Mequanent, D., & Aemro, D. (2024). Food and feeding habits of the African catfish Clarias gariepinus (Burchell, 1822) (Pisces: Clariidae) in the newly built Ribb Reservoir, north-west Ethiopia. *Indian Journal of Fisheries*, *71*(2), 248-356. https://doi.org/10.21077/ijf.2024.71.2.134268-05

Dev, S., & Babitt, J. L. (2017). Overview of Iron Metabolism in Health and Disease. *Hemodialysis International. International Symposium on Home Hemodialysis*, *21*(Suppl 1), S6–S20. https://doi.org/10.1111/hdi.12542

Dey, S., Rajak, P., & Sen, K. (2024). Bioaccumulation of metals and metalloids in seafood: A comprehensive overview of mobilization, interactive effects in eutrophic environments, and implications for public health risks. *Journal of Trace Elements and Minerals*, *8*, 100141.

Di Leo, G., & Sardanelli, F. (2020). Statistical significance: P value, 0.05 threshold, and applications to radiomics—reasons for a conservative approach. *European Radiology Experimental*, *4*(1), 18. https://doi.org/10.1186/s41747-020-0145-y

DiEnye, H., Olopade, O., & Obi, C. O. (2021). Socio-Economic and Cost Benefits of Catfish (Clarias gariepinus) Marketing in Obio-Akpor Local Government Area, Rivers State, Nigeria. *Journal of Limnology and Freshwater Fisheries Research*, *7*(1), 40–48. https://doi.org/10.17216/limnofish.768909

Dubey, I. (2021). Study on the Toxic Effects of Heavy Metals in Sediments and Water of River Ganga. *International Journal on Biological Sciences*, *12*(2), 89–97. https://doi.org/10.53390/ijbs.v12i2.7

Duffus, J. H. (2002). Prepared for publication by. *Pure and Applied Chemistry*, *74*(5), 793–807.

Dugasa, G., & Endale, T. (2019). Determination of Some Selected Heavy Metals in Water, Oreochromis niloticus and Labeobarbus intermedius Samples from Abaya and Chamo Lakes. *Food Science and Quality Management*, *18*(21), 349-356. https://doi.org/10.7176/fsqm/83-05

El-Shebly, A. (2006). Evaluation of growth performance, production and nutritive value of the African catfish, clarias gariepinus.cultured in earthen ponds. *Egyptian Journal of Aquatic Biology and Fisheries*, *10*(3), 55–67. https://doi.org/10.21608/ejabf.2006.1862

El-Taher, A., & Abbady, A. (2012). Natural radioactivity levels and associated radiation hazards in Nile river sediments from Aswan to El-Minia, Upper Egypt.

Emurotu, J. E., Olawale, O., Dallatu, E. M., Abubakar, T. A., Umudi, Q. E., Eneogwe, G. O., & Atumeyi, A. (2024). Carcinogenic and non-carcinogenic health risk assessment of heavy metals in the offal of animals from Felele Abattoir, Lokoja, Nigeria. *Toxicology Reports*, *13*, 101701. https://doi.org/10.1016/j.toxrep.2024.101701

Esilaba, F., Moturi, W. N., Mokua, M., & Mwanyika, T. (2020). Human Health Risk Assessment of Trace Metals in the Commonly Consumed Fish Species in Nakuru Town, Kenya. *Environmental Health Insights*, *14*, 1178630220917128. https://doi.org/10.1177/1178630220917128

Estokova, A., Singovszka, E., & Vertal, M. (2022). Investigation of Building Materials' Radioactivity in a Historical Building—A Case Study. *Materials*, *15*(19), 6876. https://doi.org/10.3390/ma15196876

Faure, G. (1986). Principles of isotope geology. Second edition. https://www.osti.gov/biblio/5648561

Feibel, C. S. (2011a). A Geological History of the Turkana Basin. *Evolutionary Anthropology: Issues, News, and Reviews*, *20*(6), 206–216. https://doi.org/10.1002/evan.20331

Fernandes, C., Fontaínhas-Fernandes, A., Peixoto, F., & Salgado, M. A. (2007). Bioaccumulation of heavy metals in Liza saliens from the Esmoriz-Paramos coastal lagoon, Portugal. *Ecotoxicology and Environmental Safety*, *66*(3), 426–431. https://doi.org/10.1016/j.ecoenv.2006.02.007

Francis Ekiru. (2023). Food and Agriculture Needs, Gaps, and Partnership Opportunities in Turkana County, Kenya: Areas of Focus for Development Partners, and the County Government of Turkana. https://www.researchgate.net/publication/369475128_Food_and_Agriculture_Needs_Gaps_and_Partnership_Opportunities_in_Turkana_County_Kenya_Areas_of_Focus_for_Development_Partners_and_the_County_Government_of_Turkana

Frey, P. A., & Reed, G. H. (2012). The ubiquity of iron. *ACS Chemical Biology*, *7*(9), 1477–1481. https://doi.org/10.1021/cb300323q

Friedlander, G., Kennedy, J. W., Macias, E. S., & Miller, J. M. (1981). Nuclear and radiochemistry, 3rd edition. https://www.osti.gov/biblio/7093814

Gilmore, G. R. (2008). Practical Gamma-Ray Spectrometry (1st ed.). Wiley. https://doi.org/10.1002/9780470861981

Gonzalez, A. R., Ndung'u, K., & Flegal, A. R. (2005). Natural occurrence of hexavalent chromium in the Aromas Red Sands Aquifer, California.

Environmental Science & Technology, *39*(15), 5505–5511. https://doi.org/10.1021/es048835n

Gopal, R., Narmada, S., Vijayakumar, R., & Jaleel, C. A. (2009). Chelating efficacy of CaNa2 EDTA on nickel-induced toxicity in *Cirrhinus mrigala* (Ham.) through its effects on glutathione peroxidase, reduced glutathione and lipid peroxidation. *Comptes Rendus Biologies*, *332*(8), 685–696. https://doi.org/10.1016/j.crvi.2009.03.004

Grammer, G., Slack, W., Peterson, M., & Dugo, M. (2012). Nile tilapia Oreochromis niloticus (Linnaeus, 1758) establishment in temperate Mississippi, USA: Multi-year survival confirmed by otolith ages. *Aquatic Invasions*, *7*(3), 367–376. https://doi.org/10.3391/ai.2012.7.3.008

Gure, A., Kedir, K., & Abduro, F. (2019). Heavy metal concentrations in fish tissues from Gilgel Gibe (I) Hydroelectric Dam Reservoir, Ethiopia. *Journal of Applied Sciences and Environmental Management*, *23*(8), 1411. https://doi.org/10.4314/jasem.v23i8.1

Hall, D. S., Lockwood, D. J., Bock, C., & MacDougall, B. R. (2015). Nickel hydroxides and related materials: A review of their structures, synthesis and properties. *Proceedings of the Royal Society A: Mathematical, Physical and Engineering Sciences*, *471*(2174), 20140792. https://doi.org/10.1098/rspa.2014.0792

Hama Aziz, K. H., Mustafa, F. S., Omer, K. M., Hama, S., Hamarawf, R. F., & Rahman, K. O. (2023). Heavy metal pollution in the aquatic environment: Efficient and low-cost removal approaches to eliminate their toxicity: a review. *RSC Advances*, *13*(26), 17595–17610. https://doi.org/10.1039/d3ra00723e

Hamed, Y., Ayadi, Y., Hadji, R., Ben Saad, A., Gentilucci, M., & Elaloui, E. (2024). Environmental Radioactivity, Ecotoxicology (238U, 232Th and 40K) and Potentially Toxic Elements in Water and Sediments from North Africa Dams. *Sustainability*, *16*(2), 490-510. https://doi.org/10.3390/su16020490

Harb, S., El-Kamel, A. H., Zahran, A. M., Abbady, A., & Ahmed, F. A. (2014). *Assessment of Natural Radioactivity in Soil and Water Samples from Aden Governorate South Of Yemen Region*. *1*(1), 1–7.

Hashim, N. O., Rathore, I. V. S., Kinyua, A. M., & Mustapha, A. O. (2004). Natural and artificial radioactivity levels in sediments along the Kenyan coast. *Radiation Physics and Chemistry*, *71*(3), 805–806. https://doi.org/10.1016/j.radphyschem.2004.04.101

Henckens, M. L. C. M., & Worrell, E. (2020). Reviewing the availability of copper and nickel for future generations. The balance between production growth, sustainability and recycling rates. *Journal of Cleaner Production*, *264*, 121460–121472. https://doi.org/10.1016/j.jclepro.2020.121460

Hirpa, F. A., Dyer, E., Hope, R., Olago, D. O., & Dadson, S. J. (2018). Finding sustainable water futures in data-sparse regions under climate change: Insights from the Turkwel River basin, Kenya. *Journal of Hydrology: Regional Studies*, *19*, 124–135. https://doi.org/10.1016/j.ejrh.2018.08.005

Hong, Y.-S., Song, K.-H., & Chung, J.-Y. (2014). Health Effects of Chronic Arsenic Exposure. *Journal of Preventive Medicine and Public Health*, *47*(5), 245–252. https://doi.org/10.3961/jpmph.14.035

Hossain, Md. S., Islam, Md. N., Rahman, Md. M., Mostofa, M. G., & Khan, Md. A. R. (2022). Sorghum: A prospective crop for climatic vulnerability, food and nutritional security. *Journal of Agriculture and Food Research*, *8*, 100300. https://doi.org/10.1016/j.jafr.2022.100300

ICRP. (1991). *ICRP (1991)* Recommendations of the International Commission on Radiological Protection. *ICRP Publication 60, Ann. ICRP 21 (1-3), Ottawa. - References—Scientific Research Publishing*.

Irunde, R., Ijumulana, J., Ligate, F., Maity, J. P., Ahmad, A., Mtamba, J., Mtalo, F., & Bhattacharya, P. (2022). Arsenic in Africa: Potential sources, spatial variability, and the state of the art for arsenic removal using locally available materials. *Groundwater for Sustainable Development*, *18*, 100746. https://doi.org/10.1016/j.gsd.2022.100746

Irunkwor, T. C., Abanjo N, & Ogboi, K. C. (2023). Assessment of Natural Radioactivity and Radiological Hazard indices in Cassava Cultivated in Oil Producing Area, Rivers State, Nigeria. *International Journal of Applied Science and Research*, *05*(05), 174–188. https://doi.org/10.56293/IJASR.2022.5444

Iwetan, C. N., Fuwape, I. A., Arogunjo, A. M., & Obor, G. (2015). Assessment of Activity Concentration of Radionuclides in Sediment from Oil Producing Communities of Delta State, Nigeria. *Journal of Environmental Protection*, *6*(6), 640-650. https://doi.org/10.4236/jep.2015.66058

Jamil Emon, F., Rohani, M. F., Sumaiya, N., Tuj Jannat, M. F., Akter, Y., Shahjahan, M., Abdul Kari, Z., Tahiluddin, A. B., & Goh, K. W. (2023). Bioaccumulation and Bioremediation of Heavy Metals in Fishes—A Review. *Toxics*, *11*(6), 510–532. https://doi.org/10.3390/toxics11060510

Jarup, L. (2003). *Hazards of heavy metal contamination. British Medical Bulletin, 68(1), 167—182.*

Joel, E. S., Maxwell, O., Adewoyin, O. O., Ehi-Eromosele, C. O., Embong, Z., & Oyawoye, F. (2018). Assessment of natural radioactivity in various commercial tiles used for building purposes in Nigeria. *MethodsX*, *5*, 8–19. https://doi.org/10.1016/j.mex.2017.12.002

Jung, M. Y., Kang, J. H., Choi, Y. S., Lee, D. Y., Lee, J. Y., & Park, J. S. (2019). Analytical features of microwave plasma-atomic emission spectrometry (MP-AES) for the quantitation of manganese (Mn) in wild grape (*Vitis coignetiae*) red wines: Comparison with inductively coupled plasma-optical emission spectrometry (ICP-OES). *Food Chemistry*, *274*, 20–25. https://doi.org/10.1016/j.foodchem.2018.08.114

Kage, F. G. (2012). Impact of heavy metal pollution on the composition and abundance of benthic macroinvertebrates along Nariobi river, Kenya. http://ir-library.ku.ac.ke/handle/123456789/4905

Kebwaro, J. M., Rathore, I. V. S., Hashim, N. O., & Mustapha, A. O. (2011). *Radiometric assessment of natural radioactivity levels around Mrima Hill, Kenya*. *6*(13), 3105–3110.

Kessaratikoon, P., Benjakul, S., & Udomsomporn, S. (2007). Distribution of Natural Radionuclides in Songkhla Beach Sands. *Agriculture and Natural Resources*, *41*(5), 157-164.

Khoddami, A., Messina ,Valeria, Vadabalija Venkata ,Komala, Farahnaky ,Asgar, Blanchard ,Christopher L., & and Roberts, T. H. (2023). Sorghum in foods: Functionality and potential in innovative products. *Critical Reviews in Food Science and Nutrition*, *63*(9), 1170–1186. https://doi.org/10.1080/10408398.2021.1960793

Knoll, G. F. (2010). *Radiation Detection and Measurement*. John Wiley & Sons.

Kpelly, E. D., Blay, J., & Yankson, K. (2022). The biological characteristics of the Nile tilapia (Oreochromis niloticus) in the Weija Reservoir, Ghana. *International Journal of Bonorowo Wetlands*, *12*(1), 41–54.

Krane, K. S. (1987). Introductory Nuclear Physics. An Introductory Nuclear Physics. https://ui.adsabs.harvard.edu/abs/1987inp..book.....K

Kumar, N. (2006). Copper Deficiency Myelopathy (Human Swayback). *Mayo Clinic Proceedings*, *81*(10), 1371–1384. https://doi.org/10.4065/81.10.1371

Langat, W. K., Omar, H. N., & J, W. A. (2014). Gamma Ray Spectrometric Analysis of Sedimental Deposits at the Shores of Lake Nakuru, Kenya. *Journal of Natural Sciences Research*, *4*(21), 34–40.

Lasheen, M. R., Sharaby, C. M., El-Kholy, N. G., Elsherif, I. Y., & El-Wakeel, S. T. (2008). Factors influencing lead and iron release from some Egyptian drinking water pipes. *Journal of Hazardous Materials*, *160*(2–3), 675–680. https://doi.org/10.1016/j.jhazmat.2008.03.040

Leo, W. R. (1994). Semiconductor Detectors. In W. R. Leo (Ed.), *Techniques for Nuclear and Particle Physics Experiments: A How-to Approach* (pp. 215–247). Springer. https://doi.org/10.1007/978-3-642-57920-2_10

Li, Q., Wang, Y., Li, Y., Li, L., Tang, M., Hu, W., Chen, L., & Ai, S. (2022). Speciation of heavy metals in soils and their immobilization at micro-scale interfaces among diverse soil components. *Science of The Total Environment*, *825*, 153862. https://doi.org/10.1016/j.scitotenv.2022.153862

Li, W., Simmons, P., Shrader, D., Herrman, T. J., & Dai, S. Y. (2013). Microwave plasma-atomic emission spectroscopy as a tool for the determination of copper, iron, manganese and zinc in animal feed and fertilizer. *Talanta*, *112*, 43–48. https://doi.org/10.1016/j.talanta.2013.03.029

Manahan, S. E. (2017). Environmental Chemistry (10th ed.). CRC Press. https://doi.org/10.1201/9781315160474

Matsitsi, S. M., Linturi, J. M., Kebwaro, J. M., & Kirago, L. M. (2020). Radiometric Survey of the Tyaa River Sand Mine in Kitui, Kenya. *Radiation Protection Dosimetry*, *188*(4), 405–412. https://doi.org/10.1093/rpd/ncz300

Munene, E. N., Hashim, N. O., & Ambusso, W. N. (2023 a). Human health risk assessment of heavy metal concentration in surface water of Sosian river, Eldoret town, Uasin-Gishu County Kenya. *MethodsX*, *11*, 102298–102306.

Munene, P. M., Mbugua, G. W., Wanjau, R. N., & James, N. N. (2023 b). Analysis Of Physico-Chemical Parameters And Selected Heavy Metals In Aquatic Ecosystems. *Journal of Applied Chemistry*, *16*, 59–64.

Munguti, J. M., Nairuti, R., Iteba, J. O., Obiero, K. O., Kyule, D., Opiyo, M. A., Abwao, J., Kirimi, J. G., Outa, N., Muthoka, M., Githukia, C. M., & Ogello, E. O. (2022). Nile tilapia (Oreochromis niloticus Linnaeus, 1758) culture in Kenya: Emerging production technologies and socio-economic impacts on local livelihoods. *Aquaculture, Fish and Fisheries*, *2*(4), 265–276. https://doi.org/10.1002/aff2.58

Mwegoha, W. J. S., & Kihampa, C. (2010). Heavy metal contamination in agricultural soils and water in Dar es Salaam city, Tanzania. *African Journal of Environmental Science and Technology*, *4*(11), 763-769.

Najam, L., ElTaher, A., Hussian, I., & Ali Omar, M. (2019). Evaluation of Natural Radionuclide content in Nile River Sediments and Excess Lifetime Cancer Risk due to Gamma Radioactivity. *Iranian Journal of Medical Physics*, *16*(Online First), 27–33. https://doi.org/10.22038/ijmp.2018.30622.1351

Nasirian, M., Bahari, I., & Abdullah, P. (2008). Assessment of Natural Radioactivity in Water and Sediment From Amang (Tin Tailing) Processing Ponds. *12*(1), 150–159.

Navas-Acien, A., & Nachman, K. E. (2013). Public Health Responses to Arsenic in Rice and Other Foods. *JAMA Internal Medicine*, *173*(15), 1395–1396. https://doi.org/10.1001/jamainternmed.2013.6405

Naz, R., Khan, M. S., Hafeez, A., Fazil, M., Khan, M. N., Ali, B., Javed, M. A., Imran, M., Shati, A. A., Alfaifi, M. Y., Elbehairi, S. E. I., & Ahmed, A. E. (2022). Assessment of phytoremediation potential of native plant species naturally growing in a heavy metal-polluted industrial soils. *Brazilian Journal of Biology*, *84*, e264473. https://doi.org/10.1590/1519-6984.264473

Nderitu, S. K., Maina, D. M., & Kinyua, A. M. (2001). Natural gamma radiation levels, indoor and water ^{222}Rn Concentrations in soil division of Kerio valley, kenya [Report]. University of Nairobi. http://erepository.uonbi.ac.ke/handle/11295/78235

Njoroge, P. W., & Nyambura, C. (2024). Risk Assessment of Resident Farmers in Kilimambogo, Kenya, Using RESRAD Computer Code. *International Journal of Scientific and Research Publications*, *14*(9), 188–196.

Njuguna, S. M., Yan, X., Gituru, R. W., Wang, Q., & Wang, J. (2017). Assessment of macrophyte, heavy metal, and nutrient concentrations in the water of the Nairobi River, Kenya. *Environmental Monitoring and Assessment*, *189*(9), 454–468. https://doi.org/10.1007/s10661-017-6159-0

Nyakuni, L. (2009). Habitat utilization and reproductive biology of Nile Tilapia (Oreochromis Niloticus) in Albert Nile, Nebbi District [Thesis, Makerere University]. https://makir.mak.ac.ug/handle/10570/2495

Nyarko, E., Boateng, C. M., Asamoah, O., Edusei, M. O., & Mahu, E. (2023). Potential human health risks associated with ingestion of heavy metals through fish consumption in the Gulf of Guinea. *Toxicology Reports*, *10*, 117–123. https://doi.org/10.1016/j.toxrep.2023.01.005

Obasohan, E. E. (2008). The use of heavy metals load as an indicator of the suitability of the water and fish of Ibiekuma Stream for domestic and consumption purposes. *African Journal of Biotechnology*, *7*(23), 4345-4348. https://www.ajol.info/index.php/ajb/article/view/59586

Obiero, K., Wakjira, M., Gownaris, N., Malala, J., Keyombe, J. L., Ajode, M. Z., Smith, S., Lawrence, T., Ogello, E., Getahun, A., & Kolding, J. (2023). Lake Turkana: Status, challenges, and opportunities for collaborative research. *Journal of Great Lakes Research*, *49*(6), 102120. https://doi.org/10.1016/j.jglr.2022.10.007

Ogbemudia, E. M., Nwoke, E. B., & Onisogenime, A. J. (2023). Concentrations of selected heavy metals and physicochemical properties in Forcados River in Sagbama Local Government Area of Bayelsa State, Nigeria. *Faculty of Natural and Applied Sciences Journal of Scientific Innovations*, *4*(1), 237-245.

Oguzie, F. A., & Okhagbuzo, G. A. (2010). *Concentrations of heavy metals in effluent discharges downstream of Ikpoba river in Benin City, Nigeria*. *9*(3), 319–325.

Ojekunle, O. Z., Ojekunle, O. V., Adeyemi, A. A., Taiwo, A. G., Sangowusi, O. R., Taiwo, A. M., & Adekitan, A. A. (2016). Evaluation of surface water quality indices and ecological risk assessment for heavy metals in scrap yard neighbourhood. *SpringerPlus*, *5*, 560–576.

Okelo, D. E. (2015). *Gamma Ray Spectrometric Analysis of the Naturally Occurring Radionuclides in Soils Collected Along the Shores of Lake Victoria, Migori County, Kenya* [MSc Thesis, Kenyatta University]. http://ir-library.ku.ac.ke/handle/123456789/14324

Ola, O., & Adedayo, O. (2020). Analysis of cassava production and processing by various groups in support of cassava value chain in the south west of Nigeria. *ISABB Journal of Food and Agricultural Sciences*, *9*(1), 11–19. https://doi.org/10.5897/ISABB-JFAS2020.0113

Oladele, B. B., Ugbede ,Fredrick Oghenebrorie, & and Arogunjo, A. M. (2023). Study of activity concentrations of 40K, 238U and 232Th for assessment of radiation dose in agricultural soils of southwestern Nigeria. *International Journal of Environmental Health Research*, *33*(12), 1640–1651. https://doi.org/10.1080/09603123.2022.2114593

Olagbemide P. T., & Owolabi O. D. (2023). Length-Weight Relationship and Condition Factor of Oreochromis niloticus (Linnaeus, 1758) in Selected Tropical Reservoirs of Ekiti State, Southwest Nigeria. *Journal of Experimental Biology and Agricultural Sciences*, *11*(4), 707–719.

Olatunji Ayotunde, E., Obeten Offem, B., & Bekeh Ada, F. (2012). Heavy metal profile of water, sediment and freshwater cat fish, Chrysichthys nigrodigitatus (Siluriformes: Bagridae), of Cross River, Nigeria. *Revista de Biología Tropical*, *60*(3), 1289–1301.

Olurin, T. O. (2024). Assessment of Naturally Occurring Radionuclides and Heavy Metals Level and Health Risks in Commonly Consumed African catfish, White Catfish and Nile Tilapia Fish Species from Epe Waterside Region of Lagos, Nigeria. *Journal of Applied Sciences and Environmental Management*, *28*(2), 449-457. https://doi.org/10.4314/jasem.v28i2.17

Ononugbo, C. P., Azikiwe, O., & Avwiri, G. O. (2019). Uptake and Distribution of Natural Radionuclides in Cassava Crops from Nigerian Government Farms. *Journal of Scientific Research and Reports*, *5*(23), 1–15.

Oronsaye, J. a. O., Wangboje, O. M., & Oguzie, F. A. (2010). Trace metals in some benthic fishes of the Ikpoba river dam, Benin City, Nigeria. *African Journal of Biotechnology*, *9*(51), 8860-8864.

Osman, A. G. M., & Kloas, W. (2010). Water Quality and Heavy Metal Monitoring in Water, Sediments, and Tissues of the African Catfish Clarias gariepinus (Burchell, 1822) from the River Nile, Egypt. *Journal of Environmental Protection*, *1*(4), 389-400. https://doi.org/10.4236/jep.2010.14045

Plagnard, J., Hamon, C., & Lépy, M. C. (2008). Study of scattering effects in low-energy gamma-ray spectrometry. *Applied Radiation and Isotopes: Including Data, Instrumentation and Methods for Use in Agriculture, Industry and Medicine*, *66*(6–7), 769–773. https://doi.org/10.1016/j.apradiso.2008.02.016

Plessl, C., Otachi, E. O., Körner, W., Avenant-Oldewage, A., & Jirsa, F. (2017). Fish as bioindicators for trace element pollution from two contrasting lakes in the Eastern Rift Valley, Kenya: Spatial and temporal aspects. *Environmental Science and Pollution Research*, *24*(24), 19767–19776. https://doi.org/10.1007/s11356-017-9518-z

Prasad, S., Yadav, K. K., Kumar, S., Gupta, N., Cabral-Pinto, M. M. S., Rezania, S., Radwan, N., & Alam, J. (2021). Chromium contamination and effect on environmental health and its remediation: A sustainable approaches. *Journal of Environmental Management*, *285*, 112174. https://doi.org/10.1016/j.jenvman.2021.112174

Qiao, C.-K., Wei, J.-W., & Chen, L. (2021). An Overview of the Compton Scattering Calculation. *Crystals*, *11*(5), 525. https://doi.org/10.3390/cryst11050525

Qureshi, A. A., Tariq, S., Din, K. U., Manzoor, S., Calligaris, C., & Waheed, A. (2014). Evaluation of excessive lifetime cancer risk due to natural radioactivity in the rivers sediments of Northern Pakistan. *Journal of Radiation Research and Applied Sciences*, *7*(4), 438–447. https://doi.org/10.1016/j.jrras.2014.07.008

R. Hamad, F. Ikraiam, & H. Hasan. (2023). Determination of Specific Natural Radionuclides in the Bones of Some Local Fish Commonly Consumed from the Eastern Libyan Coast. *Journal of Radiation and Nuclear Applications*, *8*(3), 283–289. https://doi.org/10.18576/jrna/080310

Radzali, N. A. M., Hidzir, N. M., & Rahman, I. A. (2018). Determination of Natural Radioactivity and Heavy Metals at the Former Mining Site of Kolej Universiti Islam Antarabangsa Selangor (Kuis) Lake. *Malaysian Journal of Analytical Science*, *22*(5), 828–838. https://doi.org/10.17576/mjas-2018-2205-10

Raghu, Y., Ravisankar, R., Chandrasekaran, A., Vijayagopal, P., & Venkatraman, B. (2017). Assessment of natural radioactivity and radiological hazards in building materials used in the Tiruvannamalai District, Tamilnadu, India, using a statistical approach. *Journal of Taibah University for Science*, *11*(4), 523–533. https://doi.org/10.1016/j.jtusci.2015.08.004

Rajeshkumar, S., & Li, X. (2018). Bioaccumulation of heavy metals in fish species from the Meiliang Bay, Taihu Lake, China. *Toxicology Reports*, *5*, 288–295. https://doi.org/10.1016/j.toxrep.2018.01.007

Rasheed, A. A., Kadhum, N. F., & Ibrahim, N. K. (2016). Natural Radioactivity and Associated Dose Rates in Soil Samples in the Destroyed Fuel Fabrication Facility, Iraq. *International Journal of Physics*, *4*(3), 50-54. https://doi.org/10.12691/ijp-4-3-1

Ravisankar, R., Vanasundari, K., Suganya, M., Raghu, Y., Rajalakshmi, A., Chandrasekaran, A., Sivakumar, S., Chandramohan, J., Vijayagopal, P., & Venkatraman, B. (2014). Multivariate statistical analysis of radiological data of building materials used in Tiruvannamalai, Tamilnadu, India. *Applied Radiation and Isotopes*, *85*, 114–127. https://doi.org/10.1016/j.apradiso.2013.12.005

Reis, V., & Duarte, A. C. (2019). Chapter One—Occurrence, distribution, and significance of arsenic speciation. In A. C. Duarte & V. Reis (Eds.), *Comprehensive Analytical Chemistry* (Vol. 85, pp. 1–14). Elsevier. https://doi.org/10.1016/bs.coac.2019.03.006

Reisz, J. A., Bansal, N., Qian, J., Zhao, W., & Furdui, C. M. (2014). Effects of Ionizing Radiation on Biological Molecules—Mechanisms of Damage and Emerging Methods of Detection. *Antioxidants & Redox Signaling*, *21*(2), 260–292. https://doi.org/10.1089/ars.2013.5489

Rosenberg, I. (2008). Radiation Oncology Physics: A Handbook for Teachers and Students. *British Journal of Cancer*, *98*(5), 1020. https://doi.org/10.1038/sj.bjc.6604224

Safia, H. Q. H. (2016). (PDF) An assessment of Some Toxic, Essential Elements and Natural Radioactivity, in Most Common Fish Consumed in Jeddah-Saudi Arabia. *ResearchGate*, *07*(04), 301–311. https://doi.org/10.4236/fns.2016.74032

Samantara, M. K., Panigrahi, S., Mohanty, A. K., Sahu, G., Mishra, S. S., Palaniswami, K., Subramanian, V., & Venkatraman, B. (2023). Heavy metal concentration in marine edible fishes and associated health risks: An assessment from Tamil Nadu coast, Bay of Bengal. *Environmental Chemistry and Ecotoxicology*, *5*, 193–204. https://doi.org/10.1016/j.enceco.2023.09.002

Sani, A., Idris, K. M., Abdullahi, B. A., & Darma, A. I. (2022). Bioaccumulation and health risks of some heavy metals in *Oreochromis niloticus*, sediment and water of Challawa river, Kano, Northwestern Nigeria. *Environmental Advances*, *7*, 100172. https://doi.org/10.1016/j.envadv.2022.100172

Saravanan, P., Saravanan, V., Rajeshkannan, R., Arnica, G., Rajasimman, M., Baskar, G., & Pugazhendhi, A. (2024). Comprehensive review on toxic heavy metals

in the aquatic system: Sources, identification, treatment strategies, and health risk assessment. *Environmental Research*, *258*, 119440.

Shin, D. Y., Lee, S. M., Jang, Y., Lee, J., Lee, C. M., Cho, E.-M., & Seo, Y. R. (2023). Adverse Human Health Effects of Chromium by Exposure Route: A Comprehensive Review Based on Toxicogenomic Approach. *International Journal of Molecular Sciences*, *24*(4), 3410–3422. https://doi.org/10.3390/ijms24043410

Soh, S. D. T., Saïdou, Hosoda, M., Ii, J. E. N. N., Akata, N., Bouba, O., & Tokonami, S. (2018). Natural radioactivity measurements and external dose estimation by car-borne survey in Douala city, Cameroon. *Radioprotection*, *53*(4), 255–263. https://doi.org/10.1051/radiopro/2018032

SureshGandhi, M., Ravisankar, R., Rajalakshmi, A., Sivakumar, S., Chandrasekaran, A., & Pream Anand, D. (2014). Measurements of natural gamma radiation in beach sediments of north east coast of Tamilnadu, India by gamma ray spectrometry with multivariate statistical approach. *Journal of Radiation Research and Applied Sciences*, *7*(1), 7–17. https://doi.org/10.1016/j.jrras.2013.11.001

Taskin, H., Karavus, M., Ay, P., Topuzoglu, A., Hidiroglu, S., & Karahan, G. (2009). Radionuclide concentrations in soil and lifetime cancer risk due to gamma radioactivity in Kirklareli, Turkey. *Journal of Environmental Radioactivity*, *100*(1), 49–53. https://doi.org/10.1016/j.jenvrad.2008.10.012

Tchounwou, P. B., Yedjou, C. G., Patlolla, A. K., & Sutton, D. J. (2012). Heavy Metals Toxicity and the Environment. *EXS*, *101*, 133–164. https://doi.org/10.1007/978-3-7643-8340-4_6

Thilakarathna, R. C. N., Madhusankha, G. D. M. P., & Navaratne, S. B. (2022). Potential food applications of sorghum (Sorghum bicolor) and rapid screening methods of nutritional traits by spectroscopic platforms. *Journal of Food Science*, *87*(1), 36–51. https://doi.org/10.1111/1750-3841.16008

Turhan, S., Baykan, U. N., & Sen, K. (2008). Measurement of the natural radioactivity in building materials used in Ankara and assessment of external doses. *Journal of Radiological Protection: Official Journal of the Society for Radiological Protection*, *28*(1), 83–91. https://doi.org/10.1088/0952-4746/28/1/005

Tzortzis, M., & Tsertos, H. (2004). Determination of thorium, uranium, and potassium elemental concentrations in surface soils in Cyprus. *J. Environ. Radioact.*, *77*, 325–338. https://doi.org/10.1016/j.jenvrad.2004.03.014

Umar, S., Muhammad, A., & Elijah, S. (2023). Assessment of heavy metal contamination in groundwater from motorized boreholes in Maitumbi, Tipa Garage Area, Minna, Niger State. *Science World Journal*, *18*(2), 212–215. https://doi.org/10.4314/swj.v18i2.7

UNSCEAR. (2000). Sources and effects of ionizing radiation. *UNSCEAR 2000 report to the General Assembly, with scientific annexes. Volume I: Sources*. https://inis.iaea.org/records/8behk-d2e65

UNSCEAR. (2011). Sources and Effects of Ionizing Radiation. *United Nations Scientific Committee on the Effects of Atomic Radiation (UNSCEAR) 2008*

Report, Volume II: Report to the General Assembly, with Scientific Annexes C, D and E - Effects: Vol. II. United Nations. https://doi.org/10.18356/ce8f288a-en

Vardhan, K. H., Kumar, P. S., & Panda, R. C. (2019). A review on heavy metal pollution, toxicity and remedial measures: Current trends and future perspectives. *Journal of Molecular Liquids*, *290*, 111197.

Vennart, J. (1991). The 1990 recommendations of the International Commission on Radiological Protection. *Journal of Radiological Protection*, *11*(3), 199–203. https://doi.org/10.1088/0952-4746/11/3/006

Verwoerd, D. P. (2017). *A study on the levels of the heavy metals in the Kenyan Eastern Rift*. *5(1)*, 308–312.

Violante, A., Cozzolino, V., Perelomov, L., Caporale, A. G., & Pigna, M. (2010). Mobility and Bioavailability of Heavy Metals and Metalloids in Soil Environments. *Journal of Soil Science and Plant Nutrition*, *10*(3), 268–292. https://doi.org/10.4067/S0718-95162010000100005

Wani, A. L., Ara, A., & Usmani, J. A. (2015). Lead toxicity: A review. *Interdisciplinary Toxicology*, *8*(2), 55–64. https://doi.org/10.1515/intox-2015-0009

Wanink, J. H., & Goudswaard, K. P. C. (1994). Effects of Nile perch (Lates niloticus) introduction into Lake Victoria, East Africa, on the diet of Pied Kingfishers (Ceryle rudis). In J. J. Kerekes (Ed.), *Aquatic Birds in the Trophic Web of Lakes* (pp. 367–376). Springer Netherlands.

Wise, J. P., Young, J. L., Cai, J., & Cai, L. (2022). Current understanding of hexavalent chromium [Cr(VI)] neurotoxicity and new perspectives. *Environment International*, *158*, 106877. https://doi.org/10.1016/j.envint.2021.106877

World Health Organization. (2011). *Guidelines for drinking-water quality*. 1–564.

World Health Organization, Food and Agriculture Organization of the United Nations, & Joint FAO/WHO Expert Committee on Food Additives. Meeting (80th: 2015, R., Italy). (2016). *Evaluation of certain food additives and contaminants: Eightieth report of the Joint FAO/WHO Expert Committee on Food Additives*. World Health Organization. https://iris.who.int/handle/10665/204410

Xu, J., Chen, Y., Zheng, L., Liu, B., Liu, J., & Wang, X. (2018). Assessment of Heavy Metal Pollution in the Sediment of the Main Tributaries of Dongting Lake, China. *Water*, *10*(8), 1060-1076. https://doi.org/10.3390/w10081060

Yu, K. N., Mao, S. Y., Young, E. C., & Stokes, M. J. (1997). A study of radioactivities in six types of fish consumed in Hong Kong. *Applied Radiation and Isotopes: Including Data, Instrumentation and Methods for Use in Agriculture, Industry and Medicine*, *48*(4), 515–519. https://doi.org/10.1016/s0969-8043(96)00283-7

Yue, C. S., You, K. Y., Tan, C. W., & Ng, K. H. (2022). Method development and determination of potassium and phosphorus in oil palm organic fertilizers by microwave plasma atomic emission spectrometry (MP-AES). *Journal of the Iranian Chemical Society*, *19*(11), 4435–4443. https://doi.org/10.1007/s13738-022-02612-w

Zhang, W., & Cheng, C. Y. (2007). Manganese metallurgy review. Part I: Leaching of ores/secondary materials and recovery of electrolytic/chemical manganese dioxide. *Hydrometallurgy*, *89*(3), 137–159. https://doi.org/10.1016/j.hydromet.2007.08.010

APPENDICES

Appendix 1: $^{235}U^{*}$ disintegration chain

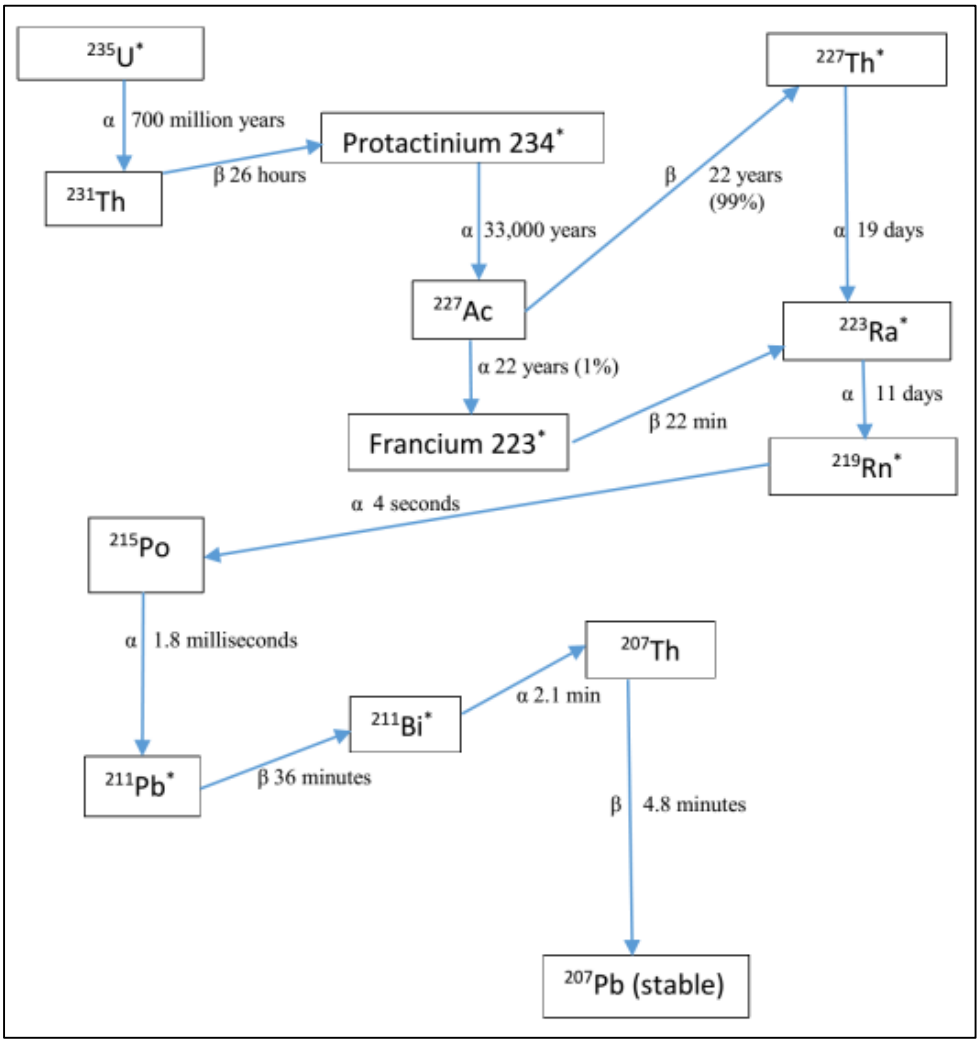


Figure A1: $^{235}U^{*}$ disintegration chain (Friedlander *et al.*, 1981).

Appendix 2: ^{238}U disintegration chain

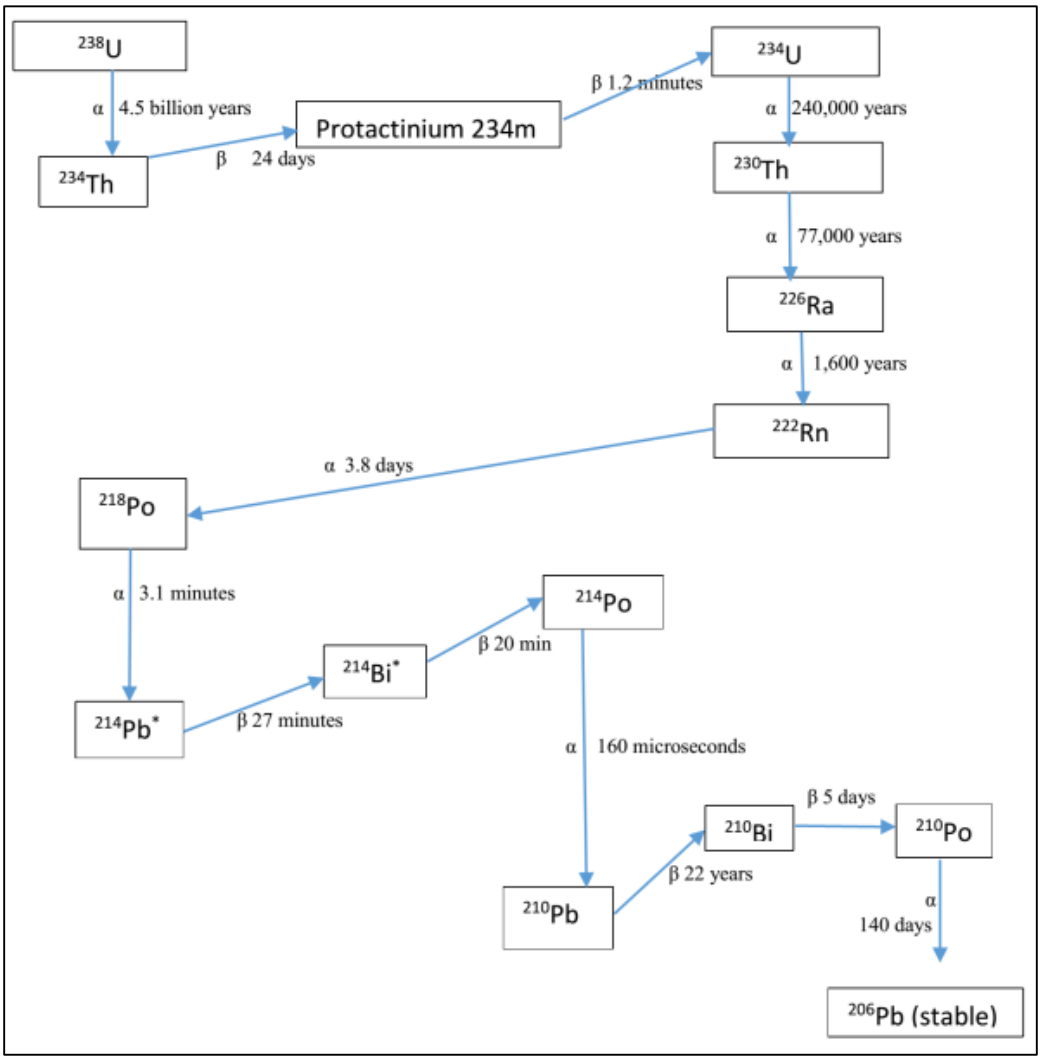


Figure A2: ^{238}U disintegration chain (Friedlander *et al.*, 1981).

Appendix 3: ^{232}Th disintegration chain

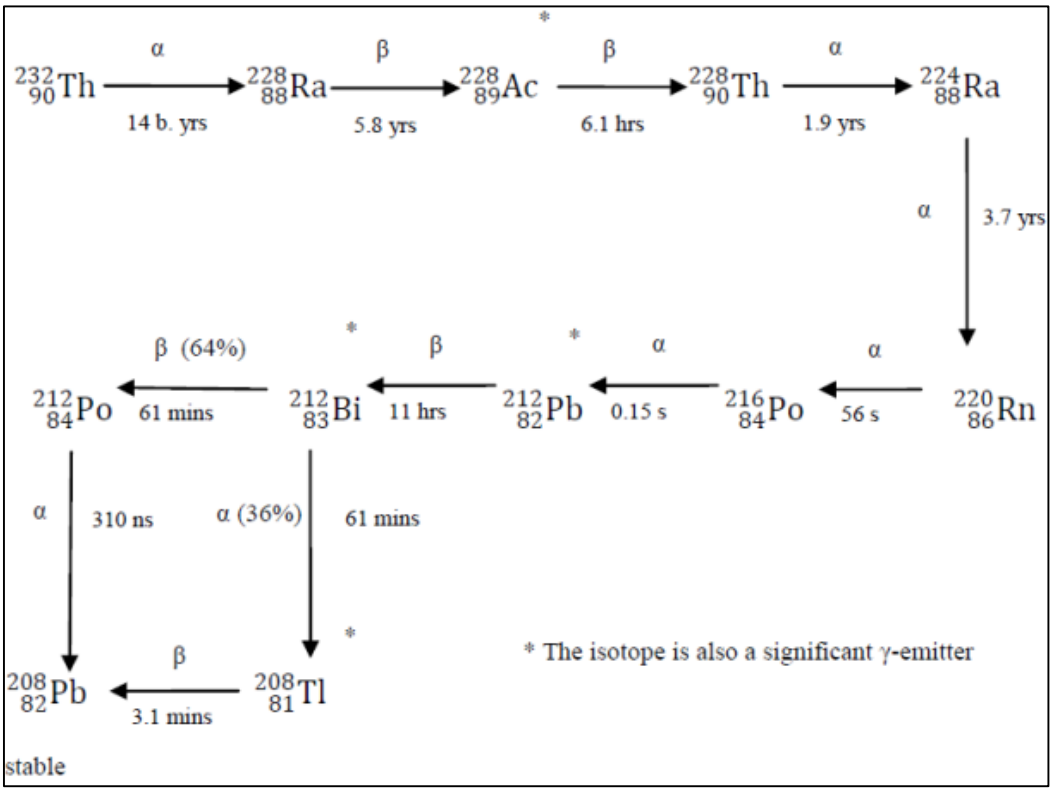


Figure A3: ^{232}Th disintegration chain (Friedlander et al., 1981).

Appendix 4: Pre-treatment Protocols for Heavy Metal Analysis

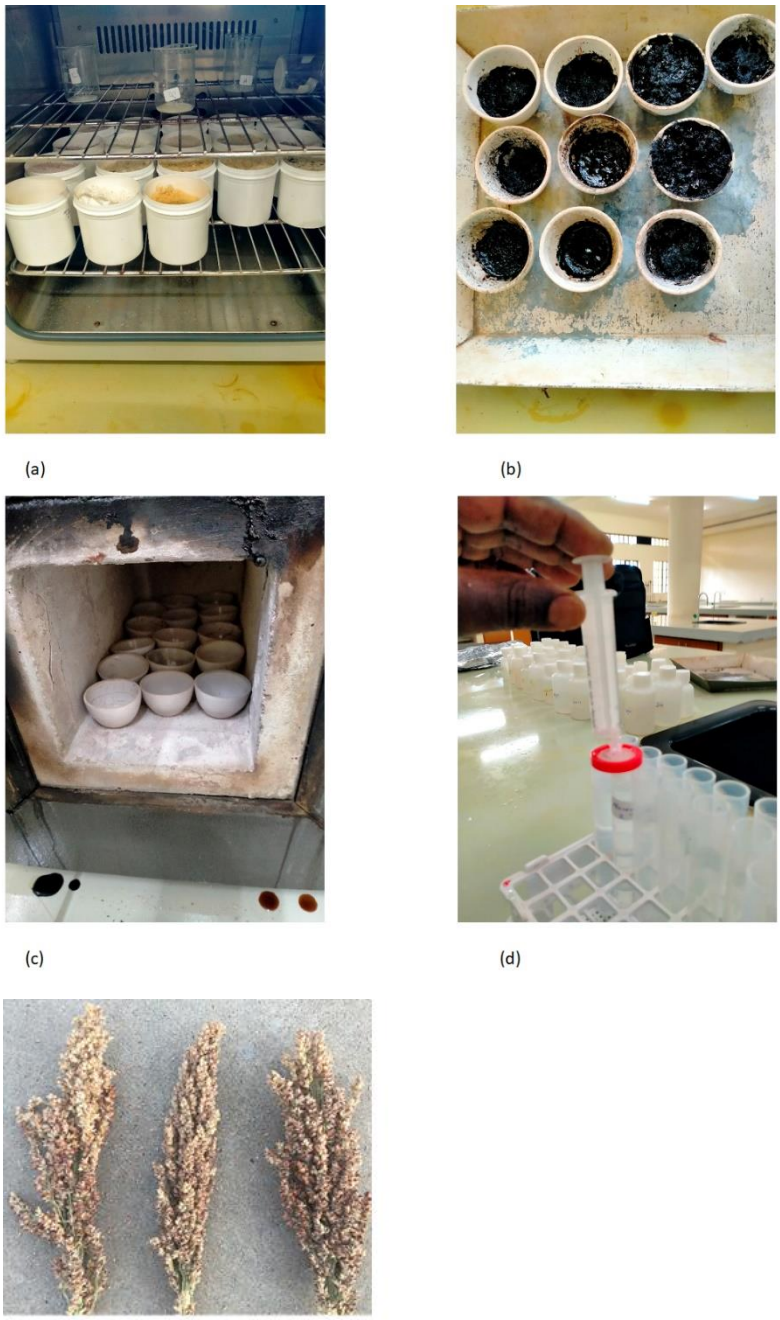


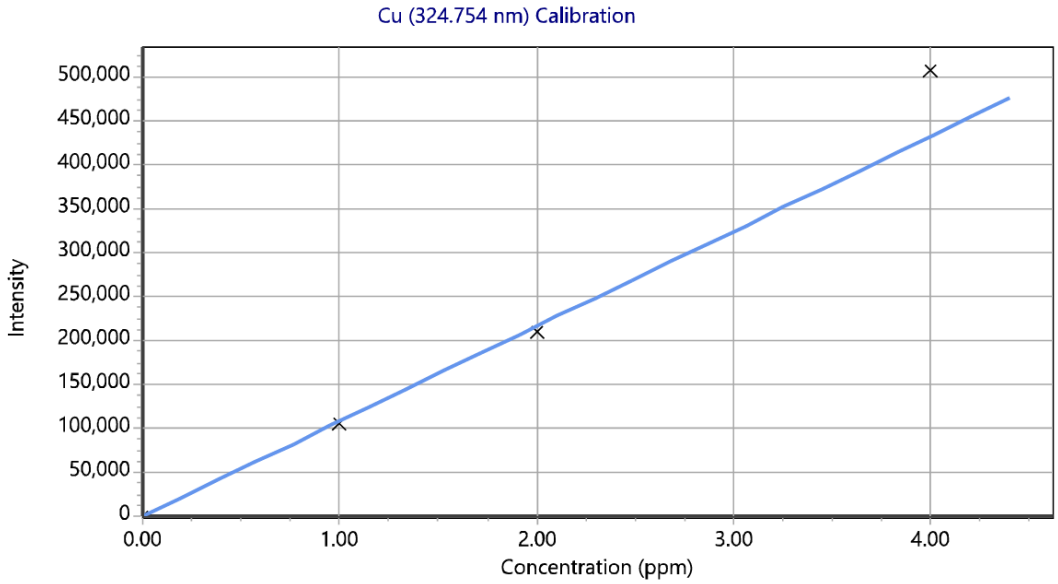
Figure A 4: Preparation of organic samples for heavy metal analysis; (a) Oven drying, (b) Charred samples, (c) Ashing in a maffle furnace, (d) Sample filtration, and (e) Sorghum flower heads

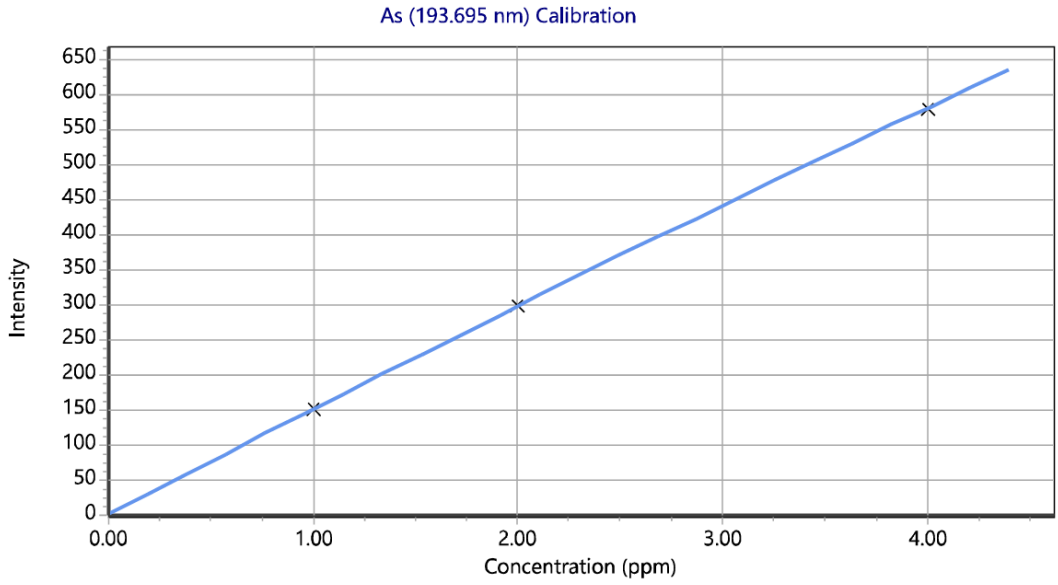
Appendix 5: The Agilent 4210 MP-AES used for heavy metal analysis.

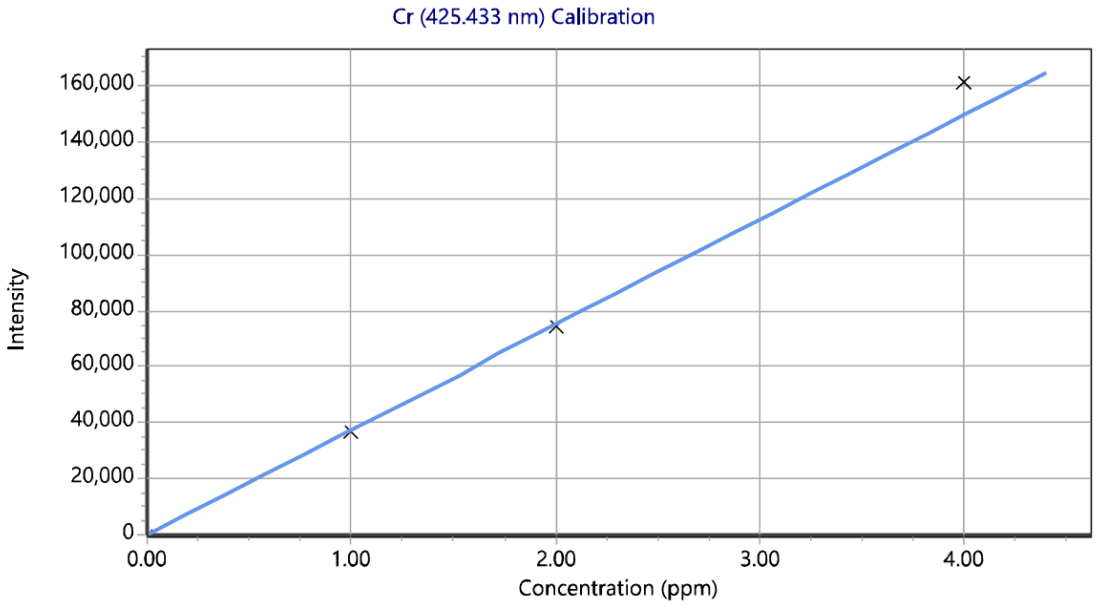


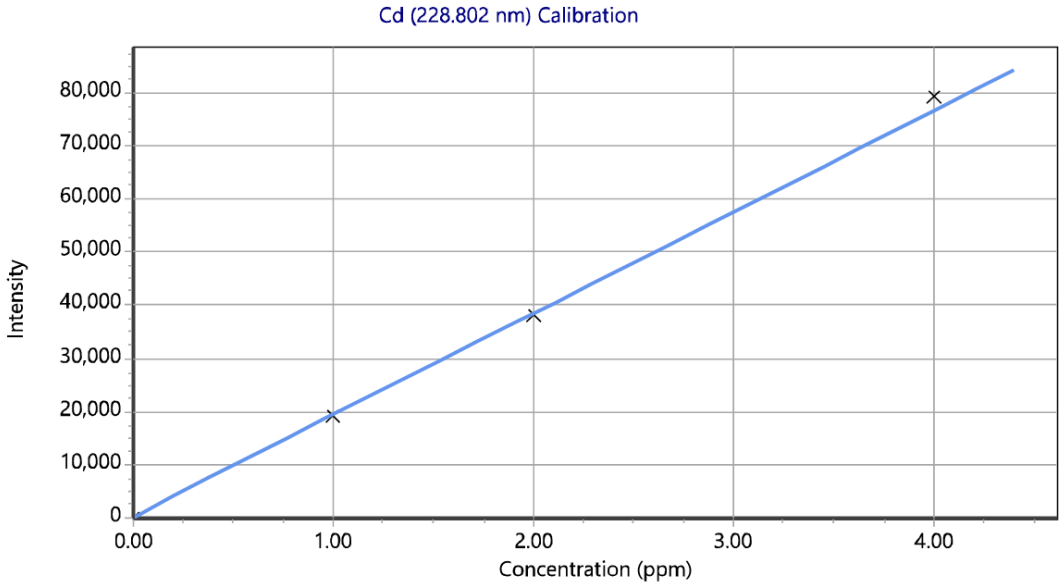
Figure A 5: The Agilent 4210 MP-AES used for elemental concentration data collection.

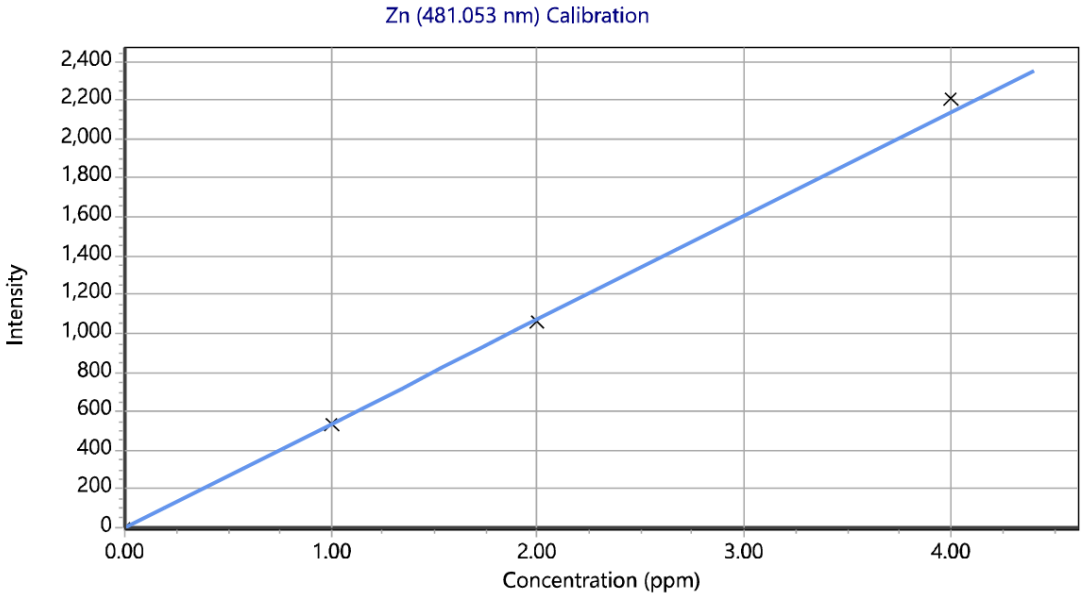
Appendix 6: Calibration curves for heavy metal analysis

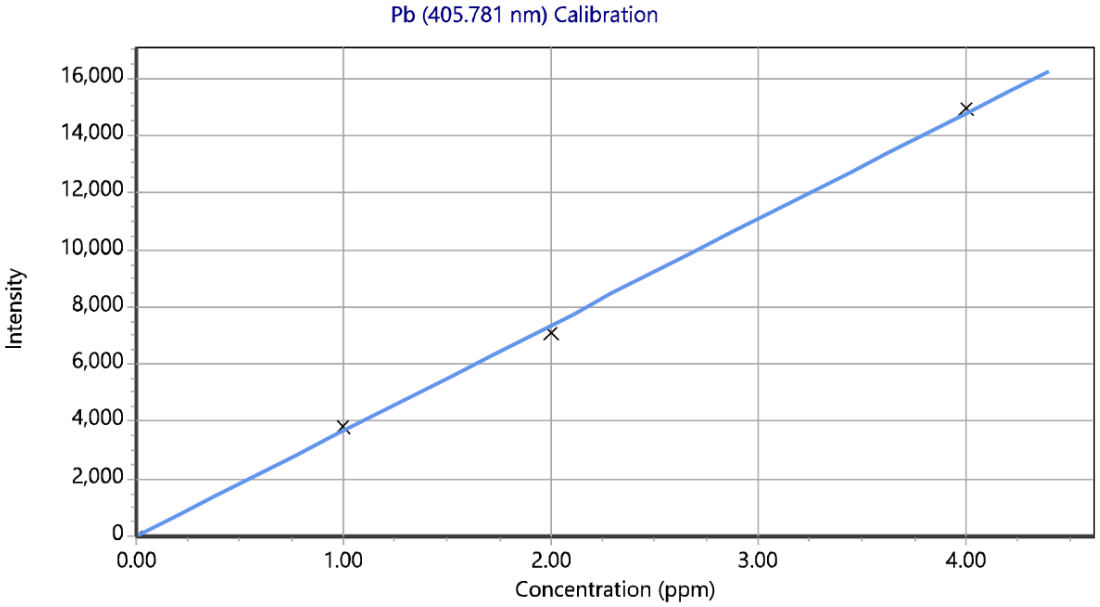





Cr (425.433 nm) Calibration
Intensity
160,000
140,000
120,000
100,000
80,000
60,000
40,000
20,000
0
0.00
1.00
2.00
3.00
4.00
Concentration (ppm)


Cd (228.802 nm) Calibration
Intensity
80,000
70,000
60,000
50,000
40,000
30,000
20,000
10,000
0
0.00
1.00
2.00
3.00
4.00
Concentration (ppm)


Zn (481.053 nm) Calibration
Intensity
2,400
2,200
2,000
1,800
1,600
1,400
1,200
1,000
800
600
400
200
0
0.00
1.00
2.00
3.00
4.00
Concentration (ppm)


Pb (405.781 nm) Calibration
Intensity
16,000
14,000
12,000
10,000
8,000
6,000
4,000
2,000
0
0.00
1.00
2.00
3.00
4.00
Concentration (ppm)

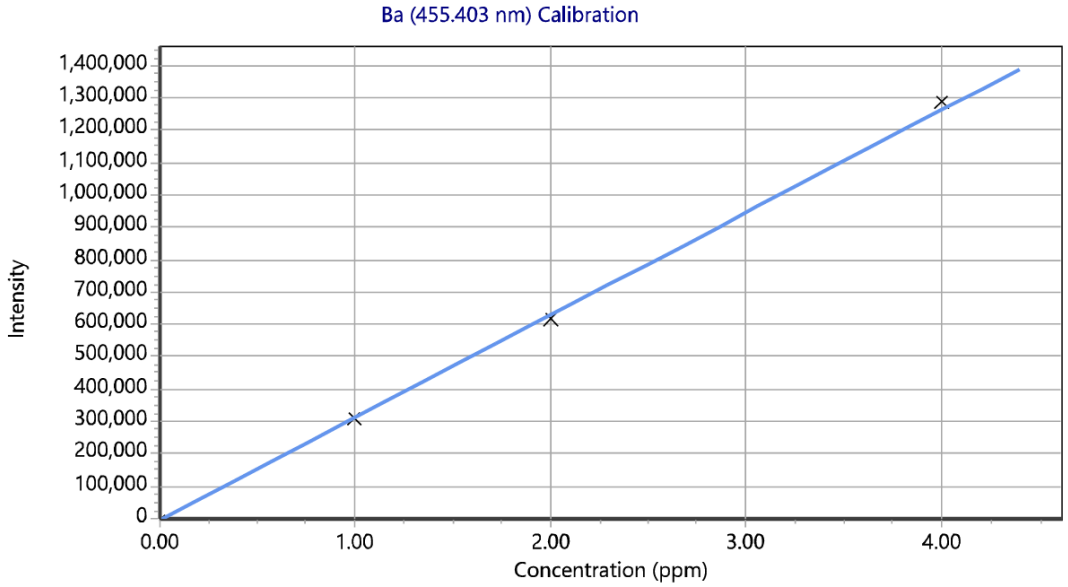
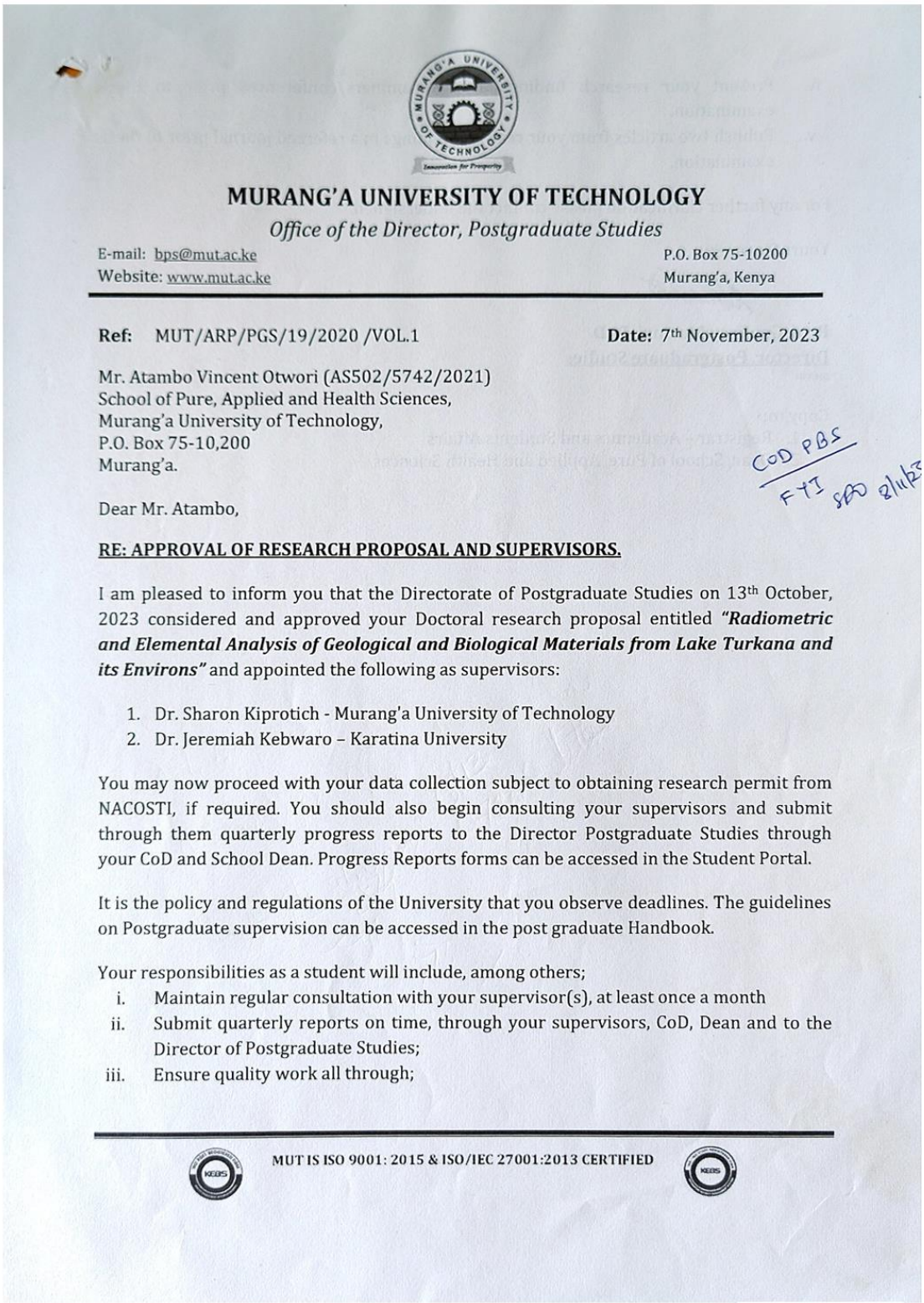


Figure A 6: Calibration curves of the studied heavy metals

Appendix 7: MUT Research Authorization Letter



MURANG'A UNIVERSITY OF TECHNOLOGY

Office of the Director, Postgraduate Studies

E-mail: bps@mut.ac.ke
Website: www.mut.ac.ke

P.O. Box 75-10200
Murang'a, Kenya

Ref: MUT/ARP/PGS/19/2020 /VOL.1

Date: 7th November, 2023

Mr. Atambo Vincent Otwori (AS502/5742/2021)
School of Pure, Applied and Health Sciences,
Murang'a University of Technology,
P.O. Box 75-10,200
Murang'a.

CoD PBS
FYI
SPD 8/11/23

Dear Mr. Atambo,

RE: APPROVAL OF RESEARCH PROPOSAL AND SUPERVISORS.

I am pleased to inform you that the Directorate of Postgraduate Studies on 13th October, 2023 considered and approved your Doctoral research proposal entitled ***"Radiometric and Elemental Analysis of Geological and Biological Materials from Lake Turkana and its Environs"*** and appointed the following as supervisors:

1. Dr. Sharon Kiprotich - Murang'a University of Technology
2. Dr. Jeremiah Kebwaro – Karatina University

You may now proceed with your data collection subject to obtaining research permit from NACOSTI, if required. You should also begin consulting your supervisors and submit through them quarterly progress reports to the Director Postgraduate Studies through your CoD and School Dean. Progress Reports forms can be accessed in the Student Portal.

It is the policy and regulations of the University that you observe deadlines. The guidelines on Postgraduate supervision can be accessed in the post graduate Handbook.

Your responsibilities as a student will include, among others;

i. Maintain regular consultation with your supervisor(s), at least once a month
ii. Submit quarterly reports on time, through your supervisors, CoD, Dean and to the Director of Postgraduate Studies;
iii. Ensure quality work all through;

MUT IS ISO 9001: 2015 & ISO/IEC 27001:2013 CERTIFIED

iv. Present your research findings at 2-3 seminars/conferences prior to thesis examination.

v. Publish two articles from your research findings in a refereed journal prior to thesis examination.

For any further clarification please contact the undersigned.

Yours Sincerely,

Prof. Geoffrey Muchiri, PhD
Director, Postgraduate Studies
GM/PIM

Copy to:
1. Registrar – Academics and Students Affairs
2. Dean, School of Pure, Applied and Health Sciences

Appendix 8: Publications

This thesis has produced the following journal articles:

1. Atambo, V. O., Opiyo, S., Kiprotich, S., & Kebwaro, J. M. (2025). Heavy metal concentration levels in surface waters of Lake Turkana and River Turkwel, Kenya. *IOSR Journal of Applied Physics (IOSR-JAP)*, *17*(3, Ser. 2), 11-16. http://www.iosrjournals.org
2. Atambo, V. O., Opiyo, S., & Kiprotich, S. (2025). Heavy metal concentration levels in some selected fish from Lake Turkana, Kenya. *International Journal of Research and Analytical Reviews (IJRAR)*, *12*(2), 272-278. http://www.ijrar.org